

Development of Chip-Based Electrochemically- and
Light-Directed Peptide Microarray Synthesis

by

Pallav Kumar

A Dissertation Presented in Partial Fulfillment
of the Requirements for the Degree
Doctor of Philosophy

Approved October 2013 by the
Graduate Supervisory Committee:

Neal Woodbury, Chair
James Allen
Stephen Johnston

ARIZONA STATE UNIVERSITY

December 2013

ABSTRACT

Peptide microarrays may prove to be a powerful tool for proteomics research and clinical diagnosis applications. Fodor et al. and Maurer et al. have shown proof-of-concept methods of light- and electrochemically-directed peptide microarray fabrication on glass and semiconductor microchips respectively. In this work, peptide microarray fabrication based on the abovementioned techniques were optimized. In addition, MALDI mass spectrometry based peptide synthesis characterization on semiconductor microchips was developed and novel applications of a CombiMatrix (CBMX) platform for electrochemically controlled synthesis were explored.

We have investigated performance of 2-(2-nitrophenyl)propoxycarbonyl (NPPOC) derivatives as photo-labile protecting group. Specifically, influence of substituents on 4 and 5 positions of phenyl ring of NPPOC group on the rate of photolysis and the yield of the amine was investigated. The results indicated that substituents capable of forming a π -network with the nitro group enhanced the rate of photolysis and yield. Once such properly substituted NPPOC groups were used, the rate of photolysis/yield depended on the nature of protected amino group indicating that a different chemical step during the photocleavage process became the rate limiting step.

We also focused on electrochemically-directed parallel synthesis of high-density peptide microarrays using the CBMX technology referred to above which uses electrochemically generated acids to perform patterned chemistry. Several issues related to peptide synthesis on the CBMX platform were studied and optimized, with emphasis

placed on the reactions of electro-generated acids during the deprotection step of peptide synthesis.

We have developed a MALDI mass spectrometry based method to determine the chemical composition of microarray synthesis, directly on the feature. This method utilizes non-diffusional chemical cleavage from the surface, thereby making the chemical characterization of high-density microarray features simple, accurate, and amenable to high-throughput.

CBMX Corp. has developed a microarray reader which is based on electro-chemical detection of redox chemical species. Several parameters of the instrument were studied and optimized and novel redox applications of peptide microarrays on CBMX platform were also investigated using the instrument. These include (i) a search of metal binding catalytic peptides to reduce overpotential associated with water oxidation reaction and (ii) an immobilization of peptide microarrays using electro-polymerized polypyrrole.

I would like to dedicate this work to my family and friends. First, to my loving parents, Shri Digvijay Kumar Sharma and Smt. Savita Sharma. Their unconditional love and support is a great source of strength to me. To my brothers, Pankaj Sharma and Neeraj Sharma who make me very proud and always love and support me. I am indebted to Neeraj for his steadfast support and faith in my abilities. I could not have accomplished this degree without his support. I would also like to dedicate this work to my sisters-in-law Aparna Sharma and Priyanka Sharma who are the new pillars of our family and are shouldering the responsibilities with great love and dedication. To the wonderful kids of my family, Vedagya, Riddhima, and Nandini who are a great source of happiness in our lives. To my wonderful friends, Abhishek Roy, Loren Howell, and Kul Bhushan who always love and support me and I feel blessed to have them.

ACKNOWLEDGEMENTS

My heartfelt thanks to my supervisory committee, Prof. Dr. Neal Woodbury, Prof. Dr. James Allen, and Prof. Dr. Stephen Johnston, for giving me a second chance to complete my degree. I shall ever remain greatly indebted to the committee.

I am very grateful to Dr. Neal Woodbury for his support throughout my academic studies, for introducing me to microarray area, for his expert advice, for the supervision of my thesis, and especially for allowing me to complete my degree. He has been a great mentor and dealt with me with great patience and perseverance. I greatly admire his dedication to science, kindness, acumen, energy, patience, perseverance, creativity, and management skills.

I offer special thanks to Dr. James Allen and Dr. JoAnn Williams for their support and guidance during the DOE project. Their focus on minute details of the experiments and strategizing future experiments always amazed me. I will try to develop these qualities earnestly and apply in my future endeavors.

I would also like to thank Dr. Stephen Johnston for his support and guidance. Like many researchers, I too benefitted a lot from his willingness to safely use several scientific instruments of his lab. Several interactions with him and talented researchers of his lab broadened my perspective about peptide microarray area.

I am very thankful to Dr. Arman Ghodousi, Dr. Zhan-Gong Zhao, and Dr. Allan Scruggs with whom I worked very closely on microarray related projects. Dr. Ghodousi taught me several key aspects of organic synthesis while studying the efficiency of different photo-labile protecting groups. His support and several discussions that we had

were very helpful. Dr. Zhao and I worked together to develop peptide microarray fabrication capability on CombiMatrix platform. His expert advice in designing experiments and analyzing results were very helpful and was a learning experience. Dr. Scruggs and I worked together in understanding the capabilities of PotentioSense unit, and developing a protocol for measuring the redox assays involving high currents/voltages. During this period the discussions that we had, and his logical reasoning about the experiments and protocol development were very useful.

I would like to thank Dr. Karl Maurer, Mr. Sho Fuji, and Dr. Kia Peyvan of CombiMatrix for all the technology support and guidance they provided. I would like to thank Mr. John Lopez and Dr. Zachary Laughrey of Proteomics Center at Arizona State University, Dr. Dan Brune of School of Life Sciences at Arizona State University, and Dr. Randall Nelson of The Biodesign Institute at Arizona State University for helping with MALDI characterization of microarray synthesis. I would also like to thank Kevin Brown for integrating Peptide synthesizer and Electro-synthesis instruments.

I am very thankful to Carole Flores for providing every possible professional assistance and my thanks also go out to Mikayla Madjidi for editing my dissertation.

Finally, I want to thank the DOE for financial support. In addition, I also want to thank the past and present members of Woodbury lab for all the fun along the way: Jinglin, Su Lin, Sean, Crystal, Jason, Shervin Shariari, Tram Lyna Vu, and Julie Noh, Matt, Jie, Guon, Wei, Evaldas, Amy, Doug, Jo, Laimonas, Terri, Haiyu, Trent, Rashaad, Michaela and April.

TABLE OF CONTENTS

	Page
LIST OF TABLES	x
LIST OF FIGURES	xii
LIST OF EQUATIONS	xvii
LIST OF SCHEMES.....	xviii
CHAPTER	
1. GENERAL INTRODUCTION TO PEPTIDE MICROARRAYS.....	1
Abstract	1
Introduction	1
Microarray Technology	3
Peptides at Molecular Level	5
Peptide Synthesis	5
Peptide Microarray Synthesis	7
Project Organization	11
Note.....	23
References.....	24
2. INVESTIGATION OF THE 2-(2-NITROPHENYL)PROPOXYCARBONYL PROTECTING GROUP SUBSTITUENT-EFFECT ON THE RATE OF PHOTOLYSIS AND YIELD OF AMINE	30
Abstract	30
Introduction	31

CHAPTER	Page
Results and Discussion	32
Materials and Methods	40
Conclusion	47
References.....	48
 3. FEATURE-LEVEL MALDI-MS CHARACTERIZATION OF ELECTROCHEMICALLY-DIRECTED IN SITU-SYNTHESIZED PEPTIDE MICROARRAYS.....	50
Abstract	50
Introduction.....	50
Results and Discussion	53
Materials and Methods	63
Conclusion	67
References.....	68
 4. OPTIMIZATION OF ELECTROCHEMICALLY-DIRECTED PEPTIDE MICROARRAY SYNTHESIS.....	72
Abstract	72
Introduction	72
Results and Discussion	77
Materials and Methods	97
Conclusion	101
References.....	102

CHAPTER	Page
5. INVESTIGATION OF NOVEL APPLICATIONS OF COMBIMATRIX MICROARRAY PLATFORM IN CONJUNCTION WITH MALDI MASS SPECTROMETRY AND ELECTROCHEMICAL DETECTION TECHNIQUES	104
.....	104
Abstract	104
Introduction	105
Results and Discussion	112
Materials and Methods	135
Conclusion	139
References.....	140
6. CONCLUSION.....	144
7. COMPLETE LIST OF REFERENCES	150
APPENDIX	16161
A. A STUDY OF ELECTROCHEMICAL DEPROTECTION EFFICIENCY OF TRITYL GROUPS USING MALDI-BASED MICROARRAY CHARACTERIZATION TECHNIQUE.....	165
B. TEST OF ALTERNATE METHODS TO ELECTROCHEMICALLY GENERATE ACIDS	174
C. STUDY OF PEPTIDE CONTAMINATION DURING MICROARRAY SYNTHESIS	178

APPENDIX	Page
D. SEARCH FOR A MILD ELECTRICAL CONDITION TO ELECTROCHEMICALLY DEPROTECT TRITYL GROUPS	186
E. PEPTIDE SYNTHESIZER AND ELECTRO-SYNTHESIS INSTRUMENT INTEGRATION AND OTHER INSTRUMENTATION ISSUES	191
F. PEPTIDE MICROARRAY FABRICATION ON SILICON SUBSTRATE USING PHOTOLITHOGRAPHY TECHNIQUE	197
G. TECHNIQUES	208
Continuous Flow Peptide Synthesizer	209
MALDI Mass Spectrometry	211
Ultraviolet-visible (UV-Vis) Spectroscopy	213
Infra-Red (IR) Spectroscopy	216
Nuclear Magnetic Resonance (NMR) Spectroscopy	218
Fluorescent Microarray Image Scanner	221
High-performance Liquid Chromatography	223
References.....	226
H. ABBREVIATIONS, SIDE-CHAIN RESIDUES, AND ACID DISSOCIATION CONSTANT VALUES OF AMINO ACIDS	228
I. MASS TO CHARGE RATIO OF AMINO ACIDS AND FEW GROUPS FREQUENTLY USED IN PEPTIDE SYNTHESIS	230

LIST OF TABLES

Table	Page
CHAPTER 1	
1. An Overview of the Electrochemical Method for Oligonucleotide Microarray Fabrication	14
CHAPTER 2	
1. Photolysis rate constants, half-lives, and the yields of amine.....	38
CHAPTER 4	
1. Details of the peaks observed in MALDI spectrum of peptide synthesis involving three electrochemical steps (without capping step; trityl glycine)	92
2. Details of the peaks observed in MALDI spectrum of peptide synthesis involving three electrochemical steps (with capping step; trityl glycine)	93
3. Details of the peaks observed in MALDI spectrum of peptide synthesis involving three electrochemical steps (with capping step; trityl chloride)	94
CHAPTER 5	
1. Details of Experiment 1 of peptide immobilization via co- electropolymerization of peptide-py and pyrrole.....	134
2. Details of Experiment 2 of peptide immobilization via co- electropolymerization of peptide-py and pyrrole.....	135
APPENDIX A	
1. % electro-deprotection of Trt and DMT groups at 3.0V, 10min condition ..	167

Table	Page
2. % deprotection of Trt and DMT groups at zero volts.....	168

APPENDIX H

1. Abbreviations, side-chain residues, and pKa values of amino acids	229
--	-----

APPENDIX I

1. Mass to charge ratio of amino acids and few groups frequently used in peptide synthesis	231
--	-----

LIST OF FIGURES

Figure	Page
CHAPTER 1	
1. Architecture of CombiMatrix chip	15
2. Photomicrograph of a CombiMatrix chip	15
3. Fluorescence detection scheme of peptide microarrays via interaction of biotin and fluorophore conjugated streptavidin molecules.....	20
4. Photograph of a PotentioSense instrument	22
5. Electrochemical detection of peptide microarrays via interaction of biotin and horseradish peroxidase conjugated streptavidin molecules	22
CHAPTER 2	
1. Photodeprotection mechanism of NPPOC analogues	37
2. Photodeprotection mechanism of NVOC group.....	37
CHAPTER 3	
1. Scheme of electrochemically-directed peptide microarray synthesis on CombiMatrix chips	54
2. MALDI-TOF characterization of Tmpp labeled peptide using photolabile linker	57
3. Schematic diagram of an electrochemical array of four peptides	58
4. MALDI-MS characterization of three peptide features with electrochemical steps ..	59
5. MALDI-MS characterization of three peptide features with electrochemical steps	60
6. MALDI-MS characterization of a peptide synthesized on top of ANP linker	62
7. MALDI-MS characterization of a peptide synthesized on top of Rink linker.....	63

Figure	Page
CHAPTER 4	
1. MALDI-MS characterization of electrochemical removal of trityl groups using N,N'-diphenylhydrazine as EGA-P	80
2. Fluorescence characterization of stability of CombiMatrix chips to trifluoroacetic acid (TFA)	84
3. MALDI-MS characterization of chemical deprotection efficiency of t-butyl groups using TFA	86
4. MALDI-MS characterization of capping reaction efficiency	88
5. MALDI-MS characterization of peptide synthesis involving three electrochemical steps	91
CHAPTER 5	
1. Electrochemical detection of synthesis using biotin-SRP-HRP assay	113
2. I/V analysis of Potentiosense microarray reader	115
3. MALDI-MS characterization of coupling of ferrocene carboxylic acid to free amines on CombiMatrix chip surface	117
4. I/V analysis of ferrocene labeled CombiMatrix chips	118
5. Sequences of designed peptides for initial round of electrocatalyst search for anodic half-reaction of water electrolysis	120
6. A sketch of peptide 3 designed for search of catalyst for anodic half-reaction of water electrolysis	121

Figure	Page
7. I/V curve comparing catalytic efficiencies of designed peptides on gold electrodes	123
8. Sequences and chemical structures of catalytic peptides and control peptide	124
9. Aspartimide formation reaction mechanism	125
10. MALDI-MS characterization of synthesis of peptide 3 on CombiMatrix chips ...	126
11. MALDI-MS characterization of synthesis of peptide 4 on CombiMatrix chips ...	127
12. Electrochemical detection of peptide immobilization on CBMX chips via co- electropolymerization of peptide-py and pyrrole	131
13. A probable mechanism of pyrrole electropolymerization	132
 APPENDIX A	
1. MALDI-MS characterization of electrochemical deprotection of Trt and DMT groups using hydroquinone as EGA-P	170
 APPENDIX B	
1. MALDI-MS characterization of electrochemical deprotection of Fmoc groups using piperidine hydrochloride	176
 APPENDIX C	
1. Pyrrole electropolymerization on selected electrodes of a CombiMatrix chip	179
2. Chip design of experiments conducted for peptide contamination study	180
3. MALDI-MS characterization of experiments conducted for peptide contamination study	182

Figure	Page
APPENDIX D	
1. Fluorescence image of the experiment to search for a mild electrical condition to electrochemically deprotect Trt groups using Hydroquinone as EGA	188
APPENDIX F	
1. Fluorescence images of the experiment to determine coupling efficiency of amino acids to available free amines on silicon substrates	201
2. Fluorescence images of the silicon substrates derivatized with β -alanine and Peg 6 linker modified with a glycine.	202
3. UV-Vis, HPLC, and IR analysis to determine composition of photoresist mixture	203
4. Fluorescence comparison of photo-deprotection efficiency at 260nm and 365nm.....	204
5. Fluorescence comparison of photo-deprotection efficiency to chemical deprotection efficiency	205
APPENDIX G	
1. A picture of continuous flow peptide synthesizer manufactured by PerSeptive Biosystems	211
2. Schematic of MALDI-TOF.....	213
3. Working principle of a UV-vis spectrophotometer	216
4. Working principle of a FT-IR spectrometer	218
5. Working principle of a NMR instrument.....	221

Figure	Page
6. Working principle of a fluorescent image scanner	224
7. Schematic of a HPLC instrument.....	226

LIST OF EQUATIONS

Equation	Page
APPENDIX B	
1. Electro-reduction of piperidine hydrochloride to piperidine	175
2. Hydrogenolysis of amine protecting Cbz groups on platinum surfaces	177
3. Electrochemical reaction to deprotect alloc groups	177
APPENDIX G	
1. Beer-Lambert's law	214
2. Equation to measure absorbance based on transmittance	214
3. Equation to determine chemical shift	220
4. Equation to calculate signal to noise ratio	222
5. Equation to calculate numerical aperture.....	223

LIST OF SCHEMES

Scheme	Page
CHAPTER 1	
1. Solid-Phase peptide synthesis scheme	7
CHAPTER 2	
1. General synthetic schemes for NPPOC carbamates and tryptophan protected with PLPGs	33
APPENDIX F	
1. General synthesis scheme of peptide microarray fabrication on silicon substrates..	200

Chapter 1

General Introduction to Peptide Microarrays

Abstract

This chapter provides an introduction to microarrays in general, and establishes the need and applications of peptide microarrays. It discusses the difficulty of fabrication of peptide microarrays and different approaches applied to this problem. A new approach for making peptide microarrays based on a CombiMatrix (CBMX) platform is described. A study to improve photo-deprotection efficiency of photo-labile protecting groups, which can be useful in photolithography based microarray fabrication, is also described. This chapter also discusses various fabrication and characterization techniques used in the following chapters.

Introduction

Proteins are considered workhorse molecules in biology. They perform a vast array of functions such as signaling, catalysis, and DNA replication¹. Binding between proteins and biomolecules plays a key role in the functioning of proteins². The binding could be based on Fischer's lock-and-key³ or Koshland's induced fit concept⁴. The lock-and-key concept involves the interaction of spatially complementary regions of binding molecules. In the induced-fit concept, the binding partners are conformationally flexible to induce a binding interaction. The binding interactions are comprised of several forces: vanderwaals, electrostatic, hydrophobic, and hydrogen bonding. The specificity of binding could vary from a protein being specific to only one binding partner (e.g., glucokinase which catalyzes conversion of glucose to glucose-6-phosphate) to a protein

being completely non-specific and interacting almost irrespective of the structural features of the binding partner (e.g. sticky proteins)⁵.

Proteins are made up of one or several three-dimensionally folded polypeptides⁶. A polypeptide is a linear chain comprising of twenty naturally occurring amino acids connected to each other through amide bonds. Although no exact definition of length of polypeptides is described in literature, some authorities have adopted 10,000 Da as an upper limit on the molecular weight of a polypeptide⁷.

The diversity of proteins arises because of two different factors. Firstly, there are twenty different possibilities (amino acids) for each position in a polypeptide chain. Secondly, there are multiple folding possibilities of a linear polypeptide chain, giving rise to innumerable conformations. Levinthal's paradox⁸ provides an idea of the vast diversity of proteins possible with twenty amino acids. It states that a protein of 101 amino acids could exist in $3^{100} = 5 \times 10^{47}$ configurations. Even if the protein is able to sample new configurations at the rate of 10^{13} per second, or 3×10^{20} per year, it will take 10^{27} years to try them all. Real proteins fold over a time scale of 10^{-1} to 10^3 sec. Thus, nature has explored a small fraction of the complete possibilities in designing proteins for various functions. It has conserved proteins in whole or in part (domains of proteins) across different species with minor modifications.

Protein interactions with a binding partner can be dependent on its constituent amino acids at various levels. Sometimes, a single amino acid plays a decisive role in protein interaction⁹. Its replacement could enhance or inhibit a protein's interaction drastically. Hence, a theoretical understanding of the role of each amino acid in a protein's functioning is important. However, there is a lack of substantial experimental

data and a difficulty in modeling various forces of interactions of twenty amino acids. This makes the prediction of the role of different entities of a protein individually as well as in combination with other entities in binding interactions very difficult.

One way to approach this problem is to limit the study to protein-peptide interactions instead of protein-protein interactions. An increasing number of protein-protein interactions are being reported to involve interaction of a protein with a peptide of the binding protein partner¹⁰. The interacting peptide may originate from a loop within a well-defined domain, or from an unstructured region between structured domains¹⁰. A number of protein-protein interactions involved in cell signaling and regulatory systems which are basically protein-peptide interactions have been studied¹⁰⁻¹². The study of protein-peptide interactions is also important for drug discovery and development of inhibitory peptides¹³⁻¹⁵.

Gaining a deeper understanding of protein-peptide interactions requires an experimental system which can evaluate the interactions of a multitude of peptides with a specific protein. Time-saving and cost-efficiency capabilities of such a system are also highly desirable. Microarray technology has proved to be an experimental system capable of meeting these desired features¹⁶⁻¹⁸. As a discovery tool, microarray technology has the advantage of reading the activity of every single probe of a library. Another great advantage of microarray technology is that peptide based systems can be integrated and used to study various protein-peptide interactions in a robust and reproducible way.

Microarray Technology

Microarray technology involves the assembling of biomolecules in an array format on a solid surface. This surface is usually a glass slide or a silicon substrate¹⁹. The

array format is useful for assaying a large number of biomolecules in a high-throughput fashion with little consumption of analyte. Each feature on the solid support is functionalized with one type of biomolecule. The activity of the biomolecules immobilized on different features of the microarray is read-out in a parallel, high-throughput way.

The microarray working principle involves the incubation of a microarray functionalized with immobilized biomolecules (target probes) such as peptides, proteins, DNA, or small molecules with analyte (proteins, virus, cells, single-stranded DNA, RNA). The analyte binds to different features of the microarray with different binding strength and specificity. Fluorescent molecules that are coupled directly to the analyte before incubation, or are bound to the analyte after incubation in a subsequent step, are then used to determine the binding characteristics of the whole array when imaged using a fluorescence scanner²⁰. Every single feature of the microarray is an assay providing information about the binding interaction between the target and analyte molecule.

Although microarrays of a variety of biomolecules can be generated in theory, DNA and peptide microarrays have progressed a great deal in last few years. DNAs composed of four building blocks (nucleotides) and peptides composed of twenty building blocks (amino acids), when fabricated in a fully combinatorial manner, gives rise to comprehensive DNA and peptide microarrays respectively. Because of the high number of building blocks (twenty amino acids) and the presence of a variety of side-chain groups in these building blocks which can lead to side reactions, fabrication of a comprehensive and synthetically robust peptide microarray has proved to be challenging.

Peptides at Molecular Level

A polymer of amino acid molecules through amide bond formation, usually less than 30 – 50 amino acids, is called a peptide. There are twenty types of naturally occurring amino acids differing from each other only in their side-chain group. The amino acid group (part of an amino acid molecule other than side-chain group) is conserved among all the twenty amino acids. All the amino acids can couple with each other through a peptide bond leading to the diversity of peptide sequences. More information on amino acids can be found in Appendix H. Further information can be found in Reference 21.

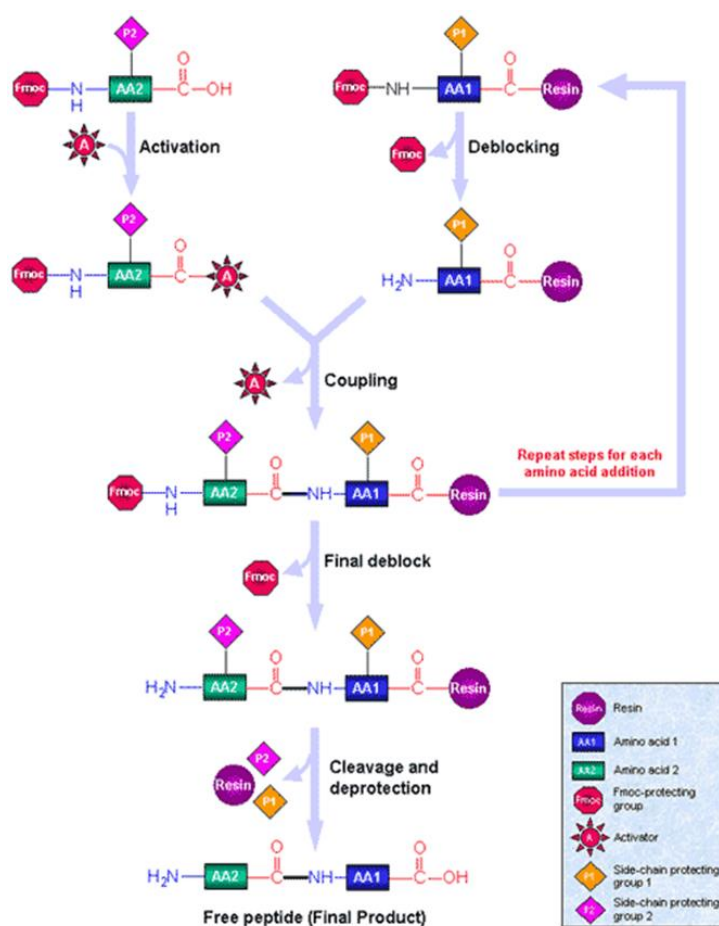
Two different stereoisomers, L-amino acid and D-amino acid, are possible for an amino acid except glycine, which does not possess any chiral center. All other amino acids occur as the L-isomer in nature. The peptide bond formation reaction between two amino acids is essentially a dehydration reaction between the α -amino group of one amino acid and the carboxyl group of another amino acid. Elongation of a peptide can take place from either end: N-terminus or C-terminus.

Peptide Synthesis

Chemical synthesis of peptides is mainly based on Bruce Merrifield's solid-phase peptide synthesis technique²². Earlier chemical synthesis was carried out in a solution phase and involved multiple synthesis, purification, and characterization steps. The development of protecting groups, mainly boc and fmoc groups, has further simplified and drastically improved the efficiency of chemical synthesis.

Merrifield Peptide Synthesis. The solid-phase peptide synthesis technique developed by Bruce Merrifield revolutionized the chemical synthesis of peptides²². Using

this technique, peptides can be synthesized on solid supports functionalized with amino or carboxyl groups. The technique overcomes multiple tedious purification and characterization steps and facilitates synthesis of very long peptides. Previously this was impossible through solution-phase methods. Once the synthesis is complete, the fabricated peptide can be cleaved from the solid support, purified, and characterized (Figure 1). This technique is also the basis for the chemical-synthesis of peptide libraries. Peptide libraries can be fabricated on beads based on a split-mix synthesis method²³ and can be fabricated on 2D solid substrates in microarray format through several successful techniques such as photolithography^{24,25} and laser printing²⁶.



SCHEME 1: Solid-phase peptide synthesis scheme²⁸.

Peptide Microarray Synthesis

Peptide synthesis is complicated compared to DNA synthesis due to considerable side-chain functional group variability between the twenty naturally occurring amino acids. Every amino acid coupling cycle required to grow a peptide on a surface takes approximately 1 - 2 hours to complete^{28,29} and synthesis efficiencies using standard Fmoc or t-boc protection strategies are approximately >98%. DNA synthesis is much simpler because it involves only four nucleotides and the formation of phosphodiester bonds between two nucleotides during oligonucleotide synthesis which is very efficient (>99%).

It is also less time consuming (Nimblegen, can now complete each synthesis cycle in 5 minutes)³⁰ and the synthesis challenges due to nucleobases have been overcome.

There are several methods of generating peptide libraries such as phage display³¹, mRNA display³² or combinatorial synthesis on solid supports such as beads. The combinatorial synthesis on beads is based on a split-mix synthesis strategy that results in one compound per bead^{33,3}. Peptide libraries can also be generated on flat surfaces in a rationally-designed pattern. Peptide microarrays with probe sequence densities up to 200K within a square cm area of a 1 × 3in microscope slide are commercially available³⁵. The advantage of an array-based synthesis over other library-generating techniques is that the sequence information of every single peptide on the surface is known. Other library-generating techniques do not have this advantage; though several labor-intensive strategies have been devised which permit probe decoding through sequencing subsequent to screening³⁶. Peptide library-generating techniques such as phage display and mRNA display can generate libraries containing up to 10¹⁰ and 10¹⁵ different peptides respectively. In comparison, the largest peptide microarray libraries commercially available at present are a few hundreds of thousands as per published information³⁷. Although, the library size of peptide microarrays is very small in comparison to the library size generated by techniques such as phage display and mRNA display, each member of a peptide microarray is defined, unlike other techniques which are largely combinatoric. Such defined high-throughput systems when merged with large-scale computation of libraries can lead to an ever-expanding database through which several algorithms can be tested and new concepts in science can be discovered. Microarrays can also assist in refining the consensus sequences obtained by other

techniques. . Microarrays are also robust and reproducible: a peptide microarray platform could be fabricated with desired sequences in replicates that could be used multiple times for various assays.

Peptide microarray synthesis may proceed in two general ways: (i) peptide printing (robotic deposition of pre-synthesized peptides)³⁸ and (ii) in situ parallel synthesis of peptides on microarray surfaces^{39,40}. Microarrays generated by peptide printing are best suited for low- and medium-throughput assays. Major issues with printed arrays in regards to high throughput assays include maintenance of the peptide library and replacement of the library.

In situ parallel peptide synthesis performed directly on microarray surfaces is a preferable method. It is capable of generating on the order of 10^6 peptide sequences; far exceeding the size and diversity possible when depositing pre-synthesized peptides directly onto microarrays³⁸. Theoretically, a new batch of chips can be generated within a week, which is comparable to other library generating techniques such as split-mix synthesis. Using a parallel, split-pool method to generate a penta-peptide library, on beads, from the twenty naturally-occurring amino acids, would involve 100 coupling cycles and likely take 9-10 days to complete. Synthesis automation instruments have the capability to perform a microarray synthesis on a chip and produce several replicates of the chip within a week's time that can be used for multiple experiments.

Several methods have been reported for the in situ parallel synthesis of peptide microarrays on 2D surfaces. Early on, one of the most successful approaches was SPOT synthesis^{39,41}. In this method, synthetic building blocks, along with the coupling reagents, are spotted on a membrane support. The membrane support is generally made up of

cellulose or nylon and has functional groups attached to it. The activated incoming synthetic building blocks couple with the functional groups. The size of the spot is decided by the volume dispensed and the absorptive capacity of the membrane support. The feature density of this technique is low (~1mm diameter features) but the site density is quite high (~ 0.1 to 1 $\mu\text{mol}/\text{cm}^2$). In the past few years, two approaches, Breitling's microparticle-deposition technology^{42,43} and photolithography based approaches^{44,45}, have been very successful in fabricating high density peptide microarrays. In Breitling's technology, spatially defined deposition of microparticles coated with aminoacids is done through laser printing. Later, the microparticle is melted and the amino acid is coupled to the functionalized microscope glass slide. A German-based company, PEPperPRINT, fabricates peptide microarrays based on this technology. Photolithography-based approaches involve light irradiation through a real or virtual photomask for the deprotection of amine protecting groups from selected features of the surface. Photolabile protecting groups (PLPGs) are directly deprotected upon irradiation, and acid-labile groups are deprotected by localized generation of acids upon light irradiation of selected features^{43,44}. This results in the patterned deprotection of these features on the surface which are then coupled with an activated incoming amino acid. This is repeated for multiple cycles selecting a different set of features at each light irradiation step. This method, although promising, has some limitations. Amino acids protected with PLPGs are not readily available, and it is not a simple process to prepare them in-house. In addition, diffraction and flare (scattering) issues during light irradiation in both photo-acid based and PLPGs based techniques can lead to insertion of moieties at undesired features.

Project Organization

This thesis was conducted with the aim of optimizing (1) light- and (2) electrochemically-directed peptide microarray synthesis, and (3) investigating innovative applications of electrochemically-directed peptide microarray synthesis on CBMX chips in conjunction with MALDI mass spectrometry and electrochemical detection techniques.

Optimization of light-directed peptide microarray synthesis. There is a great deal of interest in synthesis and characterization of photolabile protective groups (PLPGs) that are readily and efficiently removed by irradiation. The success of light directed combinatorial synthesis based on PLPGs⁴⁵ used for development of high density microarrays depends on the photo-deprotection efficiency of PLPGs^{46,47}.

Among the first protective groups used in oligonucleotide and oligopeptide synthesis was the *o*-nitroveratryloxycarbonyl group (NVOC)^{45,49,50}, which has a relatively low photo-deprotection yield. It was later discovered that methyl extension of the α -carbon would enhance the cleavage process by changing the mechanistic pathway as demonstrated by the use of α -methyl-*o*-nitropiperonyloxycarbonyl protective groups (MeNPOC)^{46,51}. Further improvement of this process was accomplished by studying the cleavage pattern of 2-(2-nitrophenyl)propoxycarbonyl (NPPOC) protected nucleotides⁵². In fact, the NPPOC group turned out to be a better choice for peptide synthesis due to the presence of an extra methylene group. This resulted in the formation of less reactive intermediates that otherwise would react with the free amine to form undesired byproducts⁵³. The NPPOC group has been studied in terms of the rate of photolysis of various protected amino acids, and it has been evaluated in terms of its utility for photolithographic peptide microarray synthesis⁵⁴. The photo-deprotection rates of

NPPOC protected amino acids were at least twice as fast as NVOC protected amino acids. These studies have demonstrated that the NPPOC group exhibits the capacity to serve as a reasonable platform for light-sensitive protection of various amines. Yet the efficiency of NPPOC is not comparable to Fmoc (base labile), and Boc (acid labile) protecting groups which are most commonly used in conventional peptide synthesis. To improve the deprotection efficiency, which limits the rate of photolysis and yield of free amines, we have tested several derivatives of NPPOC. We have also tested the photodeprotection efficiency of the most efficient NPPOC derivative towards different kinds of amines. The results derived from this investigation could be useful in preparing a more efficient photolabile amino protecting group with applications ranging from organic to combinatorial peptide synthesis.

Optimization of electrochemically-directed peptide microarray synthesis.

Peptide microarray synthesis based on an electrochemical approach is another promising technique for the fabrication of peptide microarrays. This method was devised by Maurer et al. in 2005⁵⁵. They produced an electrochemically generated acid (EGA) in a spatially defined way on microelectrodes of an electronically addressable array to remove boc protecting groups. The substrate used was a CBMX 1K chip developed by CombiMatrix Corp., Mukilteo, Washington. It had 1024 individually addressable platinum microelectrodes embedded on a silicon substrate. The platinum electrodes of the chip were coated with a proprietary polymer possessing hydroxyl groups on which was synthesized a DNA oligomer. Previously, a pentapeptide, N-terminal sequence of endorphin (YGGFL) was synthesized electrochemically on top of the DNA oligomer of

the CMOS chip. The characterization of the synthesis was done by a fluorescence detection method.

The CMOS chips produced by CombiMatrix (CBMX chips), by virtue of possessing electronically addressable arrays of electrodes, are able to fabricate molecular libraries electrochemically. The chips are primarily used for the generation of oligonucleotide microarrays^{56,57,58}. Details of oligonucleotide microarray fabrication on CBMX chips can be seen in Table 1. The YGGFL peptide, synthesized electrochemically by Maurer et al. as a proof of concept, did not provide any complications due to side-chain groups of amino acids. Furthermore, syntheses of only a single peptide and related truncated peptides on CBMX chip surface was demonstrated. Several issues in electrochemical synthesis such as stability of side-chain protecting groups during the gating step (chemical step at which a spatially defined deprotection step takes place), containment of EGA, and stability of CBMX chips to strong acids needed for deprotection of side-chain protecting groups were not explored by Maurer et al. We chose to explore these aspects and optimize the electrochemical synthesis of peptide microarrays on CBMX chips. We mainly focused on (i) generation and use of an EGA for the removal of acid labile protecting groups from selected positions of the electronically addressable CBMX chip and (ii) synthesis of peptide microarrays with the optimized EGA system.

Table 1: An Overview of the Electrochemical Method for Oligonucleotide Microarray

Fabrication^{58,59,60}.

Method	Approach	Chemistry	Current Availability
In situ parallel synthesis	Use of microarrays of individually addressable microelectrodes, diversity achieved through gating reaction before each nucleotide cycle.	Regular phosphoramidite chemistry, trityl groups are deprotected using electrogenerated acid (gating reaction), acid electrochemically generated through oxidation of hydroquinone at platinum microelectrodes, hydroquinone is oxidized to release protons by passing 0.26μA current to the addressed microelectrodes for 60s.	50-140mer arrays on 12K, 90K, and 4X2K chips, 25μm - 45μm in feature size, synthesis quality – high quality 50-mer arrays; quality long oligonucleotide arrays, synthesis characterization through fluorescence or electrochemical-based enzyme amplification, flexible in chip design, flexible in non-regular sequences.

Peptide microarray synthesis on 12K CBMX chips.

Complementary metal oxide semiconductor (CMOS) array technology. A key component of our microarray synthesis, CBMX’s CMOS array technology, allows programmable, spatially selective activation of electrodes of the CBMX chip. Each CBMX chip has 12,544 individually, electronically addressable microelectrodes present in it (Figure 1). Each microelectrode is spherical in shape, 45μm in diameter, overlaid with a three dimensional proprietary biopolymer about 50nm thick, and separated from its neighbor electrode by 75μm (Figure 2). Microarray fabrication using this technology involves a software compilation of peptide sequences to be synthesized and a software

generation of a minimum number of synthetic steps required for microarray fabrication. It also involves hardware concentrating on a selected set of electrodes at each synthesis step to generate acid from electro-generated acid precursor (EGA-P). During the gating step in each synthesis cycle, the CBMX hardware unit (electro-synthesis instrument) automatically applies voltage/current to the selected set of electrodes and generates acid locally from EGA-P that deprotects terminal amino groups of the addressed electrodes.

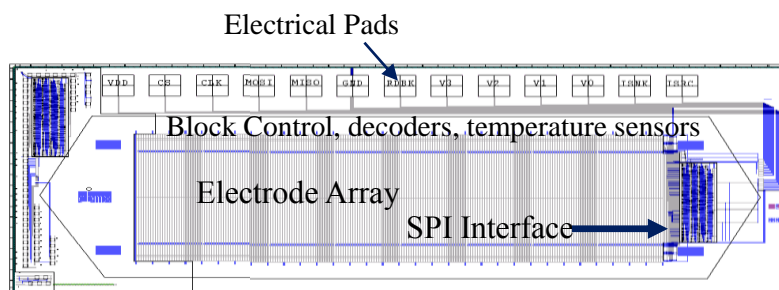


FIGURE 1: Architecture of CBMX chip.

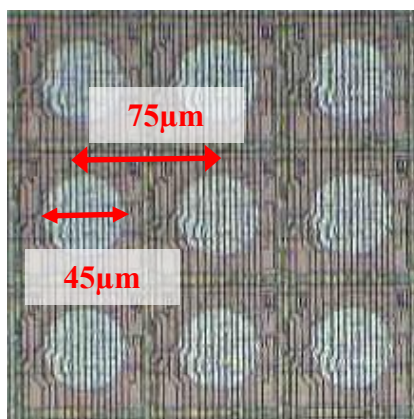


FIGURE 2: Light photomicrograph of a CBMX chip.

At the time this research was being performed, CBMX's main focus was fabricating DNA microarrays on the chip and providing products and services in the areas of drug development, genetic analysis, molecular diagnostics, nanotechnology, and

defense and homeland security markets. Currently, they are a genetics-based Clinical Laboratory Improvement Amendments (CLIA) lab in Irvine, CA. Our collaboration with CBMX was to extend the scope of their technology by developing peptide microarrays fabrication capabilities on their chips.

Electro-generated acid precursor (EGA-P). In CBMX's CMOS based array technology, gating reactions are controlled by applying voltage/current on selected electrodes. Electro-generated acid precursor molecules (EGA-P), under the influence of electric field, undergo oxidation at the anode and release protons, which deprotect the terminal amino group present of the selected electrodes. Specifically, we have tested and optimized two EGA systems in terms of the gating step: (i) N,N'-diphenylhydrazine as EGA-P, and (ii) Hydroquinone as EGA-P.

N,N'-substituted hydrazines can be chemically and electrochemically oxidized to N,N'-substituted diazene⁶¹. Application of N,N'-diphenylhydrazine as EGA-P during the gating reaction on CBMX arrays has been demonstrated earlier by Maurer et al. They used N,N'-diphenylhydrazine as EGA-P to release acid upon electro-oxidation, which then deprotected the Boc group from the terminal amino groups present on the surface. Selection of N,N'-diphenyl hydrazine has a few advantages over various other substituted hydrazines⁶¹. Substitution on Hydrazine can be both aromatic as well as aliphatic. Presence of aromatic substitution can lead to a drop in redox potential compared to unsubstituted or aliphatic substituted hydrazines. This is due to extended conjugation available for radical cation intermediates formed during oxidation. Symmetrical substitution of Hydrazines is important for the gating reaction since the corresponding

diazene, upon formation, does not decompose further into its corresponding hydrocarbon and dinitrogen - a phenomenon observed with unsymmetrical diazenes⁶¹.

Ortho and para aromatic diols can be easily oxidized to respective ketones⁶¹. This chemical transformation finds wide-scale application due to the low redox potential involved ($E^\circ = +286\text{mV}$ at $\text{pH} = 7.0$, 25°C), at which most of the redox side reactions can be avoided. Montgomery et al. has demonstrated successful use of Hydroquinone as EGA-P in the gating reaction of DNA microarray fabrication on CBMX chip⁶²⁻⁶⁴. In this chemical transformation two protons are released at the anode. The acidic environment thus generated deprotects the acid labile protecting groups, such as the trityl group, from the selected electrodes. The EGA-P solution also contains quinone which is reduced at cathode into a radical anion, which acts as a scavenger by absorbing unreacted protons and prevents their diffusion towards the neighboring electrodes.

A wide variety of protecting groups are available in synthetic chemistry to protect the amino group. In peptide chemistry, many of these protecting groups, such as 9-fluorenylmethyloxycarbonyl (Fmoc), allyloxycarbonyl (alloc) etc., have been used. The most common of these protecting groups are base labile, acid labile, catalytically reducible, and organometallic labile groups. Of these, base labile and acid labile groups are the most common. As stated earlier, we have focused on optimizing two EGA systems, N,N' -diphenylhydrazine and Hydroquinone systems, to deprotect the acid labile protecting groups. We also explored strategies to electrochemically deprotect other main classes of protecting groups. These strategies include (i) generating base electrochemically from a probase to deprotect an Fmoc group, (ii) reducing protons to hydrogen on the cathode to catalytically deprotect Carboxybenzyl (Cbz) groups on a

Platinum electrode surface, and (iii) electrochemically generating Pd(0) from Pd(II) on selectively addressed electrodes to deprotect alloc protecting groups. The details of the results of each strategy are discussed in Appendix B.

General Synthesis Scheme. In our research group, a peptide is synthesized on platinum microelectrodes of CMOS based CBMX chip. The platinum electrode is chemically altered with deposition of roughly 50nm thick proprietary organic polymer by CombiMatrix Corp. The organic polymer layer introduces hydroxyl groups to which spacers of different lengths can be coupled. The spacer that makes peptide synthesis possible on the chip is usually a 20-T or 2-T single stranded nucleotide linker with terminal thymidine (T) which is modified to possess an amino group. Another linker, an N-terminal Fmoc group protected photo-labile molecule with a carboxyl group is coupled to the 20-T or 2-T linker through amide bond formation. This linker allows cleavage of the peptides from the solid-support by UV irradiation for synthesis characterization.

The polymer coated CMOS chip displays the spacer with a terminal amino group. Each amino acid involved in the synthesis is Fmoc protected at N-terminus and its side chains are protected with acid-labile protecting groups. The C-terminus is preactivated as OBt ester, which enables direct coupling of the compound. Once a coupling reaction is complete, the unreacted amino groups are capped with acetyl glycine through a standard amide bond formation reaction. The Fmoc protecting group is then cleaved from the terminal amino acid, making new amino groups available for the next coupling cycle. The Fmoc group is deprotected with a base, usually piperidine, leaving the acid-labile side chain protecting groups intact. The coupling cycle is repeated until a gating step

(spatially controlled deprotection of amino protecting groups) is required for generation of the diversity in a peptide sequence. Finally, the peptide is side-chain deprotected with trifluoroacetic acid (TFA).

Our objective with this technique is to produce patterns with high complexity and arbitrary configuration, which should allow for a full combinatorial peptide synthesis on 12K CBMX chips. Therefore, we optimized the gating reaction efficiency by exploring the electrochemical deprotection efficiency of trityl (Trt) and dimethoxytrityl (DMT) groups using two EGA systems and various electrical titration conditions. Several aspects of peptide synthesis such as development of orthogonal synthesis strategy, synthesis automation, and other synthesis and instrumentation issues were solved.

Microarray Synthesis Characterization by MALDI Mass Spectrometry (MALDI-MS). MALDI-MS provides a way to characterize in situ-synthesized peptide microarrays at a molecular level, which is not possible by other means. The deduced masses of the peptides observed in the spectrum can be compared to those calculated for the predicted peptides on the spots of interest of the microarray⁶⁵. The working principle of MALDI-MS involves co-crystallization of the sample with an acidified matrix, which absorbs laser light energy and dissipates the energy to the sample. This rapid transfer of energy vaporizes the matrix. The vaporized sample acquires charge simultaneously from the matrix. A strong electric field between the MALDI plate and the entrance of the time-of-flight (TOF) tube of MALDI-MS instrument energizes the quasimolecular ions to more or less the same extent. Ions with different masses, but similar kinetic energies travel with different velocities in TOF and hit the detector at various points within a timeframe of

microseconds. The resolution $t/\Delta t$, which is proportional to $m/\Delta m$ is better achieved if all the ions at the entrance of the TOF tube are very close in their kinetic energy values.

A significant advantage of MALDI-TOF is that it is relatively easy to perform peptide identification with high-throughput systems. Towards this direction, we have developed a MALDI detection method wherein the peptide probes can be immobilized on the chip via a cleavable linker. After the fabrication of a microarray, the linker can be cleaved under dry conditions to prevent diffusion. A controlled deposition of the matrix solution using aerosol on the microarray chip and limiting the diffusion of analytes can then provide direct characterization of analytes from each spot of the array.

Electrochemical detection of microarrays. Currently, microarray synthesis and assay characterization based on Fluorescence is arguably the most desirable technique. In this technique, the probe molecule present on the chip surface is multiplexed with a target molecule, which is in turn conjugated directly or indirectly to a fluorophore molecule to collect fluorescence signals (Figure 3). Probes with high binding affinity to target molecules endure stringent washing steps, and the corresponding features can be visualized in a fluorescence scanner.

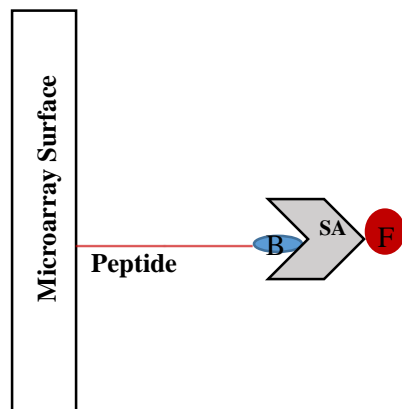


FIGURE 3: Fluorescence detection scheme of peptide microarrays via biotin-fluorophore conjugated streptavidin interaction. 'B' stands for biotin, 'SA' stands for streptavidin, and 'F' stands for fluorophore.

Surface plasmon resonance and Quartz crystal balance approaches are other techniques that are amenable for microarray detection. These are label-free detection methods which also provide information about real-time binding kinetics^{66,67}. CBMX manufactures microarray chips that have CMOS technology based underlying integrated circuitry which makes electrochemical detection possible on the chips. CBMX custom 12K array chips have 12,544 electrodes embedded on them, which can be addressed individually or in groups through the scripting interface of the PotentioSense and Electro-synthesis instrument's software. These custom instruments have been developed by CBMX for reading and fabrication of microarrays. The PotentioSense instrument is used primarily as a microarray reader based on electrochemical technique. It can also be used for fabrication of microarrays, although it would require complicated interfacing with third-party instruments. The instrument is sensitive to picoamps (pA) level current signals and does not have the problem of surface-quenching of signals observed with fluorescence detection on metal surfaces. Detection of pA level steady state currents are achieved in a serial read-out of the array in approximately 60s. There are thirteen electrical pads made of platinum on one side of the active surface area of the chip, which transmits power and electronic signals to the electrodes. The instrument is capable of applying both voltage polarities to the microelectrodes of the chip. Some features

associated with PotentioSense include low instrument cost, portability, and operational convenience.



FIGURE 4: Photograph of a potentiosense instrument. The externalized leads of the instrument provide connection between the microelectrodes of the chip and external instruments.

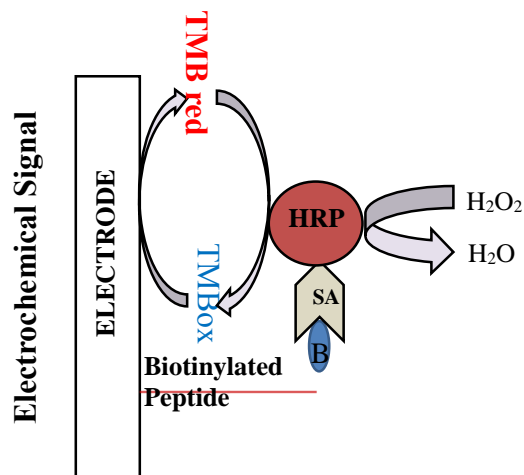


FIGURE 5: Electrochemical detection of peptide microarrays via biotin-horseradishperoxidase (HRP) conjugated streptavidin interaction. Potentiosense can

measure signals generated from the HRP mediated redox cycle of 3,3',5,5'-tetramethylbenzidine (TMB) molecule.

We have explored novel applications of peptide microarrays that are possible using the CBMX platform. Towards this end, capabilities and functioning of the Potentiosense reader was investigated and optimized. Applications such as a search for a catalyst for the anodic half-reaction of water splitting and immobilization of peptides on microelectrodes of CBMX chips by co-electropolymerization of pyrrole and pyrrole modified peptides (peptide-py) were explored.

Note

This work was performed between January 2005 and May 2011. In the past few years peptide microarray fabrication technology has made rapid progress. Some technologies, such as particle-based and photolithography-based peptide synthesis, have overcome many synthesis challenges of peptide microarray fabrication. While documenting this work, the progress made in the field was researched and contents were updated to reflect the current status of the field. The work performed is still relevant, as electrochemically-directed peptide microarray fabrication on the CBMX chip is a unique approach which no other group has yet explored. Several groups, such as Breitling et al. and Price et al., are working towards making their platform electrically active. However, no peptide microarray product on an electrically active platform is currently available in the market. Nimblegen has introduced more efficient photolabile protecting groups by attaching a sensitizer chromophore, such as thioxanthone, to NPPOC groups in their DNA microarray fabrication technology^{68,69}. Yet, a study of efficiency of derivatives of NPPOC group as photolabile protecting group still holds academic relevance.

References

1. W.P. Blackstock, M.P. Weir, Proteomics: quantitative and physical mapping of cellular proteins. *Trends Biotechnol.* **17**, 121–127 (1999).
2. D. Voet, J.G. Voet, *Biochemistry*, Vol **1** 3rd ed., Wiley: Hoboken, NJ (2004).
3. E. Fischer, *Ber. Dt. Chem. Ges.*, **27** (3): 2985–2993 (1894).
4. D.E. Koshland, Application of a theory of enzyme specificity to protein synthesis. *Proc. Natl. Acad. Sci. USA* **44**, 98–104 (1958).
5. R.P. Bahadur, P. Chakrabarti, F. Rodier, J. Janin, A dissection of specific and non-specific protein-protein interfaces. *J. Mol. Biol.* **336**, 943–955 (2004).
6. J.M. Berg, J.L. Tymoczko, L. Stryer, *Biochemistry*. 6th ed. New York: W.H. Freeman (2007).
7. <http://www.britannica.com/EBchecked/topic/450900/peptide>
8. R. Zwanzig, A. Szabo, B. Magchi, Levinthal's paradox. *Proc. Natl. Acad. Sci. USA* **89**, 20–22 (1992).
9. J. Cheng, A. Randall, P. Baldi, *Proteins: Structure, Function, and Bioinformatics* **62**, 1125–1132 (2006).
10. T. Pawson, P. Nash, Assembly of cell regulatory systems through protein interaction domains. *Science* **300**, 445–452 (2003).
11. V. Neduva, R.B. Russell, Peptides mediating interaction networks: new leads at last. *Curr. Opin. Biotechnol.* **17**, 465–471 (2006).
12. E. Petsalaki, R.B. Russell, Peptide-mediated interactions in biological systems: new discoveries and applications. *Curr. Opin. Biotechnol.* **19**, 344–350 (2008).
13. Z. Hayouka, J. Rosenbluh, A. Levin, S. Loya, M. Lebendiker, D. Veprintsev, M. Kotler, A. Hizi, A. Loyter, A. Friedler, Inhibiting HIV-1 integrase by shifting its oligomerization equilibrium. *Proc. Natl. Acad. Sci. USA* **104**, 8316–8321 (2007).
14. L. Parthasarathi, F. Casey, A. Stein, P. Aloy, D.C. Shields, Approved drug mimics of short peptide ligands from protein interaction motifs. *J. Chem. Inf. Model.* **48**, 1943–1948 (2008).

15. L. Zhao, J. Chmielewski, Inhibiting protein-protein interactions using designed molecules. *Curr. Opin. Struct. Biol.* **15**, 31–34 (2005).
16. M. Uttamchandani, S.Q. Yao, Next generation chemical proteomic tools for rapid enzyme profiling. *Acc. Chem. Res.* **42**, 1183-1192 (2009).
17. Y. Shen, B.L. Wu, Microarray-based genomic DNA profiling technologies in clinical molecular diagnostics. *Clin. Chem.* **55**, 659-669 (2009).
18. O. Poetz, J.M. Schwenk, S. Kramer, D. Stoll, M.F. Templin, T.O. Jos, Protein microarrays: catching the proteome. *Mech. Ageing. Dev.* **126**, 161-170 (2005).
19. Y.M. Foong, J. Fu, Q.Y. Shao, M. Uttamchandani, Current advances in peptide and small molecule microarray technologies. *Curr. Opi. Chem. Biol.* **16**, 234-242 (2012).
20. B.B. Haab, Methods and applications of antibody microarrays in cancer research. *Proteomics* **3**, 2116–2122 (2003).
21. <http://ionsource.com/Card/aaTable/aanav.htm>
22. B.R. Merrifield, Solid phase peptide synthesis. I. The synthesis of a tetrapeptide. *J. Am. Chem. Soc.* **85**, 14, 2149-2154 (1963).
23. A. Furka, F. Sebestyen, M. Asgedom, G. Dibo, General method for rapid synthesis of multicomponent peptide mixtures. *Int. J. Peptide Protein Res.* **37**, 487-493 (1991).
24. S. Fodor, J. Read, M. Pirrung, L. Stryer, A. Lu, D. Solas, Light-directed spatially addressable parallel chemical synthesis. *Science* **251**, 767-773 (1991).
25. S. Singh-Gasson, R.D. Green, Y.J. Yue, C. Nelson, F. Blattner, M.R. Sussman, F. Cerrina, Maskless fabrication of light-directed oligonucleotide microarrays using a digital micromirror array. *Nature Biotechnology* **17**, 974-978 (1999).
26. V. Stadler, T. Felgenhauer, M. Beyer, S. Fernandez, K. Leibe, S. Güttler, M. Gröning, K. König, G. Torralba, M. Hausmann, V. Lindenstruth, A. Nesterov, I. Block, R. Pipkorn, A. Poustka, F.R. Bischoff, F. Breitling, Combinatorial synthesis of peptide arrays with a laser printer. *Angew. Chem. Int. Ed.* **47**, 37:7132-7135 (2008).
27. Aldrich, S., In Scheme for Solid phase Peptide Synthesis.
<http://www.sigmaaldrich.com/etc/medialib/brands/sigma/solid-phase-syn-schem.Par.0001.Image.500.gif>.

28. Stadler, V., et al., Combinatorial synthesis of peptide arrays with a laser printer. *Angewandte Chemie International Edition* **47**, 37: 7132-7135 (2008).
29. J.V. Price, S. Tangsombatvisit, G. Xu, J. Yu, D. Levy, E.C. Baechler, O. Gozani, M. Varma, P.J. Utz, C.L. Liu, On silico peptide microarrays for high-resolution mapping of antibody epitopes and diverse protein-protein interactions. *Nature Medicine* **18**, 1434-1441 (2012).
30. C. Agbavwe1, C. Kim, D. Hong, K. Heinrich, T. Wang, M.M. Somoza, Efficiency, error, and yield in light-directed maskless synthesis of DNA microarrays. *Journal of Nanobiotechnology* **9**, 57 (2011).
31. D. Montgomery, U.S. Patent 6, 280, 595 (2001).
32. R.W. Roberts, Totally In vitro protein selection using mRNA-protein fusions and ribosome display. *Curr. Opin. Chem. Biol.* **3**, 268–273 (1999).
33. S.E. Cwirla, E.A. Peters, R.W. Barrett, W.J. Dower, Peptides on phage: a vast library of peptides for identifying ligands. *Proc. Natl. Acad. Sci. USA* **87**, 6378–6382 (1990).
34. A. Furka, In G. Jung (Ed.), A handbook, VCH, New York, 111–138 (1996).
35. <http://www.pepperprint.com/products/pepperchip-custom-microarrays/>
36. X.Y. Xiao, R. Li, H. Zhuang, B. Ewing, K. Karunaratne, J. Lillig, R. Brown K.C. Nicolaou, Solid-phase combinatorial synthesis using MicroKan reactors, Rf tagging, and directed sorting. *Biotechnol Bioeng.* **71**, 44–50 (2000).
37. C.M. Salisbury, D.J. Maly, J.A. Ellman, Peptide microarrays for the determination of protease substrate specificity. *J. Am. Chem. Soc.* **124**, 14868–14870 (2002).
38. R. Frank, The SPOT-synthesis technique. Synthetic peptide arrays on membrane supports – principles and applications. *J. Immunol. Methods* **267**, 13–26 (2002).
39. K. Komolpis, O. Srivannavit, E. Gulari, Light-directed simultaneous synthesis of oligopeptides on microarray substrate using a photogenerated acid. *Biotechnol. Prog.* **18**, 641–646 (2002).
40. K. Bialek, A. Swistowski, R. Frank, Anal. Bioanal. Chem.[Epub ahead of print] PMID: 12677339 (2003).

41. J.P. Pellois, W. Wang, X. Gao, Peptide synthesis based on t-boc chemistry and solution photogenerated acids. *J. Comb. Chem.* **2**, 355–360 (2000).
42. J.V. Price, S. Tangsombatvisit, G. Xu, J. Yu, D. Levy, E.C. Baechler, O. Gozani, M. Varma, P.J. Utz, C.L. Liu, *On silico* peptide microarrays for high resolution mapping of antibody epitopes and diverse protein-protein interactions. *Nature Medicine* **18**, 1434-1441 (2012).
43. V. Stadler et al., Combinatorial synthesis of peptide arrays with a laser printer. *Angewandte Chemie International Edition* **47**, 7132-7135 (2008).
44. S. Fodor, J. Read, M. Pirrung, L. Stryer, A. Lu, D. Solas, Light-directed, spatially addressable parallel chemical synthesis. *Science* **251**, 767-773 (1991).
45. S. Fodor, J. Read, M. Pirrung, L. Stryer, A. Lu, D. Solas, Light-directed, spatially addressable parallel chemical synthesis. *Science* **251**, 767-773 (1991).
46. R.J. Lipshutz, S.P.A. Fodor, T.R. Gingeras, High density synthetic oligonucleotide arrays. *Nature Genetics Supplements* **21**, 20-24 (1999).
47. G.H. McGall, A.D. Barone, M. Diggelmann, The efficiency of light-directed synthesis of DNA arrays on glass substrates. *Journal of the American Chemical Society* **119**, 5081- 5090 (1997).
48. T.J. Albert, J. Norton, M. Ott, T. Richmond, K. Nuwaysir, F. Emile, K.P. Stengele, R.D. Green, Light-directed synthesis of complex oligonucleotide microarrays. *Nucl. Acids Res.* **31**, e35 (2003).
49. A. Patchornik, B. Amit, R.B. Woodward, Photosensitive protecting groups. *Journal of the American Chemical Society* **92**, 6333-6335 (1970).
50. V.N.R. Pillai, Photoremovable protecting groups in organic synthesis. *Synthesis* **1**, 1-26 (1980).
51. C.P. Holmes, D.W. Solas, B. Kiangsoontra, WO 9410128, P.I. Appl., Editor. 1994.
52. M. Beier, J.D. Hoheisel, Production by quantitative photolithographic synthesis of individually quality checked DNA microarrays. *Nucleic Acid Research* **28**, e11 (2000).
53. C.G. Bochet, Wavelength-selective cleavage of photolabile protecting groups. *Tetrahedron Letters* **41**, 6341 (2000).

54. K.R. Bhushan, D. Charles, R.A. Laursen, Synthesis of photolabile 2-(2-nitrophenyl)propyloxycarbonyl protected amino acids. *Tetrahedron Letters* **44**, 8585-8588 (2003).
55. K. Maurer, A. McShea, M. Strathmann, K. Dill, The removal of the t-boc group by electrochemically generated acid and use of an addressable electrode array for peptide synthesis. *J. Combi. Chem.* **7**, 637-640 (2005).
56. K. Dill, D. Montgomery, W. Wang, J.C. Tsai, Antigen detection using microelectrode array microchips. *Anal. Chim. Acta* **444**, 69 (2001).
57. Montgomery, D. U.S. Patent 6,093,302, 2000.
58. Montgomery, D. U.S. Patent 6,280, 595, 2001.
59. www.customarrayinc.com
60. M. Baker, Microarrays, megasynthesis. *Nature Methods* **8**, 457-460 (2011).
61. J. March, M.B. Smith, Advanced Organic Chemistry (5th edition), John Wiley & Sons, Inc. (2005).
62. K. Maurer, J. Cooper, M. Strathmann, A. Gindilis, United States Patent Application Publication 2006/0102471 (2006).
63. R.D. Egeland, E.M. Southern, Electrochemically directed synthesis of oligonucleotides for DNA microarray fabrication. *Nucleic Acids Res.* **33**, e125 (2005).
64. K. Maurer, J. Cooper, M. Caraballo, J. Crye, D. Suciu, A. Ghindilis, J.A. Leonetti, W. Wang, W.M. Rossi, A.G. Stover, C. Larson, H. Gao, K. Dill, A. McShea, Electrochemically generated acid and its containment to 100 micron reaction areas for the production of DNA microarrays. *PLoS One* **1**, e34 (2006).
65. P. Kumar, M.P. Greving, Z.G. Zhao, N.W. Woodbury, Feature-level MALDI-MS characterization of in situ-synthesized peptide microarrays. *Langmuir* **26**, 1456-1459 (2010).
66. Y. Li, J. Xiang, F. Zhou, Sensitive and label-free detection of DNA by surface plasmon resonance. *Plasmonics* **2**, 79-87 (2007).
67. B. Becker, M. A. Cooper, A survey of the 2006-2009 quartz crystal microbalance biosensor literature. *Journal of Molecular Recognition.* **24**, 754-787 (2011).

68. D. Woll, J. Smirnova, M. Galetskaya, T. Prykota, J. Bühler, K.P. Stengele, W. Pfleiderer, U.E. Steiner, Intramolecular sensitization of photocleavage of the photolabile NPPOC protecting group: photoproducts and photokinetics of the release of nucleosides. *Chem. Eur. J.* **14**, 6490-6497 (2008).
69. D. Woll, W. Dominik, J. Smirnova, W. Pfleiderer, U.E. Steiner, Highly efficient photolabile protecting groups with intramolecular energy transfer. *Angew. Chem. Int. Ed.* **45**, 2975-2978 (2006).

Chapter 2

Investigation of the 2-(2-nitrophenyl)propoxycarbonyl Protecting Group

Substituent-Effect on the Rate of Photolysis and Yield of Amine

Abstract

The protecting group 2-(2-nitrophenyl)propoxycarbonyl (NPPOC) has been used as a β -linked *o*-nitrobenzyl protecting group for in situ nucleotide array preparation. It was demonstrated that NPPOC can be used as an efficient photo-labile amino protecting group. Mechanistic studies have revealed that the photo-cleavage process of this group involves the formation of less reactive intermediates than those formed during the photocleavage of NVOC and MeNPOC groups leading to suppression of side products and increase in yield of free amines. In this chapter, we have investigated the influence of substituents on the rate of photolysis and the yield of the amine. The results indicate that substituents capable of forming a π -network with the nitro group enhanced the rate of photolysis and yield. Once such properly substituted NPPOC groups were used, the rate of photolysis/yield depended on the nature of protected amino group (aromatic amines were found to be more efficient than aliphatic amines). This indicated a different chemical step during photocleavage process, and became the rate limiting step. The deprotection from a primary amine group is faster than deprotection from a secondary amine group. Similarly, deprotection from an amine group bonded to an electron donating group is faster than deprotection from an amine group bonded to an electron withdrawing group.

Introduction

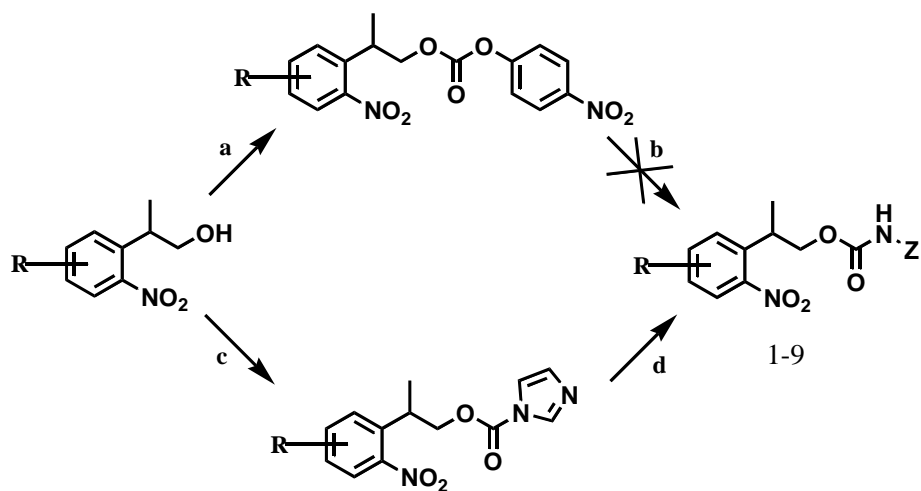
Since their first report by Barltrop and Schofield¹, photo-labile protective groups have been utilized in a wide range of applications. One the most commonly used groups, 6-nitroveratroyloxycarbonyl (NVOC), was originally introduced by Patchornik, Amit, and Woodward². The mechanistic studies on the NVOC photo-cleavage process revealed formation of a Norrish-type II diradical species³ - a characteristic of all *o*-nitrobenzylalcohols⁴. Despite its popularity photo-cleavage of NVOC protected amines can result in poor yields due to the formation of the nitrosobenzaldehyde, a chemically labile product, which further reacts with the deprotected amine to form diazo or/and imine-type products^{5,6}. Thus, presence of additives and scavengers is often required for improvement in the yield⁷. However, the photo-cleavage studies of α -methyl-*o*-nitropiperonyloxycarbonyl (MeNPOC) by Holmes et al.⁸ did reveal some improvements due to presence of electron-donating methyl group. However, the mechanism of photocleavage is similar to that of NVOC groups and therefore, several side-products are formed during photolytic cleavage.

Various groups have utilized 2-(2-nitrophenyl)propyloxycarbonyl (NPPOC) and its thioxanthone derivative for nucleotide protection and reported improved cleavage yields⁹⁻¹². The improved yield was attributed to the NPPOC group having a different photo-cleavage mechanism, which resulted in formation of a less reactive end-product, as was demonstrated by Hasan et al.¹³ Finally, the utility of NPPOC for photolithography-based peptide synthesis was demonstrated by Bhushan et al.¹⁴ where relative half-lives of protected amino acids and deprotection yields were studied. The higher yields of photo-

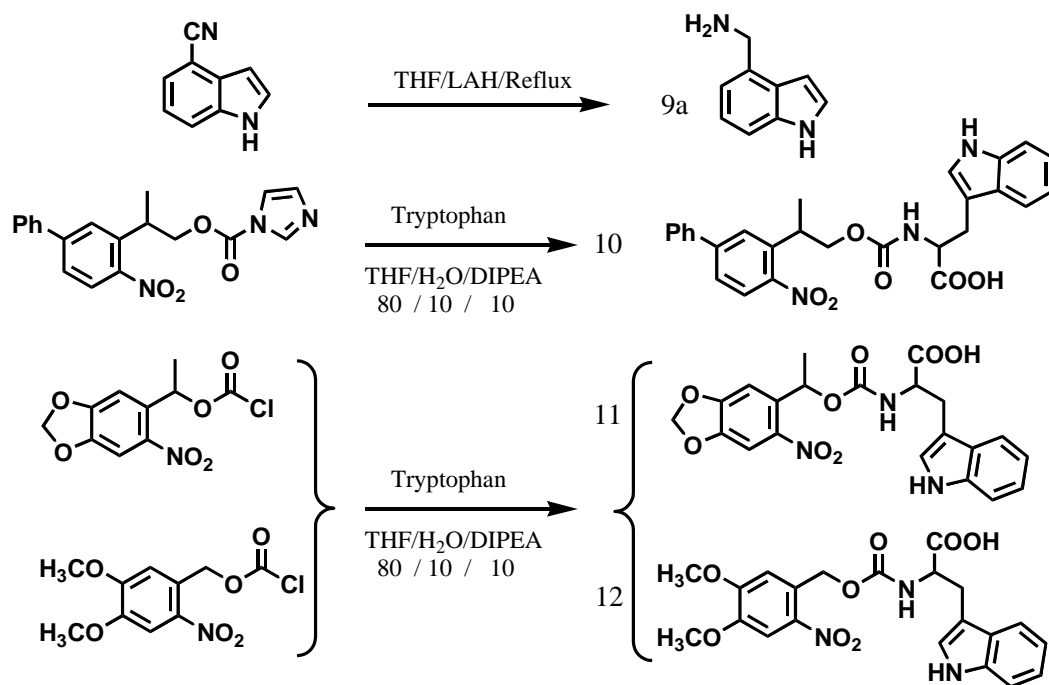
cleavage yield using NPPOC protected amines has inspired us to investigate the influence of the substituent on the photo-cleavage rates, half-lives, and yields of various NPPOC protected amines. Here, we report synthesis and photolysis studies of various NPPOC-based carbamate analogues.

Results and Discussion

This study included the unsubstituted and six differently substituted NPPOC analogues combined with three different amines, *N*-benzylamine, 4-aminoindole, and 4-(aminomethyl)-indole. For comparison of efficiency of NVOC, MeNPOC, and NPPOC as a photolabile protecting group, tryptophan protected with NVOC, MeNPOC, and NPPOC were prepared and studied. Starting from the alcohol forms of the NPPOC analogues, two general synthetic strategies were considered for preparation of the corresponding carbamates. The first method involved the formation of carbonate analogues by reacting NPPOC alcohols with 4-nitrophenylchloroformate (Scheme 1). However, it was found that formation of the carbamate was not feasible due to high stability of the carbonate bond. Despite multiple attempts using various conditions, this route did not result in appreciable product. Alternatively, alkyloxycarbonylimidazole NPPOC analogues were prepared by reacting NPPOC alcohols with 1,1'-carbonyldiimidazole (CDI) and subsequent reaction with various amines, affording the carbamate products **1-9** (Scheme 1). The carbamate **10** was prepared from the reaction between (L)-tryptophan and the NPPOC-imidazole while carbamates **11** and **12** were generated from (L)-tryptophan and MeNPOC/NVOC-chloroformate (Scheme 1).



(a) 4-Nitrophenylchloroformate, DIPEA, DCM; (b) Amine, DMF, DIPEA;
 (c) 1,1'-Carbonyldimidazole, THF; (d) Amine, THF, DIPEA.



SCHEME 1: General synthetic schemes for compounds 1-12. Top: General synthesis of various NPPOC carbamates. Reaction 'b' did not occur, as p-nitro phenoxy group proved

to be a poor leaving group. Bottom: Reduction of cyanoindole and preparation of NPPOC, MeNPOC, and NVOC protected tryptophan.

The rates of photolysis were determined using UV/Vis spectroscopy with results summarized in Table 1. The rate constants varied from 0.756 to 0.009 min⁻¹ corresponding to half-lives ranging from 0.917 to 77.0 minutes. The comparison among analogues **1-7** indicated that the rate of photolysis was improved when an aromatic substituent was present at the 5th position of the ring (**4, 7**). Between these, the rate constant was greater for the carbamate bearing the electron rich 3,4-dimethoxyphenyl substituent (**7**) as compared to the phenyl group (**4**). In comparison, the rate of cleavage was significantly decreased for the di-substituted NPPOC (**5**) bearing both an alkyl and an aromatic group. The presence of bromine on the ring adversely affected the photolysis rate (**2**) as compared to the aromatic or unsubstituted NPPOCs. The combination of bromo and ethyl groups (**3**) further decreased the rate of photolysis. Finally, the phenylketone substituent (**6**) did not drastically change the rate of photolysis and indicated a half-life similar to that of the unsubstituted NPPOC analogue.

The comparison among carbamates **4, 8, 9, and 10** indicated that the nature of the protected amine significantly influenced the rate of cleavage. This resulted in half-lives ranging from 0.917 to 5.55 minutes. The rate was especially accelerated when the protected amine was aromatic (**8**). The comparison between NPPOC, MeNPOC, and NVOC protected tryptophan (**10, 11, and 12**) revealed that the NPPOC did exhibit a faster cleavage rate. In fact, the rate constant associated with photo-deprotection of NPPOC-Tryptophan was twice as fast as MeNPOC which was still faster than NVOC.

The yield of the complete deprotection of amine was quantitatively determined using HPLC analysis with the 3,4-dimethoxyphenyl substituted NPPOC, displaying the highest yield of 88.7%. The patterns of substitution among carbamates **1-7** indicated that the brominated analogue (**2**) displayed lower yields as compared to the unsubstituted NPPOC (**1**). The presence of the additional ethyl group on the ring (**3**) decreased the yield even more. Furthermore, the electron withdrawing phenylketone (**6**) also indicated a drastic decrease in the yield of the free amine, while the phenyl analogue (**4**) resulted in only 14% reduction as compared to the parent molecule. The comparison between carbamates **4, 8, 9, 10** revealed that the yield associated with the aromatic amine was slightly higher than those of benzylic/aliphatic amines. Finally, evaluation of the three different classes of protective groups indicated that NPPOC-protected tryptophan demonstrated 13% higher cleavage yield compared to the MeNPOC-protected tryptophan. The MeNPOC-protected tryptophan cleavage yield was 10% higher than that of the NVOC-protected amine.

The photo-cleavage of NPPOC, MeNPOC, and NVOC-protected amines all demonstrated first order kinetics as seen from half-life values of photolysis. The half-lives decreased from NVOC to MeNPOC (as reported in literature) to NPPOC. Among the substituents, the half-life values decreased when electron-donating groups were substituted, compared to NPPOC groups. The half-life values increased when electron-withdrawing groups were substituted. The numerical values of half-lives can be seen in Table 1. In general, the substitution patterns of the NPPOC ring indicated that presence of a π -network *para* to the nitro group enhanced the rate of cleavage, while halogens/non-

aromatic substituents adversely affected this process. It appears that conjugation to the nitro group provides extra delocalization for the Norrish-type II radical. This is seen in the mechanism discussed by Patchomik, Amit, and Woodward, making formation of the di-radical species more favorable resulting in an increased rate constant^{13,16}. Consistent with this concept, the larger rate constant associated with carbamate **6**, compared with **2**, can be attributed to the additional delocalization provided by the carbonyl group. In contrast, the influence of ethyl substituent on the rate constant is less clear. Perhaps the presence of an ethyl substitution in the ring makes the phenyl ring twist away from coplanar conformation, a steric constraint in **5**, and changes the electronic conjugation of the ring in **3**, resulting in a drastic rate decrease. In other words, an ethyl group as a substituent distorts the coplanarity and hence the molecule is no longer as aromatic, leading to a decrease in photolysis rate and percent yield. Such distortion is not usually seen with Br or phenyl groups. From the work performed, it seems with respect to carbamates 1-7, formation of the diradical species is the key step in determining the rate of the reaction. However, we have observed that rate constants associated with molecules **4**, **8**, **9**, and **10**, all of which have the same substituent, also depend on the elimination of the CO₂ step as carbamate **8** displayed a significantly faster cleavage process. Perhaps, all the transformations during photodeprotection takes place in a concerted manner and therefore the nature of the protected amine also plays a role in determining the photolysis rate. The photodeprotection mechanism of NPPOC and NVOC groups can be seen in Figure 1 & 2.

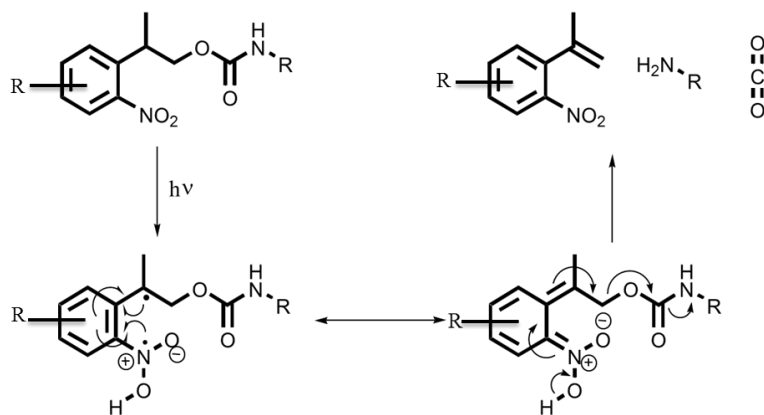


FIGURE 1: Photoprotection mechanism of NPPOC analogues.

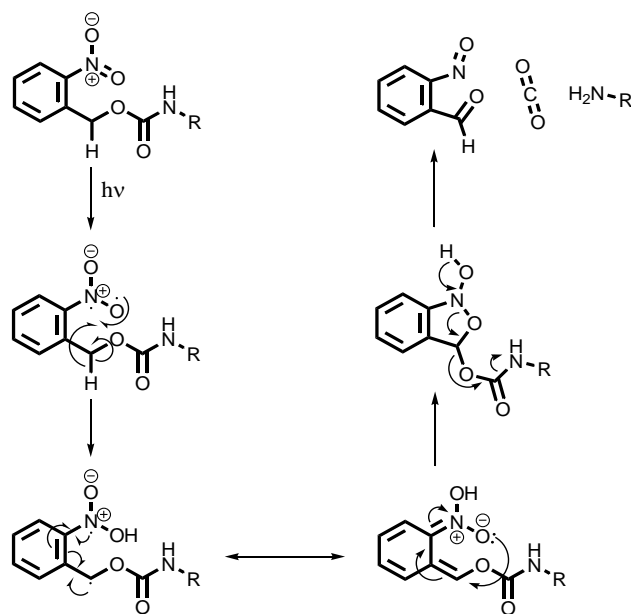


FIGURE 2: Photoprotection mechanism of NVOC group.

Thus, it appears that nature of the substituent greatly influences the formation of the Norrish-type II di-radical. However, having the right substituent, this process occurs fast enough that elimination of the CO_2 becomes the slow step in the overall process.

TABLE 1: Photolysis rate constants, half-lives, and the yields of amine

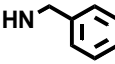
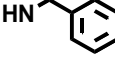
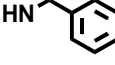
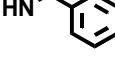
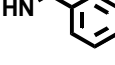
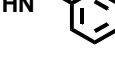
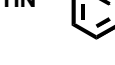
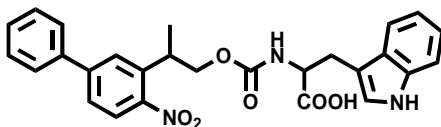
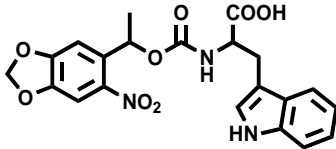
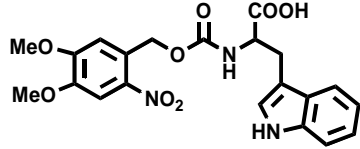
Entry	R ₁	R ₂	R ₃	k(min ⁻¹)	t/2(min)	Yield of Amine
1	H	H		0.108	6.42	86.7%
2	Br	H		0.088	7.88	59.3%
3	Br	Ethyl		0.009	77.0	25.1%
4	Phenyl	H		0.185	3.75	74.0%
5	Phenyl	Ethyl		0.011	63.0	48.1%
6	Phenylketone	H		0.103	6.72	31.0%
7	3,4-Dimethoxy phenyl	H		0.192	3.61	88.7%
8	Phenyl	H	4-Aminoindole	0.756	0.917	81.0%
9	Phenyl	H	4-(Aminomethyl)-indole	0.274	2.53	76.3%
10				0.125	5.55	78.6%
11				0.058	11.9	68.2%
12				0.041	16.9	61.0%

TABLE 1: All photolysis, UV/Vis, and HPLC analysis were carried out in 0.80M HCl in CH₃CN solution. Initial rates were taken at 280-300 nm. Half-lives were determined from rate constants, and yields were measured by calculating the area under each HPLC peak.

With respect to measured yields, there appears to be a correlation between the rate of the reaction and the yield of the amine (Table 1). Rates and yields were found to improve in tandem, with different substituents, with the exception of carbamate **6**. It is believed that low yield, in this case, is due to the formation of an imine-type side-product (molecules 1-7), as deprotected amine reacts with the carbonyl of the phenylketone. Nevertheless, none of the protective groups could be removed quantitatively (> 95%). Thus, it appears that some side reactions may have taken place during the cleavage process. This is easily explained with regard to MeNPOC and NVOC, where formation of a reactive side product has been documented by McGall⁶, resulting in depletion of the deprotected amine. However, the data also indicates that NPPOC photo-cleavage results in one or more side-reactions, resulting in a lower yield of the amine. Therefore, the addition of nucleophilic scavengers may also be necessary in the NPPOC photo-cleavage process. Finally, the comparison between carbamates **10**, **11**, and **12** further corroborated the fact that functional group protection via the β -position of *o*-nitrobenzyl group would result in a faster, cleaner, and more efficient photo-cleavage process as demonstrated for nucleotides by Hasan et al.¹³

Materials and Methods

The NPPOC analogues were obtained as alcohols from NimbleGen system Inc. and all reagents were purchased from Sigma-Aldrich. Light-sensitive reactions were carried out in the presence of red light only, and kept at 4.0 °C in a dark environment. Irradiations were carried out in the dark for 30 sec, 1.0 min, and every 30 sec after, up to 10 min. The UV/Vis spectroscopy was performed using a Cary 50 Bio Varian Spectrometer. HPLC data was obtained using Agilent 1100 series instrument, NMR spectra were recorded with a 300 MHz instrument, and elemental analyses were performed in the Gold Water Center at Arizona State University.

General Procedure for Photo-cleavage, UV/Vis Spectroscopy and HPLC analysis

Experiments were carried out in a 2.00 mL-quartz cuvette with a total reaction volume of 1.00 mL. For each set of experiments a background spectrum of the solvent was first recorded [988 μ L of stock solution containing CH₃CN/HCl (0.800M HCl)], followed by 2.00 μ L addition of each NPPOC (5.00 mM stock solution in CH₃CN). The cuvette was then irradiated at 375-400 nm using a 2mW/cm² UV-lamp while recording a scanning kinetics of the photolysis at 220-370 nm for 12 minutes. The initial rates at 280-300 nm were then fitted to a first order rate law and the rate constants were obtained. For the HPLC analysis, a 10 mM solution of each carbamate in CH₃CN/HCl (0.800M HCl) was prepared. The solution was then divided into 6 reaction samples (1.0 mL each) and samples 1-6 were irradiated from 0, 1, 2, 4, 8, and 16 minutes respectively using a 2 mW/cm² UV-lamp. All the groups were deprotected at various time points from 0 to 16 minutes irradiation as seen from HPLC. Each sample was then analyzed with the HPLC

and the areas corresponding to the initial carbamate and final amine were calculated. The overall quantitative yield of the amine was obtained by dividing the area of the amine by the area of the initial carbamate.

Synthesis Procedures

General synthesis of carbamates via 1,1'-carbonyldiimidazole. A solution of 1,1'-carbonyldiimidazole (1.3 molar excess) dissolved in a minimum amount of anhydrous THF was added to a solution of NPPOC-alcohol in anhydrous THF under a nitrogen atmosphere. The resulting solution was then warmed up to 45 °C and stirred at this temperature for 4.0 hours. After completion, (indicated by TLC) the solution was poured over neutral water and the product was extracted with chloroform. The extract was washed a few times with water, the organic layer was dried over sodium sulfate, and the solvent was removed under reduced pressure. The resulting product was then dissolved in anhydrous THF under a nitrogen atmosphere and DIPEA was added (10 molar excess). The desired amine was then added to this solution (1.0-5.0 molar excess depending on the nature of amine), the resulting mixture was warmed up to 80 °C, and stirred at this temperature for 12 hours. The product was then extracted out of 2.0N HCl solution with chloroform and the extract was washed multiple times with 2.0N HCl, then water. The organic layer was dried over sodium sulfate and removed under reduced pressure. Product was purified with silica gel chromatography using DCM/Ethanol 98:2 as the eluant, resulting in the oily desired carbamate.

General synthesis of carbonate derivatives. A solution of 4-nitrophenyl chloroformate dissolved in a minimum amount of pyridine was added to a solution of

NPPOC-alcohol in anhydrous pyridine under nitrogen atmosphere. The resulting mixture was brought to reflux and stirred overnight. After the reaction completed (TLC), the product was extracted out of 2.0N HCl with DCM. The organic layer was washed multiple times with 2.0N HCl solution, dried over sodium sulfate, and removed under reduced pressure resulting in the oily carbonate product.

General Synthesis of Phenyl-NPPOC, MeNPOC, and NVOC Tryptophan. A solution of tryptophan (2.0 mM) dissolved in 28 mL CH₃CN, 4 mL H₂O, 4 mL DIPEA in an ice bath was added to phenyl-NPPOC-imidazole/MeNPOC-chloroformate/NVOC-chloroformate (1.0mM) dissolved in 4 mL CH₃CN. The resulting mixture was kept in the ice bath and stirred for 4.0 h. The solution was concentrated under reduced pressure and the product was extracted with ethyl acetate out of 2.0N HCl solution. The organic layer was dried over sodium sulfate and removed under reduced pressure. The product was recrystallized from hexanes.

4-(Aminomethyl)-indole (9a). 4-cyanoindole (0.40g, 2.8mmol) dissolved in minimum amount of THF was added drop-wise to a solution of LAH (0.50g, 13mmol) in anhydrous THF under a nitrogen atmosphere. The resulting solution was refluxed for 4.0 hours. The reaction was then cooled down in an ice bath and very carefully a drop of water was added every 1-2 minutes until no more hydrogen gas evolved. The solution was then filtered and the precipitate was washed with THF. The organic solution was then dried over sodium sulfate and removed under reduced pressure. Product was recrystallized from hexanes resulting in **9a**. **Yield:** 83%; **TLC:** 0.12 (DCM/Ethanol 96:4); **IR:** 3347, 2987, 2899, 1575, 1423, 1346, 1053 cm⁻¹; **¹H NMR** [DMF] δ 11.2 (1H, broad,

indole proton); δ 7.44 (1H, t, $J = 3.0$ Hz, aromatic proton); δ 7.40 (1H, m, $J = 2.1$ Hz, aromatic proton); δ 7.12 (2H, m, aromatic protons); δ 6.64 (1H, m, aromatic proton); δ 4.12 (2H, s, methylene protons); δ 3.14 (2H, broad, amine protons). Anal. ($C_9H_{10}N_2$): C, 73.94; H, 6.890; N, 19.16. Found: C, 74.38; H, 7.044; N, 19.18.

2-(2-Nitrophenyl)-propyl *N*-Benzyl Carbamate (1). Yield: 82%; TLC: 0.64 (DCM/Ethanol 96:4); IR: 3329, 3056, 2925, 1703, 1511, 1446, 1343, 1229 cm^{-1} ; 1H NMR [$CDCl_3$] δ 7.72 (1H, dd, $J = 1.8$ Hz, $J = 7.5$ Hz, aromatic proton); δ 7.55 (1H, m, aromatic proton); δ 7.47 (1H, m, aromatic proton); δ 7.37 (1H, d, $J = 8.4$ Hz, aromatic proton); δ 7.27 (5H, m, aromatic protons); δ 4.92 (1H, broad, carbamate proton); δ 4.31 (2H, d, $J = 6.0$ Hz, methylene protons); δ 4.18 (2H, d, $J = 8.1$ Hz, methylene protons); δ 3.75 (1H, m, $J = 7.2$ Hz, methine proton); δ 1.35 (3H, d, $J = 7.2$ Hz, methyl protons). Anal. ($C_{17}H_{18}N_2O_4$): C, 64.96; H, 5.770; N, 8.910. Found: C, 64.13; H, 5.580; N, 8.510.

2-(5-Bromo-2-nitro-phenyl)-propyl *N*-Benzyl Carbamate (2). Yield: 89%; TLC: 0.63 (DCM/Ethanol 96:4); IR: 3434, 3047, 2925, 1715, 1556, 1519, 1453, 1262, 1225 cm^{-1} ; 1H NMR [$CDCl_3$] δ 7.53 (1H, d, $J = 9.0$ Hz, aromatic proton); δ 7.49 (1H, d, $J = 1.5$ Hz, aromatic proton); δ 7.40 (1H, dd, $J = 1.8$ Hz, $J = 6.6$ Hz, aromatic proton); δ 7.18 (5H, m, aromatic protons); (1H, broad, carbamate proton); δ 4.23 (2H, d, $J = 5.4$ Hz, methylene protons); δ 4.19 (2H, d, $J = 6.0$ Hz, methylene protons); δ 3.66 (1H, m, $J = 7.2$ Hz, methine proton); δ 1.26 (3H, d, $J = 7.2$ Hz, methyl protons). Anal. ($C_{17}H_{17}BrN_2O_4$): C, 51.92; H, 4.360; N, 7.120. Found: C, 52.34; H, 4.490; N, 6.850.

2-(5-Bromo-4-ethyl-2-nitro-phenyl)-propyl *N*-Benzyl Carbamate (3). Yield: 85%; TLC: 0.68 (DCM/Ethanol 96:4); IR: 3419, 3321, 2970, 2929, 1703, 1515, 1450,

1352, 1225 cm^{-1} ; $^1\text{H NMR}$ [CDCl_3] δ 7.51 (1H, s, aromatic proton); δ 7.50 (1H, s, aromatic proton); δ 7.18 (5H, m, aromatic protons); δ 4.85 (1H, broad, carbamate proton); δ 4.22 (2H, d, $J = 3.3$ Hz, methylene protons); δ 4.17 (1H, m, methine proton); δ 4.00 (1H, m, methylene proton); δ 3.61 (1H, m, methylene proton); δ 2.68 (2H, q, $J = 7.8$ Hz, methylene protons); δ 1.82 (6H, m, methyl protons). Anal. ($\text{C}_{19}\text{H}_{21}\text{BrN}_2\text{O}_4$): C, 54.17; H, 5.020; N, 6.650. Found: C, 54.15; H, 5.030; N, 6.100.

2-(5-Phenyl-2-nitro-phenyl)-propyl *N*-Benzyl Carbamate (4). Yield: 85%; **TLC:** 0.70 (DCM/Ethanol 96:4); **IR:** 3333, 2917, 1707, 1523, 1453, 1356, 1258 cm^{-1} ; $^1\text{H NMR}$ [CDCl_3] δ 7.75 (1H, d, $J = 8.4$ Hz, aromatic proton); δ 7.54 (1H, d, $J = 2.1$ Hz, aromatic proton); δ 7.46 (6H, m, aromatic protons); δ 7.16 (5H, m, aromatic protons); δ 4.85 (1H, broad, carbamate proton); δ 4.22 (4H, m, methylene protons); δ 3.75 (1H, m, methine proton); δ 1.31 (3H, d, $J = 6.6$ Hz, methyl protons). Anal. ($\text{C}_{23}\text{H}_{22}\text{N}_2\text{O}_4$): C, 70.75; H, 5.680; N, 7.170. Found: C, 70.66; H, 5.830; N, 7.190.

2-(5-Phenyl-4-ethyl-2-nitro-phenyl)-propyl *N*-Benzyl Carbamate (5). Yield: 82%; **TLC:** 0.72 (DCM/Ethanol 96:4); **IR:** 3329, 3000, 2917, 1719, 1515, 1348, 1258 cm^{-1} ; $^1\text{H NMR}$ [CDCl_3] δ 7.62 (1H, s, aromatic proton); δ 7.34 (5H, m, aromatic protons); δ 7.20 (6H, m, aromatic protons); δ 4.95 (1H, broad, carbamate proton); δ 4.21 (4H, m, methylene protons); δ 3.65 (1H, m, methine proton); δ 2.55 (2H, q, $J = 7.2$ Hz, methylene protons); δ 1.26 (3H, d, $J = 6.0$ Hz, methyl protons); δ 1.02 (3H, t, $J = 1.2$ Hz, methyl protons). Anal. ($\text{C}_{25}\text{H}_{26}\text{N}_2\text{O}_4$): C, 71.75; H, 6.260; N, 6.690. Found: C, 71.30; H, 6.950; N, 6.080.

2-(5-Phenylketone-2-nitro-phenyl)-propyl N-Benzyl Carbamate (6). Yield: 87%; **TLC:** 0.63 (DCM/Ethanol 96:4); **IR:** 3332, 3058, 2968, 1709, 1659, 1522, 1448, 1255 cm^{-1} ; **$^1\text{H NMR}$** [CDCl_3] δ 7.79 (1H, d, $J = 1.8$ Hz, aromatic proton); δ 7.67 (4H, m, aromatic protons); δ 7.51 (1H, m, aromatic proton); δ 7.40 (2H, m, aromatic protons); δ 7.16 (5H, m, aromatic protons); δ 4.91 (1H, broad, carbamate proton); δ 4.22 (2H, d, $J = 4.8$ Hz, methylene protons); δ 4.08 (2H, m, methylene protons); δ 3.66 (1H, m, $J = 6.6$ Hz, methine proton); δ 1.29 (3H, d, $J = 6.6$ Hz, methyl protons). Anal. ($\text{C}_{24}\text{H}_{22}\text{N}_2\text{O}_5$): C, 68.89; H, 5.300; N, 6.690. Found: C, 68.76; H, 5.270; N, 6.430.

2-[5-(3,4-Dimethoxyphenyl)-2-nitro-phenyl]-propyl N-Benzyl Carbamate (7). Yield: 84%; **TLC:** 0.70 (DCM/Ethanol 96:4); **IR:** 3434, 3052, 2958, 1715, 1601, 1515, 1462, 1343, 1245 cm^{-1} ; **$^1\text{H NMR}$** [CDCl_3] δ 7.74 (1H, d, $J = 8.7$ Hz, aromatic proton); δ 7.51 (1H, d, $J = 1.8$ Hz, aromatic proton); δ 7.42 (1H, dd, $J = 1.8$ Hz, $J = 8.7$ Hz, aromatic proton); δ 7.11 (5H, m, aromatic protons); δ 7.04 (1H, d, $J = 1.5$ Hz, aromatic proton); δ 7.00 (1H, d, $J = 1.5$ Hz, aromatic proton); δ 6.87 (1H, d, $J = 8.1$ Hz, aromatic proton); δ 4.97 (1H, broad, carbamate proton); δ 4.19 (4H, m, methylene protons); δ 3.84 (3H, s, methoxy protons); δ 3.82 (3H, s, methoxy protons); δ 3.75 (1H, m, methine proton); δ 1.30 (3H, d, $J = 6.6$ Hz, methyl protons). Anal. ($\text{C}_{25}\text{H}_{26}\text{N}_2\text{O}_6$): C, 66.65; H, 5.820; N, 6.220. Found: C, 66.97; H, 6.010; N, 6.060.

2-(5-Phenyl-2-nitro-phenyl)-propyl N-4-Indole Carbamate (8). Yield: 68%; **TLC:** 0.57 (DCM/Ethanol 96:4); **IR:** 3401, 3301, 2956, 1701, 1602, 1547, 1323, 1232 cm^{-1} ; **$^1\text{H NMR}$** [CDCl_3] δ 7.83 (1H, d, $J = 8.4$ Hz, aromatic proton); δ 7.61 (1H, d, $J = 1.8$ Hz, aromatic proton); δ 7.41 (9H, m, aromatic protons); δ 6.96 (1H, t, $J = 8.1$ Hz,

aromatic proton); δ 6.40 (1H, m, aromatic proton); δ 4.59 (2H, d, $J = 7.2$ Hz, methylene protons); δ 3.93 (1H, m, methine proton); δ 3.79 (1H, broad, carbamate proton); δ 1.44 (3H, d, $J = 7.2$ Hz, methyl protons). Anal. ($C_{24}H_{21}N_3O_4$): C, 69.39; H, 5.100; N, 10.11.

2-(5-Phenyl-2-nitro-phenyl)-propyl *N*-4-methylindole Carbamate (9). Yield: 76%; TLC: 0.58 (DCM/Ethanol 96:4); IR: 3406, 3305, 2923, 1694, 1603, 1510, 1342, 1225 cm^{-1} ; 1H NMR [$CDCl_3$] δ 8.21 (1H, broad, indole proton); δ 7.74 (1H, d, $J = 8.7$ Hz, aromatic proton); δ 7.41 (7H, m, aromatic protons); δ 7.23 (1H, d, $J = 7.8$ Hz, aromatic protons); δ 7.08 (1H, m, aromatic proton); δ 7.01 (1H, t, $J = 7.8$ Hz, aromatic proton); δ 6.88 (1H, d, $J = 7.2$ Hz, aromatic proton); δ 6.46 (1H, s, aromatic proton); δ 4.87 (1H, broad, carbamate proton); δ 4.53 (2H, d, $J = 5.7$ Hz, methylene protons); δ 4.26 (2H, m, methylene protons); δ 3.74 (1H, m, $J = 7.2$ Hz, methine proton); δ 1.30 (3H, d, $J = 6.9$ Hz, methyl protons). Anal. ($C_{25}H_{23}N_3O_4$): C, 69.92; H, 5.400; N, 9.780.

2-(5-Phenyl-2-nitro-phenyl)-propyl *N*-(L)-Tryptophan Carbamate (10). Yield: 38%; TLC: 0.15 (DCM/Ethanol 96:4); IR: cm^{-1} ; 1H NMR [$CDCl_3$] δ (1H, broad, indole proton); δ (1H, d, $J = 8.7$ Hz, aromatic proton); δ (7H, m, aromatic protons); δ (1H, d, $J = 7.8$ Hz, aromatic protons); δ (1H, m, aromatic proton); δ (1H, t, $J = 7.8$ Hz, aromatic proton); δ (1H, d, $J = 7.2$ Hz, aromatic proton); δ (1H, s, aromatic proton); δ (1H, broad, carbamate proton); δ (2H, d, $J = 5.7$ Hz, methylene protons); δ (2H, m, methylene protons); δ (1H, m, $J = 7.2$ Hz, methine proton); δ (3H, d, $J = 6.9$ Hz, methyl protons). Anal. ($C_{27}H_{25}N_3O_6$): C, 66.52; H, 5.170; N, 8.620.

1-(4,5-Methylenedioxy-2-nitro-phenyl)-ethyl *N*-(L)-Tryptophan Carbamate (11). Yield: 52%; TLC: 0.13 (DCM/Ethanol 96:4); IR: cm^{-1} ; 1H NMR [$DMSO-d_6$] δ

10.8 (1H, d, indole proton); δ 7.58 (3H, m, aromatic protons); δ 7.32 (1H, t, $J = 8.4$ Hz, aromatic protons); δ 7.06 (3H, m, aromatic protons); δ 6.22 (2H, s, methylene protons); δ 5.96 (1H, m, $J = 6.6$ Hz, methine proton); δ 4.14 (1H, m, $J = 4.5$ Hz, methine proton); δ 3.13 (1H, m, $J = 5.1$ Hz, methylene proton); δ 2.98 (1H, dd, $J = 9.3$ Hz, $J = 5.4$ Hz, methylene proton); δ 1.47 (3H, dd, $J = 6.6$ Hz, $J = 6.0$ Hz methyl protons). Anal. ($C_{21}H_{19}N_3O_8$): C, 60.60; H, 4.580; N, 10.60.

(4,5-Dimethoxy-2-nitro-phenyl)-methyl *N*-(L)-Tryptophan Carbamate (12).

Yield: 42%; **TLC:** 0.17 (DCM/Ethanol 96:4); **IR:** cm^{-1} ; **1H NMR** [DMSO- d_6] δ 10.7 (1H, s, indole proton); δ 7.78 (1H, d, $J = 8.1$ Hz, aromatic proton); δ 7.58 (1H, s, aromatic proton); δ 7.44 (1H, d, $J = 8.4$ Hz, aromatic proton); δ 7.24 (1H, d, $J = 8.1$ Hz, aromatic proton); δ 7.05 (1H, s, aromatic proton); δ 7.00 (1H, m, aromatic proton); δ 6.85 (1H, m, aromatic proton); δ 4.13 (1H, m, methine proton); δ 3.79 (3H, s, methoxy protons); δ 3.74 (3H, s, methoxy protons); δ 3.51 (2H, s, methylene protons); δ 3.03 (1H, m, methylene proton); δ 2.92 (1H, m, methylene proton). Anal. ($C_{21}H_{21}N_3O_8$): C, 56.88; H, 4.770; N, 9.480.

Conclusion

With increasing development and interest in in situ preparation of peptide arrays^{15,16}, photo-labile protective groups that exhibit efficient and quantitative yields have great appeal. A comparison between NPPOC, MeNPOC, and NVOC revealed that all three groups were viable amino photo-labile protective groups, but that NPPOC and its derivatives had the highest rates and yields. By comparing the rates and yields of photo-cleavage using various substituted NPPOC-amino protective groups, it was

determined that aromatic substituents resulted in most effective cleavage. Normally, di-radical formation is rate limiting in the mechanism. However, for the substituted NPPOC groups that gave the highest deprotection rates, formation of the di-radical occurs fast enough so that the rate determining step was the elimination of the CO₂.

References

1. J.A. Barltrop, P. Schofield, Photosensitive protecting groups. *Tetrahedron Letters*, 697-699 (1962).
2. A. Patchornik, B. Amit, R. Woodward, Photosensitive protecting groups. *Journal of the American Chemical Society* **92**, 6333-6335 (1970).
3. C.H. Bamford, R.G.W. Norrish, Primary photochemical reactions. VII. Photochemical decomposition of isovaleraldehyde and dipropyl ketone. *Journal of the American Chemical Society*, 1504-1511 (1935).
4. P. Wan, K. Yates, Photoredox chemistry of nitrobenzyl alcohols in aqueous solution. Acid and base catalysis of reaction. *Canadian Journal of Chemistry* **64**, 2076-2086 (1986).
5. C.G. Bochet, Photolabile protecting groups as linkers. *Perkin Trans.* **1**, 125-142 (2002).
6. G.H. McGall et al., The efficiency of light-directed synthesis of DNA arrays on glass substrates. *Journal of the American Chemical Society* **119**, 5081-5090 (1997).
7. M.C. Pirrung et al., Pentadienylnitrobenzyl and pentadienylnitropiperonyl photochemically removable protecting groups. *Journal of Organic Chemistry* **64**, 5042-5047 (1999).
8. C.P. Holmes et al., Preparation of novel nitrobenzyl derivative photoreactive protecting reagents., P.I. Appl., Editor. (1994).
9. M. Beier, J.D. Hoheisel, Production by quantitative photolithographic synthesis of individually quality checked DNA microarrays. *Nucleic Acids Research* **28**, e11 (2000).

10. T.J. Albert, J. Norton, M. Ott, T. Richmond, K. Nuwaysir, E.F. Nuwaysir, K.P. Stengele, R.D. Green, Light-directed synthesis of complex oligonucleotide microarrays. *Nucl. Acids Res.* **31**, e35 (2003).
11. D. Woll, W. Dominik, J. Smirnova, W. Pfliederer, U.E. Steiner, Highly efficient photolabile protecting groups with intramolecular energy transfer. *Angew. Chem. Int. Ed.* **45**, 2975-2978 (2006).
12. D. Wöll, J. Smirnova, M. Galetskaya, T. Prykota, J. Bühler, K.P. Stengele, W. Pfliederer, U.E. Steiner, Intramolecular sensitization of photocleavage of the photolabile NPPOC protecting group: photoproducts and photokinetics of the release of nucleosides. *Chem. Eur. J.* **14**, 6490-6497 (2008).
13. A. Hasan et al., Photolabile protecting groups for nucleosides. *Tetrahedron* **53**, 4247-4264 (1997).
14. K.R. Bhushan, D. Charles, R.A. Laursen, Synthesis of photolabile 2-(2-nitrophenyl)propyloxycarbonyl protected amino acids. *Tetrahedron Letters* **44**, 8585-8588 (2003).
15. D.H. Min, M. Mrksich, Peptide arrays: toward routine implementation. *Current opinion in chemical biology* **8**, 554-558 (2004).
16. P. Klán, T. Šolomek, C.G. Bochet, A. Blanc, R. Givens, M. Rubina, V. Popik, A. Kostikov, J. Wirz, Photoremovable Protecting Groups in Chemistry and Biology: Reaction Mechanisms and Efficacy. *Chem. Rev.* **113**, 119-191 (2013).

Chapter 3

Feature-Level MALDI-MS Characterization of Electrochemically-Directed In situ-Synthesized Peptide Microarrays

The contents of this chapter has been extracted from an already published article¹.

Abstract

Characterizing the chemical composition of microarray features is a difficult yet important task in the production of in situ-synthesized microarrays. Here, we describe a method to determine the chemical composition of microarray features, directly on the feature. This method utilizes non-diffusional chemical cleavage from the surface along with techniques from MALDI-MS tissue imaging, thereby making the chemical characterization of high-density microarray features simple, accurate, and amenable to high-throughput.

Introduction

Microarrays are one of the leading platforms used in high-throughput experimentation and data acquisition. A primary example is the DNA microarray, which serves as an integral experimental platform in genomics². The information content and the throughput achieved with microarrays continue to advance, partly because of advances in the fabrication of in situ-synthesized DNA microarrays²⁻⁸. This has resulted in greatly increased feature densities.

Advances in DNA microarray fabrication are being applied to the production of peptide and other non-nucleic acid microarrays⁸⁻¹⁷. Synthesis efficiency is essential for reliable microarray data; even minor inefficiencies result in cumulative in situ stepwise

synthesis errors¹⁸. Characterization of the synthesis efficiency of in situ-synthesized DNA microarrays is facilitated by the ability to hybridize a complementary strand of DNA and the sensitivity of hybridization to base-pair mismatches¹⁹⁻²¹. However, characterizing the synthetic fidelity of peptide arrays and other non-nucleic acid-based microarrays is much more difficult given that the hybridization of a complementary strand is not possible.

In the absence of hybridization, characterization of microarrays is typically done using direct-label fluorescence or staining^{13,15,22}, antibody binding to a synthesized epitope^{8,15}, protein binding to a known ligand^{12,23}, or molecules are cleaved from the surface and then analyzed using traditional methods such as HPLC and mass spectrometry^{9,24,25}. Although these methods provide information about the success or failure of a particular microarray synthesis, much of the information about the chemical composition of the microarray features remains unknown. Labeling particular groups using fluorescence simply provides a measure of the number of reactive sites. An antibody binding to a known epitope or protein binding to a known ligand indicates if the epitope or ligand exists at the spot, but gives no information about what side products may be there or in what quantity²⁶⁻²⁸. Finally, cleaving in situ-synthesized molecules from the microarray surface does provide a complete characterization of the synthesis. However, this analysis is not compatible with arrayed chemical libraries because of diffusion and mixing at the surface upon cleavage and sample collection.

Here, we describe a mass spectrometry approach to fully characterize the composition of arrayed, in situ-synthesized peptide libraries, directly on each feature. Direct characterization of in situ-synthesized small-molecule microarrays has been

previously described^{29,30}. These studies utilized TOF-SIMS and a custom-synthesized cleavable linker. In the characterization of microarrays, TOF-SIMS has significant spatial resolution advantages when compared to MALDI-TOF. In addition, TOF-SIMS does not require the application of a matrix, thereby limiting the diffusion of analyte between microarray features. However, TOF-SIMS is generally limited to low-mass ions, such as short peptides or small molecules; whereas, high molecular-weight ions can be detected with MALDI-TOF³¹. The high-mass range of TOF-SIMS can be extended with the application of a matrix, similar to that used with MALDI-TOF³¹. However, the application of a matrix confounds the advantage of limited diffusion offered by matrix-free TOF-SIMS. Also, the hard ionization technique on which TOF-SIMS is based produces unwanted fragmentation of analyte molecules. Therefore, although TOF-SIMS would likely offer higher spatial resolution than MALDI-TOF, analyte fragmentation represents the definitive limitation.

In the approach described below, microarrays containing various peptide sequences, attached to surfaces via commercially-available cleavable linkers, are synthesized in situ using electrochemically-patterned synthesis. The resulting features are then cleaved and the MALDI matrix is applied in such a way as to limit analyte diffusion. After applying the MALDI matrix, the chemical composition of each feature is analyzed using MALDI-TOF mass spectrometry directly on the feature. Though MALDI-TOF was used to demonstrate the approach in this work, TOF-SIMS could also presumably be used, in conjunction with the MALDI matrix to obtain in situ mass spectra from the peptide array features³².

Results and Discussion

To demonstrate the generality of this approach in characterizing in situ-synthesized microarrays on different platforms, both electrochemically- and photolithographically-synthesized peptide microarrays have been tested. Electrochemical in situ synthesis utilizes electrochemically-generated acids to remove acid-labile protecting groups and addressable electrodes to produce distinct microarray features¹² whereas, photolithographic in situ synthesis utilizes photolabile protecting groups and masks to selectively deprotect features on a microarray². In these experiments, microarray feature dimensions were limited to several hundred micrometers to demonstrate the approach. Here, we focus solely on the characterization of electrochemical in situ synthesis, since the photolithographic in situ synthesis characterization work was conducted by another graduate student of the Woodbury Lab.

Direct MALDI-MS Characterization of Electrochemically-Synthesized Peptide Microarrays

Electrochemical peptide microarray synthesis was performed using a mixed protecting group approach on 12K CombiMatrix (CBMX) chips sold by CombiMatrix Corp., Mukilteo, WA. This strategy utilized base-labile/acid-labile (FMOC/trityl) protecting groups (Figure 1). This strategy allowed for the use of commercially available amino acids with amino groups protected by FMOC at positions in the peptide that were constant across the array and highly acid-labile trityl groups at variable positions in the peptide. Using a very acid-labile protecting group, such as trityl, allowed for deprotection with electrochemically-generated acids at low applied electrode potentials.

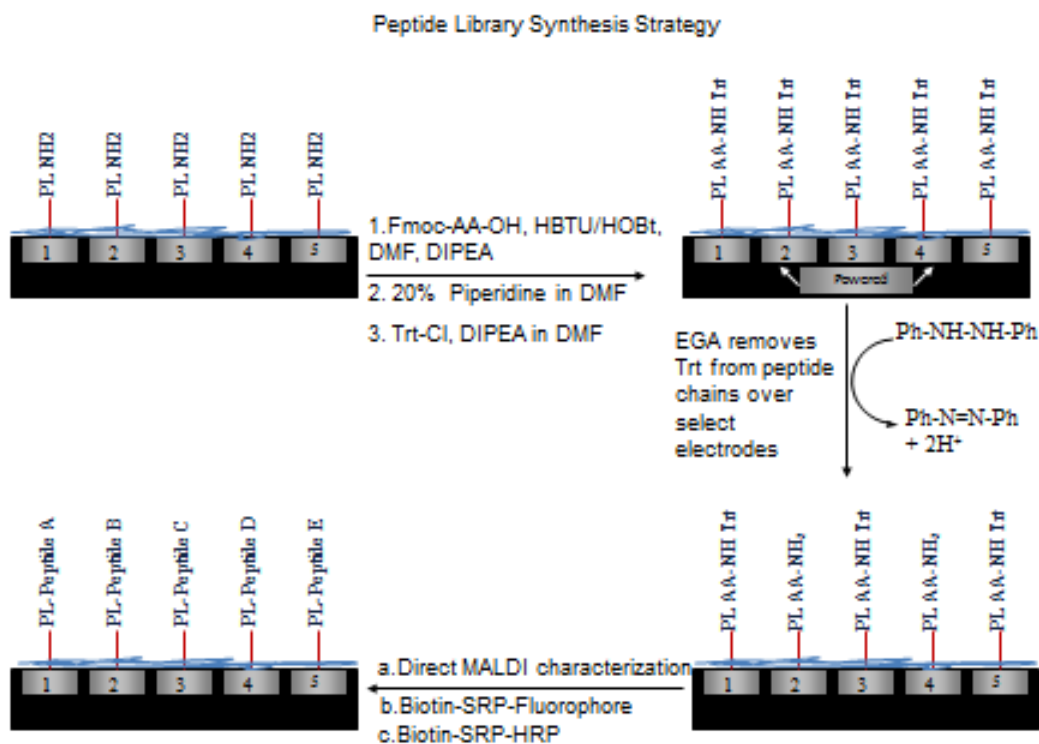


FIGURE 1: Scheme of electrochemically directed peptide synthesis on CBMX chips.

For this work, a cleavable linker to the electrode surface was needed for release of the peptide at the end of the synthesis for MALDI-TOF analysis. Because the electrochemical peptide array synthesis generates acid at each electrode surface, the acid-cleavable Rink linker could not be used. Instead, an orthogonal linker strategy was used to attach peptides to the electrode surface. Use of HMBA linker (base-labile) did not prove to be a successful strategy for MALDI-based synthesis characterization due to the required application of strong basic conditions for removal of the linker after synthesis. The strong basic conditions deteriorated the electrode surfaces and clean removal of the

peptide was not possible (no peaks were observed in the appropriate mass range). Instead, a photolabile linker (4-{4-[1-(9-Fluorenylmethyloxycarbonyl)ethyl]-2-methoxy-5-nitrophenoxy}butanoic acid, (Fmoc-Photolabile linker-OH, Cat # RT1095, Advanced Chemtech) was used and proved to be beneficial in several ways; (a) the linker could be cleaved by UV exposure without damaging the slide or the synthesized molecule and (b) UV cleavage could be done under dry conditions. UV cleavage under dry conditions gave the flexibility to characterize the synthesis directly from the chip surface and made the protocol simpler because there was no need to purify samples collected after cleavage.

Initially, synthesized peptides were labeled with TMPP [(N-Succinimidyl)oxycarbonylmethyl]tris(2,4,6-trimethoxyphenyl)phosphonium bromide] on the N-terminus in order to improve their ionization ability in the mass spectrometer (Figure 2)³³. Later, we successfully tested peptides without TMPP labels. During synthesis optimization experiments, we observed that peptide sequences containing lysine possessed improved ionization ability due to facile positive charge formation associated with lysine. Peptides that did not contain lysine, still resulted in MALDI peaks, but sodium and potassium adducts dominated.

An electrochemical array of four peptides of different lengths; KAFGAFGAFG, K(G)AFGAFGAFG, K(FG)AFGAFGAFG, and K(AFG)AFGAFGAFG; was synthesized. The residues in parentheses were added electrochemically; all other amino acids were coupled using Fmoc chemistry. To simplify the task of visualizing array features during MALDI-MS analysis, the array was synthesized as a collection of several, individual, neighboring electrodes. For MALDI-TOF analysis, the chip was divided in

four regions and each peptide was synthesized in a quarter of the chip. Schematic diagram of the experiment can be seen in Figure 3 and the corresponding MALDI analysis in Figure 4.

After array synthesis, the dry chip was irradiated with UV light to cleave the peptides from the surface without diffusion. The MALDI matrix was applied to the surface as small drops with a pipette, and the chip (75 mm X 25 mm dimensions) was mounted in the MALDI target plate and then analyzed with MALDI-MS. Surface charging during MALDI spectrum acquisition was not a problem because of the conductive nature of the electrochemical chip. The resulting spectra (Figure 4) from each array feature shows the desired peptide as a dominant peak along with several side-product peaks. A second electrochemical array using the same array layout but with modified peptide sequences produced a similar result (Figure 5).

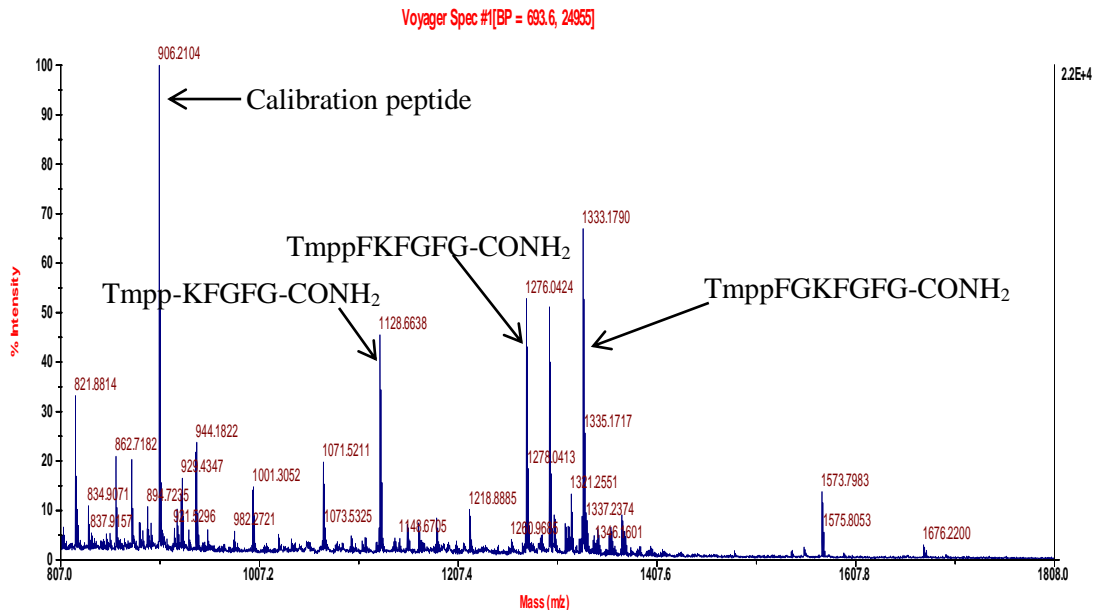


FIGURE 2: MALDI-TOF characterization of Tmpp labeled peptide: Tmpp-FGKFGFG-CONH₂ using Photolabile linker. Peaks in the spectrum correspond to the peptide, peptide with deletion of certain amino acids, and an internal calibration peptide. The synthesis was performed using Fmoc chemistry.

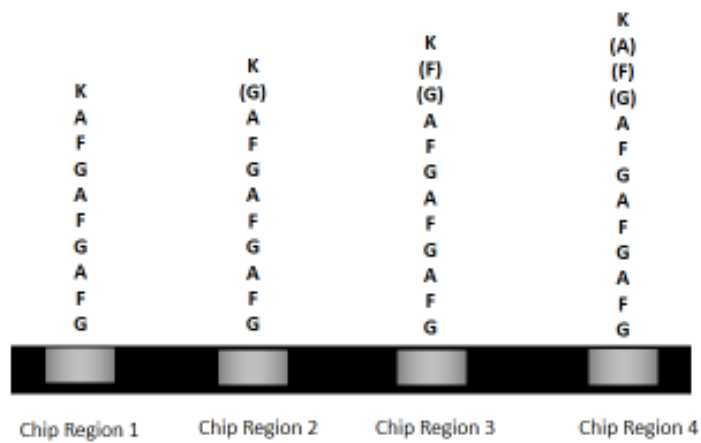


FIGURE 3: Schematic diagram of an electrochemical array of four peptides. Each region is made up of a quarter of 12K electrodes present on the chip. Letters in parentheses denote electrochemical synthesis of corresponding amino acid.

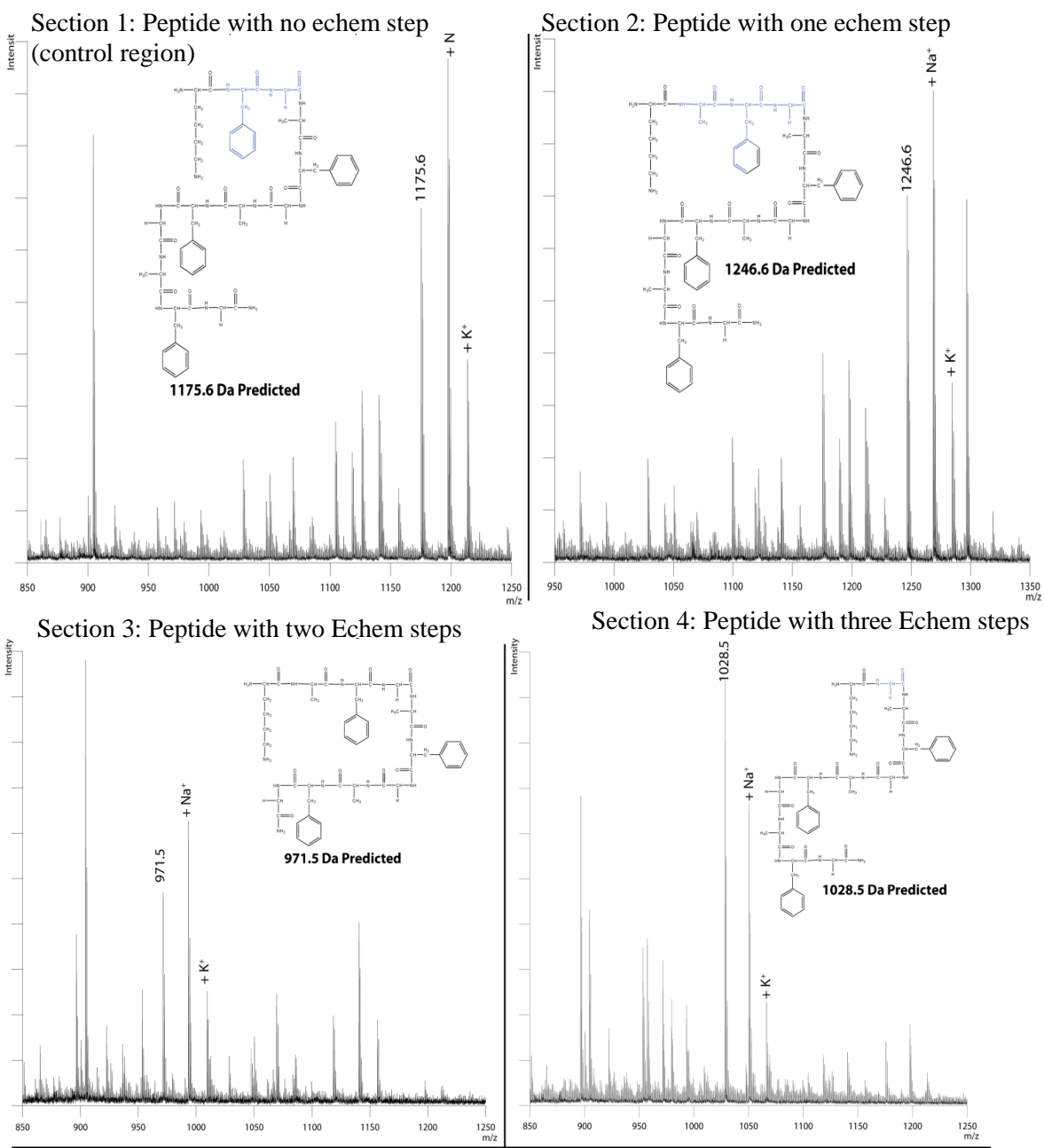


FIGURE 4: MALDI-MS characterization of three peptide features with 1, 2 or 3 electrochemical steps (in parentheses below). Feature 1 was synthesized using Fmoc chemistry.

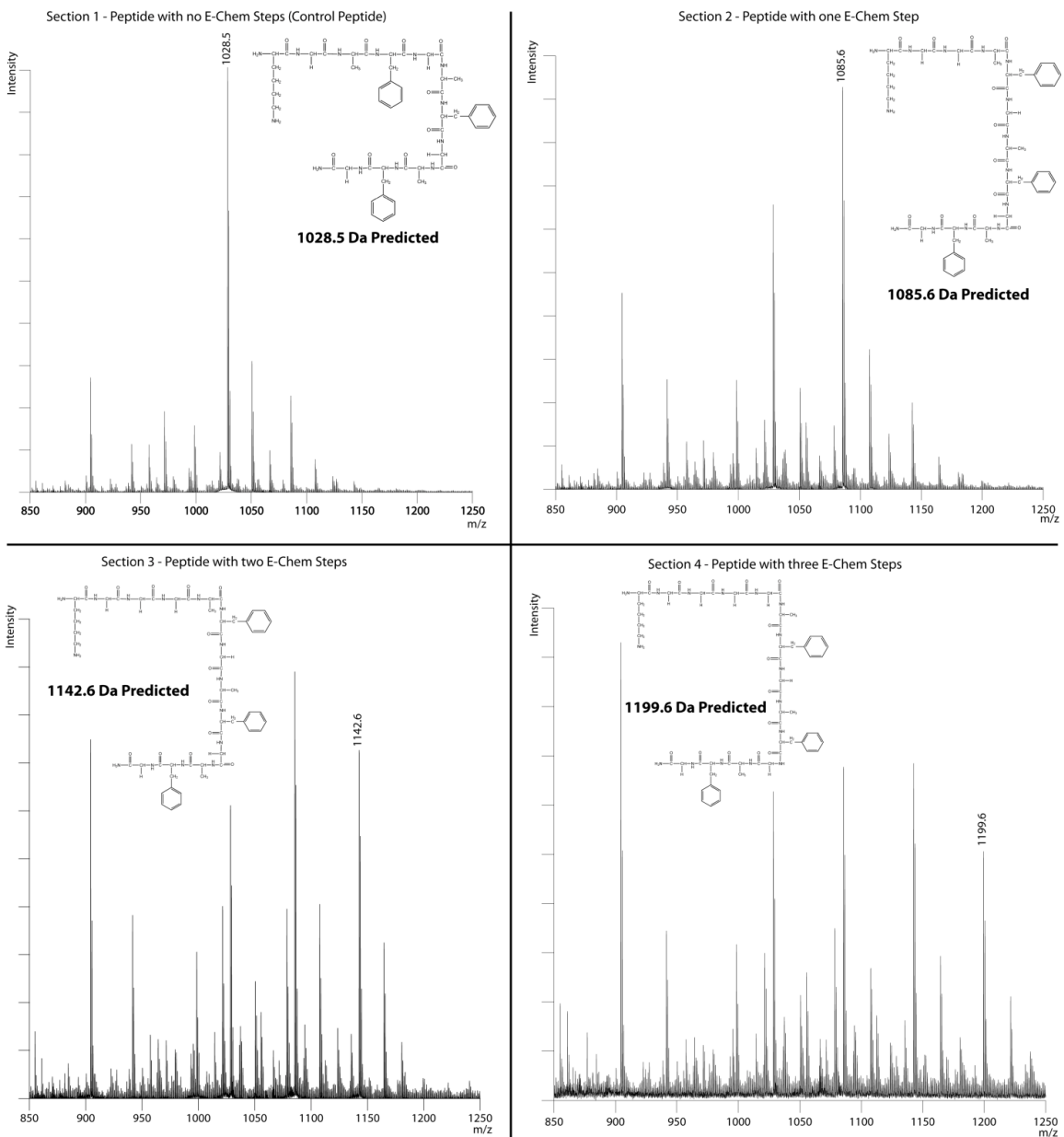


FIGURE 5: MALDI-MS characterization of three peptide features with 1, 2 or 3 electrochemical steps (in parentheses below). Feature 1 was synthesized using Fmoc chemistry only. Sequences of the peptides synthesized are: 1) KGAFGAFGAFG, 2) K(G)GAFGAFGAFG, 3) K(GG)GAFGAFGAFG, 4) K(GGG)GAFGAFGAFG. Desired product peak mass is noted in each spectrum.

The photolabile linker became unavailable at one point during the experimental process. Therefore, another photolabile linker (ANP linker) was successfully adapted for use in MALDI characterization of synthesis products (Figure 6). This ANP linker is also UV-cleavable and is readily available from several vendors. In addition, MALDI characterization of synthesis using TFA vapor cleavage of acid-labile linker (Rink linker) was also optimized (Figure 7). Though the use of acid-labile linker did not provide an orthogonal system for electrochemically-patterned synthesis, several optimization experiments were performed which did not require any electrochemical steps. These experiments tested the synthesis efficiency of difficult peptide sequences on the CBMX chips. Rink linker, an acid-labile linker, was used for these experiments. The linker was cleaved by overnight exposure to TFA vapor.

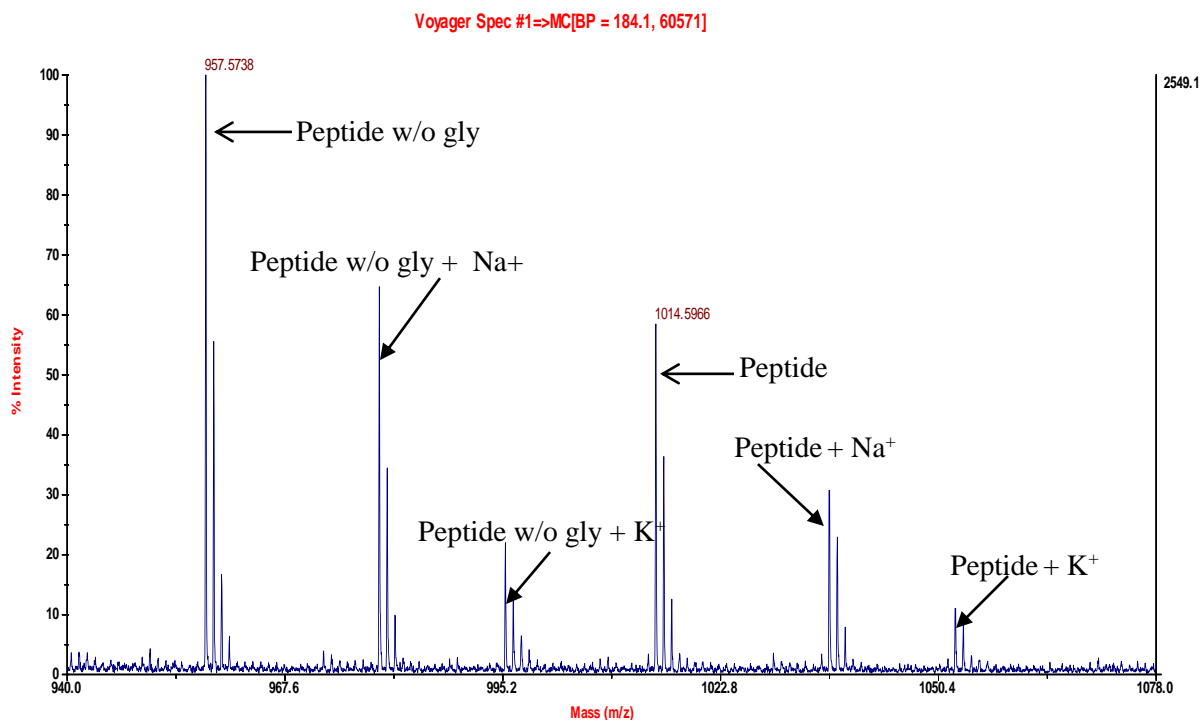


FIGURE 6: MALDI-MS characterization of peptide (NH₂-KFGKFGKFG-CONH₂) synthesized on ANP linker.

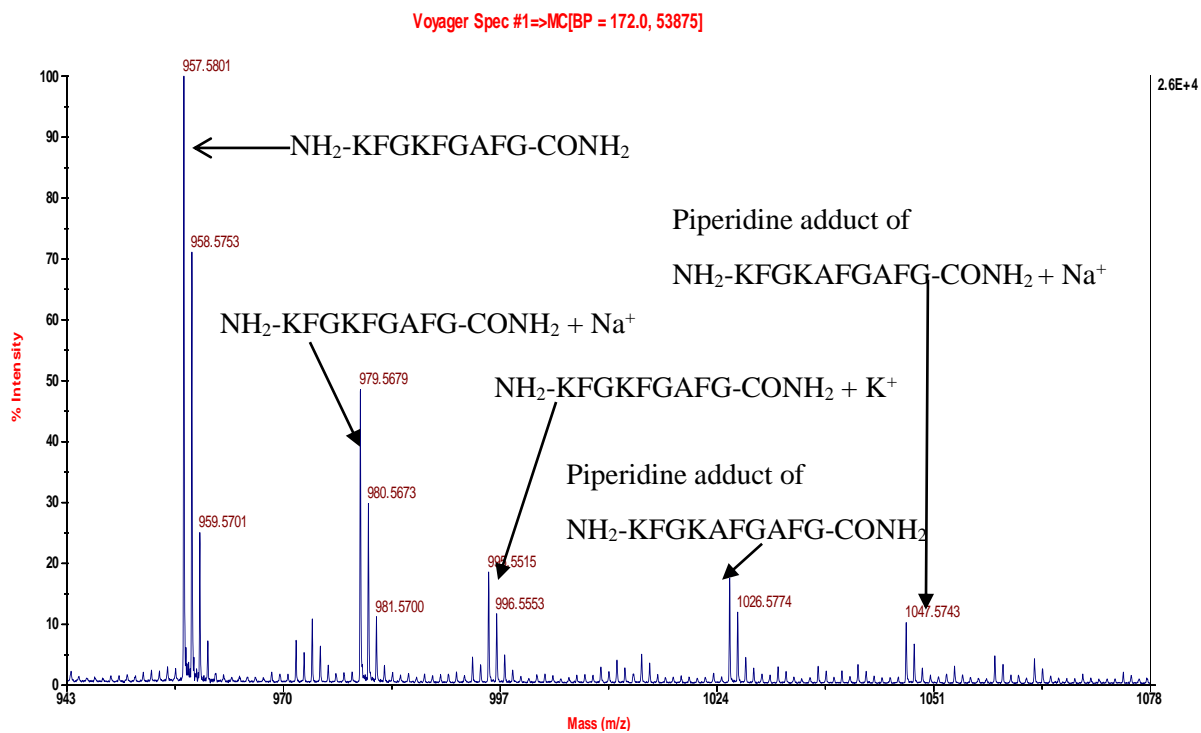


FIGURE 7: MALDI-MS characterization of a peptide synthesized on Rink linker.

Materials and Methods

Electrochemical Array Synthesis

Peptide synthesis was performed on 12,500 electrode (12K) Semiconductor microchips (CBMX Corporation, Mukilteo, WA). Chip fabrication and its surface morphology has been described in detail in Chapter 1. Briefly, the 12K semiconductor microchip has 12,500 individually-addressable, circular, porous polymer-coated platinum electrodes fabricated in rows and columns on silicon substrate. Electrodes contain either a 20-nucleotidepoly-T-spacer or 2-nucleotidepoly-T-spacer with an amine-modified terminal thymidine protected by monomethoxy trityl group. In all syntheses, an Fmoc-protected photolabile linker (Advanced Chemtech, Louisville, KY) was coupled as the C-terminal residue. Amino acid residues that are constant in all peptides in the array were

coupled and deprotected using standard Fmoc synthesis protocols and commercially available Fmoc-protected amino acids from either NovaBiochem (Affiliate of Merck, Darmstadt, Germany) or Anaspec (San Jose, CA). Variable amino acid residues were coupled and deprotected using electrochemically-directed peptide synthesis. Briefly, during variable amino acid coupling, the Fmoc group from N-terminal amines is deprotected and replaced chemically with a trityl group. Later, trityl groups from selected electrodes are deprotected by spatially controlled electro-generated acid and finally, the variable amino acid is coupled to the addressed electrodes. The following modifications to the described electrochemically-directed protocol were made: First, the localized generation of acids from 1,2-diphenylhydrazine (Sigma-Aldrich, Milwaukee, WI) by application of voltage to the addressed electrodes was conducted on 12K chips instead of a 1K chip. Second, voltage and time conditions for the electrochemical generation of acids were optimized to 3V and 10 min. for 12K chips.

Acid based chemical deprotection

t-butyl groups were chemically deprotected using a cocktail of 94% TFA (Sigma-Aldrich, St. Louis, MO) + 2.5% triisopropylsilane (TIS) (Sigma-Aldrich, Milwaukee, WI) + 3.5% water. The wafer was placed in an acid-resistant chamber and exposed to the deprotection cocktail for thirty minutes. At regular time intervals the setup was shaken for a better reaction. After thirty minutes, the solution was discarded in acid waste and the reaction setup was rinsed 5x with dichloromethane, 5x with 5% DIEA in dichloromethane, 3x with DMF, and 5x with water. The chip was then dried with argon gas.

Non-Diffusional UV-Cleavage of Arrayed Peptides

After synthesis, the chip was rinsed with N,N'-dimethylformamide (Sigma-Aldrich, Milwaukee, WI) for 6 minutes, with acetonitrile (Sigma-Aldrich, Milwaukee, WI) for 10 minutes, then dried with argon gas. Dry UV cleavage of the photolabile linker was carried out by exposing the chip with active surface area of 25 mm² to 7 mw of 365 nm UV irradiation for 3 hours. UV light was generated by inserting a U-360 1" bandpass filter (Edmund Optics Inc., Barrington, NJ) in front of the fiber optic cable from a white light source (Fiber-lite MH-100, Dollan-Jenner Ind., Boxborough, MA).

Non-Diffusional TFA Vapor based Cleavage of Arrayed Peptides

To prevent diffusion across the array, peptides were cleaved from the surface of the electrode in a dry state, using acid vapor cleavage. An array substrate containing the synthesized peptides was placed in a small glass vacuum chamber, evacuated by vacuum and sealed. A corked 100 mL Buchner flask containing 15 mL of neat trifluoroacetic acid (TFA) (Sigma-Aldrich, St. Louis, MO) was connected to the evacuated vacuum chamber containing the microarray substrate via a tube, thereby connecting the side-vent of the flask to the vacuum chamber inlet port. Once connected, the evacuated vacuum chamber inlet valve was opened, allowing gas flow between the Buchner flask and the vacuum chamber. The low-pressure of this system causes rapid evaporation of the neat TFA, forming a saturated TFA vapor in both the vacuum chamber and the Buchner flask. The microarray substrate was exposed to the TFA vapor for 2 hours, which was sufficient for nearly complete cleavage of Rink-linked peptide from the array substrate as well as complete cleavage of acid-labile side-chain protecting groups.

MALDI Matrix Application and Characterization of Array Features

CombiMatrix chips with cleaved peptides were characterized with either an ultraflex III MALDI-TOF-TOF (Bruker, Billerica, MA) or a Voyager-DE STR MALDI-TOF (Applied Biosystems, Foster City, CA). For characterization with the ultraflex III TOF-TOF MALDI, microarray substrates containing cleaved peptides and crystallized MALDI matrix were mounted in a Bruker (Billerica, MA) MTP Slide-Adapter, which holds up to two 75 X 25 mm substrates for MALDI Imaging. Calibration was performed by spotting peptide calibration standard II (Bruker, Billerica, MA) and MALDI matrix at the array corners to provide a close external standard. Final MALDI Spectra were acquired as an average of ~300 individual spectra at 25 Hz laser shot frequency and 40% laser power on an ultraflex III TOF-TOF (Bruker, Billerica, MA). MALDI spectra were analyzed using FlexAnalysis (Bruker, Billerica, MA). For characterization with Voyager-DE STR MALDI-TOF, a custom MALDI target plate was used to mount the chip and α -cyano-4- hydroxycinnamic acid (Sigma-Aldrich, St. Louis, MO) MALDI matrix was prepared in 1:1 acetonitrile:H₂O with 0.1% trifluoroacetic acid and an internal calibrant peptide mixture containing des-Arg1-Bradykinin peptide (904.47Da), Angiotensin1 peptide (1296.66Da), and Glu1-Fibrinopeptide B peptide (1570.68Da), all purchased from Applied Biosystems (Foster city, CA). Stock peptide calibrant was diluted 20x with saturated MALDI matrix solution and spotted on the chip surface with a pipette. MALDI spectra were analyzed using FlexAnalysis (Bruker, Billerica, MA) or Data Explorer (Applied Biosystems, Foster city, CA).

Conclusion

We have developed a simple, accurate, and general MALDI-MS based approach to characterize the chemical composition of an in situ-synthesized microarray directly on array features. As demonstrated, this approach has sufficient sensitivity to characterize array features synthesized on 2D surfaces, in this case, a carbohydrate matrix on an electrode. This approach provides significantly more information about microarray spot composition than can be gained from traditional approaches, such as fluorescence and antibody binding. In addition to the in situ determination of amino acid composition, with MALDI-TOF-TOF (MS-MS), it is likely possible to obtain peptide sequence information directly from the microarray feature. We recognize that this approach, as described, has spatial limitations that make it difficult to analyze array features that are less than 100 μm in diameter. The two most significant factors limiting the spatial resolution of this work are the limit to which the MALDI laser can be focused and the limited precision in positioning the array features inline with the laser. Improvements in either of these limiting factors would significantly reduce the array feature sizes that can be analyzed with MALDI-TOF. Array spatial resolutions as small as 25 μm may be possible, as has already been demonstrated in tissue imaging³⁴.

Another limitation we need to address is the successful MALDI-TOF characterization of large-scale arrays. We have been manually spotting MALDI matrix, through pipetting, which covers an area of approximately 750 μm X 750 μm . This area is large enough to cover several substrate features. Therefore, the peptide profiles of several different features covered in the spotted area appear in the MALDI spectrum, making it

complicated to discriminate between them. To overcome this problem, we attempted to apply a matrix aerosol using an air brush. However, manual handling of the air brush did not result in an even application of the tiny matrix droplets that we were hoping would only cover single features at a time. There are precise instruments available which apply matrix aerosols to tissue samples but these instruments were unavailable for this study. Another approach is to synthesize a subset of peptides (approximately ten) in the region covered by the pipetted matrix. The MALDI spectrum of a particular spot would then consist of ten peptides whose analysis will be straightforward and easier to interpret. Using this method, a small array could be characterized (about 10% of a 1K array), though large-scale characterization is not possible with this strategy.

References

1. P. Kumar, M.P. Greiving, Z.G. Zhao, N.W. Woodbury, Feature-level MALDI-MS characterization of in situ-synthesized peptide microarrays. *Langmuir* 26, 1456-1459 (2010).
2. M. Chee, R. Yang, E. Hubbell, A. Berno, X.C. Huang, D. Stern, J. Winkler, D.J. Lockhart, M.S. Morris, S.P. Fodor, Accessing genetic information with high-density DNA arrays. *Science* 274, 610–614 (1996).
3. X. Gao, E. LeProust, H. Zhang, O. Srivannavit, E. Gulari, P. Yu, C. Nishiguchi, Q. Xiang, X. Zhou, A flexible light-directed DNA chip synthesis gated by deprotection using solution photogenerated acids. *Nucleic Acids Res.* 29, 4744–4750 (2001).
4. T.R. Hughes, M. Mao, A.R. Jones, J. Burchard, M.J. Marton, K.W. Shannon, S.M. Lefkowitz, M. Ziman, J.M. Schelter, M.R. Meyer, S. Kobayashi, C. Davis, H. Dai, Y.D. He, S.B. Stephaniants, G. Cavet, W.L. Walker, A. West, E. Coffey, D.D. Shoemaker, R. Stoughton, A.P. Blanchard, S.H. Friend, P.S. Linsley, Expression profiling using microarrays fabricated by an ink-jet oligonucleotide synthesizer. *Nat. Biotechnol.* 19, 342–347 (2001).
5. R.J. Lipshutz, S.P. Fodor, T.R. Gingeras, D.J. Lockhart, High density synthetic oligonucleotide arrays. *Nat. Genet.* 21, 20–24 (1999).

6. A.C. Pease, D. Solas, E.J. Sullivan, M.T. Cronin, C.P. Holmes, S.P. Fodor, Light-generated oligonucleotide arrays for rapid DNA sequence analysis. *Proc. Natl. Acad. Sci. U.S.A.* **91**, 5022–5026 (1994).
7. S. Singh-Gasson, R.D. Green, Y. Yue, C. Nelson, F. Blattner, M.R. Sussman, F. Cerrina, Maskless fabrication of light-directed oligonucleotide microarrays using a digital micromirror array. *Nat. Biotechnol.* **17**, 974–978 (1999).
8. M. Beyer, A. Nesterov, I. Block, K. König, T. Felgenhauer, S. Fernandez, K. Leibe, G. Torralba, M. Hausmann, U. Trunk, V. Lindenstruth, F.R. Bischoff, V. Stadler, F. Breitling, Combinatorial synthesis of peptide arrays onto a chip. *Science* **318**, 1888 (2007).
9. R. Frank, The SPOT-synthesis technique. Synthetic peptide arrays on membrane supports--principles and applications. *J. Immunol. Methods* **267**, 13–26 (2002).
10. F.G. Kuruvilla, A.F. Shamji, S.M. Sternson, P.J. Hergenrother, S.L. Schreiber, Dissecting glucose signalling with diversity-oriented synthesis and small-molecule microarrays. *Nature* **416**, 653–657 (2002).
11. G. MacBeath, S.L. Schreiber, Printing proteins as microarrays for high-throughput function determination. *Science* **289**, 1760–1763 (2000).
12. K. Maurer, A. McShea, M. Strathmann, K. Dill, The removal of the t-boc group by electrochemically generated acid and use of an addressable electrode array for peptide synthesis. *J. Comb. Chem.* **7**, 637–640 (2005).
13. T.R. Northen, M.P. Greving, N.W. Woodbury, Combinatorial screening of biomimetic protein affinity materials. *Adv. Mater.* **20**, 4691–4697 (2008).
14. S. Park, I. Shin, Fabrication of carbohydrate chips for studying protein-carbohydrate interactions. *Angew. Chem., Int. Ed.* **41**, 3180–3182 (2002).
15. J.P. Pellois, X. Zhou, O. Srivannavit, T. Zhou, E. Gulari, X. Gao, Individually addressable parallel peptide synthesis on microchips. *Nat. Biotechnol.* **20**, 922–926 (2002).
16. M. Pirrung, Spatially addressable combinatorial libraries. *Chem. Rev.* **97**, 473–488 (1997).
17. N. Ramachandran, E. Hainsworth, B. Bhullar, S. Eisenstein, B. Rosen, A.Y. Lau, J.C. Walter, J. Labaer, Self-assembling protein microarrays. *Science* **305**, 86–90 (2004).

18. M. Pirrung, How to make a DNA chip. *Angew. Chem., Int. Ed.* **41**, 1276–1289 (2002).
19. R.B. Wallace, J. Shaffer, R.F. Murphy, J. Bonner, T. Hirose, K. Itakura, Hybridization of synthetic oligodeoxyribonucleotides to phi chi 174 DNA: the effect of single base pair mismatch. *Nucleic Acids Res.* **6**, 3543–3557 (1979).
20. B.J. Conner, A.A. Reyes, C. Morin, K. Itakura, R.L. Teplitz, R.B. Wallace, Detection of sickle cell beta S-globin allele by hybridization with synthetic oligonucleotides. *Proc. Natl. Acad. Sci. U.S.A.* **80**, 278–282 (1983).
21. U. Maskos, E.M. Southern, Oligonucleotide hybridisations on glass supports: a novel linker for oligonucleotide synthesis and hybridisation properties of oligonucleotides synthesised *in situ*. *Nucleic Acids Res.* **20**, 1679–1684 (1992).
22. K. Hilpert, D.F.H. Winkler, R.E.W. Hancock, Peptide arrays on cellulose support: SPOT synthesis, a time and cost efficient method for synthesis of large numbers of peptides in a parallel and addressable fashion. *Nat. Protoc.* **2**, 1333–1349 (2007).
23. O. Michel, B.J. Ravoo, Carbohydrate microarrays by microcontact ‘Click’ chemistry. *Langmuir* **24**, 12116–12118 (2008).
24. K.R. Bhushan, Light-directed maskless synthesis of peptide arrays using photolabile amino acid monomers. *Org. Biomol. Chem.* **4**, 1857–1859 (2006).
25. T.R. Northen, D.C. Brune, N.W. Woodbury, Synthesis and characterization of peptide grafted porous polymer microstructures. *Biomacromolecules* **7**, 750–754 (2006).
26. S. Chen, M.F. Phillips, F. Cerrina, L.M. Smith, Controlling oligonucleotide surface density in light-directed DNA array fabrication. *Langmuir* **25**, 6570–6575 (2009).
27. V. Tapia, J. Bongartz, M. Schutkowski, N. Bruni, A. Weiser, B. Ay, R. Volkmer, M. Or-Guil, Affinity profiling using the peptide microarray technology: A case study. *Anal. Biochem.* **363**, 108–118 (2007).
28. D. Zichi, B. Eaton, B. Singer, L. Gold, Proteomics and diagnostics: let’s get specific, again. *Curr. Opin. Chem. Biol.* **12**, 78–85 (2008).
29. C. Chen, G. Nagy, A.V. Walker, K. Maurer, A. McShea, K.D. Moeller, Building addressable libraries: the use of a mass spectrometry cleavable linker for monitoring reactions on an microelectrode array. *J. Am. Chem. Soc.* **128**, 16020–16021 (2006).

30. C. Chen, P. Lu, A. Walker, K. Maurer, K.D. Moeller, Building addressable molecular libraries: the use of a detectable mass spectrometry cleavable linker. *Electrochem. Commun.* **10**, 973–976 (2008).
31. R.M. Heeren, Proteome imaging: a closer look at life's organization. *Proteomics* **5**, 4316–4326 (2005).
32. L. MacAleese, J. Stauber, R.M. Heeren, Perspectives for imaging mass spectrometry in the proteomics landscape. *Proteomics* **9**, 819–834 (2009).
33. Z.H. Huang, J. Wu, K.D.W. Roth, Y. Yang, D.A. Gage, J. T. Watson, A Picomole-Scale Method for Charge Derivatization of Peptides for Sequence Analysis by Mass Spectrometry. *Anal. Chem.* **69**, 137-144 (1997).
34. M. Stoeckli, P. Chaurand, D.E. Hallahan, R.M. Caprioli, Imaging mass spectrometry: a new technology for the analysis of protein expression in mammalian tissues. *Nat. Med.* **7**, 493–496 (2001).

Chapter 4

Optimization of Electrochemically-Directed Peptide Microarray Synthesis

Abstract

Technologies enabling the creation of large-scale, miniaturized, spatially addressable peptide microarrays are emerging. The focus of this chapter is on the synthesis optimization of peptide microarrays; specifically, the electrochemically-directed parallel synthesis of individually addressable high-density peptide microarrays using the electrochemical patterning platform described in previous chapters developed by CBMX¹. Synthesis concepts are discussed, with emphasis placed on the reactions of electrogenerated acids in the deprotection step of peptide synthesis. Peptide microarrays potentially represent a versatile tool for probing antigen-antibody, peptide-protein, and peptide-ligand interactions and may prove to be a powerful tool for proteomics research and clinical diagnosis applications.

Introduction

Microarray technology has become a powerful research means in proteomics and genomics studies^{1,2}. Microarrays are used to explore chemical spaces such as oligonucleotides, peptides, peptidomimetics, proteins, and small molecules for functional activity. This includes binding interactions with proteins, catalytic activity, and fitness as enzyme substrate. Microarray based assays involve probing several molecular interactions, concurrently on a single platform, at resolutions high enough to discriminate between single building blocks at specific positions. DNA Microarrays with probe numbers in millions and Peptide Microarrays with probe numbers in tens of thousands

are commercially available now^{3,4}. Microarrays have become one of the leading platforms used in high-throughput experimentation and data acquisition. Although, only DNA and peptides have been explored at a high density, microarrays in principle enjoy the advantage of incorporating a varied range of synthetic building blocks when compared to other library generating techniques⁵⁻⁹.

Proteins experience a much more diverse set of chemical interactions, as compared to DNA and RNA, since there are twenty different naturally occurring amino acids that may comprise proteins versus four nucleotide species that are found in nucleic acids. Proteins perform a vast array of functions for e.g., catalysis, regulation, inhibition, signaling, etc. They are therefore identified as important biomolecules for several research applications, such as therapeutic targets for several diseases, targets for drug discovery, models for artificial catalyst development, biomarkers for medical diagnosis, etc. Many of the biological interactions are based on the interaction of a protein with another protein¹⁰. One way to gain a deeper insight into protein-protein interactions is to restrict study to protein-peptide interactions, as protein interaction is sometimes only with a small continuous (linear) or discontinuous (conformational) region of its partner protein. For example, in the immune system, antibodies (protein) interact with a small portion of antigen (commonly protein) called epitope. Accordingly, it is desirable to fabricate peptide microarrays capable of probing interactions of several peptides with a binding protein. These peptide microarrays must be produced at a fast pace and at low cost. They must be reproducible, possess high sensitivity and a large dynamic detection range, and they should be stable for long-term storage.

Peptide microarray fabrication technologies fall into two broad categories; (i) direct deposition of presynthesized peptides on surfaces and (ii) parallel in situ synthesis of peptides on surfaces. We focused on parallel in situ synthesis of peptides on surfaces. The main aim of the research in our lab is to understand chemical spaces. We fabricate large arrays of heteropolymers, such as peptides, on surfaces by in situ synthesis utilizing technologies developed in the electronics industry.

Peptide Microarray Synthesis Techniques

Several techniques have been devised for peptide microarray synthesis. A survey of some of the important techniques is described below.

SPOT peptide synthesis. This technique was developed by Ronald Frank¹⁰. It involves spotting liquefied amino acids on a nitrocellulose substrate using a hollow needle. The working principle of the SPOT synthesis technique involves spotting of amino acid dissolved in a solvent on the substrate. This is done using a print head with a hollow needle placed relative to the substrate. The synthesis reaction takes place as soon as the drop contacts the surface. The peptide density on a feature using this technique is quite high, but the feature density (roughly 25 features per cm²) is quite low. Smaller features involve smaller droplets, which tend to evaporate. This limits the feature density.

Photolithography based peptide synthesis. It was developed by Fodor in 1991¹¹. In this technique light is irradiated through a real or virtual photomask to deprotect N-terminal protecting groups. The N-terminal amino groups can be protected with photo-labile protecting groups (PLPGs) or acid-labile protecting groups. The real and virtual mask approaches can be employed to shine light on selected features in order

to deprotect the protecting groups. PLPGs are directly deprotected upon irradiation, and acid-labile groups are deprotected by localized generation of acids upon light irradiation on selected features^{11,12}. This method has proved to be very successful in DNA microarray fabrication, and in the past few years large peptide microarrays also have been fabricated successfully. A few limitations are (1) PLPG protected amino acids are not readily available and are not simple to prepare in-house and (2) diffraction and scattering during light irradiation can lead to insertion of unwanted amino acids at neighboring silent features.

Particle-based peptide synthesis. It was developed by Frank Breitling and has proved to be very successful in fabricating large peptide microarrays^{13,14}. In this technique, different particles embedding different activated amino acid (-OPfp ester of amino acid) are deposited using a laser printer on a substrate (usually glass or silicon) functionalized with amino groups. Once the particles are deposited, they are melted so that the activated amino acids diffuse and couple with the free amino groups of the substrate. The excess particles are then washed away and the unreacted amino groups of the substrate are blocked using acetic anhydride. The Fmoc group is then deprotected, and the surface is ready for the next coupling cycle. Particles with different amino acids are then patterned on the surface through laser printing for the next round of the coupling cycle.

Electrochemical Synthesis of Peptide Microarrays

Another conceptually interesting method of in situ peptide microarray synthesis for producing high density peptide chips is electrochemical parallel synthesis using acid

labile protected amino acids as building blocks. This method was first reported by Maurer et al. in 2005¹⁵. An electrochemically generated acid (EGA) was used for the removal of the BOC protecting group at selected positions on an electronically addressable array. The substrate used was a CBMX chip, which is a semiconductor silicon surface with 1024 individually electronically addressable platinum microelectrodes¹⁵. The platinum electrode surface is overlaid with a three-dimensional polymer matrix on which is synthesized a DNA oligomer. A successful electrochemical synthesis of a pentapeptide, N-terminal sequence of endorphin (YGGFL), was performed on top of the DNA oligomer and its characterization by fluorescence was demonstrated.

The CBMX chips were developed by CombiMatrix Corp. in Seattle, Washington. These chips have been primarily used for the generation of DNA microarrays^{16,17}. The CBMX chips, by virtue of possessing electronically addressable arrays of electrodes, have an additional capability of conducting redox assays on microarrays compared to other surfaces. The peptide synthesis demonstrated by Maurer et al. on CBMX chips did not involve any complications due to side chain chemistry of amino acids. This is because all of the amino acids of the pentapeptide (YGGFL) synthesized did not require any side chain protection groups. One of the major factors that contributes to making peptide synthesis a difficult synthetic process is the stability of the orthogonal protecting groups during peptide synthesis. Also, synthesis of only a single peptide was demonstrated on the CBMX chip surface as a proof of the concept. We decided to take this work further and optimize the CBMX chips (next generation CBMX chips which have 12,544 platinum electrodes present on the silicon surface were used) for peptide

microarray synthesis. We focused on various aspects of peptide microarray synthesis on CBMX chips. Most notably the (i) generation and use of an electrochemically generated acid (EGA) for the removal of acid labile protecting groups from selected positions of an electronically addressable CBMX chip and (ii) the synthesis of peptide microarrays with the optimized EGA system.

The MALDI detection method described in the previous chapter was used to characterize the chemical composition of arrayed, in situ synthesized peptide libraries.

Results and Discussion

General Synthesis Scheme

Our method of fabrication of peptide microarrays is based on three components: (i) CBMX's CMOS array technology, (ii) electro-generated acid precursors (EGA-P), and (iii) automated solid phase peptide synthesis. The fabrication of peptide and other biopolymer microarrays requires a gating step in every synthesis cycle so that the biopolymer sequence generation can be spatially controlled. Such synthesis cycles, involving a gating step, when executed multiple times, results in fabrication of a microarray with a large sequence diversity of biopolymer (in our case, microarray of 12,544 peptides, peptidomimetics, and other biopolymers can be fabricated) (Scheme 1 in Chapter 3). In our method we accomplish gating by generating acid from an electro-generated acid precursor (EGA-P) molecule. Upon application of electric potential to the addressed electrodes, the EGA-P undergoes an electrolytic reaction to generate acid (EGA), which deprotects the terminal amino group present on the chip surface. The EGA

replaces the use of Trifluoroacetic acid (TFA) as the deprotection reagent commonly used in conventional peptide synthesis.

The synthesis is performed on a CBMX chip surface functionalized with monomethoxytrityl (MMT)-protected amino-linker (a 20-nucleotidepoly-T-spacer with an amine-modified terminal thymidine protected by MMT group), in a solvent-leak-free reaction chamber. A computer-generated voltage/current pattern for the application of potential across selected electrodes is focused to the microchip's constituent electrodes.

At the selectively addressed electrodes, the electrolytic reaction of EGA-P yields acid, which removes the Trityl (Trt) protecting group from the terminal amino group of the chip surface. Diffusion of acid from the selected electrode to the neighboring silent electrodes is prevented in three ways. Firstly, every single electrode is surrounded by a ring-shaped electrode called getter electrode, with opposite polarity which prevents protons from diffusing to the neighbor electrode. Then, each electrode is separated from its neighbor electrodes through passive silicon nitride layer, and finally, an EGA-P solution involves scavenger molecules to absorb unreacted protons and prevent diffusion. After every gating reaction, the reaction chamber is washed with diisopropylethylamine (DIEA) in dichloromethane (DCM) and N,N'-dimethylformamide (DMF). Then, a Trt-protected monomer such as Trt-Gly-OH is coupled to deprotected amino groups. The unreacted amino groups are capped using Acetyl glycine (Ac-Gly-OH). We have observed that the capping reaction (acetylation of unreacted surface amino groups using acetic anhydride) does not happen on our chip surface. Therefore, the unreacted amino

groups are capped via an amino acid coupling reaction, where the incoming amino acid is acetyl glycine.

Trt deprotection using EGA

Trityl (Trt) protecting groups require mild acidic conditions for their deprotection from amino groups. Treatment with aqueous solution of 5% trifluoroacetic (TFA) acid for 30 minutes is enough for its deprotection. This is compared to Boc groups, which require 30 minutes of exposure to 50% TFA in dichloromethane (DCM), and tert-butyl (t-bu) groups which require 30 – 90 minutes of exposure to 95% aq. TFA. We tested and optimized electrochemical deprotection of Trt groups during the gating step using N,N'-diphenylhydrazine and hydroquinone systems. In this study, a modified Trt group, Dimethoxytrityl (DMT) group, which is even more acid labile than Trt, was also included. Details of the study can be found in Appendix B.

From a MALDI based detection, Trt deprotection efficiency at 3.0V and 1 minute using N,N'-diphenylhydrazine as EGA-P was found to be approximately 60% per electrochemical deprotection step. Titration experiments were then conducted for improving the deprotection efficiency. Different conditions, ranging from 3.0V 1 min to 3.0V 10 min, were tested. At 3.0V 10 min, the deprotection efficiency was approximately 70%. From 3.0V 4min to 3.0V 10min, not much improvement in deprotection efficiency was observed (Figure 1).

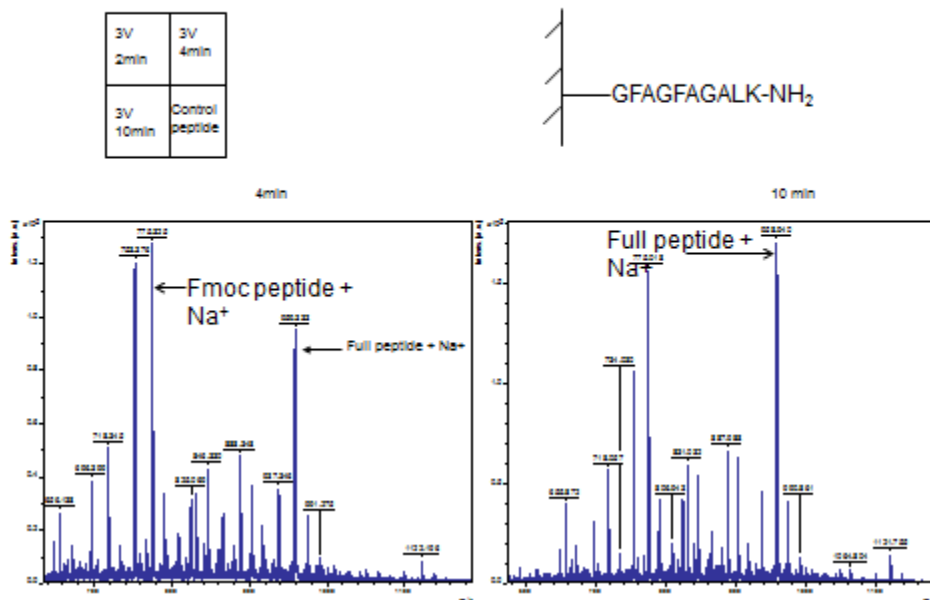


FIGURE 1: MALDI-MS characterization of electrochemical removal of trityl groups using *N,N'*-diphenylhydrazine as EGA. The two MALDI spectrums correspond to electro-deprotection of the trityl group under two different titration conditions, (i) 3.0V 4 min. and (ii) 3.0V 10 min. The label 'Fmoc Peptide' corresponds to NH₂-LAGAFGAFG-CONH₂, and the label 'Full Peptide' corresponds to NH₂-KLAGAFGAFG-CONH₂, where K was coupled after the gating step. Not much improvement was seen from 3.0V 4min to 3.0V 10 min. Approximately 70% of Trityl groups got electrochemically deprotected at 3.0V 10 min.

Based on this study, it was determined that with *N,N'*-diphenylhydrazine as EGA-P and at 3.0V 10 min, about 70% electrochemical deprotection efficiency of Trt could be achieved without any non-specific deprotection.

Boc electrochemical deprotection efficiency study using MALDI Mass Spectrometry

Electrochemical deprotection efficiency of boc group using EGA was tested for parallel synthesis on CBMX chips. Maurer et al. has reported its deprotection using EGA on 1K CBMX chips¹⁴. They analyzed the efficiency of the gating step by the fluorescence method. Using this method, percent deprotection yield appeared to be in the low nineties similar to what Maurer et al. has observed at 3.0V 3 min. In the meantime, we developed a MALDI mass spectrometry detection method of parallel syntheses on CBMX chips and glass slides. Similar experiments were conducted to confirm the percent deprotection yield, however, this time using the MALDI detection method. Surprisingly, the yields were not in the low nineties, and instead were in the low sixties. Various side products of the synthesis such as deletion peptides and truncated peptides were observed.

Titration experiments were then planned and different deprotection conditions were tested. Concentration of *N,N'*-diphenylhydrazine, electric potential, and the duration of application of potential were varied. Concentrations from 250mM to 750mM, potential difference from 2.0V to 3.3V and duration from 1min to 4mins were tested. The deprotection yield did not improve significantly and remained in the low sixties. From the MALDI detection method it was also observed that the Boc electro-deprotection using EGA was inconsistent. In a few trials, Boc electrochemical deprotection could be observed and in others no deprotection was seen at all. Some of the experiments which

involved two electrochemical deprotection steps in the peptide synthesis, either showed one deprotection or none using EGA. Several measures were taken to produce consistency in the electrochemical deprotection step. For example, fresh reagents and fresh deprotection solution were used, and the chips were kept in an inert atmosphere until the completion of the synthesis. Later on, the measurements consistently started showing less than 10% deprotection of Boc groups per deprotection step. During this series of experiments, CBMX made changes in the fabrication of their chips and started providing upgraded chips. In the earlier version of the chips, a bulk electrode of the electro-synthesis instrument was employed as a common counter electrode, whereas, in the upgraded version, a grid present within the chip can be employed as a counter electrode. It is possible that the changes made in chip fabrication resulted in consistent results of less than 10% deprotection of Boc groups.

One of the possible explanations for consistent stability of Boc groups seen during N,N'-diphenylhydrazine based gating step with the upgraded version of the instrumentation could be due to the ability of platinum to absorb large amounts of hydrogen. Microelectrodes involve fast mass transport of the electroactive species whereas the distance between the microelectrode and the grid counter electrode is extremely small. As a result, reduction of protons at the counter electrode to dihydrogen and its absorption by the platinum surface may become a competing reaction to the acidic reduction of the Boc groups at the anode. The changes in the chip fabrication may have made this phenomenon more prominent and hence Boc groups, which require stronger acidic conditions for deprotection via acidic reduction, could no longer be removed.

Stability of CBMX Chips to Strong Acids

Stability of CBMX chips to several acidic conditions was tested in order to optimize the side-chain deprotection conditions for in situ peptide synthesis. The general synthesis scheme on CBMX chips involves use of amino acids protected by acid-labile groups. The side-chains of such amino acids are usually protected with groups which are acid-labile under more stringent conditions. Some of these common side-chain protecting groups are Pbf (2,2,4,6,7-pentamethyldihydrobenzofuran-5-sulfonyl), Cbz (carboxybenzyl), Bn (benzyl), Bz (benzoyl), and t-butyl groups. Of these groups, Pbf, Cbz, Bn, and Bz require use of superacids for deprotection and t-butyl groups require use of highly concentrated TFA. In comparison, Boc and trityl groups can be removed using relatively weak acidic conditions, such as 50% TFA in DCM and 1% TFA in DCM respectively.

In order to determine the stability of CBMX chips to strong acids, the chip functionalized with MMT protected amines was used. The bottom one-third of the chip was electrochemically deprotected and 5(6)-carboxy fluorescein dye was coupled.

Fluorescence imaging of the chip was then carried out. The chip was then exposed to 95% TFA for 30 min and imaged using a fluorescence scanner. The fluorescence signals from the bottom one-third of the chip reduced, but the chip showed no signs of damage. The middle portion of the chip was then electrochemically deprotected, labeled with 5(6)-carboxy fluorescein dye and imaged for fluorescence. It was then exposed to 95% TFA for another 30 min, rinsed, and imaged. This time the chip showed signs of deterioration indicating that the chip remains stable to 95% TFA for 30 min, but not for a 60 min time

interval (Figure 2). In a similar experiment, the chip was exposed to trifluoromethane sulfonic acid. The chip did not withstand this treatment for the first 30 min time interval, indicating its susceptibility to superacids.

The stability of CBMX chips to 95% TFA for 30 mins proved to be sufficient for acid based chemical deprotection of t-butyl groups.

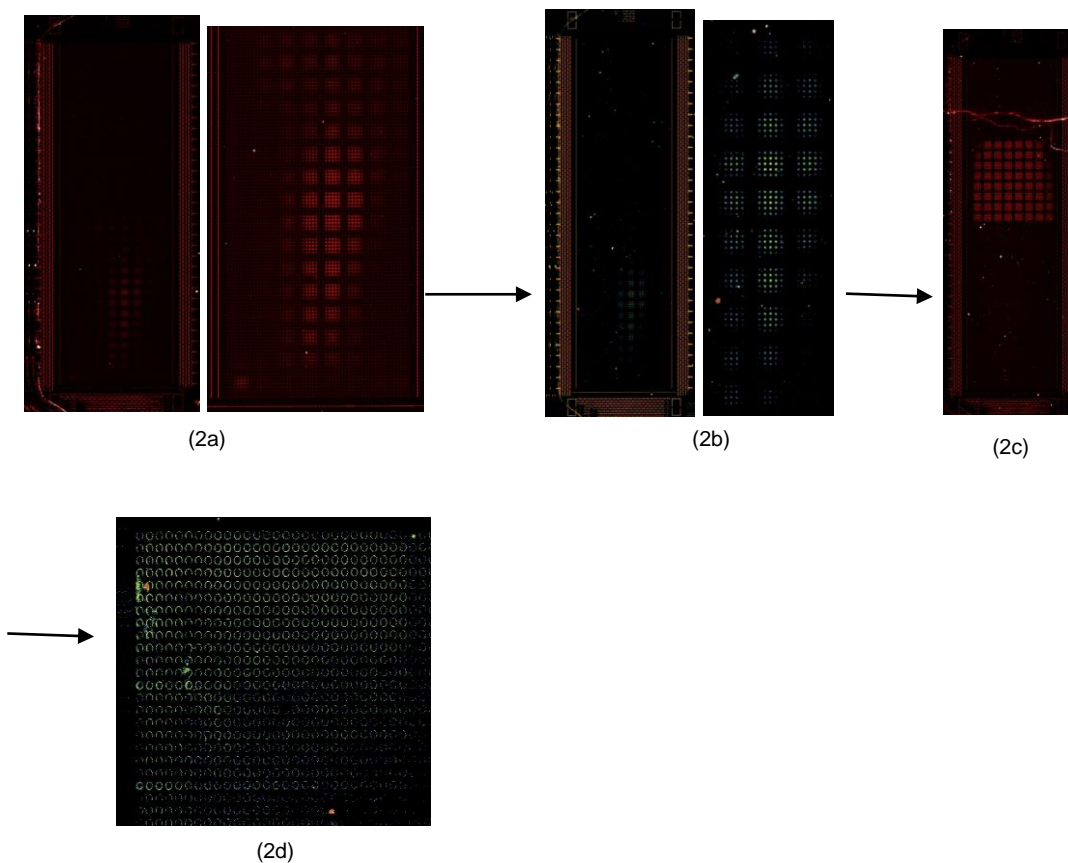


FIGURE 2: Fluorescence characterization of stability of CBMX chips to trifluoroacetic acid. A selected region of the chip was electrochemically deprotected and 5(6)-carboxy Fluorescein (fluorophore) was coupled to the free amines generated. Image (2a) is a fluorescence scanning image of the selected region after fluorophore coupling to the

electrochemically-deprotected region. Image (2b) is a fluorescence scanning image of the selected region after 30 min of exposure to 95% TFA and 5% H₂O. Image (2c) is a fluorescence scanning image of the chip after fluorophore coupling to the electrochemically-deprotected middle region of the chip. Image (2d) is a fluorescence scanning image after an additional 30 min of exposure to 95% TFA and 5% H₂O.

The above observations, (1) consistent stability of Boc groups towards N,N'-diphenylhydrazine system during the gating step, across many experiments with upgraded chips, and (2) stability of chips to 95% TFA for 60 mins exposure enabled the development of an orthogonal system, where the primary amine groups protected with trt could be deprotected using EGA, keeping the sidechain protecting groups (boc and t-bu) intact. The boc and t-bu groups can later be chemically deprotected without deteriorating the chip as it was observed in an experiment where t-bu groups got deprotected in near stoichiometric ratio upon treatment of the chip with 94% TFA for 30 min. Earlier, it was difficult to develop an orthogonal system when Boc was employed as primary amine protecting group. This was due to the inability of the chips to sustain superacid conditions required for deprotection of side chain groups.

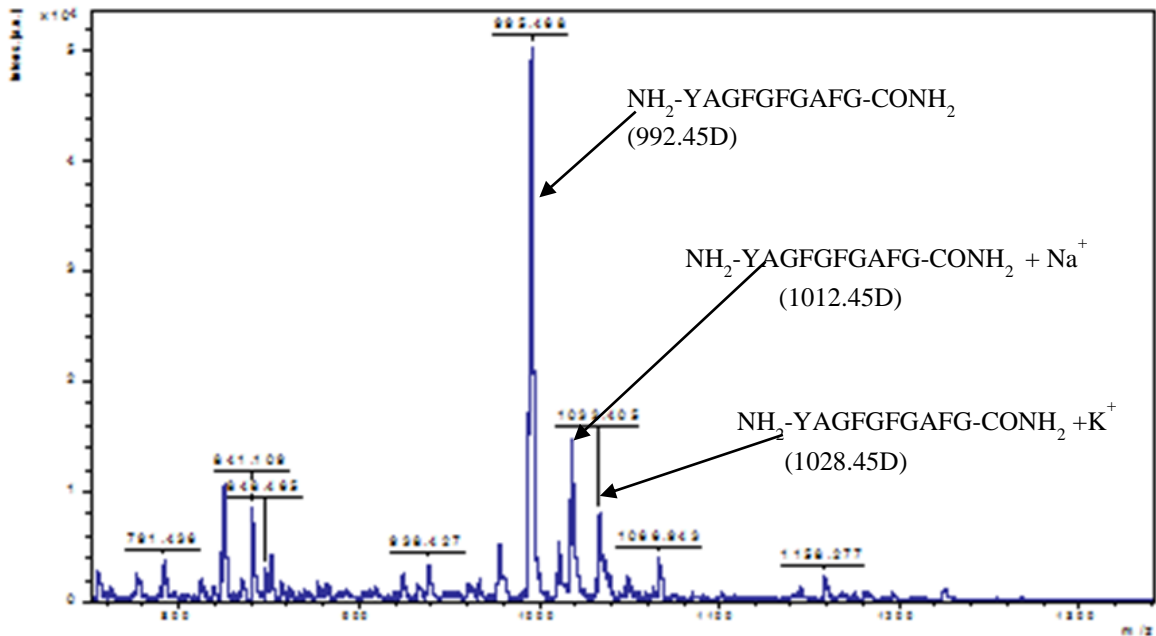


FIGURE 3: MALDI-MS characterization of chemical deprotection efficiency of t-butyl groups using TFA. A peptide $\text{NH}_2\text{-YAGFGFGAFG-CONH}_2$ was synthesized by Fmoc chemistry. The t-butyl group of Tyrosine was chemically deprotected using 94% TFA+ 5% H_2O +1% TIS for 30 minutes. The deprotection was complete as can be seen from the MALDI spectrum.

Capping Reaction Efficiency

In conventional peptide synthesis, after every coupling step a capping reaction is executed. This is done in order to cap the unreacted amines which did not participate in coupling step. These amines get capped with an acetyl group, and do not participate in further coupling steps. The capping reaction involves acetylation of free amines. The acetylation reaction is generally conducted using about 40 fold excess acetic anhydride and an organic base, such as pyridine or diisopropylethylamine. The duration of the step

is around 30 minutes. Although capping steps were included during syntheses, MALDI spectra truncated and deleted peptides with uncapped N-terminal amino group were often observed. One possible reason for the failure of a capping reaction could be the hydrolysis of the acetamide bond upon repeated exposure of the chip to EGA-P solution containing N,N'-diphenylhydrazine. Hydrazine can hydrolyze an acetamide bond, although it normally requires approximately 70°C and 1-12 h for this reaction to reach completion. Possibly, the platinum surface and /or voltage application on the chip facilitated the reaction. As a result, N-acetyl glycine was coupled after each coupling step. The coupling of N-acetyl glycine to the N-terminal of the peptide was done using a regular HBTU-based coupling reaction. The efficiency of N-acetyl glycine coupling was found to be nearly stoichiometric, similar to any other amino acid coupling in conventional Fmoc synthesis Figure 4.

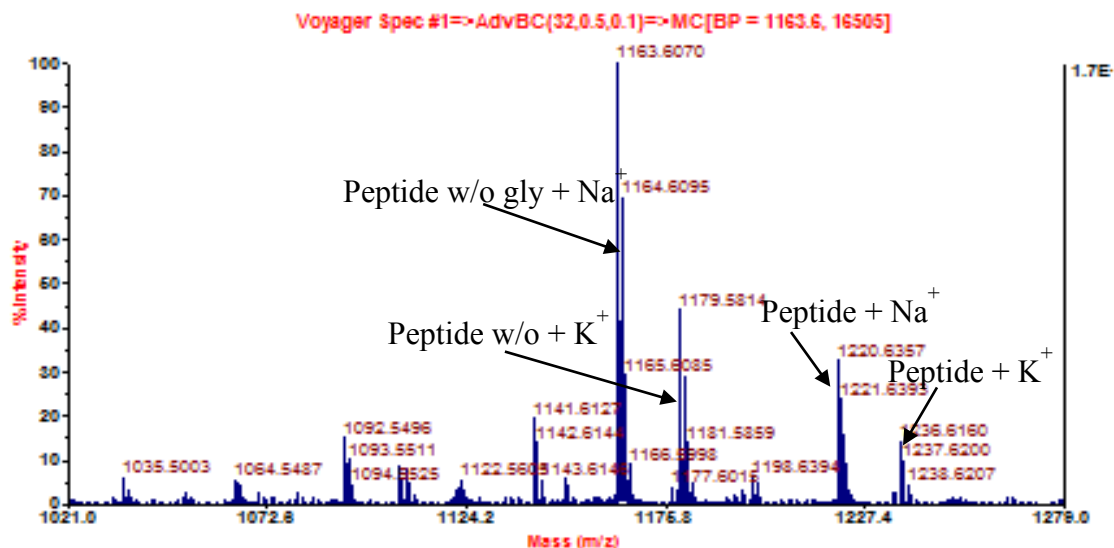


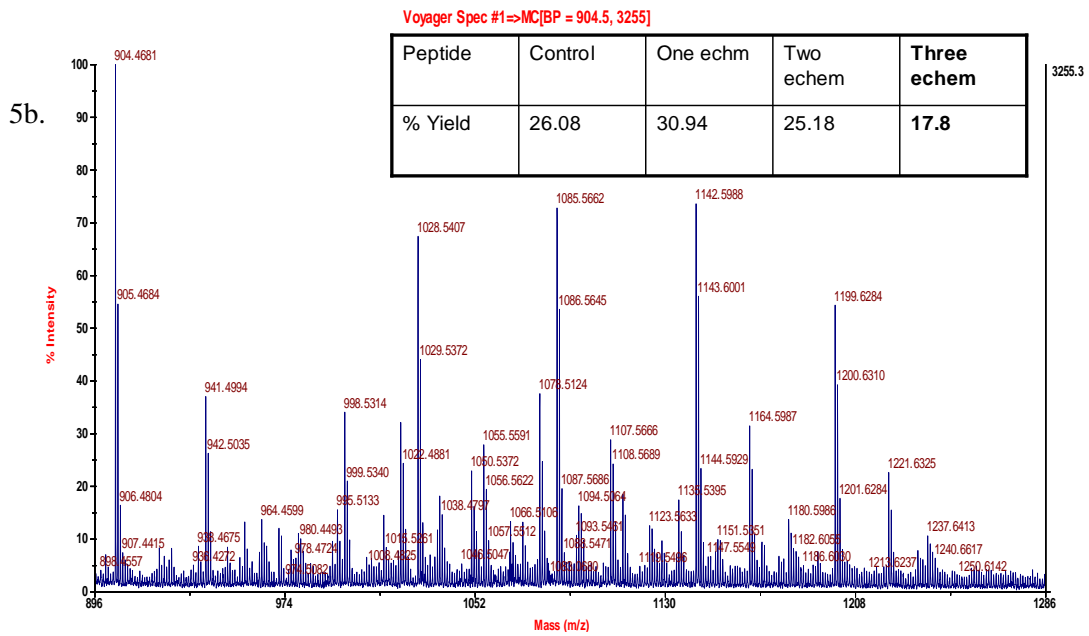
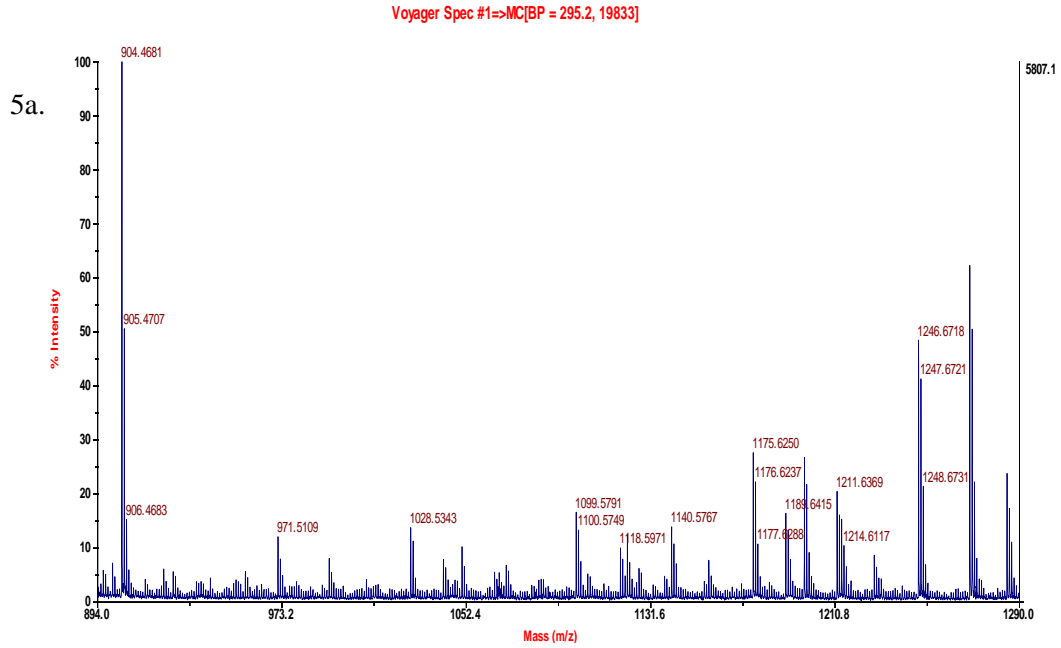
FIGURE 4: MALDI-MS characterization of capping reaction efficiency. A peptide N-Ac-GFAGFAGFAGAGAG-CONH₂ (peptide) was synthesized using Fmoc chemistry. The final amino acid coupled was N-acetyl glycine. The coupling efficiency of N-acetyl glycine was similar to coupling efficiency of any other amino acid in conventional Fmoc synthesis.

Peptide Synthesis with Three Electrochemical Deprotection Steps

Having developed an orthogonal system, in which the Trt from primary amine groups can be deprotected at the gating step with a 70% stepwise yield without deprotecting side-chain groups (boc and t-bu) considerably (less than 10%), we moved ahead to optimize peptide library synthesis with these capabilities. We aimed to

synthesize a peptide including three gating steps. The MALDI detection method discussed in Chapter 3 was convenient for optimizing the chemistry. A peptide sequence, $\text{NH}_2\text{-KAFGAFGAFG-CONH}_2$, was synthesized in which the first six coupling steps were performed using conventional Fmoc chemistry, and next three coupling steps involved electrochemical deprotection. Final coupling of lysine was done using Fmoc chemistry. Lysine was coupled in the final step to make the peptide protonable via its side chain amine group for MALDI detection. Only charged molecules can be detected by MALDI mass spectrometry and Lysine ϵ -amino group is highly protonable ($\text{pK}_a = 10.5$). The rest of the peptide sequence does not have strong protonable groups and can only show sodium and potassium adducts in the MALDI spectrum, which can be difficult to analyze. Amino acids used in the synthesis were Fmoc protected. For electrochemical removal of Trt groups, first the Trt was introduced by deprotecting Fmoc and coupling Trt in its place using Trt-Cl. Electrochemical deprotection involved N,N' -diphenylhydrazine as EGA-P and application of 3.0V for 10 minutes. The chip was divided into four sections: a control region involving no electrochemical step, a region involving one electrochemical step, a region involving two electrochemical steps, and a region involving three electrochemical steps. The MALDI spectra of the experiment showed that the peptide made with three electrochemical steps can be synthesized with approximately 42% yield. In this experiment, no capping step was involved after Trt protection of N-terminal amine groups using Trt-Cl. The synthesis conditions were made more stringent in the next experiment by involving capping via N-acetyl glycine after the

Trt coupling step. A similar experiment was performed, and the overall synthesis yield was found to be approximately 18%.



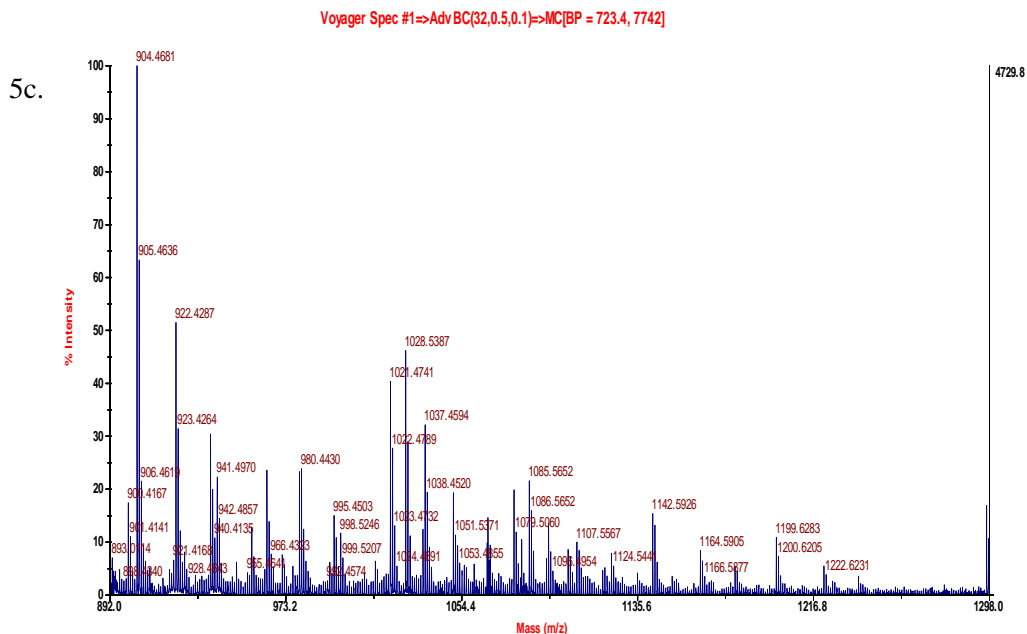


Figure 5: MALDI mass spectra 5a, 5b, and 5c correspond to peptide syntheses involving three electrochemical steps; (5a) does not involve capping step, Trt-cl used for Trityl incorporation, (5b) involves capping step, Trt-cl used for Trityl incorporation, and (5c) involves capping step, Trt-Gly-OH used for Trityl incorporation. Details of the peaks observed in MALDI spectra 5a, 5b, and 5c can be found in Tables 1, 2, and 3 respectively.

Table 1.

Details of the MALDI peaks observed in Figure 5a.

Peptide	Chemical Formula of Peptide	Peptide m/z Peak	% yield
Peptide with three electrochemical steps	NH ₂ -KAFGAFGAFGAFG-CONH ₂	1246.6718	41.59
Sodium adduct of Peptide with three electrochemical steps	NH ₂ -KAFGAFGAFGAFG-CONH ₂ + Na ⁺	1268.6718	
Potassium adduct of Peptide with three electrochemical steps	NH ₂ -KAFGAFGAFGAFG-CONH ₂ + K ⁺	1284.672	58.41
Peptide with two electrochemical steps	NH ₂ -KFGAFGAFGAFG-CONH ₂	1175.625	
Peptide with one electrochemical step	NH ₂ -KGAFGAFGAFG-CONH ₂	1028.5343	N/A
Control Peptide (no electrochemical step)	NH ₂ -KAFGAFGAFG-CONH ₂	971.511	
Calibration Peptide		904.4681	

Table 2.

Details of the MALDI peaks observed in Figure 5b

Peptide	Chemical Formula of Peptide	Peptide m/z Peak	% Yield	
Peptide with three electrochemical steps	NH ₂ -KGGGGAGAFGAFG-CONH ₂	1199.6283	9.4	
Sodium adduct of Peptide with three electrochemical steps	NH ₂ -KGGGGAGAFGAFG-CONH ₂ + Na ⁺	1221.6325		
Potassium adduct of Peptide with three electrochemical steps	NH ₂ -KGGGGAGAFGAFG-CONH ₂ + K ⁺	1237.6413		
Peptide with two electrochemical steps	NH ₂ -KGGGAGAFGAFG-CONH ₂	1142.5926		
Sodium of Peptide with two electrochemical steps	NH ₂ -KGGGAGAFGAFG-CONH ₂ + Na ⁺	1164.5905	90.6	
Potassium adduct of Peptide with two electrochemical steps	NH ₂ -KGGGAGAFGAFG-CONH ₂ + K ⁺	1180.5886		
Peptide with one electrochemical step	NH ₂ -KGGAGAFGAFG-CONH ₂	1085.5652		
Sodium adduct of Peptide with one electrochemical step	NH ₂ -KGGAGAFGAFG-CONH ₂ + Na ⁺	1107.5567		
Potassium adduct of Peptide with one electrochemical step	NH ₂ -KGGAGAFGAFG-CONH ₂ + K ⁺	1124.4441		
Control Peptide (no electrochemical step)	NH ₂ -KGAGAFGAFG-CONH ₂	1028.5387		
Sodium adduct of Control Peptide	NH ₂ -KGAGAFGAFG-CONH ₂ + Na ⁺	1051.5371		
Calibration Peptide		904.4681		N/A

Table 3.

Details of the MALDI peaks observed in Figure 5c

Peptide	Chemical Formula of Peptide	Peptide m/z Peak	% Yield
Peptide with three electrochemical steps	NH ₂ -KGGGGAGAFGAFG-CONH ₂	1199.6284	17.8
Sodium adduct of Peptide with three electrochemical steps	NH ₂ -KGGGGAGAFGAFG-CONH ₂ + Na ⁺	1221.6325	
Pottassium adduct of Peptide with three electrochemical steps	NH ₂ -KGGGGAGAFGAFG-CONH ₂ + K ⁺	1237.6413	82.2
Peptide with two electrochemical steps	NH ₂ -KGGGAGAFGAFG-CONH ₂	1142.5988	
Sodium of Peptide with two electrochemical steps	NH ₂ -KGGGAGAFGAFG-CONH ₂ + Na ⁺	1164.5987	N/A
Pottassium adduct of Peptide with two electrochemical steps	NH ₂ -KGGGAGAFGAFG-CONH ₂ + K ⁺	1180.5886	
Peptide with one electrochemical step	NH ₂ -KGGAGAFGAFG-CONH ₂	1085.5662	N/A
Sodium adduct of Peptide with one electrochemical step	NH ₂ -KGGAGAFGAFG-CONH ₂ + Na ⁺	1107.5666	
Pottassium adduct of Peptide with one electrochemical step	NH ₂ -KGGAGAFGAFG-CONH ₂ + K ⁺	1123.5683	N/A
Control Peptide (no electrochemical step)	NH ₂ -KGAGAFGAFG-CONH ₂	1028.5407	
Calibration Peptide		904.4681	N/A

The drop in overall percent yield from 42% to 18% after introduction of the capping step clearly indicated that Trt coupling using Trt-Cl was not 100% efficient. In related literature, the best overall yield achieved in coupling Trt to amine groups is approximately 80%. We emulated those conditions mentioned in the literature in our synthesis: 4hrs coupling with Trt-Cl in DMF. In order to improve the overall synthesis yield, Trt-Br and Trt-Gly were also tested instead of Trt-Cl. Overall synthesis yield with Trt-Br was similar to Trt-Cl, and overall synthesis yield dropped to approximately 9% from 18% when Trt-Gly was used instead of Trt-Cl (Figure 5). Trt-Br did not improve Trt coupling efficiency, even though Br is a good leaving group compared to Cl. Probably, the solvent involved during the step, DMF, was not optimum for maximizing the yield of the step. The reaction here is a unimolecular nucleophilic substitution reaction, which is favoured by protic solvents (the synthesizer is only compatible with a selected number of solvents, mostly aprotic solvents; ethanol, a protic solvent compatible with synthesizer, would have competed with amines of the surface as nucleophile). In contrast, here we are employing an aprotic solvent, N,N'-dimethylformamide (DMF). Low efficiency with Trt-Gly was expected because Trt-Gly is a large hydrophobic molecule. Its reactivity in a polar solvent, such as DMF, as well as owing to its large size, was expected to be low when compared to a facile S_N1 reaction using Trt-Cl.

Test of Alternate Linkers

Two alternate linkers, one photo-labile (ANP linker) and another acid-labile (Rink linker) were tested as substitute to Fmoc-Photo-labile linker. ANP linker underwent efficient deprotection under similar conditions as employed for Fmoc-Photo-labile linker.

Rink linker was deprotected using TFA acid-vapor rather than TFA acid solution in order to preserve the capability to characterize the peptide synthesis directly from the chip surface using chip MALDI mass spectrometry. Its deprotection efficiency was found to be similar to photolabile linkers. A discussion on this topic can be found in Results and Discussion section of Chapter 3.

Peptide Synthesizer and Electro-Synthesis Instrument Integration and Other Instrumentation Issues

In order to achieve synthesis automation, Peptide Synthesizer and Electrosynthesis instruments were integrated using LabView software. The peptide synthesizer was programmed to halt during the gating step in a synthesis cycle. During this halt period, the electrosynthesis instrument was activated to load a chip map and execute the gating step. A manual chamber made of PTFE with low reaction volume (100 μ L) was fabricated for peptide synthesis. Two types of chambers that were available at the time had issues. Firstly, a reaction chamber of the manifold, due to greater volume (200 μ L), led to contamination of chemicals from different synthesis steps (the internal pressure of peptide synthesizer was not enough to push the chemicals of the chamber out for incoming chemicals). Second, a reaction chamber of electrosynthesis instrument had a low volume of 100 μ L, but electronic circuitry present in it would get deteriorated due to the seeping of chemicals during synthesis. The electrical pads present on the side of the chip get deteriorated upon exposure to chemicals. These pads provide electrical connectivity with the electrosynthesis instrument and potentiostatic microarray reader. Therefore, a teflon based reaction chamber similar to polytetrafluoroethylene (PTFE)

based reaction chamber was fabricated to prevent exposure of the pads to TFA solution during the side-chain deprotection step. Details of the instrumentation issues are discussed in Appendix F.

Materials and Methods

Electrochemical Array Synthesis

Peptide synthesis is performed on 12,544 electrode (12K) semiconductor microchips (CBMX Corporation, Seattle, WA). Chip fabrication and its surface morphology has been described in detail in Chapter 1. Briefly, the 12K semiconductor microchip has 12,544 individually addressable, circular, porous polymer-coated platinum electrodes fabricated in rows and columns on silicon substrate. Electrodes contain either a 20-nucleotidepoly-T-spacer or 2-nucleotidepoly-T-spacer with an amine-modified terminal thymidine protected by monomethoxy trityl group. In all syntheses, an Fmoc-protected photolabile linker (Advanced Chemtech, Louisville, KY) was coupled as the C-terminal residue. Amino acid residues that are constant in all peptides in the array were coupled and deprotected using standard Fmoc synthesis protocols and commercially available Fmoc-protected amino acids purchased from either EMD Biosciences (Darmstadt, Germany) or Anaspec (San Jose, CA). Variable amino acid residues were coupled and deprotected using electrochemically-directed peptide synthesis. The following modifications to the described electrochemically-directed protocol were made. First, the localized generation of acids from *N,N'*-diphenylhydrazine (Sigma-Aldrich, Milwaukee, WI) by application of voltage to the addressed electrodes was conducted on

12K chips instead of a 1K chip. Second, voltage and time conditions for the electrochemical generation of acids were optimized to 3V 10 min for 12K chips.

MALDI Matrix Application and Characterization of Array Features

Experimental protocol for MALDI matrix application and characterization of features is discussed in Chapter 3 Materials and Methods section.

Non-Diffusional UV-Cleavage of Arrayed Peptides

Experimental protocol for non-diffusional UV-cleavage of arrayed peptides is discussed in Chapter 3 Materials and Methods section.

Non-Diffusional TFA Vapor Based Cleavage of Arrayed Peptides

Experimental protocol for non-diffusional TFA vapor based cleavage of arrayed peptides is discussed in Chapter 3 Materials and Methods section.

Preparation of N,N'-diphenylhydrazine Based EGA-P Solution

N,N'-diphenylhydrazine (200mg, 0.1M) and tetrabutylammoniumhexafluorophosphate (400mg, 0.1M) were weighed and added to a clean Erlenmeyer flask. Then 10mL of dichloromethane was added and shaken until all of the solid is dissolved and forms a pale yellow solution. The flask with the solution is kept loosely corked so that dichloromethane does not evaporate and alter the concentration of the solution. Once the electrosynthesis software is ready for the application of electric potential to the chip, the synthesis reaction chamber was filled with the solution. After the gating step, the solution is discarded and the chamber is rinsed 5x with dichloromethane, 3x with 5% DIEA in dichloromethane, and 5x with DMF. At this point, the chip is ready to undergo the coupling reaction.

Amino Acid Coupling Reaction

To achieve amino acid coupling, the chip terminating with free amines is exposed to a mixture of amino acid (Fmoc-Gly-OH: 37 mg, 137 mM, Trt-Gly-OH: 52mg, 137 mM), HBTU (*O*-benzotriazol-1-yl-*N,N,N',N'*-tetramethyluronium hexafluorophosphate, 95 mg, 137 mM), HOBT (*N*-hydroxybenztriazole, 33.5 mg, 137 mM), and diisopropylethylamine (130.5 μ L, 350mM) in DMF (2mL) for 30 minutes. The chip is then rinsed with DMF 3x, dichloromethane 3x, and again with DMF 3x, then re-exposed to the coupling mixture for another 30 minutes. After repeating the washing procedure (with an additional ethanol rinse to remove any residual DMF or dichloromethane), the chip is allowed to dry.

Trityl Coupling Reaction

To achieve trityl coupling, the chip terminating with free amines is exposed to a mixture of Trt-Cl (76.4mg, 137mM), and diisopropylethylamine (130.5 μ L, 350mM) in DMF (2mL) for 2hrs. The chip is then rinsed with DMF 3x, dichloromethane 3x, and again with DMF 3x, then re-exposed to a fresh mixture for another 2hrs. After repeating the washing procedure (with an additional ethanol rinse to remove any residual DMF or dichloromethane), the chip is allowed to dry.

Capping with Acetic anhydride

The chip is first washed 3x with 20mL DMF. It is then incubated with 50% acetic anhydride in DMF solution for 30min. The chip is then washed 3x with DMF, 3x with DCM, and dried with Argon gas.

Dye-Labeling Protocol and Fluorescence Detection

To achieve dye coupling, the CBMX chip terminated with free amines is exposed to a mixture of 5(6)-carboxy fluorescein (103.2mg, 137mM), DIC (diisopropylcarbodiimide, 43 μ L, 137mM), and HOBT (*N*-hydroxybenzotriazole, 33.5mg, 137mM), in 2mL of 2:1 DMF: DMSO for 60 minutes. The chip is then rinsed 3x with DMF, 3x with ethanol, and allowed to dry using argon gas. The chip is then removed and washed 3x with 1XTBST, for five minutes each. Next, the chip is washed 3x with ddH₂O, again for five minutes each. Then the chip is scanned at a 517nm wavelength with 70% PMT and 100% laser. ScanArray Express HT (Perkin Elmer Wellesley, MA) was used for fluorescence imaging.

Acid Based Chemical Deprotection

(a) A cocktail of 95% TFA (Sigma-Aldrich, St. Louis, MO) + 2.5% triisopropylsilane (TIS) (Sigma-Aldrich, Milwaukee, WI) + 2.5% water was used for a stability test of the CBMX chips to TFA. The chip was placed in an acid-resistant chamber and exposed to the deprotection cocktail for thirty minutes. At regular time intervals, the setup was shaken for a better reaction. After thirty minutes, the solution was discarded in acid waste and the reaction setup was rinsed 5x with dichloromethane, 5x with 5% DIEA in dichloromethane, 3x with DMF, and 5x with water. The chip was then dried with argon gas.

(b) The chip was rinsed 3x with DMF, 3x with DCM, and thoroughly dried. The chip was then placed in a glass cuvette and 20 μ L of thioanisole and 10 μ L of ethanedithiol were added. The glass cuvette was then cooled in an ice bath and 1mL of

TFA was added. The reaction setup was stirred for 10 minutes. Next 20 μ L of TFMSA was added slowly, drop-wise, with vigorous stirring. The reaction setup was stirred at room temperature for 60 minutes. The chip was then rinsed with a small amount of TFA, 3x with DCM, 3x with DMF, and 5x with H₂O followed by drying with argon gas.

Conclusion

In conclusion, we have optimized several aspects of peptide synthesis on 12K CBMX chips. Specifically, we can deprotect trityl groups per gating step with 70% efficiency using N,N'-diphenylhydrazine as EGA-P solution. We have optimized the electrosynthesis system to synthesize a peptide with three gating steps involved, with an overall yield of 18%. We have developed an orthogonal system for peptide microarray synthesis, where the primary amines are protected with trityl groups and side-chain groups are protected with t-butyl or Boc groups. The acid generated during the gating step is strong enough to remove trityl groups without affecting t-butyl or Boc groups. We have done careful study of stability of Trityl and Dimethoxytrityl groups upon exposure to N,N'-diphenylhydrazine and Hydroquinone based EGA-P solutions. We determined that Trityl groups are stable to N,N'-diphenylhydrazine-based EGA-P solution and have optimized peptide synthesis employing trityl as primary amine protecting group. We have optimized several aspects of peptide synthesis, such as in situ coupling of trityl groups to N-terminal free amines of peptides, efficiency of chemical deprotection of t-butyl groups, and stability of chips upon exposure to TFA for t-butyl deprotection. In addition we have optimized the efficiency of the capping reaction, efficiency of alternate linkers, and stability of Boc groups during the gating step. Several issues related to the electro-

synthesis instrument and peptide synthesizer were solved. These were the integration of both the instruments to fully automate the synthesis as well as the fabrication of manual reaction chambers with low reaction volumes so that peptide synthesizer can push the solutions forward and avoid contamination of solutions from different steps of synthesis cycle. Lastly, this included the fabrication of acid resistant chambers to carry out acid-based chemical deprotection reactions.

References

1. O. Stoevesandt, M. J. Taussig, M. He, Protein microarrays: high-throughput tools for proteomics. *Expert Review of Proteomics* **6**, 145 (2009).
2. V. Tapia, J. Bongartz, M. Schutkowski, N. Bruni, A. Weiser, B. Ay, R. Volkmer, M. Or-Guil, Affinity profiling using the peptide microarray technology: A case study. *Analytical Biochemistry* **363**, 108 (2007).
3. K. Stoffel, H.V. Leeuwen, A. Kozik, D. Caldwell, H. Ashrafi, X. Cui, X. Tan, T. Hill, S. Reyes, C. Wo, M. Jose, R.W. Micheltore, A.V. Deynze, *BMC Genomics* **13**, 185 (2012).
4. H. Park, J. Kim, Y.S. Ju, O. Gokcumen, R.E. Mills, S. Kim, S. Lee, D. Suh, D. Hong, H.P. Kang, Y.J. Yoo, J.Y. Shin, H.J. Kim, M. Yavartanoo, Y.W. Chang, J.S. Ha, W. Chong, G.R. Hwang, K. Darvishi, H.R. Kim, S.J. Yang, K.S. Yang, H. Kim, M.E. Hurler, S.W. Scherer, Discovery of common Asian copy number variants using integrated high-resolution array CGH and massively parallel DNA sequencing. *Nature Genetics* **42**, 400–405 (2010).
5. J.C. Mills, K.A. Roth, R.L. Cagan, J.I. Gordon, DNA microarrays and beyond: completing the journey from tissue to cell. *Nature Cell Biology* **3**, E175-E178 (2001).
6. G. MacBeath, S.L. Schreiber, Printing proteins as microarrays for high-throughput function determination. *Science* **289**, 1760-1763 (2000).
7. O.P. Kallioniemi, U. Wagner, J. Kononen, G. Sauter, Tissue microarray technology for high-throughput molecular profiling of cancer. *Mol. Genet.* **10**, 657-662 (2001).

8. H. Wu, J. Ge, M. Uttamchandani, S.Q. Yao, Small molecule microarrays: the first decade and beyond. *Chem Commun(Camb)* **47**, 5664-5670 (2011).
9. K. Hattori, S. Sugiura, T. Kanamori, Microenvironment array chip for cell culture environment screening. *Lab on a Chip* **11**, 212-214 (2011).
10. R. Frank, SPOT-synthesis: an easy technique for the positionally addressable, parallel chemical synthesis on a membrane support. *Tetrahedron* **48**, 42:9217-9232 (1992).
11. S. Fodor, J. Read, M. Pirrung, L. Stryer, A. Lu, D. Solas, Light-directed, spatially addressable parallel chemical synthesis. *Science* **251**, 767-773 (1991).
12. S. Singh-Gasson, R.D. Green, Y.J. Yue, C. Nelson, F. Blattner, M.R. Sussman, F. Cerrina, Maskless fabrication of light-directed oligonucleotide microarrays using a digital micromirror array. *Nature Biotechnology* **17**, 974-978 (1999).
13. V. Stadler, T. Felgenhauer, M. Beyer, S. Fernandez, K. Leibe, S. Güttler, M. Gröning, K. König, G. Torralba, M. Hausmann, V. Lindenstruth, A. Nesterov, I. Block, R. Pipkorn, A. Poustka, F.R. Bischoff, F. Breitling, Combinatorial synthesis of peptide arrays with a laser printer. *Angew. Chem. Int. Ed.*, **47**, 7132-7135 (2008).
14. V. Stadler et al., Combinatorial synthesis of peptide arrays with a laser printer. *Angewandte Chemie International Edition* **47**, 7132-7135 (2008).
15. K. Maurer, A. McShea, M. Strathmann, K. Dill, The removal of the t-boc group by electrochemically generated acid and use of an addressable electrode array for peptide synthesis. *J. Combi. Chem.* **7**, 637-640 (2005).
16. E. LeProust, J.P. Pellois, P. Yu, H. Zhang, O. Srivannavit, E. Gulari, X. Zhou, X. Gao, Digital light-directed synthesis. A microarray platform that permits rapid reaction optimization on a combinatorial basis. *J. Comb. Chem.* **2**, 349-354 (2000).
17. X.Y. Xiao, R. Li, H. Zhuang, B. Ewing, K. Karunaratne, J. Lillig, R. Brown, K.C. Nicolaou, Solid-phase combinatorial synthesis using MicroKan reactors, Rf tagging, and directed sorting. *Biotechnol Bioeng.* **71**, 44-50 (2000).
18. K. Dill, D. Montgomery, W. Wang, J.C. Tsai, Antigen detection using microelectrode array microchips. *Anal.Chim. Acta* **444**, 69 (2001). (b) D. Montgomery, U.S. Patent 6,093,302 (2000). (c) D. Montgomery, U.S. Patent 6,280, 595 (2001).

Chapter 5

Investigation of Novel Applications of CombiMatrix Microarray Platform In Conjunction With MALDI Mass Spectrometry and Electrochemical Detection Techniques

Abstract

Novel applications of CBMX microarray platform were explored such as searching metal binding catalytic peptides to reduce overpotential associated with water oxidation reactions. In addition the fabrication of peptide microarrays via co-electropolymerization of pyrrole as well as peptide derivatized with pyrrole were also explored. MALDI mass spectrometry and electrochemical detection techniques were used in the investigation of these applications. The Potentiosense microarray reader designed for CBMX custom arrays was used for electrochemical detection. Using this reader, electrochemical signals from the 12K custom microarray can be collected in approximately 60-second time intervals. Several parameters of the instrument have been studied and optimized, including its noise characteristics at high and low voltages and the manipulation of software to scan in different ways based on voltage, current, and chip-map parameters. In addition, the determination of the length of the linker for optimal signal detection was studied and optimized. Due to the portability of the equipment, the absence of quenching of signals, and the capability to measure redox activity, electrochemical detection techniques based microarray readers have interesting potential applications.

Introduction

Microarray-based research involves probing several molecular interactions, concurrently, on a single platform, at resolutions high enough to discriminate between single building blocks at specific positions^{1,2,3}. It enjoys the advantage of incorporating a varied range of synthetic building blocks when compared to other library generating techniques¹. Some other advantages of microarray technology are the use of a small amount of analyte, a fast and direct read out of the activity of the whole library, reproducibility of the microarray for multiple experiments, and the ability to integrate systems with desired features. Fluorescence detection methods⁴ are the most widely-employed technique in microarray synthesis and binding analysis. In this technique a fluorescent dye is associated either directly or indirectly with the analyte and imaged using a fluorescence scanner. Fluorescence signals proportional to the strength of binding are observed. However, there are some drawbacks of this method. They include the difficulty to determine the chemical make-up of microarray synthesis products, possibility of influence of fluorophore in peptide-protein binding due to modification in surface characteristics of proteins and peptides after labeling. In addition, real-time binding kinetics cannot be determined, signal-to-noise ratio is sometimes difficult to improve, and labeling efficiency could vary, making quantification of detection error-prone. Also, the fluorescent microarray scanner is cumbersome, delicate, expensive, and usually requires a separate benchtop area. In the past few years microarray analysis based on other detection methods have made rapid progress. Examples of this include surface plasmon resonance imaging (SPRi)^{5,6}, electrochemical impedance spectroscopy (EIS)^{7,8},

and mass spectrometry (MS)^{9,10,11}. Different detection methods bring different analytical capabilities, and can serve a compliment to the fluorescence detection method or to each other. For example, SPRi can be used to study real-time binding kinetics and MS can be used to directly characterize microarray synthesis and protein-peptide binding. Similarly, electrochemical detection methods bring unique analytical capabilities. The instrumentation involved in these methods is simple, portable, and less expensive. Conductivity, capacitance and impedance measurements have the capability to directly monitor the changes occurring on the electrode surfaces^{12,13,14,15}. An added advantage with redox label mediated electrochemical detection method is that signals can be amplified, thereby making the detection highly sensitive¹⁶.

Redox Enzyme Mediated Measurements

One approach to redox enzyme based detection involves a three electrode system¹⁷. In this approach the enzyme converts a redox inactive compound to a product that can be oxidized at one electrode and reduced at another. In this approach, signal amplification is dependent on enzyme concentration. A drawback of this approach is that the density of electrodes on a single platform is limited, due to large number of leads required per electrode. Another approach involves a unique combination of a redox enzyme, redox substrate, and an electrode to generate an electronic signal¹⁶. With this method, signal amplification is independent of the concentration of the enzyme. Since the electrode is used to monitor signals, a three-electrode system is not required. As a result, the fabrication of a high density of electrodes on a single platform can be achieved. CBMX has developed a microarray reader, Potentiosense, which is based on this

approach. It reads each electrode in a serial fashion and measures the redox activity from each site.

In the CBMX electrochemical detection method, horseradish peroxidase is usually the redox enzyme. It oxidizes 3,3',5,5'-Tetramethylbenzidine (TMB) in the presence of hydrogen peroxide. The oxidized product is then reduced at the microelectrode of the CBMX chip. Signal amplification is achieved in this method because the redox enzyme is capable of rapidly oxidizing TMB. The CBMX chip is placed in a chamber and exposed to buffers and enzyme substrate. The whole arrangement (chamber with chip and buffer) is then placed within the instrument's holder and an electrical connection with the instrument is made. This is done through contact between the electrical pads of the chip and several pins of the reader. Each electrode has a capacitor associated with it, in which charge gets built-up during the redox process. The built-up charge, when released, results in a current flow which upon detection and processing, results in a digital image of the binding activity.

MALDI mass spectrometry is one of the most widely-used analytical techniques in proteomics^{18,19,20}. As microarray research advances toward more mature systems, it is important to develop protein identification and characterization techniques to meet the requirements of high-throughput systems. The combination of microarrays and MALDI-MS has the potential to become a potent tool to meet this requirement⁹.

MALDI-MS can provide chemical make-up information about microarray synthesis⁹ and protein-peptide interaction²¹. This is difficult to obtain through other techniques. Combining MALDI-MS and electrochemical detection techniques could offer

new capabilities in protein analysis. In this chapter, we investigate novel applications of CBMX microarray platform in conjunction with MALDI mass spectrometry and electrochemical detection technique. PotentioSense microarray reader, designed for CBMX custom arrays, was used for electrochemical detection. Specifically, microarray experiments were conducted to search for metal binding catalytic peptides to reduce overpotential associated with anodic half reaction of water splitting^{22,23}. Experiments were also conducted to develop a new method of fabricating peptide microarrays using electro-polymerized pyrrole polymer. Before conducting these tests several parameters of the PotentioSense were studied and optimized. These parameters include inherent noise associated with the instrument during electrical measurements at high and low voltages and the determination of the length of linker suitable for efficient electrochemical detection using HRP conjugated avidin-biotin interaction. Additionally, we investigated the electronic communication between peptide probes and electrodes by examining redox behavior of Ferrocene, when it was placed at varying distances from the electrode surface via peptides of varying lengths.

Overpotential associated with anodic half-reaction of water splitting: Direct conversion of water to molecular hydrogen and oxygen via electrolysis followed by regeneration of electrical power in a hydrogen fuel cell would be, in principle, an ideal mechanism for the generation and utilization of hydrogen^{24,25}. However, there are a number of problems that still have yet to be solved. One of these problems stems from the fact that the conversion of water to hydrogen via electrolysis using conventional metal electrodes involves substantial activation energy. This necessitates that the

reaction be driven by a considerably higher potential than simple thermodynamics would demand. This overpotential represents a significant energy loss during conversion, impacting the economic practicality of using hydrogen as a fuel in this way.

The biggest part of this overpotential comes from the water-splitting reaction at the oxygen evolving electrode (the anode). This is because of the multi-electron nature of the reaction and the high energy, as well as the partially oxidized intermediates that must be formed in order to generate molecular oxygen and protons from water. Fortunately, nature has developed a catalyst, the oxygen evolving complex (OEC) of photosystem II, which works with almost no overpotential for this reaction^{22,26}. The OEC contains four manganese atoms that have a structure and chemical environment defined by the surrounding protein. The manganese cluster is directly involved in the redox process and stabilizes the highly reactive intermediates in the oxidation of water. In recent years, a considerable amount has been learned about the characteristics of this complex. This includes the redox properties of the manganese atoms at various stages during the four electron oxidation of water as well as the structure of the surrounding protein at 1.9 Å high resolution²².

We tested a novel combinatorial biochemical approach to develop manganese binding peptides for modification of the surface of the electrolysis anode used during hydrogen production. The design of these peptides included features of the OEC and of a model system developed at Arizona State University. In this design, the bacterial reaction centers lacking the OEC have been modified to bind and oxidize manganese²⁷. The approach involves the electrochemically-mediated production of a library of manganese-

binding peptides using a process developed in our lab, with support from researchers at CBMX. It involves electrochemical generation of peptide microarrays on CBMX chips. Each member of the library is attached to a different microelectrode on a fabricated surface. The current/voltage characteristics of each electrode is measured in series, using the PotentioSense microarray reader, looking for the peptide/Mn complexes that result in the lowest overpotential for water splitting. These peptide sequences will then be used as the initial guesses for a subsequent round of molecular evolution, etc. In principle, similar techniques could also be used to develop catalysts for the hydrogen evolving cathode (e.g., using hydrogenase as a model) or for the electrodes in hydrogen fuel cells.

Peptide immobilization via co-electro-polymerization of pyrrole modified peptide (peptide-py) with pyrrole: Co-electro-polymerization of a peptide-py and pyrrole molecules can prove to be an alternative method of fabricating peptide microarrays on CBMX chips. Minehan et al. has demonstrated immobilization of oligonucleotides on electrodes using electro-polymerized pyrrole polymer²⁸. Since then, several electro-active polymers have been studied for DNA immobilization^{29,30}. The immobilized oligonucleotides were detected using fluorescence, cyclic voltammetry, and impedance-based detection methods. Maurer et al. and Cooper et al. have reported immobilization of antibodies and oligonucleotides on CBMX chips using electro-polymerized pyrrole polymer^{31,32}. They incubated antibodies and oligonucleotides in the porous pyrrole polymer, electro-deposited on the electrode surface. Several parameters, such as electrical conditions and pyrrole concentration, were optimized to achieve optimal incubation. A more pertinent study for our research has been reported by

scientists at Bio International. They performed co-electro-polymerization of pyrrole and pyrrole modified oligonucleotides on a chip possessing a set of 128 individually addressable microelectrodes^{33,34}. We have investigated the possibility of immobilizing peptides on CBMX chips by co-electro-polymerizing Ppy with pyrrole molecules. The efficiency of the approach was evaluated using the PotentioSense microarray reader.

Ferrocene as a reference molecule: The ferrocene molecule undergoes reversible one-electron reduction/oxidation at 0.5V vs a saturated calomel electrode. Substituents on the cyclopentadienyl rings of the molecule alter its redox potential either in a positive or negative direction. The electron-donating substituents alter it in a positive direction, and the electron-withdrawing substituents alter it in a negative direction. Due to its low redox potential and reversible nature, ferrocene is often used as reference molecule in electrochemistry³⁵. The cyclopentadienyl rings coupled to the iron atom in the ferrocene molecule are amenable for synthetic chemistry³⁶. This capability is leveraged to couple the ferrocene molecule to the electrode surface via amide bond formation between the carboxylic acid group of ferrocene carboxylic acid and amine group present on the surface. Several redox assays would require confirming that electronic communication between electrodes and the fabricated molecule on it is possible. The ferrocene molecule is an ideal external standard for this purpose due to the low and reversible redox potential associated with it, as well as the synthetic maneuverability possible with it. The redox behavior of ferrocene tagged on top of a peptide of a certain length, if communicates with the electrode would establish that the

redox activity of the probe peptides of certain lengths of a microarray could be investigated.

Results and Discussion

PotentialSense Detection Principle

A CBMX 12K microarray consists of 12,544 individually addressable microelectrodes, underlying CMOS based circuitry, and thirteen electrical contact pads. This provides electrical connectivity to the PotentialSense microarray reader. The microelectrodes are made up of platinum, and are 45 microns in diameter and spaced from each other by 75 microns. These electrodes are coated with a bio-polymer, which provides a three dimensional porous milieu. Each electrode is surrounded by a circular ring, like a platinum electrode, which acts as counter electrode. The PotentialSense reader can read the electrical signals from all the electrodes in approximately 60 seconds, taking no more than 5 milliseconds, to read an individual electrode. The instrument is sensitive to electrical signals between 100 – 200,000pA, therefore, assays involving large signals can be measured using the instrument. A peptide probe on an electrode, chemically coupled to biotin at N-terminus, multiplexes with SRP-HRP fusion protein present in the solution. The chip, after multiplexing, is exposed to a solution containing 3,3',5,5'-tetramethylbenzidine (TMB) and hydrogen peroxide. The oxidized product of TMB released from HRP is reduced at the surface of the electrode. The electrochemical signal thus obtained is measured using the PotentialSense microarray reader.

Determination of the Optimal Length of Linker for Electrochemical Detection

Initial tests were performed to verify the electrochemical detection capability on an array containing biotin-labeled oligos of varying lengths (purchased from CBMX for the purposes of testing). This array was incubated with a HRP-streptavidin fusion protein. HRP emits a continuous electrochemical signal. We looked at linker-length dependence of the electrochemical signals and found that the shorter linkers, which positioned the biotin within a nanometer (nm) of the surface, showed the strongest signals. It also showed that the signal decreased rapidly as the linker became longer (Figure 1). The strong linker length dependence was surprising, given the size of the HRP-streptavidin fusion protein.

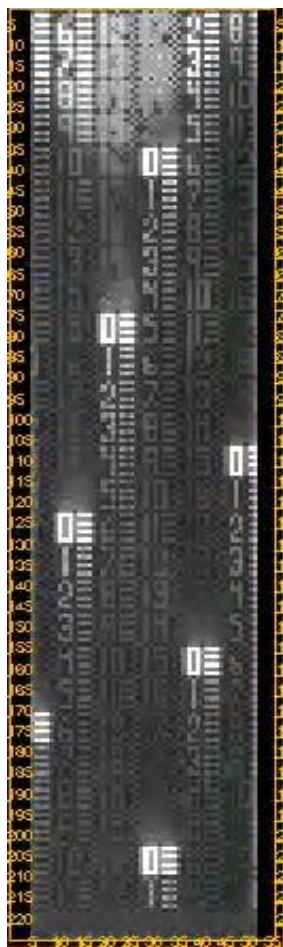


FIGURE 1: Electrochemical detection of synthesis by Biotin-SRP-HRP assay. Each number represents the length of the Poly T linker on top of which biotin was chemically coupled.

Noise Characteristics of PotentioSense Instrument

Electrical current signals were read from each electrode in the presence of TRIS buffer upon application of voltages ranging from 0.6V – 2.4V. The 12,544 electrodes are embedded on the chip in 224 rows and 56 columns. The PotentioSense instrument reads current values from each electrode in a serial fashion. Three kinds of noises were observed with the instrument. Firstly, a periodic noise; current values from the electrodes near the edges were greater compared to the current values from electrodes present in the middle of the row. Secondly, a drift in current signals; the electrodes that were read first, under the same measurement conditions, gave less current values compared to the electrodes that were read later. Lastly, with increase in applied voltage, the periodic as well as the drift noise increased. The abovementioned three noise characteristics can be seen in Figure 2. The real current values can be differentiated from the noise of the instrument by employing mapping strategies and performing statistical analysis. For example, several replicates of electrodes can be planned on different parts of the chip so that the noise related to drift can be corrected, and high current values from the electrodes present at the edges can be neglected. Such steps were taken while searching for catalytic peptides for a water oxidation reaction. It can be seen in Figure 2 that no such correction steps are required when the applied voltage is less than 1.0V during measurements.

Therefore, assays such as one based on HRP, which requires electrodes at low potential (100mV) to monitor electrical signals, does not need any correction.

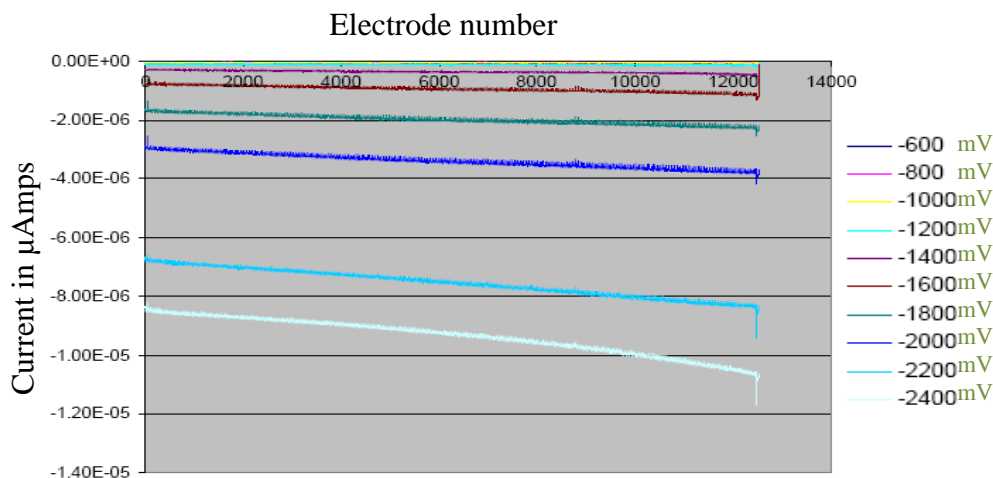


FIGURE 2: I/V analysis of Potentiosense microarray reader. Currents from all electrodes, while stepping down the voltage 200mV each time. Tris Buffer was used for measurements.

Ferrocene as a Reference Molecule

Because the redox activity of ferrocene is well known, it can be used to determine the degree to which synthesized peptides were communicating with electrodes. It can also be used to differentiate the peptide signals from the instrument noise. Various ferrocene-containing peptides were synthesized on a CBMX slide at 40% yield (Figure 3). Some positions on the slide contained ferrocene only. Some contained peptides that were four amino acids in length ($\text{NH}_2\text{-Fc-GKFG-CONH}_2$) with N-terminal ferrocenes, and some peptides were full-length (9 amino acids, $\text{NH}_2\text{-Fc-KFGKFGKFG-CONH}_2$) with N-

terminal ferrocenes. Some positions on the slide contained neither ferrocene nor peptide. All variants occurred in replicate on regions distributed throughout the slide. We then measured the redox activity on the slides with a voltage sweep. Figure 4 is an I-V comparison of the two extremes: the full-length, ferrocene-coupled peptide versus the plain slide containing neither ferrocene nor peptide. In order to get a more complete picture, we attempted to run a piece-wise current-voltage curve for the different electrodes by cycling through voltages and measuring currents. A bump in the curve at the right oxidation potential for ferrocene was observed. This was lacking in the same region of the control curve, where no ferrocene was coupled. It is likely the case that under the conditions we were running the tests, it was not possible to achieve true equilibrium current/voltage relationships. The PotentioSense instrument scans the electrodes at fixed voltages, and the scan rates are fixed and cannot be altered. This is very different from the Cyclic Voltametry instrument, where the voltage sweep is continuous and scan rates can be varied. However, ferrocene, at least, appeared to give a signal, which suggested that there was some communication between the surface and the peptides.

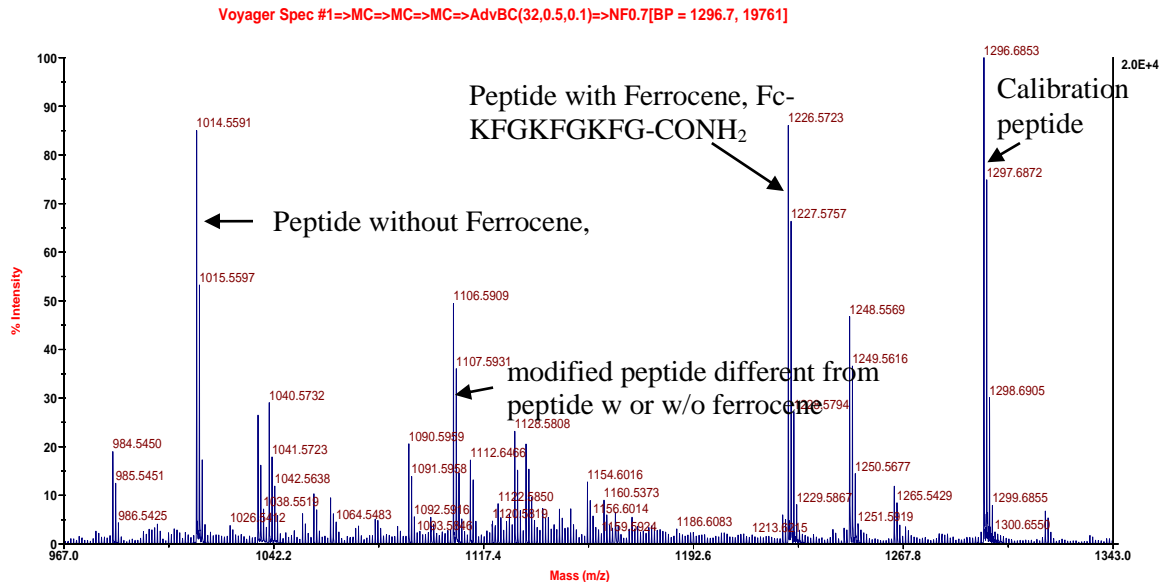


FIGURE 3: MALDI-MS characterization of coupling of ferrocene carboxylic acid to free amines on CBMX chip surface. A modified peptide containing ferrocene (Fc), $\text{NH}_2\text{-Fc-KFGKFGKFG-CONH}_2$, was synthesized and analyzed by MALDI Mass Spectrometry. Ferrocene was attached to the peptide through an amide bond formation reaction between the ferrocene carboxylic acid and the N-terminal Lysine of the peptide which was synthesized in situ on the chip using conventional Fmoc synthesis.

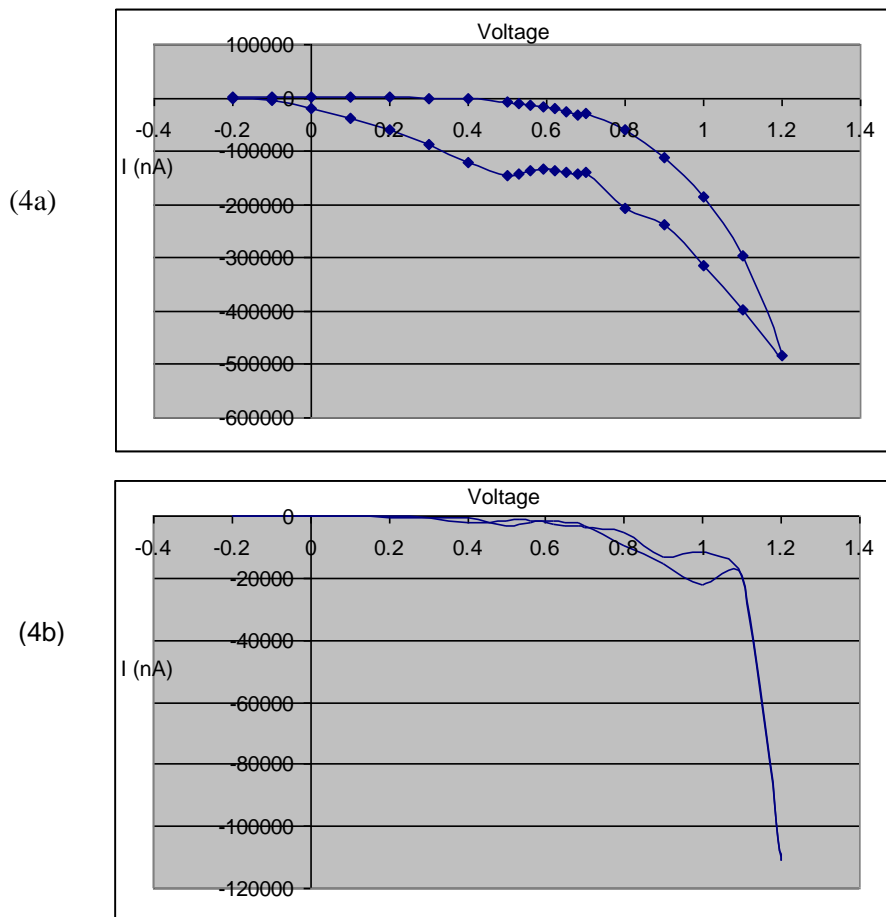


FIGURE 4: I/V analysis of ferrocene labeled CBMX chips. Panel (4a) represents current measurements at various fixed voltages corresponding to electrodes possessing full-length, ferrocene-coupled 9-mer peptides and panel (4b) represents measurements from the control region.

Search for peptide catalysts for water oxidation reaction: We (a team of members from Prof. Dr. Neal Woodbury, Prof. Dr. James Allen, and Prof. Dr. Trevor Thornton's group) fabricated electrodes in-house to search for peptide catalysts for the anodic oxidation of water. Gold electrodes were functionalized with a polyindole layer via electropolymerization of aminated indole molecules. Peptides were attached to the gold

electrode through amine groups of the polyindole layer. IR analysis revealed the successful attachment of the aminated polyindole and the peptide derivatized polyindole to the gold electrode. The I/V curves of water electrolysis on bare electrodes, electrodes functionalized with electro-polymerized aminated polyindole, and electrodes functionalized with electro-polymerized polyindole-peptide all revealed that currents from functionalized electrodes were less in comparison to bare electrodes. This was expected, due somewhat to insulation caused by the polyindole layer. For the robust attachment of polyindole to the electrode, 2% thiolated-indole was added to an indole electro-polymerization solution. This improved the attachment as several runs of electrolysis experiments could be executed.

Manganese binding peptides were designed by Prof. Dr. James Allen's group to search for a catalyst for the anodic half-reaction of water splitting. We intended to emulate the metal-protein environment in OEC in our catalyst design. In OEC, metal atoms, a cluster of four manganese atoms and a calcium atom, coordinated with surrounding amino acids catalyze water oxidation reaction. In our initial round of the catalyst search, the peptide sequences that would bind single manganese atoms were designed. Sequences of some of the designed peptides for the initial round can be seen in Figure 5.

1:	E	G	H	P	G	E	G	Y	A
2:	E	G	H	P	G	E	S	S	A
3:	D	G	H	P	G	E	G	A	A
C:	N	G	H	P	G	Q	G	A	A "control"
H:	H	H	H	H	H	H	H	A	A

FIGURE 5: Sequences of designed peptides for initial round of catalyst search for anodic half-reaction of water electrolysis.

Some of the important considerations in the design of the peptide are as follows:

(1) The presence of proline amino acid to provide a bend in the structure of the peptide,
(2) The presence of three metal coordinating amino acid residues in the sequence from Asp, Glu, and His, (3) The presence of glycine amino acid as spacer, and (4) The presence of three non-coordinating amino acids at the C-terminal of the sequence to serve as linker. Tyrosine or serine was included in Peptide 1 & 2 to enhance the electron transfer between the peptide and the electrode. Peptide 4, the control peptide, did not contain metal coordinating amino acids in its sequence. Peptide 5, a polyhistidine, which is known to bind Nickel and Cobalt, was designed to test whether the peptide can coordinate with a manganese atom and show catalytic activity. A sketch of peptide 3 can be seen in Figure 6.

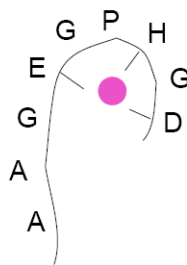


FIGURE 6: A sketch of Peptide 3. The magenta colored ball in the sketch represents manganese atom.

Early measurements on a simple gold electrode showed that peptide 2 & 3 improved I/V efficiency of water electrolysis. The voltage (and thus the power consumption) required to achieve 1.3mA of current dropped by 10% for peptide 2, which corresponds to a 15% drop in the overpotential required to achieve this current (Figure 7).

Subsequently peptide 2, peptide 3 and the control peptide were synthesized in situ on CBMX chips, and their catalytic activity was tested using PotentioSense microarray reader. Chemical structures of peptide 2, 3, & 4 can be seen in Figure 8.

MALDI characterization of in situ synthesis of peptides revealed common side-products associated with specific sequences present in a peptide. For example, peptide 3 involved Asp-Gly in its sequence. Asp-Gly, when present in a sequence, are known to undergo aspartimide formation side-reaction whose corresponding peak can be observed at $m/z = \text{peptide} + 67D$. This side-reaction can be suppressed using 1% HOBt in DMF during the final Fmoc deprotection step. The mechanism of aspartimide formation reaction and the MALDI spectrum of peptide 3 before and after use of 1% HOBt in DMF can be seen in Figure 9 & 10 respectively. Similarly, the MALDI spectrum of peptide 4 showed a peak associated with the dehydration reaction when unprotected Asn and Gln

were used. Upon use of trityl protected Asn and Gln, a peak related to the dehydration reaction disappeared from the MALDI spectrum (Figure 11).

The catalytic activity of peptides 2, 3, and the control peptide was measured using the PotentioSense microarray reader. The I/V step was used to measure currents from water electrolysis. The scan involved 0.0V to -2.4V. Currents from peptide 2 and 3 were similar to currents from control peptide region. No catalytic activity could be seen on CBMX platform. Some of the reasons that could explain why the catalytic activity of the peptide could not be seen on CBMX platform are as follows: the signals could not be differentiated from the noise of the instrument, and/or the communication between peptide and electrode is not optimal. Nevertheless, the instrument has the potential to measure electrical signals from high voltage involving redox reactions. Improvement in deciphering signals from noise, increase in efficiency in communication of peptides and electrodes, and measurements like CV using third-party instruments could make this a very useful approach to search for catalytic peptides. A bit of relevant information from this experiment is that MALDI based microarray synthesis characterization in conjunction with PotentioSense based assay detection could prove to be a powerful technique in the microarray field.

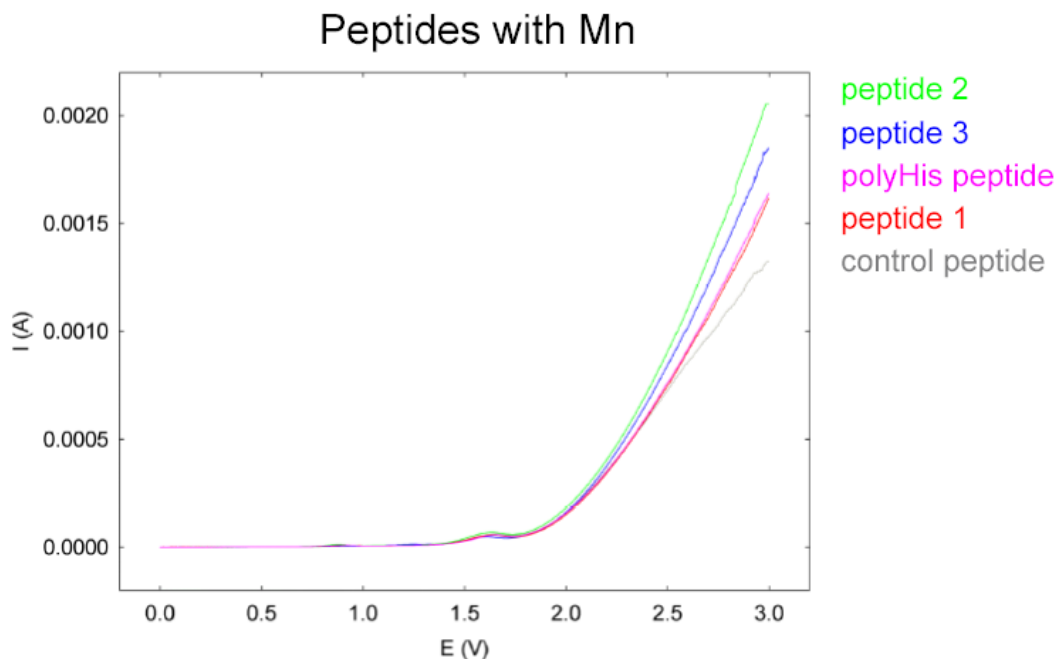


FIGURE 7: I/V curve comparing catalytic efficiencies of peptides 1, 2, 3 & polyHis, bound with Mn and the control peptide (which does not bind Mn) on gold electrodes, for anodic oxidation of water during water electrolysis. Full-length peptides were coupled to polyindole surfaces on gold electrodes and incubated with sub-mM MnCl_2 in PBS buffer. Electrolysis measurements were done in TRIS buffer.

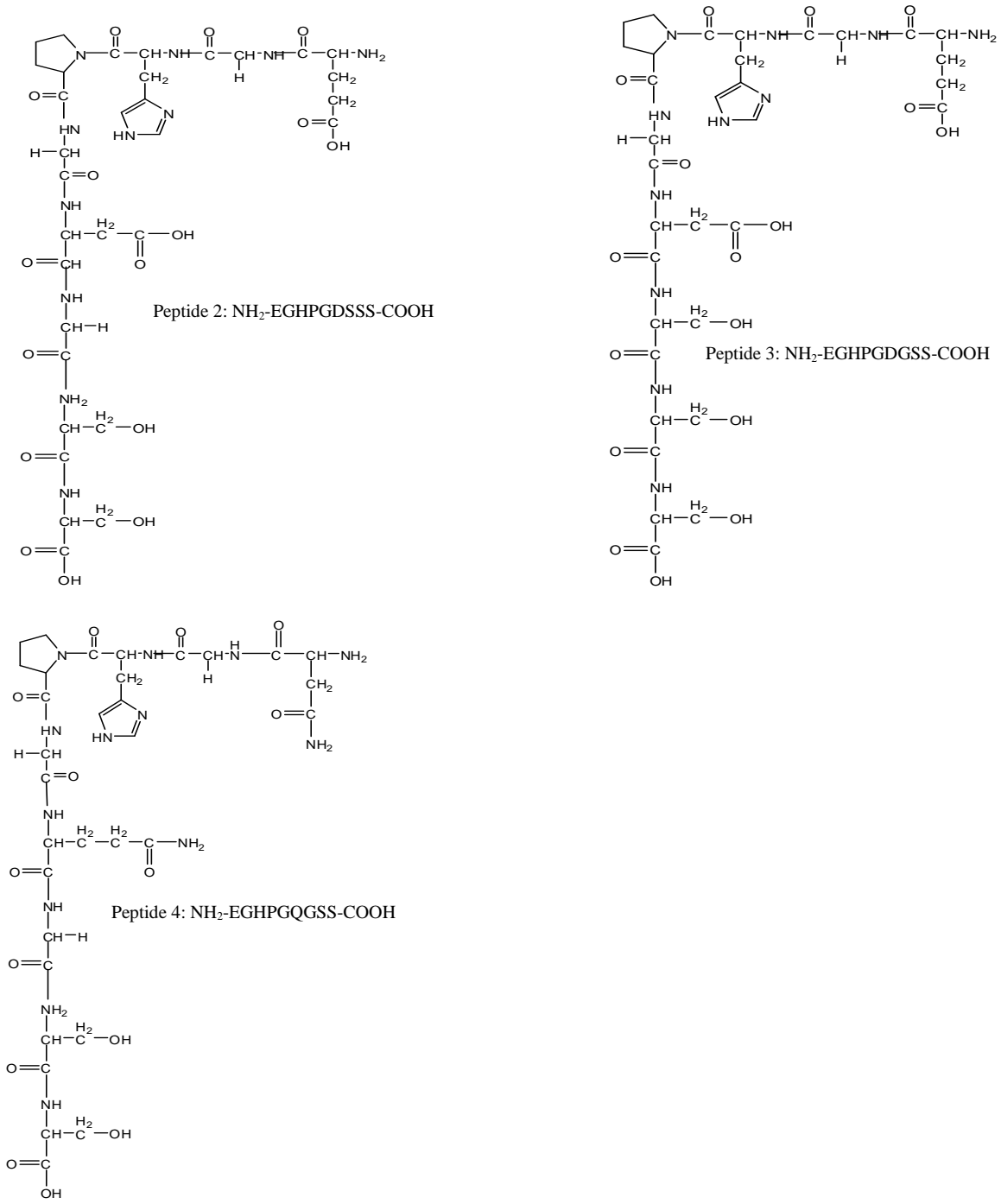


FIGURE 8: Sequences and chemical structures of catalytic peptides 2, 3, and control peptide 4.

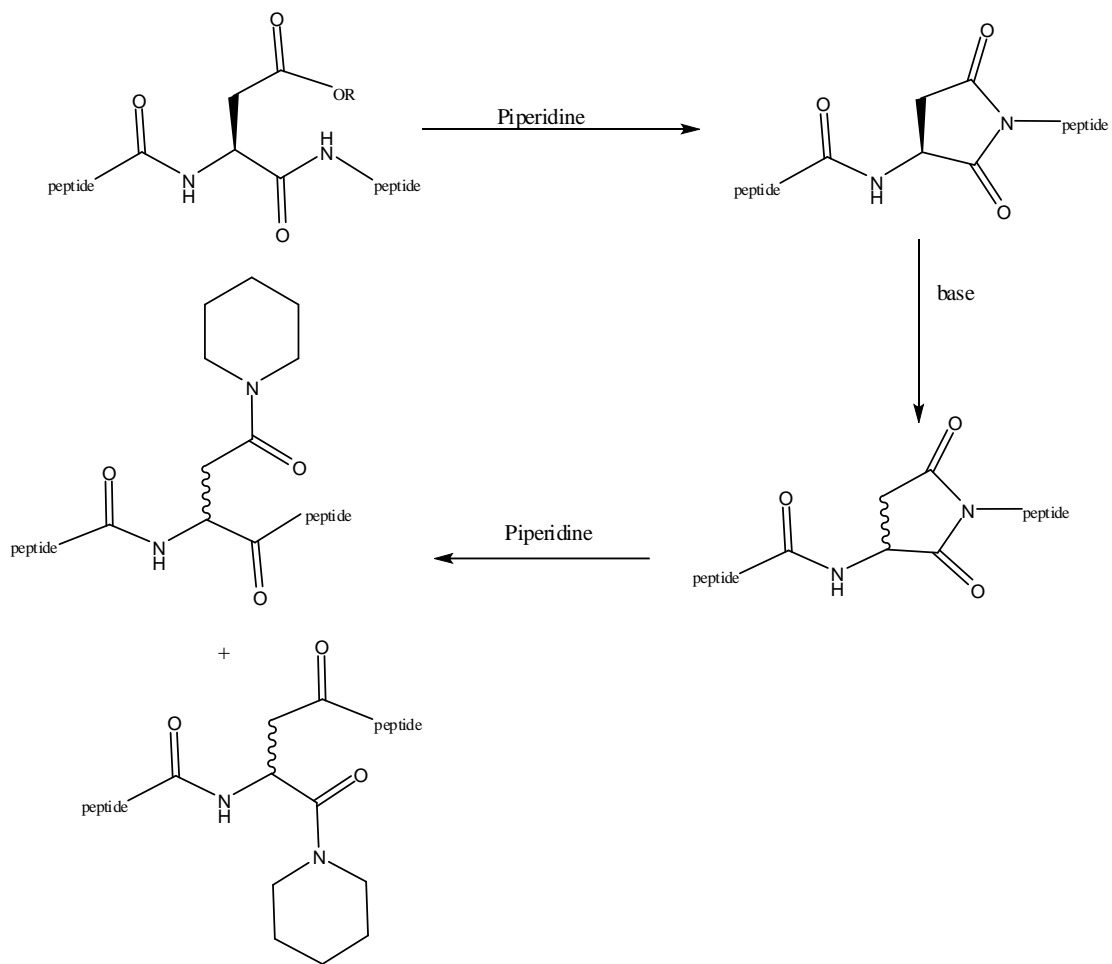


FIGURE 9: Aspartimide formation reaction mechanism.

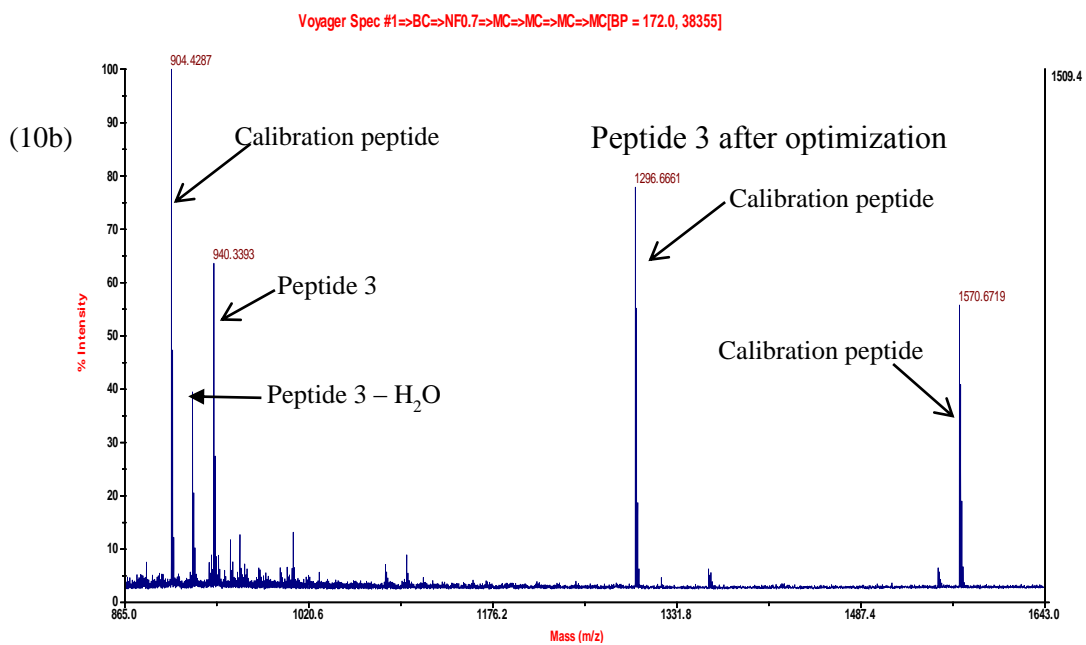
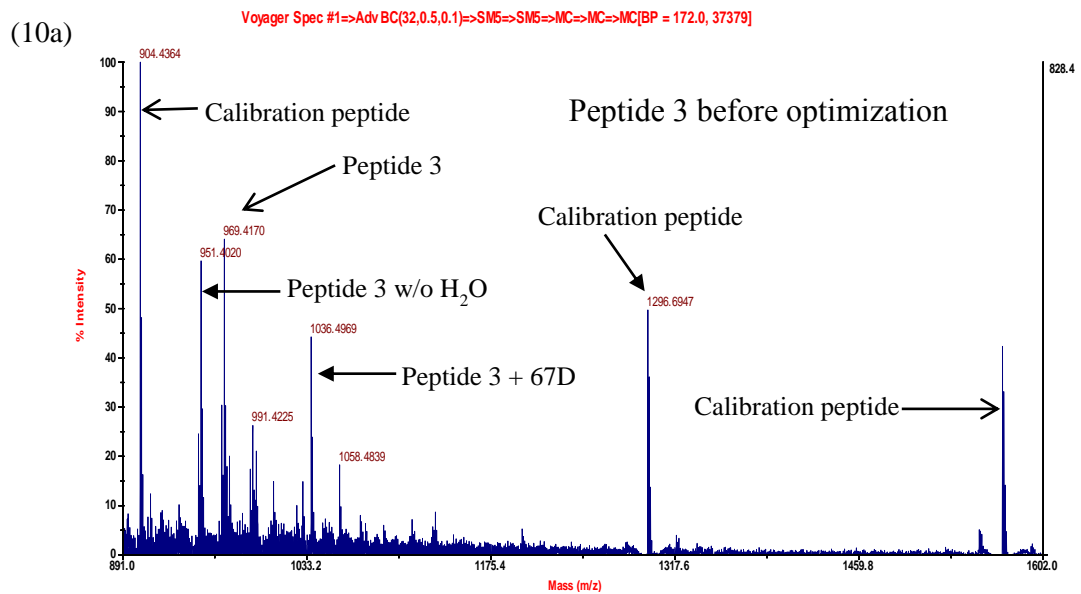


FIGURE 10: MALDI-MS characterization of synthesis of peptide 3 on CBMX chips. MALDI spectrum (10a) corresponds to peptide 3 before optimization: peaks corresponding to loss of water molecule and piperidide adduct of peptide (peptide +67D)

can be seen. The MALDI spectrum (10b) corresponds to peptide 3 after optimization: the peak corresponding to piperidide adduct of peptide (peptide + 67D) is absent.

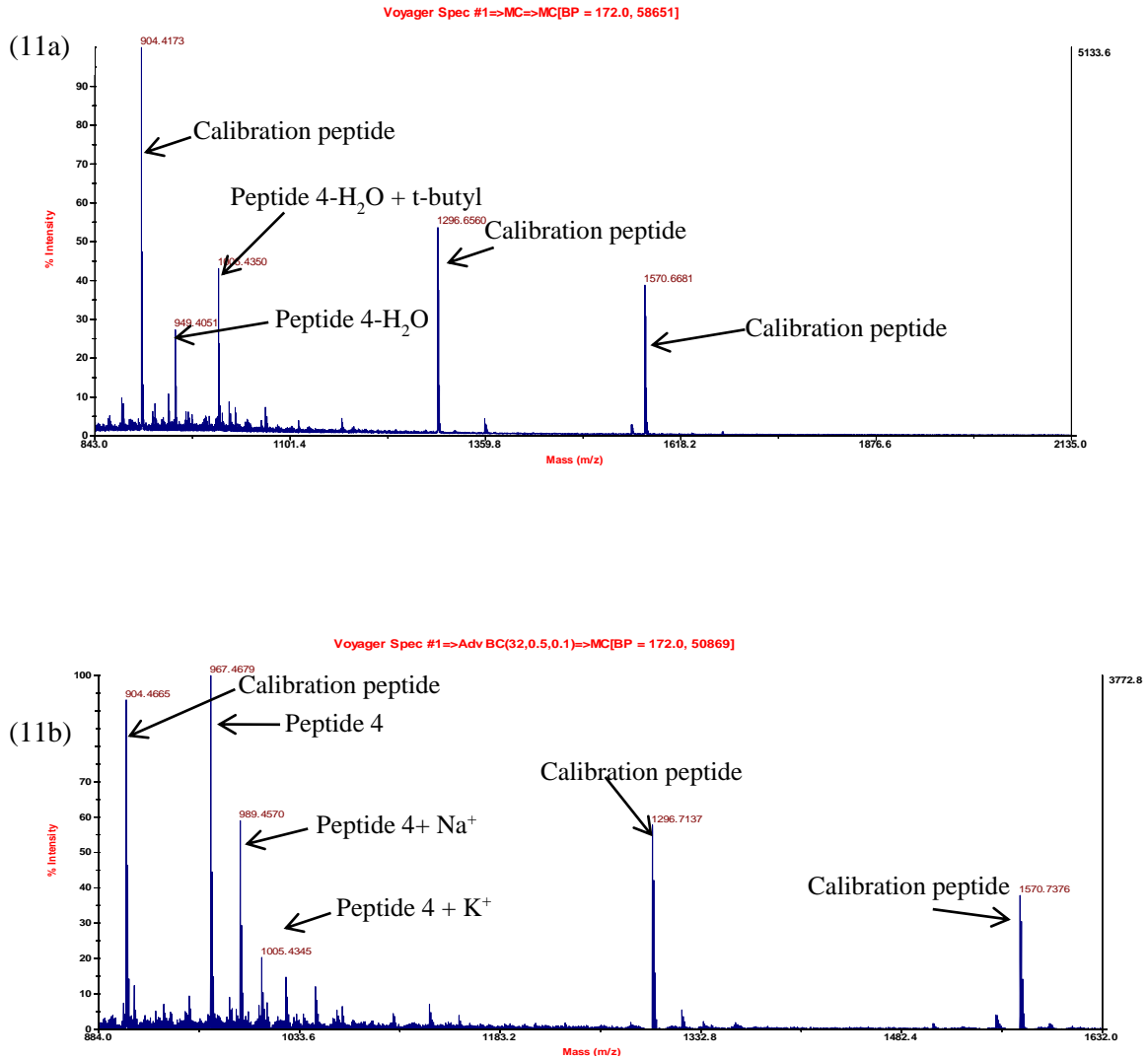


Figure 11: The MALDI spectrum (11a) corresponds to peptide 4 before optimization: the peak corresponding to loss of water molecule can be seen. The MALDI spectrum (11b) corresponds to peptide 4 after optimization: peak corresponding to loss of water molecule is absent.

Co-Electropolymerization of Peptide-py with Pyrrole

We explored another innovative application of CBMX platform: to fabricate peptide microarrays via spatially addressed co-electropolymerization of pyrrole modified peptide (peptide-py) with pyrrole molecules. Figure 12a shows different 11x5 sectors of a CBMX chip treated with solutions of different concentrations of peptide-py in pyrrole. The peptide-py used in the experiments was a pyrrole modified N-terminal endorphin sequence containing peptide (NH₂-YGGFLGGGK(py)-COOH). The numbers reflected in the Figure represent a micromolar concentration of peptide-py in pyrrole solution that was electrodeposited on the corresponding set of electrodes. After co-electropolymerization of solutions with different concentrations of peptide-py, the array was treated with biotin-labeled goat anti-mouse IgG to which HRP-SRP fusion protein was multiplexed. The electrochemical detection of YGGFL containing peptide-py using the Potentiosense microarray reader showed that the peptides were localized only on electrodes on which electrodeposition took place. The electrodes which remained silent during electrodeposition did not show any signal.

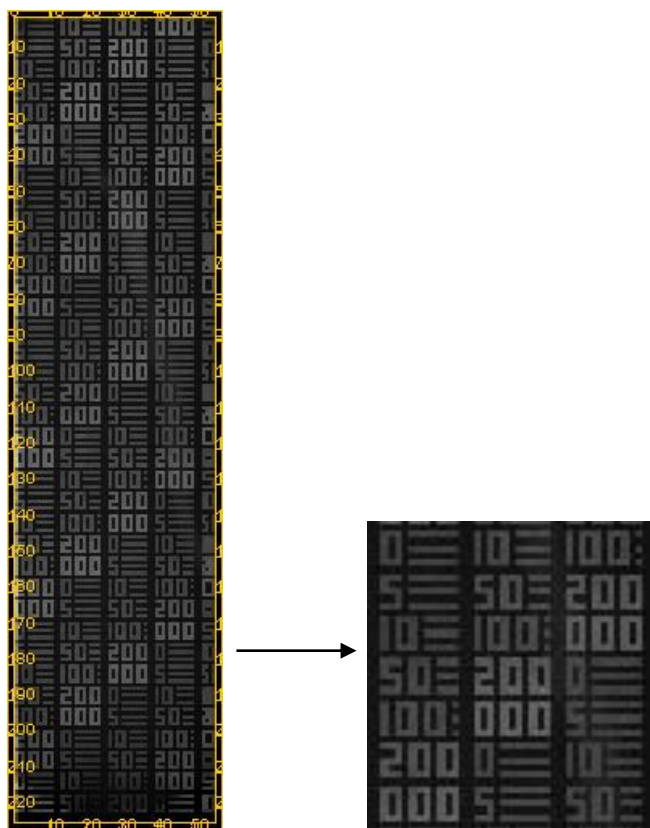


FIGURE 12a: Electrochemical detection of peptide immobilization via co-electropolymerization of peptide-py and pyrrole by YGGFL-antibody-HRP assay. Specifically, YGGFL containing peptide sequence binds to the biotinylated antibody which is multiplexed with SRP-HRP fusion protein. Each number represents micromolar concentration of peptide-py in pyrrole solution.

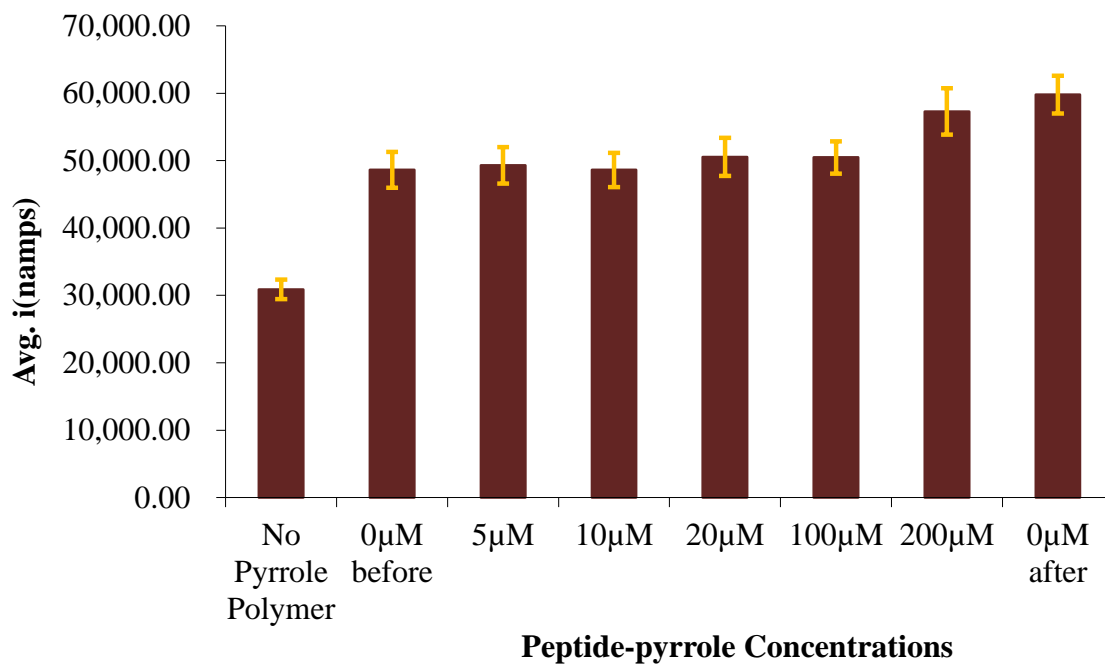


Figure 12b. Electrochemical detection of co-electropolymerization of peptide-py and pyrrole using constant voltage 1.0V for 10s. Different concentrations of peptide-py (0.0, 5, 10, 20, 100, 200 µM) in pyrrole solution were electro-deposited in different sections of a CBMX chip, and peptide immobilization efficiency was detected using YGGFL-antibody-SRP-HRP assay.

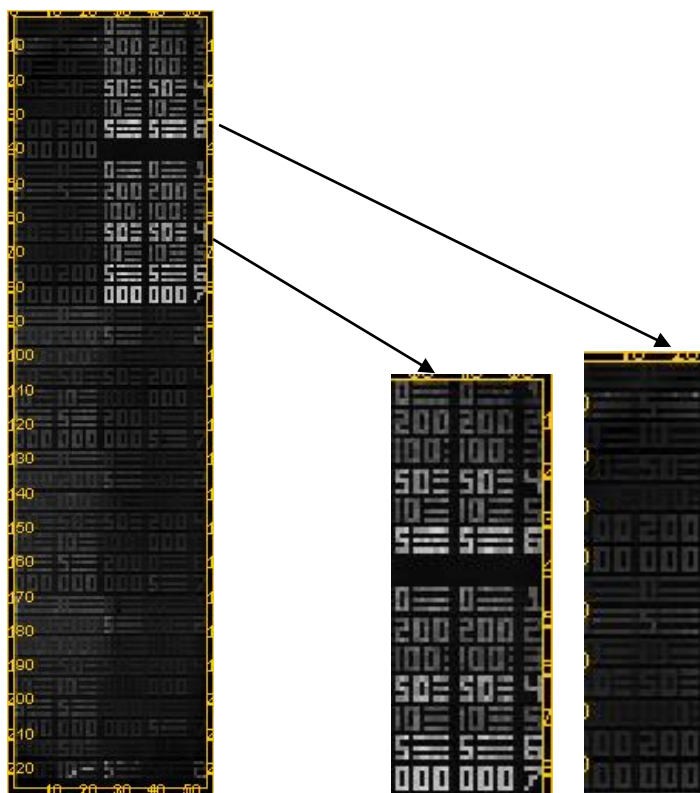


FIGURE 12c: Electrochemical detection of peptide immobilization via co-electropolymerization of peptide-py and pyrrole by YGGFL-antibody-HRP assay. Specifically, YGGFL containing peptide sequence binds to the biotinylated antibody which is multiplexed with SRP-HRP fusion protein. Each number represents micromolar concentration of peptide-py in pyrrole solution. The brighter region did not involve DMF wash.

The experiment involved three kinds of controls: (1) Control-1: electrodes on which no electrodeposition of pyrrole took place, (2) Control-2: electrodes on which pyrrole was electrodeposited before electrodeposition of mixtures containing peptide-py and pyrrole, and (3) Control-3: electrodes on which pyrrole was electrodeposited after electrodeposition of different mixtures containing peptide-py and pyrrole. It was

observed that with the increase in concentration of peptide-py in the mixture, an increase in the electrochemical signal was observed. This is expected if the pyrrole group of peptide-py is polymerizing with simple pyrrole molecules. Details of the mechanism of electropolymerization of pyrrole which are not clear can be found in Reference 37, 38 and Figure 13.

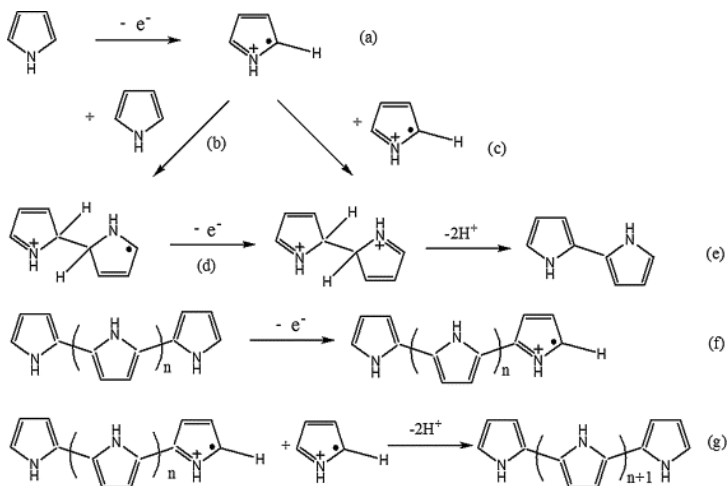


FIGURE 13: A probable mechanism of pyrrole electropolymerization³⁸.

However, control-3 showed highest signal (Figure 12b). These were simple pyrrole molecules, which were electro-polymerized at the last step after the deposition of series of solutions with different peptide-py concentrations. If the signals were dependent on the concentration of peptide-py in the mixture, control-3 should have shown the lowest signal similar to control-2.

To understand this intriguing observation, in another experiment, solutions were electro-deposited in reverse order in a section of the chip. The mixture with highest peptide-py concentration was deposited first and mixture with lowest peptide-py concentration was deposited last. Similar to the previous experiment, control-2 was

electrodeposited before electrodeposition of different mixtures and control-3 was electrodeposited after electrodeposition of different mixtures. In this experiment, a stringent DMF-based washing step was also included to check if the peptide immobilization was covalent or non-covalent. If the immobilization was non-covalent, the signal intensities should decrease with stringent washing conditions. The results of the experiment can be seen in Figure 12c. It was observed that the electrodes on which the peptide-py and pyrrole mixture was deposited last showed the highest signals. The signals observed from electrodes on which 5 μ M peptide-py mixture was electrodeposited showed higher signals than electrodes on which 200 μ M peptide-py mixture was electrodeposited. Control-3, which was electro-deposited at the very end, showed the highest signals. At the same time, electrodes that remained silent throughout the experiment did not show any relevant signal. It can be inferred that the signals are not dependent on peptide-py concentration in mixture, but on the timing of the electrodeposition. If the same mixture is electro-deposited first in the series, the corresponding electrodes show the lowest signal. If it is electro-deposited last in the series, the corresponding electrodes would show the highest signal. It can also be inferred that once a pyrrole polymer is electro-deposited on an electrode surface, no more peptide-py can non-specifically deposit on that electrode. Additionally, the already immobilized peptide-py (stuck inside the pyrrole polymer) does not get rinsed during washing steps. Otherwise, signals from all the electrodes on which electro-polymerization took place should be similar, and no signal gradation should be seen. In this experiment, a section of the chip showed brighter signals compared to rest of the chip (Figure 12c). In this section, DMF wash was not

included, whereas in rest of the chip DMF wash was included. From this observation it is clear that the majority of the signal, if not the entire signal, is due to non-covalent trapping of the peptide-py in the pyrrole polymer. Further experiments, are needed to understand the nature of immobilization, whether specific or non-specific, and to optimize the peptide immobilization strategy via co-electropolymerization with an electroactive molecule.

TABLE 1: Details of Experiment 1 of peptide immobilization via co-electropolymerization of peptide-py and pyrrole.

Experiment 1		
Electrodeposition Steps (does not include DMF wash)	Peptide-py conc'n (μM) in pyrrole solution	Signal Intensity Trend
Step 1	0	Lowest
Step 2	5	↓
Step 3	10	
Step 4	20	
Step 5	100	
Step 6	200	
Step 7	0	Highest

TABLE 2: Details of Experiment 2 of peptide immobilization via co-electropolymerization of peptide-py and pyrrole.

Experiment 2								
Electrodeposition Steps (includes DMF Wash)	Peptide-py conc'n (μM) in pyrrole solution	Signal Intensity Trend	Electrodeposition Steps (includes DMF Wash)	Peptide-py conc'n (μM) in pyrrole solution	Signal Intensity Trend	Electrodeposition Steps (does not include DMF Wash)	Peptide-py conc'n (μM) in pyrrole solution	Signal Intensity Trend
Step 1	0	Lowest	Step 1	0	Lowest	Step 1	0	Lowest
Step 2	5	↓	Step 2	200	↓	Step 2	200	↓
Step 3	10		Step 3	100		Step 3	100	
Step 4	20		Step 4	20		Step 4	20	
Step 5	100		Step 5	10		Step 5	10	
Step 6	200		Step 6	5		Step 6	5	
Step 7	0	Highest	Step 7	0	Highest	Step 7	0	Highest

Materials and Methods

Biotin Coupling Reaction

The coupling reaction of biotin to free amines is comparable to any other amino acid coupling reaction, the difference being only in concentrations. The biotin coupling reaction is difficult to achieve due to solubility issues. It is a highly polar molecule and, therefore, even most polar organic solvents such as DMF (*N,N'*-dimethylformamide) and DMSO (dimethylsulfoxide) are unable to couple biotin in regular concentrations (150-200 μM concentration). To achieve biotin coupling, the CBMX chip terminated with free amines is exposed to a mixture of biotin (67mg, 137mM), HBTU (*O*-benzotriazol-1-yl-*N,N,N',N'*-tetramethyluronium hexafluorophosphate, 95mg, 137mM), HOBT (*N*-hydroxybenzotriazole, 33.5mg, 137mM), and diisopropylethylamine (130.5 μL , 350mM) in DMF (2mL) for 30 minutes. The chip is then rinsed with DMF 3x, dichloromethane 3x, and again with DMF 3x, then re-exposed to the coupling mixture for another 30 minutes. After repeating the washing procedure (with an additional ethanol rinse to remove any residual DMF or dichloromethane), the chip is allowed to dry.

Ferrocene Coupling Reaction

The coupling reaction of ferrocene modified with a carboxylic acid group to free amines is comparable to any other amino acid coupling reaction. To achieve ferrocene coupling, the CBMX chip terminated with free amines is exposed to a mixture of ferrocene carboxylic acid (126mg, 250mM), HBTU (*O*-benzotriazol-1-yl-*N,N,N',N'*-tetramethyluronium hexafluorophosphate, 190mg, 250mM), HOBT (*N*-hydroxybenzotriazole, 67mg, 250mM), and diisopropylethylamine (130.5 μ L, 350mM) in DMF (2mL) for 30 minutes. The chip is then rinsed with DMF 3x, dichloromethane 3x, and again with DMF 3x, then re-exposed to the coupling mixture for another 30 minutes. After repeating the washing procedure (with an additional ethanol rinse to remove any residual DMF or DCM), the chip is allowed to dry.

Synthesis of Pyrrole Modified Peptide

The coupling reaction of pyrrole modified with a carboxylic acid group to free amines is comparable to any other amino acid coupling reaction. To achieve pyrrole coupling, the NH₂-YGGFLGGGK-COOH functionalized polystyrene beads with free ϵ -amines is exposed to a mixture of 1H-pyrrole-1-acetic acid (35mg, 137mM), HBTU (*O*-benzotriazol-1-yl-*N,N,N',N'*-tetramethyluronium hexafluorophosphate, 95mg, 137mM), HOBT (*N*-hydroxybenzotriazole, 33.5mg, 137mM), and diisopropylethylamine (130.5 μ L, 350mM) in DMF (2mL) for 30 minutes. The beads are then rinsed with DMF 3x, dichloromethane 3x, and again with DMF 3x, then re-exposed to the coupling mixture for another 30 minutes. After repeating the washing procedure (with an additional ethanol rinse to remove any residual DMF or DCM), the beads are allowed to dry.

Biotin–SRP-HRP Binding and Electrochemical Detection

The microarray was fitted with a hybridization cap and washed with PBSC before incubating with 5X PBSC (BioFX, Owings Mills, MD) for 20 min at 25°C and washed three times with 2XPBST. Microarrays were incubated for 30 min with Poly-80-HRP Streptavidin (Fitzgerald Industries International, Acton, MA) diluted 1:1000 in PBST. Arrays were washed four times with PBSC, once with PBS, and twice with pH 4 Conductivity Buffer Substrate (BioFX). TMB Conductivity 1 Component HRP Microwell Substrate (BioFX) was added to the array, and it was scanned immediately with a PotentioSense microarray reader (CBMX Corp.). Data was quantified using ElectraSense software (CBMX Corp.) for ECD.

N-terminal Endorphin Sequence – Antibody Binding and Electrochemical Detection

This procedure is similar to biotin-SRP-HRP binding. In this procedure three rounds of incubation took place, the first incubation involved anti- β -endorphin antibody (mouse), the second involved biotin-labeled donkey anti-mouse antibody, and the third incubation involved SRP-HRP fusion protein. Clone 3-E7 (monoclonal, mouse) diluted 1/1000 in 2X PBS + 0.05% Tween from stock purchased from Chemicon International. Imaging was done using a PotentioSense microarray reader (CBMX Corp.). Data was quantified using ElectraSense software (CBMX Corp.) for ECD.

Pyrrole Electro-Polymerization

2 μ L of Pyrrole (Sigma-Aldrich, Milwaukee, WI) is added to 0.5% SDS solution and vortexed for approximately five minutes until pyrrole gets dissolved in 0.5% SDS solution. Maps defining the electrodes to be addressed are prepared and loaded in electro-

synthesis software. Once the electro-synthesis software is ready, the pyrrole solution prepared is loaded into the reaction chamber of the electro-synthesis instrument. Electro-synthesis software is commanded to apply 1.0 V for 10 s to the selected electrodes of the chip. Once the polymerization reaction is over, the polymerization solution is discarded and the reaction chamber is rinsed 2x with 0.5% SDS solution and then 2x with water. The chip is then taken out of the reaction chamber and dried with argon gas and imaged under a microscope to detect pyrrole electro-polymerization.

Co-Electropolymerization of Pyrrole and Peptide-Py

Different concentrations of peptide-py ($\text{NH}_2\text{-YGGFLGGGK(py)-COOH}$) were added in different rounds of polymerization to polymerization solution consisting of 2 μL of pyrrole (Sigma-Aldrich, Milwaukee, WI) in 0.5% SDS solution and vortexed for approximately two minutes until the pyrrole dissolved in 0.5% SDS solution. For copolymerization of pyrrole with peptide-py of a specific concentration, maps defining the electrodes to be addressed were prepared and loaded in the electrosynthesis software. The polymerization solution prepared was then loaded in the reaction chamber of the electrosynthesis instrument. Electrosynthesis software is commanded to apply 1.0 V for 10s to the selected electrodes of the chip. Once the polymerization reaction was complete, the polymerization solution is discarded and the reaction chamber is rinsed 2x with 0.5% SDS solution and then 2x with water. Abovementioned series of steps was performed again with polymerization solution containing peptide-py of a different concentration and a different map. At last, the chip was taken out of the reaction

chamber, dried with argon gas, imaged under a microscope to detect pyrrole electropolymerization, and readied for HRP based electrochemical detection.

MALDI Matrix Application and Characterization of Array Features

Experimental protocol for the MALDI matrix application and characterization of array features is discussed in Chapter 3 Materials and Methods section.

Non-Diffusional UV-Cleavage of Arrayed Peptides

Experimental protocol for non-diffusional UV-cleavage of arrayed peptides is discussed in Chapter 3 Materials and Methods section.

Conclusion

Microarray detection based on electrochemical techniques is one of the effective approaches for analysis of biointeractions. The method has some advantages and limitations. Limitations are mainly due to complex circuitry and multi-channel electrical signal measurements. CBMX has developed the PotentioSense instrument, which overcomes these technical difficulties and thus CBMX custom 12K arrays can be used for redox applications. We have tested PotentioSense based different electrochemical techniques for peptide microarrays and analyzed the performance and limitations of the instrument. We have shown that the PotentioSense based different electrochemical techniques, in conjunction with MALDI mass spectrometry, can be applied to CBMX 12K custom arrays for analyzing several microarray based redox assays. Both the techniques in tandem can prove to be a powerful tool in peptide microarray area.

References

1. Y.M. Foong, J. Fu, S.Q. Yao, M. Uttamchandani, Current advances in peptide and small molecule microarray technologies. *Curr. Op. Chem. Biol.* **16**, 234-242 (2012).
2. Y. Shen, B.L. Wu, Microarray-based genomic DNA profiling technologies in clinical molecular diagnostics. *Clin. Chem.* **55**, 659-669 (2009).
3. J.C. Mills, K.A. Roth, R.L. Cagan, J.I. Gordon, DNA microarrays and beyond: completing the journey from tissue to cell. *Nat. Cell. Biol.* **3**, e175-e178 (2001).
4. B.B. Haab, Methods and applications of antibody microarrays in cancer research. *Proteomics* **3**, 2116–2122 (2003).
5. E.A. Smith, M. Kyo, H. Kumasawa, K. Nakatani, Chemically induced hairpin formation in DNA monolayers. *J. Am. Chem. Soc.* **124**, 6810–6811 (2002).
6. Y. Li, J. Xiang, F. Zhou, Sensitive and label-free detection of DNA by surface plasmon resonance. *Plasmonics* **2**, 79-87 (2007).
7. C. Berggren, G. Johansson, Capacitance measurements of antibody-antigen interactions in a flow system. *Anal. Chem.* **69**, 3651– 3657 (1997).
8. D. Jiang, J. Tang, B. Liu, P. Yang, J. Kong, Ultrathin aluminasol-gel-derived films: allowing direct detection of the liver fibrosis markers by capacitance measurement. *Anal. Chem.* **75**, 4578–4584 (2003).
9. P. Kumar, M.P. Greving, Z.G. Zhao, N.W. Woodbury, Feature-level MALDI-MS characterization of in situ-synthesized peptide microarrays. *Langmuir* **26**, 1456-1459 (2010).
10. D. Nedelkov, R.W. Nelson, Delineating protein-protein interactions via biomolecular interaction analysis-mass spectrometry. *J. Mol. Recognit.* **16**, 9–14 (2003).
11. D. Nedelkov, R.W. Nelson, Design and use of multi-affinity surfaces in biomolecular interaction analysis-mass spectrometry (BIA/MIS): a step toward the design of SPR/MS arrays. *J. Mol. Recognit.* **16**, 15– 19 (2003).
12. L. Yang, Y. Li, G.F. Erf, Interdigitated Array microelectrode-based electrochemical impedance immunosensor for detection of Escherichia coli O157:H7. *Anal. Chem.* **76**, 1107–1113 (2004).

13. M. Wang, L. Wang, G. Wang, X. Ji, Application of impedance spectroscopy for monitoring colloid Au-enhanced antibody immobilization and antibody-antigen reactions. *Biosens. Bioelectron.* **19**, 575–582 (2004).
14. X. Yu, D. Xu, D. Xu, Z. Liu, An impedance biosensor array for label-free detection of multiple antigen-antibody reactions. *Front. Biosci.* **11**, 983–990 (2006).
15. D. Xu, D. Xu, X. Yu, Z. Liu, Label-free electrochemical detection for aptamer-based array electrodes. *Anal. Chem.* **77**, 5107–5113 (2005).
16. K. M. Roth, K. Peyvan, K. R. Schwarzkopf, A. Ghindilis, Electrochemical detection of short DNA oligomer hybridization using the CombiMatrix Electrasense microarray reader. *Electroanalysis* **18**, 1982–1988 (2006).
17. J.J. Gau, E.H. Lan, B. Dunn, A MEMS based amperometric detector for E-Coli bacteria using self-assembled monolayers. *Biosens. Bioelectron.* **16**, 745–755 (2001).
18. R.J. Cotter, Time-of-flight mass-spectrometry for the structural-analysis of biological molecules. *Anal. Chem.* **64**, A1027–A1039 (1992).
19. B.T. Chait, S.B.H. Kent, Weighing naked proteins: practical high accuracy mass measurement of peptides and proteins. *Science* **257**, 1885–1894 (1992).
20. F. Hillenkamp, M. Karas, R.C. Beavis, B.T. Chait, Matrix-assisted laser desorption ionization mass spectrometry of biopolymers. *Anal. Chem.* **63**, A1193–A1202 (1991).
21. R. Aebersold, M. Mann, Mass spectrometry-based proteomics. *Nature* **422**, 198–207 (2003).
22. Y. Umena, K. Kawakami, J. Shen, N. Kamiya, Crystal structure of oxygen-evolving system Photosystem II at a resolution of 1.9Å. *Nature* **473**, 55–60 (2011).
23. T.A. Betley, Q. Wu, T.V. Voorhis, D.G. Nocera, Electronic design criteria for O—O bond formation via metal—oxo complexes. *Inorg. Chem.* **47**, 1849 (2008).
24. Y. Wang, K.S. Chen, J. Mishler, S.C. Cho, X.C. Adroher, A review of polymer electrolyte membrane fuel cells: Technology, applications, and needs on fundamental research. *Applied Energy* **88**, 981 (2011).

25. H. Zhang, G. Lin, J. Chen, Evaluation and calculation on the efficiency of a water electrolysis system for hydrogen production. *International Journal of Hydrogen Energy* **35**, 10851-10858 (2010).
26. W. Cady, R.H. Crabtree, G.W. Brudvig, Functional models for the oxygen-evolving complex of photosystem II. *Coord. Chem. Rev.* **252**, 444-455 (2008).
27. Kalman, L., Williams, J.C., Allen, J.P., Comparison of bacterial reaction centers and Photosystem II. *Photosynthesis Research* **98**, 643-655 (2008).
28. D.S. Minehan, K.A. Marx, S.K. Tripathy, Kinetics of DNA binding to electrically conducting polypyrrole films. *Macromolecules* **27**, 777-783 (1994).
29. M. Rahman, P. Kumar, D.S. Park, Y.B. Shim, Electrochemical sensors based on organic conjugated polymers. *Sensors* **8**, 118-141 (2008).
30. H. Peng, L. Zhang, C. Soeller, Travas-Sejdic, Conducting polymers for electrochemical DNA sensing. *Biomaterials* **30**, 2132-2148 (2009).
31. K. Maurer, N. Yazvenko, J. Wilmoth, J. Cooper, W. Lyon, D. Danley, Use of a multiplexed CMOS microarray to optimize and compare oligonucleotide binding to DNA probes synthesized or immobilized on individual electrodes. *Sensors* **10**, 7371-7385 (2010).
32. J. Cooper, N. Yazvenko, K. Peyvan, K. Maurer, C.R. Taitt, W. Lyon, D.L. Danley, Targeted Deposition of Antibodies on a Multiplex CMOS Microarray and Optimization of a Sensitive Immunoassay Using Electrochemical Detection. *PLoS ONE* **5**, e9781 (2010).
33. T. Livache, A. Roget, E. Dejean, C. Barthet, G. Bidan, R. Teoule, Preparation of a DNA matrix via an electrochemically directed copolymerization of pyrrole and oligonucleotides bearing a pyrrole group. *Nucleic Acids Research* **22**, 2915-2921 (1994).
34. T. Livache, E. Maillart, N. Lassalle, P. Mailley, B. Corso, P. Guedon, A. Roget, Y. Levy, Polypyrrole based DNA hybridization assays: Study of label free detection processes versus fluorescence on microchips. *J. Pharm. Biomed. Anal.* **32**, 687 (2003).
35. O. Niwa, M. Morita, H. Tabei, Electrochemical behaviour of reversible redox species at interdigitated array electrodes with different geometries: consideration of redox cycling and collection efficiency. *Anal. Chem.* **62**, 447-452 (1990).

36. F. Rebiere, O. Samuel, H.B. Kagan, A convenient method for the preparation of monolithioferrocene. *Tetrahedron Letters* **31**, 3121 (1990).
37. S. Sadki, P. Schottland, N. Brodie, B. Sabouraud, The mechanisms of pyrrole electropolymerization. *Chem. Soc. Rev.* **29**, 283-293 (2000).
38. Y. Tan, K. Ghandi, Kinetics and mechanism of pyrrole chemical polymerization. *Synthetic Metals* **175**, 183-191 (2013).

Chapter 6

Conclusion

In the scope of this thesis, electrochemically directed microarray fabrication technique on CBMX platform was optimized. Also, the photo-deprotection efficiency of the NPPOC protective group and its derivatives was investigated.

Fabrication of high density peptide microarrays at a low cost, and their characterization, is a difficult problem. One approach to this problem that has been described here in detail is to make electrochemically-directed peptide microarrays on CBMX chips. This approach has a tremendous advantage over traditional microarrays in that the arrays can be characterized electrochemically in addition to fluorescence. The CBMX platform is also amenable to MALDI detection without any modifications. Chapters 3, 4, 5 and Appendices A-F discuss the optimization of different aspects of peptide microarray fabrication, its characterization, and its applications.

Chapter 3 discusses a simple, accurate, and general MALDI mass spectrometry (MALDI-MS) based approach that we have developed to characterize the chemical composition of an in situ-synthesized microarray directly on array features. This approach provides chemical composition information about each microarray spot, which is not possible using other approaches. Due to some restrictive factors this approach has spatial limitations. These limitations include a greater MALDI laser focus area, difficulty in precisely aligning the microarray features with the laser, and difficulty in applying the MALDI matrix without cross-contamination of cleaved peptides of different features. By

improvements in these limiting factors, the spatial resolution can be significantly increased allowing detection of large number of array features.

Chapter 4 and Appendices A-G discuss aspects of peptide microarray synthesis that were optimized. Using MALDI-MS detection method, we optimized the gating step efficiency; trityl groups can be deprotected electrochemically using N,N'-diphenylhydrazine as EGA-P solution with approximately 70% efficiency. Stability tests of trityl and dimethoxytrityl groups to N,N'-diphenylhydrazine and hydroquinone based EGA-P solutions revealed that trityl groups were stable to N,N'-diphenylhydrazine but not to hydroquinone based EGA-P solution. DMT groups were not stable to any of the EGA-P solutions. Based on this study we employed trityl as amino protecting groups towards optimization of peptide microarray synthesis. In situ-coupling efficiency of trityl groups to N-terminal amino groups was also optimized. We determined the stability of t-butyl and Boc groups during trt electrochemical deprotection and their chemical deprotection efficiency on CBMX chips. Less than 10% Boc and t-butyl groups were deprotected at the gating step. We concluded that the CBMX chips are stable to TFA for 30 minutes through the fluorescence method and that it proved to be sufficient for complete deprotection of Boc and t-butyl groups. We were able to develop an orthogonal system where the primary amino groups are protected with trityl group, and sidechain groups were protected with boc and t-butyl groups. With this capability, we synthesized a peptide with three gating steps with an overall yield of 18%. The chemical composition and quantification of the synthesis products was determined by MALDI-MS detection. To avoid contamination caused during peptide synthesis a milder condition, 0.75 μ A for

45s using hydroquinone as EGA-P solution was developed. Several instrumentation challenges, such as synthesis automation, fabrication of two kinds of manual chambers one with low reaction volume and another which is acid-resistant to carry out TFA based deprotection step were solved. Some preliminary work to generate electro-reagents that can deprotect different kinds of protecting groups such as base-labile, catalytically reducible, and organometallic labile groups were performed. The strategy to generate piperidine, an organic base, in situ by reducing its probase (piperidine hydrochloride), piperidine hydrochloride looks promising and further work should be done to optimize the strategy. At present we can deprotect approximately 25% of Fmoc groups upon application of -2.0V for 20 minutes.

Redox enzyme mediated electrochemical detection of microarrays is one of the effective methods of studying protein-peptide interactions. Potentiosense microarray reader developed by CBMX overcomes the technical limitations of this method. These technical limitations include a complex circuitry and multichannel electrical signal measurements. A microarray system comprising of CBMX platform, MALDI-MS, and Potentiosense was used to search for peptide catalysts that can reduce overpotential associated with anodic half-reaction of water splitting, as well as to fabricate a peptide microarray on CBMX chip via co-electropolymerization of peptide-pyrrole and pyrrole. In this regard, several characteristics of Potentiosense were studied, including noise behavior at various voltages. We fabricated three designed peptides on a CBMX chip. Two of these peptides bind to manganese and showed catalytic activity on bulk gold electrode; the third was a control peptide. Although no catalytic activity could be detected

using Potentiosense, the direct characterization of synthesis using MALDI-MS and the ability to measure currents from microelectrodes of the chip at high voltages holds promise. Initial results w.r.t peptide microarray fabrication by co-electropolymerization of peptide-pyrrole and pyrrole suggested immobilization of peptides using this method is possible, but several more optimization experiments need to be conducted for optimization. Although the study has been primitive, we have demonstrated the potential of coupling CBMX chips with MALDI-MS. We have also demonstrated ECD detection methods to search for peptide based catalysts for challenging redox reactions, and the fabrication of peptide microarrays via electropolymerization, with recognizable applications in electrocatalyst development and drug discovery.

A comparison study of photolysis rates and yields of free amines for NPPOC, derivatives of NPPOC, MeNPOC and NVOC protecting groups is described in Chapter 2. Firstly, a simple, efficient, and relatively non-toxic method for synthesis of NPPOC protected amines without using phosgene was developed. Secondly, the efficiency of NPPOC and its derivatives as photolabile amino protecting groups was determined. Photolysis studies revealed that presence of pi-system conjugated to the benzene ring of NPPOC group enhances the rate of photolysis and overall yield of the amines. Probably, the improvement in the rate of photolysis is due to enhanced stability of the reactive intermediate formed (Norrish Type II – diradical species) during UV cleavage. The improvement in overall yield of amine is due to the formation of relatively inert nitrostyrene side-product, compared to nitrosobenzaldehyde seen during MeNPOC and NVOC cleavage. Once the phenyl derivative of NPPOC was chosen as a suitable group

for protecting amines, it was found that the nature of protected amine (aromatic or aliphatic) had a strong affect on the rate of photolysis. These results could be useful in preparing a more efficient photolabile amino protecting group, with applications ranging from organic to combinatorial peptide synthesis.

In conclusion, the electrochemical technique has interesting future applications. This technique can be extended to D-amino acids and unnatural amino acids, making it suitable for synthetic peptide library generation and drug discovery. The platform could be well-suited for generation of other kinds of libraries, such as oligosaccharides, peptide nucleic acids, and peptoids with some chemical modifications. With current yields (approximately 56% yield per electrochemical step), the CBMX peptide microarray platform could be useful to study influence of point mutations on binding characteristics. The features showing high binding affinity can be carefully analyzed in next rounds of microarray experiments to elucidate the chemical composition of real binders to the analyte molecule. Currently, peptide arrays are well-suited for linear epitope mapping. With advances in electrochemically-directed peptide synthesis, the CBMX platform could become well-suited for conformational epitope mapping too. Another interesting application of the CBMX platform involves monitoring conformational changes in peptide probes. Both metallo- and non-metallo-peptides could be monitored through redox behavior of metals as well as redox active amino acids such as tyrosine and tryptophan. Currently, conformational changes in proteins are detected through techniques such as NMR, UV absorption, electron spin resonance, circular dichroism, birefringence, and fluorescence spectroscopy. CBMX microarray platforms can not only

detect conformational changes, but they can also provide fast, relatively inexpensive, and detailed information about the causes of conformational changes such as nucleation points of folding. They can also provide clues to control and manipulate those changes. For example, the redox behavior of single amino acid mutations of secondary structure forming probe sequences can give an idea of amino acids that are important for a sequence to assume a secondary structure. Such amino acids, upon identification, can be replaced with other amino acids for manipulation of the conformation of the probe sequence. This could be extremely useful in finding solutions to a wide range of diseases called amyloidoses, which occur due to incorrect folding of proteins.

Complete List of References

Chapter 1

1. W.P. Blackstock, M.P. Weir, Proteomics: quantitative and physical mapping of cellular proteins. *Trends Biotechnol.* **17**, 121–127 (1999).
2. D. Voet, J.G. Voet, *Biochemistry*, Vol 1 3rd ed., Wiley: Hoboken, NJ (2004).
3. E. Fischer, *Ber. Dt. Chem. Ges.*, **27** (3): 2985–2993 (1894).
4. D.E. Koshland, Application of a theory of enzyme specificity to protein synthesis. *Proc. Natl. Acad. Sci. USA* **44**, 98–104 (1958).
5. R.P. Bahadur, P. Chakrabarti, F. Rodier, J. Janin, A dissection of specific and non-specific protein-protein interfaces. *J. Mol. Biol.* **336**, 943–955 (2004).
6. J.M. Berg, J.L. Tymoczko, L. Stryer, *Biochemistry*. 6th ed. New York: W.H. Freeman (2007).
7. <http://www.britannica.com/EBchecked/topic/450900/peptide>
8. R. Zwanzig, A. Szabo, B. Magchi, Levinthal's paradox. *Proc. Natl. Acad. Sci. USA* **89**, 20–22 (1992).
9. J. Cheng, A. Randall, P. Baldi, *Proteins: Structure, Function, and Bioinformatics* **62**, 1125–1132 (2006).
10. T. Pawson, P. Nash, Assembly of cell regulatory systems through protein interaction domains. *Science* **300**, 445–452 (2003).
11. V. Neduva, R.B. Russell, Peptides mediating interaction networks: new leads at last. *Curr. Opin. Biotechnol.* **17**, 465–471 (2006).
12. E. Petsalaki, R.B. Russell, Peptide-mediated interactions in biological systems: new discoveries and applications. *Curr. Opin. Biotechnol.* **19**, 344–350 (2008).
13. Z. Hayouka, J. Rosenbluh, A. Levin, S. Loya, M. Lebendiker, D. Veprintsev, M. Kotler, A. Hizi, A. Loyter, A. Friedler, Inhibiting HIV-1 integrase by shifting its oligomerization equilibrium. *Proc. Natl. Acad. Sci. USA* **104**, 8316–8321 (2007).

14. L. Parthasarathi, F. Casey, A. Stein, P. Aloy, D.C. Shields, Approved drug mimics of short peptide ligands from protein interaction motifs. *J. Chem. Inf. Model.* **48**, 1943–1948 (2008).
15. L. Zhao, J. Chmielewski, Inhibiting protein-protein interactions using designed molecules. *Curr. Opin. Struct. Biol.* **15**, 31–34 (2005).
16. M. Uttamchandani, S.Q. Yao, Next generation chemical proteomic tools for rapid enzyme profiling. *Acc. Chem. Res.* **42**, 1183-1192 (2009).
17. Y. Shen, B.L. Wu, Microarray-based genomic DNA profiling technologies in clinical molecular diagnostics. *Clin. Chem.* **55**, 659-669 (2009).
18. O. Poetz, J.M. Schwenk, S. Kramer, D. Stoll, M.F. Templin, T.O. Jos, Protein microarrays: catching the proteome. *Mech. Ageing. Dev.* **126**, 161-170 (2005).
19. Y.M. Foong, J. Fu, Q.Y. Shao, M. Uttamchandani, Current advances in peptide and small molecule microarray technologies. *Curr. Opi. Chem. Biol.* **16**, 234-242 (2012).
20. B.B. Haab, Methods and applications of antibody microarrays in cancer research. *Proteomics* **3**, 2116–2122 (2003).
21. <http://ionsource.com/Card/aaTable/aanav.htm>
22. B.R. Merrifield, Solid phase peptide synthesis. I. The synthesis of a tetrapeptide. *J. Am. Chem. Soc.* **85**, 14, 2149-2154 (1963).
23. A. Furka, F. Sebestyen, M. Asgedom, G. Dibo, General method for rapid synthesis of multicomponent peptide mixtures. *Int. J. Peptide Protein Res.* **37**, 487-493 (1991).
24. S. Fodor, J. Read, M. Pirrung, L. Stryer, A. Lu, D. Solas, Light-directed spatially addressable parallel chemical synthesis. *Science* **251**, 767-773 (1991).
25. S. Singh-Gasson, R.D. Green, Y.J. Yue, C. Nelson, F. Blattner, M.R. Sussman, F. Cerrina, Maskless fabrication of light-directed oligonucleotide microarrays using a digital micromirror array. *Nature Biotechnology* **17**, 974-978 (1999).
26. V. Stadler, T. Felgenhauer, M. Beyer, S. Fernandez, K. Leibe, S. Güttler, M. Gröning, K. König, G. Torralba, M. Hausmann, V. Lindenstruth, A. Nesterov, I. Block, R. Pipkorn, A. Poustka, F.R. Bischoff, F. Breitling, Combinatorial synthesis of peptide arrays with a laser printer. *Angew. Chem. Int. Ed.* **47**, 37:7132-7135 (2008).

27. Aldrich, S., In Scheme for Solid phase Peptide Synthesis.
<http://www.sigmaaldrich.com/etc/medialib/brands/sigma/solid-phase-syn-schem.Par.0001.Image.500.gif>.
28. Stadler, V., et al., Combinatorial synthesis of peptide arrays with a laser printer. *Angewandte Chemie International Edition* **47**, 37: 7132-7135 (2008).
29. J.V. Price, S. Tangsombatvisit, G. Xu, J. Yu, D. Levy, E.C. Baechler, O. Gozani, M. Varma, P.J. Utz, C.L. Liu, On silico peptide microarrays for high-resolution mapping of antibody epitopes and diverse protein-protein interactions. *Nature Medicine* **18**, 1434-1441 (2012).
30. C. Agbavwe1, C. Kim, D. Hong, K. Heinrich, T. Wang, M.M. Somoza, Efficiency, error, and yield in light-directed maskless synthesis of DNA microarrays. *Journal of Nanobiotechnology* **9**, 57 (2011).
31. D. Montgomery, U.S. Patent 6, 280, 595 (2001).
32. R.W. Roberts, Totally In vitro protein selection using mRNA-protein fusions and ribosome display. *Curr. Opin. Chem. Biol.* **3**, 268–273 (1999).
33. S.E. Cwirla, E.A. Peters, R.W. Barrett, W.J. Dower, Peptides on phage: a vast library of peptides for identifying ligands. *Proc. Natl. Acad. Sci. USA* **87**, 6378–6382 (1990).
34. A. Furka, In G. Jung (Ed.), A handbook, VCH, New York, 111–138 (1996).
35. <http://www.pepperprint.com/products/pepperchip-custom-microarrays/>
36. X.Y. Xiao, R. Li, H. Zhuang, B. Ewing, K. Karunaratne, J. Lillig, R. Brown K.C. Nicolaou, Solid-phase combinatorial synthesis using MicroKan reactors, Rf tagging, and directed sorting. *Biotechnol Bioeng.* **71**, 44–50 (2000).
37. C.M. Salisbury, D.J. Maly, J.A. Ellman, Peptide microarrays for the determination of protease substrate specificity. *J. Am. Chem. Soc.* **124**, 14868–14870 (2002).
38. R. Frank, The SPOT-synthesis technique. Synthetic peptide arrays on membrane supports – principles and applications. *J. Immunol. Methods* **267**, 13–26 (2002).
39. K. Komolpiss, O. Srivannavit, E. Gulari, Light-directed simultaneous synthesis of oligopeptides on microarray substrate using a photogenerated acid. *Biotechnol. Prog.* **18**, 641–646 (2002).

40. K. Bialek, A. Swistowski, R. Frank, Anal. Bioanal. Chem.[Epub ahead of print] PMID: 12677339 (2003).
41. J.P. Pellois, W. Wang, X. Gao, Peptide synthesis based on t-boc chemistry and solution photogenerated acids. *J. Comb. Chem.* **2**, 355–360 (2000).
42. J.V. Price, S. Tangsombatvisit, G. Xu, J. Yu, D. Levy, E.C. Baechler, O. Gozani, M. Varma, P.J. Utz, C.L. Liu, *On silico* peptide microarrays for high resolution mapping of antibody epitopes and diverse protein-protein interactions. *Nature Medicine* **18**, 1434-1441 (2012).
43. V. Stadler et al., Combinatorial synthesis of peptide arrays with a laser printer. *Angewandte Chemie International Edition* **47**, 7132-7135 (2008).
44. S. Fodor, J. Read, M. Pirrung, L. Stryer, A. Lu, D. Solas, Light-directed, spatially addressable parallel chemical synthesis. *Science* **251**, 767-773 (1991).
45. S. Fodor, J. Read, M. Pirrung, L. Stryer, A. Lu, D. Solas, Light-directed, spatially addressable parallel chemical synthesis. *Science* **251**, 767-773 (1991).
46. R.J. Lipshutz, S.P.A. Fodor, T.R. Gingeras, High density synthetic oligonucleotide arrays. *Nature Genetics Supplements* **21**, 20-24 (1999).
47. G.H. McGall, A.D. Barone, M. Diggelmann, The efficiency of light-directed synthesis of DNA arrays on glass substrates. *Journal of the American Chemical Society* **119**, 5081- 5090 (1997).
48. T.J. Albert, J. Norton, M. Ott, T. Richmond, K. Nuwaysir, F. Emile, K.P. Stengele, R.D. Green, Light-directed synthesis of complex oligonucleotide microarrays. *Nucl. Acids Res.* **31**, e35 (2003).
49. A. Patchornik, B. Amit, R.B. Woodward, Photosensitive protecting groups. *Journal of the American Chemical Society* **92**, 6333-6335 (1970).
50. V.N.R. Pillai, Photoremovable protecting groups in organic synthesis. *Synthesis* **1**, 1-26 (1980).
51. C.P. Holmes, D.W. Solas, B. Kiangsoontra, WO 9410128, P.I. Appl., Editor. 1994.
52. M. Beier, J.D. Hoheisel, Production by quantitative photolithographic synthesis of individually quality checked DNA microarrays. *Nucleic Acid Research* **28**, e11 (2000).

53. C.G. Bochet, Wavelength-selective cleavage of photolabile protecting groups. *Tetrahedron Letters* **41**, 6341 (2000).
54. K.R. Bhushan, D. Charles, R.A. Laursen, Synthesis of photolabile 2-(2-nitrophenyl)propyloxycarbonyl protected amino acids. *Tetrahedron Letters* **44**, 8585-8588 (2003).
55. K. Maurer, A. McShea, M. Strathmann, K. Dill, The removal of the t-boc group by electrochemically generated acid and use of an addressable electrode array for peptide synthesis. *J. Combi. Chem.* **7**, 637-640 (2005).
56. K. Dill, D. Montgomery, W. Wang, J.C. Tsai, Antigen detection using microelectrode array microchips. *Anal. Chim. Acta* **444**, 69 (2001).
57. Montgomery, D. U.S. Patent 6,093,302, 2000.
58. Montgomery, D. U.S. Patent 6,280, 595, 2001.
59. www.customarrayinc.com
60. M. Baker, Microarrays, megasynthesis. *Nature Methods* **8**, 457-460 (2011).
61. J. March, M.B. Smith, Advanced Organic Chemistry (5th edition), John Wiley & Sons, Inc. (2005).
62. K. Maurer, J. Cooper, M. Strathmann, A. Gindilis, United States Patent Application Publication 2006/0102471 (2006).
63. R.D. Egeland, E.M. Southern, Electrochemically directed synthesis of oligonucleotides for DNA microarray fabrication. *Nucleic Acids Res.* **33**, e125 (2005).
64. K. Maurer, J. Cooper, M. Caraballo, J. Crye, D. Suciu, A. Ghindilis, J.A. Leonetti, W. Wang, W.M. Rossi, A.G. Stover, C. Larson, H. Gao, K. Dill, A. McShea, Electrochemically generated acid and its containment to 100 micron reaction areas for the production of DNA microarrays. *PLoS One* **1**, e34 (2006).
65. P. Kumar, M.P. Greving, Z.G. Zhao, N.W. Woodbury, Feature-level MALDI-MS characterization of in situ-synthesized peptide microarrays. *Langmuir* **26**, 1456-1459 (2010).
66. Y. Li, J. Xiang, F. Zhou, Sensitive and label-free detection of DNA by surface plasmon resonance. *Plasmonics* **2**, 79-87 (2007).

67. B. Becker, M. A. Cooper, A survey of the 2006-2009 quartz crystal microbalance biosensor literature. *Journal of Molecular Recognition*. **24**, 754-787 (2011).
68. D. Woll, J. Smirnova, M. Galetskaya, T. Prykota, J. Bühler, K.P. Stengele, W. Pfleiderer, U.E. Steiner, Intramolecular sensitization of photocleavage of the photolabile NPPOC protecting group: photoproducts and photokinetcs of the release of nucleosides. *Chem. Eur. J.* **14**, 6490-6497 (2008).
69. D. Woll, W. Dominik, J. Smirnova, W. Pfleiderer, U.E. Steiner, Highly efficient photolabile protecting groups with intramolecular energy transfer. *Angew. Chem. Int. Ed.* **45**, 2975-2978 (2006).

Chapter 2

1. J.A. Barltrop, P. Schofield, Photosensitive protecting groups. *Tetrahedron Letters*, 697-699 (1962).
2. A. Patchornik, B. Amit, R. Woodward, Photosensitive protecting groups. *Journal of the American Chemical Society* **92**, 6333-6335 (1970).
3. C.H. Bamford, R.G.W. Norrish, Primary photochemical reactions. VII. Photochemical decomposition of isovaleraldehyde and dipropyl ketone. *Journal of the American Chemical Society*, 1504-1511 (1935).
4. P. Wan, K. Yates, Photoredox chemistry of nitrobenzyl alcohols in aqueous solution. Acid and base catalysis of reaction. *Canadian Journal of Chemistry* **64**, 2076-2086 (1986).
5. C.G. Bochet, Photolabile protecting groups as linkers. *Perkin Trans.* **1**, 125-142 (2002).
6. G.H. McGall et al., The efficiency of light-directed synthesis of DNA arrays on glass substrates. *Journal of the American Chemical Society* **119**, 5081-5090 (1997).
7. M.C. Pirrung et al., Pentadienylnitrobenzyl and pentadienylnitropiperonyl photochemically removable protecting groups. *Journal of Organic Chemistry* **64**, 5042-5047 (1999).
8. C.P. Holmes et al., Preparation of novel nitrobenzyl derivative photoreactive protecting reagents., P.I. Appl., Editor. (1994).

9. M. Beier, J.D. Hoheisel, Production by quantitative photolithographic synthesis of individually quality checked DNA microarrays. *Nucleic Acids Research* **28**, e11 (2000).
10. T.J. Albert, J. Norton, M. Ott, T. Richmond, K. Nuwaysir, E.F. Nuwaysir, K.P. Stengele, R.D. Green, Light-directed synthesis of complex oligonucleotide microarrays. *Nucl. Acids Res.* **31**, e35 (2003).
11. D. Woll, W. Dominik, J. Smirnova, W. Pfliederer, U.E. Steiner, Highly efficient photolabile protecting groups with intramolecular energy transfer. *Angew. Chem. Int. Ed.* **45**, 2975-2978 (2006).
12. D. Wöll, J. Smirnova, M. Galetskaya, T. Prykota, J. Bühler, K.P. Stengele, W. Pfliederer, U.E. Steiner, Intramolecular sensitization of photocleavage of the photolabile NPPOC protecting group: photoproducts and photokinetics of the release of nucleosides. *Chem. Eur. J.* **14**, 6490-6497 (2008).
13. A. Hasan et al., Photolabile protecting groups for nucleosides. *Tetrahedron* **53**, 4247-4264 (1997).
14. K.R. Bhushan, D. Charles, R.A. Laursen, Synthesis of photolabile 2-(2-nitrophenyl)propyloxycarbonyl protected amino acids. *Tetrahedron Letters* **44**, 8585-8588 (2003).
15. D.H. Min, M. Mrksich, Peptide arrays: toward routine implementation. *Current opinion in chemical biology* **8**, 554-558 (2004).
16. P. Klán, T. Šolomek, C.G. Bochet, A. Blanc, R. Givens, M. Rubina, V. Popik, A. Kostikov, J. Wirz, Photoremovable Protecting Groups in Chemistry and Biology: Reaction Mechanisms and Efficacy. *Chem. Rev.* **113**, 119-191 (2013).

Chapter 3

1. P. Kumar, M.P. Greiving, Z.G. Zhao, N.W. Woodbury, Feature-level MALDI-MS characterization of in situ-synthesized peptide microarrays. *Langmuir* **26**, 1456-1459 (2010).
2. M. Chee, R. Yang, E. Hubbell, A. Berno, X.C. Huang, D. Stern, J. Winkler, D.J. Lockhart, M.S. Morris, S.P. Fodor, Accessing genetic information with high-density DNA arrays. *Science* **274**, 610-614 (1996).
3. X. Gao, E. LeProust, H. Zhang, O. Srivannavit, E. Gulari, P. Yu, C. Nishiguchi, Q. Xiang, X. Zhou, A flexible light-directed DNA chip synthesis gated by

- deprotection using solution photogenerated acids. *Nucleic Acids Res.* **29**, 4744–4750 (2001).
4. T.R. Hughes, M. Mao, A.R. Jones, J. Burchard, M.J. Marton, K.W. Shannon, S.M. Lefkowitz, M. Ziman, J.M. Schelter, M.R. Meyer, S. Kobayashi, C. Davis, H. Dai, Y.D. He, S.B. Stephanians, G. Cavet, W.L. Walker, A. West, E. Coffey, D.D. Shoemaker, R. Stoughton, A.P. Blanchard, S.H. Friend, P.S. Linsley, Expression profiling using microarrays fabricated by an ink-jet oligonucleotide synthesizer. *Nat. Biotechnol.* **19**, 342–347 (2001).
 5. R.J. Lipshutz, S.P. Fodor, T.R. Gingeras, D.J. Lockhart, High density synthetic oligonucleotide arrays. *Nat. Genet.* **21**, 20–24 (1999).
 6. A.C. Pease, D. Solas, E.J. Sullivan, M.T. Cronin, C.P. Holmes, S.P. Fodor, Light-generated oligonucleotide arrays for rapid DNA sequence analysis. *Proc. Natl. Acad. Sci. U.S.A.* **91**, 5022–5026 (1994).
 7. S. Singh-Gasson, R.D. Green, Y. Yue, C. Nelson, F. Blattner, M.R. Sussman, F. Cerrina, Maskless fabrication of light-directed oligonucleotide microarrays using a digital micromirror array. *Nat. Biotechnol.* **17**, 974–978 (1999).
 8. M. Beyer, A. Nesterov, I. Block, K. König, T. Felgenhauer, S. Fernandez, K. Leibe, G. Torralba, M. Hausmann, U. Trunk, V. Lindenstruth, F.R. Bischoff, V. Stadler, F. Breitling, Combinatorial synthesis of peptide arrays onto a chip. *Science* **318**, 1888 (2007).
 9. R. Frank, The SPOT-synthesis technique. Synthetic peptide arrays on membrane supports--principles and applications. *J. Immunol. Methods* **267**, 13–26 (2002).
 10. F.G. Kuruvilla, A.F. Shamji, S.M. Sternson, P.J. Hergenrother, S.L. Schreiber, Dissecting glucose signalling with diversity-oriented synthesis and small-molecule microarrays. *Nature* **416**, 653–657 (2002).
 11. G. MacBeath, S.L. Schreiber, Printing proteins as microarrays for high-throughput function determination. *Science* **289**, 1760–1763 (2000).
 12. Maurer, A. McShea, M. Strathmann, K. Dill, The removal of the t-boc group by electrochemically generated acid and use of an addressable electrode array for peptide synthesis. *J. Comb. Chem.* **7**, 637–640 (2005).
 13. T.R. Northen, M.P. Greving, N.W. Woodbury, Combinatorial screening of biomimetic protein affinity materials. *Adv. Mater.* **20**, 4691–4697 (2008).

14. S. Park, I. Shin, Fabrication of carbohydrate chips for studying protein-carbohydrate interactions. *Angew. Chem., Int. Ed.* **41**, 3180–3182 (2002).
15. J.P. Pellois, X. Zhou, O. Srivannavit, T. Zhou, E. Gulari, X. Gao, Individually addressable parallel peptide synthesis on microchips. *Nat. Biotechnol.* **20**, 922–926 (2002).
16. M. Pirrung, Spatially addressable combinatorial libraries. *Chem. Rev.* **97**, 473–488 (1997).
17. N. Ramachandran, E. Hainsworth, B. Bhullar, S. Eisenstein, B. Rosen, A.Y. Lau, J.C. Walter, J. Labaer, Self-assembling protein microarrays. *Science* **305**, 86–90 (2004).
18. M. Pirrung, How to make a DNA chip. *Angew. Chem., Int. Ed.* **41**, 1276–1289 (2002).
19. R.B. Wallace, J. Shaffer, R.F. Murphy, J. Bonner, T. Hirose, K. Itakura, Hybridization of synthetic oligodeoxyribonucleotides to phi chi 174 DNA: the effect of single base pair mismatch. *Nucleic Acids Res.* **6**, 3543–3557 (1979).
20. B.J. Conner, A.A. Reyes, C. Morin, K. Itakura, R.L. Teplitz, R.B. Wallace, Detection of sickle cell beta S-globin allele by hybridization with synthetic oligonucleotides. *Proc. Natl. Acad. Sci. U.S.A.* **80**, 278–282 (1983).
21. U. Maskos, E.M. Southern, Oligonucleotide hybridisations on glass supports: a novel linker for oligonucleotide synthesis and hybridisation properties of oligonucleotides synthesised *in situ*. *Nucleic Acids Res.* **20**, 1679–1684 (1992).
22. Hilpert, D.F.H. Winkler, R.E.W. Hancock, Peptide arrays on cellulose support: SPOT synthesis, a time and cost efficient method for synthesis of large numbers of peptides in a parallel and addressable fashion. *Nat. Protoc.* **2**, 1333–1349 (2007).
23. O. Michel, B.J. Ravoo, Carbohydrate microarrays by microcontact ‘Click’ chemistry. *Langmuir* **24**, 12116–12118 (2008).
24. K.R. Bhushan, Light-directed maskless synthesis of peptide arrays using photolabile amino acid monomers. *Org. Biomol. Chem.* **4**, 1857–1859 (2006).
25. T.R. Northen, D.C. Brune, N.W. Woodbury, Synthesis and characterization of peptide grafted porous polymer microstructures. *Biomacromolecules* **7**, 750–754 (2006).

26. S. Chen, M.F. Phillips, F. Cerrina, L.M. Smith, Controlling oligonucleotide surface density in light-directed DNA array fabrication. *Langmuir* **25**, 6570–6575 (2009).
27. V. Tapia, J. Bongartz, M. Schutkowski, N. Bruni, A. Weiser, B. Ay, R. Volkmer, M. Or-Guil, Affinity profiling using the peptide microarray technology: A case study. *Anal. Biochem.* **363**, 108–118 (2007).
28. D. Zichi, B. Eaton, B. Singer, L. Gold, Proteomics and diagnostics: let's get specific, again. *Curr. Opin. Chem. Biol.* **12**, 78–85 (2008).
29. C. Chen, G. Nagy, A.V. Walker, K. Maurer, A. McShea, K.D. Moeller, Building addressable libraries: the use of a mass spectrometry cleavable linker for monitoring reactions on an microelectrode array. *J. Am. Chem. Soc.* **128**, 16020–16021 (2006).
30. C. Chen, P. Lu, A. Walker, K. Maurer, K.D. Moeller, Building addressable molecular libraries: the use of a detectable mass spectrometry cleavable linker. *Electrochem. Commun.* **10**, 973–976 (2008).
31. R.M. Heeren, Proteome imaging: a closer look at life's organization. *Proteomics* **5**, 4316–4326 (2005).
32. MacAleese, J. Stauber, R.M. Heeren, Perspectives for imaging mass spectrometry in the proteomics landscape. *Proteomics* **9**, 819–834 (2009).
33. Z.H. Huang, J. Wu, K.D.W. Roth, Y. Yang, D.A. Gage, J. T. Watson, A Picomole-Scale Method for Charge Derivatization of Peptides for Sequence Analysis by Mass Spectrometry. *Anal. Chem.* **69**, 137-144 (1997).
34. Stoeckli, P. Chaurand, D.E. Hallahan, R.M. Caprioli, Imaging mass spectrometry: a new technology for the analysis of protein expression in mammalian tissues. *Nat. Med.* **7**, 493–496 (2001).

Chapter 4

1. O. Stoevesandt, M. J. Taussig, M. He, Protein microarrays: high-throughput tools for proteomics. *Expert Review of Proteomics* **6**, 145 (2009).
2. V. Tapia, J. Bongartz, M. Schutkowski, N. Bruni, A. Weiser, B. Ay, R. Volkmer, M. Or-Guil, Affinity profiling using the peptide microarray technology: A case study. *Analytical Biochemistry* **363**, 108 (2007).

3. K. Stoffel, H.V. Leeuwen, A. Kozik, D. Caldwell, H. Ashrafi, X. Cui, X. Tan, T. Hill, S. Reyes, C. Wo, M. Jose, R.W. Micheltore, A.V. Deynze, *BMC Genomics* **13**, 185 (2012).
4. H. Park, J. Kim, Y.S. Ju, O. Gokcumen, R.E. Mills, S. Kim, S. Lee, D. Suh, D. Hong, H.P. Kang, Y.J. Yoo, J.Y. Shin, H.J. Kim, M. Yavartanoo, Y.W. Chang, J.S. Ha, W. Chong, G.R. Hwang, K. Darvishi, H.R. Kim, S.J. Yang, K.S. Yang, H. Kim, M.E. Hurles, S.W. Scherer, Discovery of common Asian copy number variants using integrated high-resolution array CGH and massively parallel DNA sequencing. *Nature Genetics* **42**, 400–405 (2010).
5. J.C. Mills, K.A. Roth, R.L. Cagan, J.I. Gordon, DNA microarrays and beyond: completing the journey from tissue to cell. *Nature Cell Biology* **3**, E175-E178 (2001).
6. G. MacBeath, S.L. Schreiber, Printing proteins as microarrays for high-throughput function determination. *Science* **289**, 1760-1763 (2000).
7. O.P. Kallioniemi, U. Wagner, J. Kononen, G. Sauter, Tissue microarray technology for high-throughput molecular profiling of cancer. *Mol. Genet.* **10**, 657-662 (2001).
8. H. Wu, J. Ge, M. Uttamchandani, S.Q. Yao, Small molecule microarrays: the first decade and beyond. *Chem Commun(Camb)* **47**, 5664-5670 (2011).
9. K. Hattori, S. Sugiura, T. Kanamori, Microenvironment array chip for cell culture environment screening. *Lab on a Chip* **11**, 212-214 (2011).
10. R. Frank, SPOT-synthesis: an easy technique for the positionally addressable, parallel chemical synthesis on a membrane support. *Tetrahedron* **48**, 42:9217-9232 (1992).
11. S. Fodor, J. Read, M. Pirrung, L. Stryer, A. Lu, D. Solas, Light-directed, spatially addressable parallel chemical synthesis. *Science* **251**, 767-773 (1991).
12. S. Singh-Gasson, R.D. Green, Y.J. Yue, C. Nelson, F. Blattner, M.R. Sussman, F. Cerrina, Maskless fabrication of light-directed oligonucleotide microarrays using a digital micromirror array. *Nature Biotechnology* **17**, 974-978 (1999).
13. V. Stadler, T. Felgenhauer, M. Beyer, S. Fernandez, K. Leibe, S. Güttler, M. Gröning, K. König, G. Torralba, M. Hausmann, V. Lindenstruth, A. Nesterov, I. Block, R. Pipkorn, A. Poustka, F.R. Bischoff, F. Breitling, Combinatorial synthesis of peptide arrays with a laser printer. *Angew. Chem. Int. Ed.*, **47**, 7132-7135 (2008).

14. V. Stadler et al., Combinatorial synthesis of peptide arrays with a laser printer. *Angewandte Chemie International Edition* **47**, 7132-7135 (2008).
15. K. Maurer, A. McShea, M. Strathmann, K. Dill, The removal of the t-boc group by electrochemically generated acid and use of an addressable electrode array for peptide synthesis. *J. Combi. Chem.* **7**, 637-640 (2005).
16. E. LeProust, J.P. Pellois, P. Yu, H. Zhang, O. Srivannavit, E. Gulari, X. Zhou, X. Gao, Digital light-directed synthesis. A microarray platform that permits rapid reaction optimization on a combinatorial basis. *J. Comb. Chem.* **2**, 349-354 (2000).
17. X.Y. Xiao, R. Li, H. Zhuang, B. Ewing, K. Karunaratne, J. Lillig, R. Brown, K.C. Nicolaou, Solid-phase combinatorial synthesis using MicroKan reactors, Rf tagging, and directed sorting. *Biotechnol Bioeng.* **71**, 44-50 (2000).
18. K. Dill, D. Montgomery, W. Wang, J.C. Tsai, Antigen detection using microelectrode array microchips. *Anal. Chim. Acta* **444**, 69 (2001). (b) D. Montgomery, U.S. Patent 6,093,302 (2000). (c) D. Montgomery, U.S. Patent 6,280, 595 (2001).

Chapter 5

1. Y.M. Foong, J. Fu, S.Q. Yao, M. Uttamchandani, Current advances in peptide and small molecule microarray technologies. *Curr. Op. Chem. Biol.* **16**, 234-242 (2012).
2. Y. Shen, B.L. Wu, Microarray-based genomic DNA profiling technologies in clinical molecular diagnostics. *Clin. Chem.* **55**, 659-669 (2009).
3. J.C. Mills, K.A. Roth, R.L. Cagan, J.I. Gordon, DNA microarrays and beyond: completing the journey from tissue to cell. *Nat. Cell. Biol.* **3**, e175-e178 (2001).
4. B.B. Haab, Methods and applications of antibody microarrays in cancer research. *Proteomics* **3**, 2116-2122 (2003).
5. E.A. Smith, M. Kyo, H. Kumasawa, K. Nakatani, Chemically induced hairpin formation in DNA monolayers. *J. Am. Chem. Soc.* **124**, 6810-6811 (2002).
6. Y. Li, J. Xiang, F. Zhou, Sensitive and label-free detection of DNA by surface plasmon resonance. *Plasmonics* **2**, 79-87 (2007).

7. C. Berggren, G. Johansson, Capacitance measurements of antibody-antigen interactions in a flow system. *Anal. Chem.* **69**, 3651–3657 (1997).
8. D. Jiang, J. Tang, B. Liu, P. Yang, J. Kong, Ultrathin aluminasol-gel-derived films: allowing direct detection of the liver fibrosis markers by capacitance measurement. *Anal. Chem.* **75**, 4578–4584 (2003).
9. P. Kumar, M.P. Greving, Z.G. Zhao, N.W. Woodbury, Feature-level MALDI-MS characterization of in situ-synthesized peptide microarrays. *Langmuir* **26**, 1456–1459 (2010).
10. D. Nedelkov, R.W. Nelson, Delineating protein-protein interactions via biomolecular interaction analysis-mass spectrometry. *J. Mol. Recognit.* **16**, 9–14 (2003).
11. D. Nedelkov, R.W. Nelson, Design and use of multi-affinity surfaces in biomolecular interaction analysis-mass spectrometry (BIA/MIS): a step toward the design of SPR/MS arrays. *J. Mol. Recognit.* **16**, 15–19 (2003).
12. L. Yang, Y. Li, G.F. Erf, Interdigitated Array microelectrode-based electrochemical impedance immunosensor for detection of Escherichia coli O157:H7. *Anal. Chem.* **76**, 1107–1113 (2004).
13. M. Wang, L. Wang, G. Wang, X. Ji, Application of impedance spectroscopy for monitoring colloid Au-enhanced antibody immobilization and antibody-antigen reactions. *Biosens. Bioelectron.* **19**, 575–582 (2004).
14. X. Yu, D. Xu, D. Xu, Z. Liu, An impedance biosensor array for label-free detection of multiple antigen-antibody reactions. *Front. Biosci.* **11**, 983–990 (2006).
15. D. Xu, D. Xu, X. Yu, Z. Liu, Label-free electrochemical detection for aptamer-based array electrodes. *Anal. Chem.* **77**, 5107–5113 (2005).
16. K. M. Roth, K. Peyvan, K. R. Schwarzkopf, A. Ghindilis, Electrochemical detection of short DNA oligomer hybridization using the CombiMatrix Electrasense microarray reader. *Electroanalysis* **18**, 1982–1988 (2006).
17. J.J. Gau, E.H. Lan, B. Dunn, A MEMS based amperometric detector for E-Coli bacteria using self-assembled monolayers. *Biosens. Bioelectron.* **16**, 745–755 (2001).
18. R.J. Cotter, Time-of-flight mass-spectrometry for the structural-analysis of biological molecules. *Anal. Chem.* **64**, A1027–A1039 (1992).

19. B.T. Chait, S.B.H. Kent, Weighing naked proteins: practical high accuracy mass measurement of peptides and proteins. *Science* **257**, 1885–1894 (1992).
20. F. Hillenkamp, M. Karas, R.C. Beavis, B.T. Chait, Matrix-assisted laser desorption ionization mass spectrometry of biopolymers. *Anal. Chem.* **63**, A1193–A1202 (1991).
21. R. Aebersold, M. Mann, Mass spectrometry-based proteomics. *Nature* **422**, 198–207 (2003).
22. Y. Umena, K. Kawakami, J. Shen, N. Kamiya, Crystal structure of oxygen-evolving system Photosystem II at a resolution of 1.9Å. *Nature* **473**, 55–60 (2011).
23. T.A. Betley, Q. Wu, T.V. Voorhis, D.G. Nocera, Electronic design criteria for O—O bond formation via metal—oxo complexes. *Inorg. Chem.* **47**, 1849 (2008).
24. Y. Wang, K.S. Chen, J. Mishler, S.C. Cho, X.C. Adroher, A review of polymer electrolyte membrane fuel cells: Technology, applications, and needs on fundamental research. *Applied Energy* **88**, 981 (2011).
25. H. Zhang, G. Lin, J. Chen, Evaluation and calculation on the efficiency of a water electrolysis system for hydrogen production. *International Journal of Hydrogen Energy* **35**, 10851–10858 (2010).
26. W. Cady, R.H. Crabtree, G.W. Brudvig, Functional models for the oxygen-evolving complex of photosystem II. *Coord. Chem. Rev.* **252**, 444–455 (2008).
27. Kalman, L., Williams, J.C., Allen, J.P., Comparison of bacterial reaction centers and Photosystem II. *Photosynthesis Research* **98**, 643–655 (2008).
28. D.S. Minehan, K.A. Marx, S.K. Tripathy, Kinetics of DNA binding to electrically conducting polypyrrole films. *Macromolecules* **27**, 777–783 (1994).
29. M. Rahman, P. Kumar, D.S. Park, Y.B. Shim, Electrochemical sensors based on organic conjugated polymers. *Sensors* **8**, 118–141 (2008).
30. H. Peng, L. Zhang, C. Soeller, Travas-Sejdic, Conducting polymers for electrochemical DNA sensing. *Biomaterials* **30**, 2132–2148 (2009).
31. K. Maurer, N. Yazvenko, J. Wilmoth, J. Cooper, W. Lyon, D. Danley, Use of a multiplexed CMOS microarray to optimize and compare oligonucleotide binding

- to DNA probes synthesized or immobilized on individual electrodes. *Sensors* **10**, 7371-7385 (2010).
32. J. Cooper, N. Yazvenko, K. Peyvan, K. Maurer, C.R. Taitt, W. Lyon, D.L. Danley, Targeted Deposition of Antibodies on a Multiplex CMOS Microarray and Optimization of a Sensitive Immunoassay Using Electrochemical Detection. *PLoS ONE* **5**, e9781 (2010).
 33. T. Livache, A. Roget, E. Dejean, C. Barthet, G. Bidan, R. Teoule, Preparation of a DNA matrix via an electrochemically directed copolymerization of pyrrole and oligonucleotides bearing a pyrrole group. *Nucleic Acids Research* **22**, 2915-2921 (1994).
 34. T. Livache, E. Maillart, N. Lassalle, P. Mailley, B. Corso, P. Guedon, A. Roget, Y. Levy, Polypyrrole based DNA hybridization assays: Study of label free detection processes versus fluorescence on microchips. *J. Pharm. Biomed. Anal.* **32**, 687 (2003).
 35. O. Niwa, M. Morita, H. Tabei, Electrochemical behaviour of reversible redox species at interdigitated array electrodes with different geometries: consideration of redox cycling and collection efficiency. *Anal. Chem.* **62**, 447-452 (1990).
 36. F. Rebiere, O. Samuel, H.B. Kagan, A convenient method for the preparation of monolithioferrocene. *Tetrahedron Letters* **31**, 3121 (1990).
 37. S. Sadki, P. Schottland, N. Brodie, B. Sabouraud, The mechanisms of pyrrole electropolymerization. *Chem. Soc. Rev.* **29**, 283-293 (2000).
 38. Y. Tan, K. Ghandi, Kinetics and mechanism of pyrrole chemical polymerization. *Synthetic Metals* **175**, 183-191 (2013).

APPENDIX A

A STUDY OF ELECTROCHEMICAL DEPROTECTION EFFICIENCY OF TRITYL GROUPS USING MALDI-BASED MICROARRAY CHARACTERIZATION TECHNIQUE

The starting point in titration, 3.0V 3min, was based on the condition used by Maurer et al. for deprotecting boc groups. At this point, in order to further improve the deprotection efficiency of Trt groups, dimethoxytrityl (DMT) protecting group and hydroquinone as EGA-P were included in our studies. Montgomery et al. has described the use of Hydroquinone as EGA-P for electrochemical deprotection of DMT groups during oligonucleotide synthesis on CBMX chips. They employed 0.26 μ A and 30seconds condition for its deprotection. Therefore, we investigated the electrochemical deprotection efficiency of DMT using N,N'-diphenylhydrazine at 3.0V 10min condition, and Hydroquinone at 0.26 μ A 30s condition. It was observed that N,N'-diphenylhydrazine as EGA-P deprotected DMT with approximately 88.7% stepwise yield, and hydroquinone as EGA-P deprotected DMT with approximately 85% stepwise yield. The control regions of the chip in these experiments, where no gating step was involved, also underwent electrochemical deprotection. The MALDI spectra of the control regions of these experiments showed that 75% of the control peptide with N,N'-diphenylhydrazine, and 80% with Hydroquinone, got electrochemically deprotected. Such electrochemical deprotection from the control region was undesired. Because of this, the cause of non-specific deprotection was investigated. We also investigated the behavior of Trt with Hydroquinone as EGA-P. Approximately 75% of the Trt was deprotected in the gating step. Approximately 17% of peptides from the control region were also deprotected when Hydroquinone was used as EGA-P. It should be noted that when Trt was removed electrochemically, using N,N'-diphenylhydrazine as EGA-P, no such undesired deprotection from the control region was seen. Therefore, we developed a desired system

(250mM N,N'-diphenylhydrazine and 250mM tetrabutylammoniumhexafluorophosphate in DCM, 3.0V 10min) which could selectively deprotect Trt groups. The system was developed so that no non-specific deprotection could be seen. The results are summarized in Table A-1 below.

TABLE A-1: % electro-deprotection of Trt and DMT groups at 3.0V 10min condition.

% electro-deprotection efficiency	N,N'- diphenyl hydrazine as EGA-P	Hydroquinone as EGA-P
Trityl protecting groups	68.4% deprotection No deprotection in control region	70% deprotection 17% deprotection in control region
Dimethoxytrityl protecting groups	88.7% deprotection 75.8% deprotection in control region	85% deprotection 80% deprotection in control region

TABLE A-1: Data shown in Table A1 corresponds to the deprotection efficiency of Trt and DMT groups using N,N'-diphenylhydrazine and Hydroquinone. Also shown is the unwanted deprotection of these groups from the control region without any application of voltage when exposed to the two EGA-P solutions.

To understand such non-specific deprotection during the gating step, we first considered any undesired electric potential, which was applied across the chip due to hardware malfunctioning. Consequently, similar experiments were conducted with the electrosynthesis instrument turned 'ON', but maintained at 0.0V. Surprisingly, DMT

groups present on the chip surface were deprotected when the chip was exposed to EGA-P solutions at zero volts. The results are summarized in Table A2 below.

TABLE A-2: % deprotection of DMT and Trt groups at zero volts

Hydroquinone as EGA-P	% deprotection at zero volts	N,N'-diphenyl hydrazine as EGA-P	% deprotection at zero volts
DMT	80%	DMT	80%
Trt	15%	Trt	stable

TABLE A-2: Data shown in Table A-2 corresponds to % deprotection of DMT and Trt groups when exposed to Hydroquinone and N,N'-diphenylhydrazine solution. During this exposure the instrument was turned ON, but maintained at 0.0 volts.

Here again, Trt remained stable to N,N'-diphenylhydrazine. At this point, it was inferred that there were three possible reasons for the instability of the Trt and DMT groups. These included (i) instability from EGA-P solutions, (ii) EGA-P solution in conjunction with Platinum electrode surface, or (iii) a chip with some electric potential due to hardware malfunctioning. Diffusion of protons from the selectively addressed region to the control region may not be the cause, though this aspect could not be completely ignored. It cannot be discounted because the deprotection was observed even at zero volts. The stability of Trt and DMT groups present on the chip to EGA-P solutions was determined by exposing the chip to EGA-P solutions without turning on the electro-synthesis instrument. The Trt and DMT groups underwent deprotection and showed similar results as observed with the application of zero volts. It was then assumed that either the Trt and DMT groups are not stable to EGA-P solutions or it was possible

that the Platinum electrode surface was influencing the deprotection when exposed to EGA-P solutions. Therefore, the stability of Trt and DMT groups to EGA-P solutions was tested using beads, instead of on the chip surface. In this experiment, a peptide NH₂-GFKGFKGFK-CONH₂ with a photo-labile linker at the C-terminal was synthesized on PAL-resin by conventional Fmoc chemistry. The N-terminal amine of the peptide was protected with Trt group on one set of beads, and with DMT group on another set of beads. Subsets of such beads were exposed to EGA-P solutions with different concentrations of base, Lutidine, ranging from 0.1M to 0.5 M. The beads were then washed with dichloromethane and N,N'-dimethylformamide solvents and the peptide present on the beads were cleaved photolytically. The cleaved peptides were collected by filtration and characterized by MALDI mass spectrometry. The MALDI spectra showed peaks corresponding to the peptide with Trt and DMT groups present, intact, on the N-terminal amine. No peaks were seen in the MALDI spectra corresponding to Trt or DMT deprotection upon exposure to EGA-P solutions (Figure A-1).

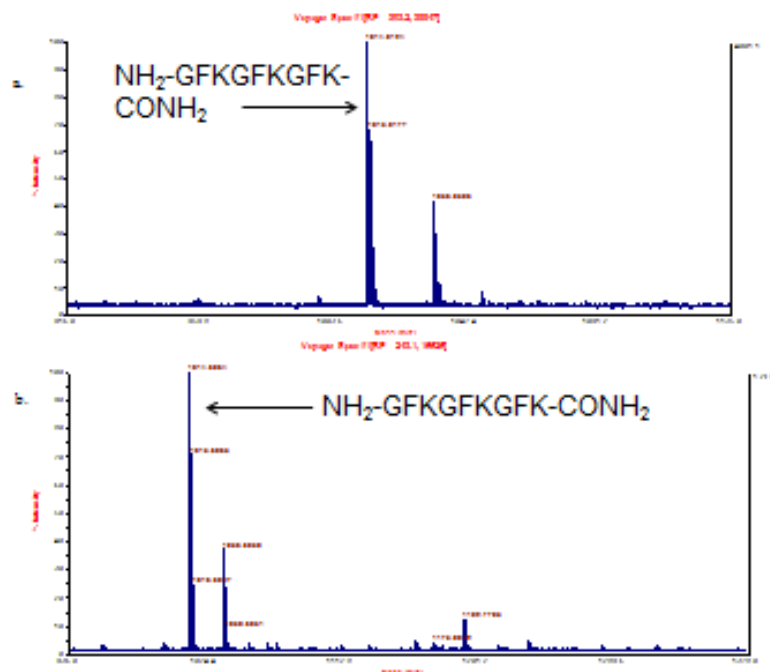


FIGURE A-1: MALDI-MS characterization of electrochemical deprotection of Trt and DMT groups using Hydroquinone as EGA-P. The two MALDI spectra, a & b, correspond to peptides with terminal glycine protected with DMT and Trt groups respectively. Both the peptides were exposed to Hydroquinone EGA-P solution. The MALDI spectrum did not show any cleavage of Trt or DMT group upon exposure to Hydroquinone solution. If the cleavage had taken place, a phenylalanine group should have been added to the N-terminal of the peptide. However, the peaks in the spectrum do not show the presence of phenylalanine at all. Similar results were observed with N,N'-diphenylhydrazine as EGA-P solution.

Based on the abovementioned set of experiments, it seems that Trt and DMT groups are unstable to EGA-P solutions on the chip surface. The platinum electrode surface is influencing the deprotection of Trt and DMT groups by EGA-P solutions. The mechanism of this observation is not yet clear. In literature, there are reports of Trt deprotection by catalytic hydrogenolysis. One of the problems with this hypothesis is that the catalytic hydrogenolysis reactions generally require high-pressure conditions, ranging from 3atm to 200atm for different kind of substrates, whereas the pressure inside the peptide synthesizer is usually 6psi, less than 1 atm. Another argument against this hypothesis could be that catalytic hydrogenolysis is not usually a fast reaction, whereas the chips were exposed to EGA-P solutions for not more than ten minutes. It is possible that some other kind of organometallic reaction mechanism was deprotecting the Trt and DMT groups by EGA-P solutions. Collaboration with research labs focused on organometallic chemistry would be helpful to discern these observations. A part of our research lab is focused in bioorganic chemistry, with an aim to develop tools for medical applications. However, organometallic chemistry, an exclusive class of synthetic organic chemistry, does not have much scope in our research goals.

Nevertheless, based on this study, it was determined that with N,N'-diphenylhydrazine as EGA-P and at 3.0V, under a 10 minute electrical condition, about 70% electrochemical deprotection efficiency of Trt could be achieved without any non-specific deprotection. Here we would like to demonstrate the advantages of an application of fluorescence and use of the MALDI detection method in conjunction with parallel synthesis optimization. This is compared to an application of sole fluorescence

method or MALDI detection method. Although we developed a system to electrochemically deprotect Trt using N,N'-diphenylhydrazine, the electrical condition, (3.0V 10min) associated with it is quite stringent. At this potential, several side redox transformations could be possible. Titration experiments were conducted in order to find an optimal electrical condition at which deprotection is high and chances of side redox transformations is low.

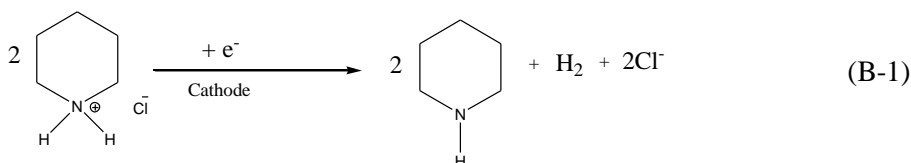
Since several electrical conditions were to be tested, fluorescence detection method instead of MALDI detection method was opted. As discussed earlier, with fluorescence detection methods, the chemical nature of the synthesis products cannot be determined. However, fluorescence methods are useful for titration experiments, in which a large number of conditions along with multiple replicates of each condition are tested. The MALDI detection method is useful for direct characterization of parallel synthesis, but at present, not many titration conditions can be tested at once on a single chip. At best, we can only test six different titration conditions on a chip at one time. This constraint is due to the difficulty associated with applying the fine MALDI matrix across the chip in such a way that cleaved peptides from one feature does not get diffused to neighboring features. Such precise application of matrix is possible only through expensive instrumentation, which is generally available only in MALDI mass spectrometry based research labs. In addition, difficulty is associated with the software program that can store thousands of MALDI spectra, collected from single features of a microarray. It can generate a heat map based on intensities of desired and undesired peaks seen from each spectrum/feature.

Therefore, a total of twenty different titration conditions along with five replicates of each condition were tested using the fluorescence method on a single chip. Hydroquinone was used as EGA-P due to a low redox potential associated with it. A fluorescence assay was performed based on an N-terminal endorphin sequence (YGGFL) interaction with a fluorophore conjugated antibody against it. Titration conditions ranged from 0.25 μ A, 60 seconds to 0.25 μ A, 210 seconds and 1.2V, 60 seconds to 3.0V, 60 seconds. The electrical conditions that were 0.75 μ A, 60 seconds and stronger showed high fluorescence signal intensities. This indicated that Trt groups were electrochemically deprotected from respective features. Earlier in this section we discussed the instability of Trt and DMT groups to the Hydroquinone system. The MALDI spectrum associated with the electrochemical deprotection of Trt using Hydroquinone as EGA-P at 0.5 μ A, 60 seconds, showed approximately 17% deprotection of Trt from the control region. By the application of fluorescence and the MALDI based detection method we were able to develop a mild electrical condition for Trt deprotection using Hydroquinone as EGA-P, but also discovered that Trt is unstable to Hydroquinone on CBMX chips. Hence, although Trt can be deprotected at a mild electrical condition, due to its instability to hydroquinone it may not be an optimal system for parallel synthesis. Such analysis of Trt deprotection would not have been possible solely by the fluorescence method and would have been very tedious to determine with only the MALDI method.

APPENDIX B

TEST OF ALTERNATE METHODS TO ELECTROCHEMICALLY GENERATE ACIDS

Alongside optimizing the peptide microarray synthesis based on electro-generated acids, a few strategies for generating other kinds of reagents electrochemically were also tested. Specifically, we tried to generate base, oxidize metal, and generate hydrogen electrochemically. The idea behind this effort was to replace electro-generated acids with an even more efficient system of electro-deprotection. One of the ideas tested was to reduce piperidine hydrochloride to generate in situ piperidine, an organic base widely used for deprotection of Fmoc group. The chemical reaction is as follows:



Many different electrical and concentration conditions were tested to generate an adequate amount of piperidine from piperidine hydrochloride via an electrochemical reduction reaction. The range of the titration conditions was 0.1M piperidine hydrochloride, -2.0V, and 1minute to 0.6M piperidine hydrochloride, -2.0V, and 20 minutes. At -2.0V, 20 minutes, approximately 25% of Fmoc groups were deprotected. The deprotection results were inconsistent; in few trials the deprotection of approximately 25% of Fmoc groups (Figure B-1) was observed, but the results could not be replicated in all of the trials. The deprotection yields also remained constant at about 25% and did not improve, even when stronger titration conditions were applied.

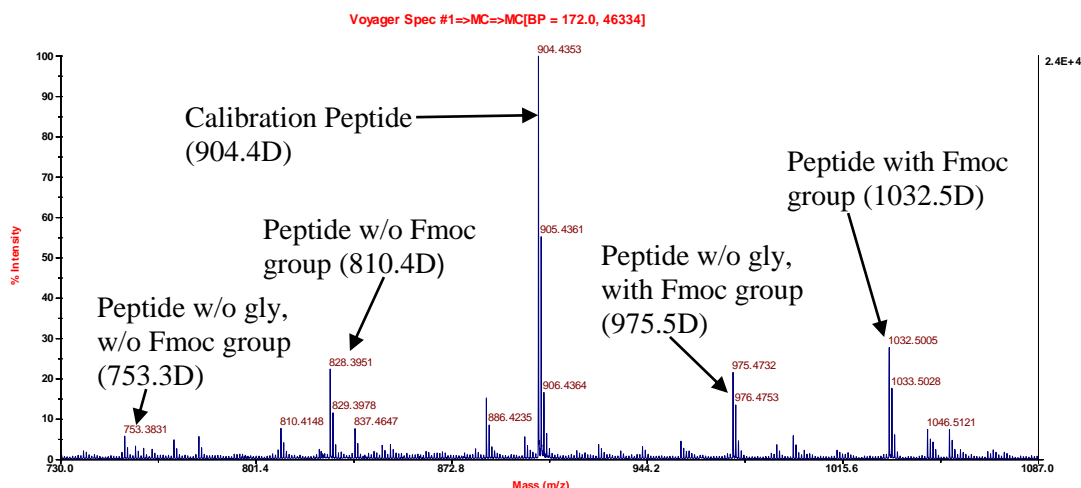
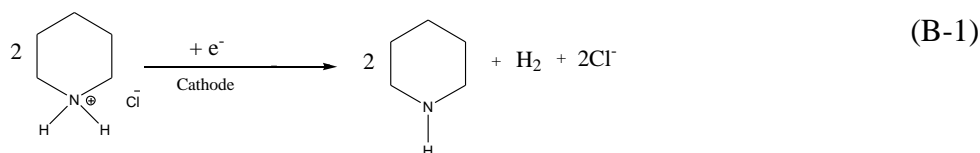
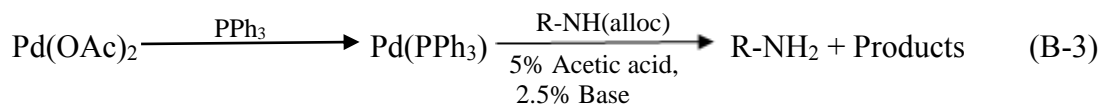
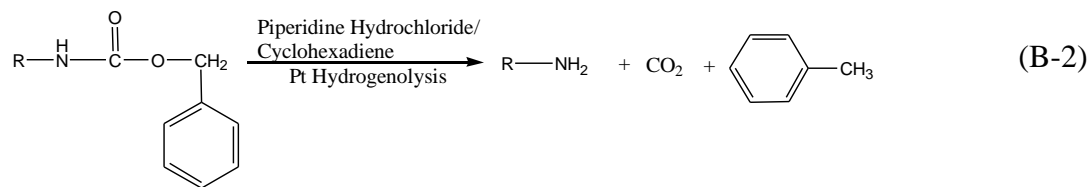


FIGURE B-1: MALDI-MS characterization of electrochemical deprotection of Fmoc groups using piperidine hydrochloride as electro-generated base precursor (EGB-P). A peptide, $\text{NH}_2\text{-AKFGAFGAFG-CONH}_2$ was synthesized where the final alanine was coupled after electrochemical deprotection of Fmoc group of lysine via reduction of piperidine hydrochloride to piperidine. The MALDI spectrum corresponding to 0.6M piperidine Hydrochloride solution and -2.0V, 20-minute condition showed approximately 25% removal of Fmoc groups.

Two more strategies were tested to generate electrochemical reagents: (1) generate in situ hydrogen, which can deprotect Cbz groups by hydrogenolysis (Equations B1 & B2), and (2) oxidizing Pd(0) to Pd(II) in situ to deprotect alloc groups (Equation B3). The chemical equations of these strategies are as follows:





The equation B-1 shows that the chemical reaction to generate hydrogen in situ is the same as the one carried out to reduce piperidine from piperidine hydrochloride. The only difference was that the Cbz group was present on the N-terminal of the peptide instead of the Fmoc group for deprotection. The titration conditions for in situ generation of Pd (II) from Pd (0) was 2.4V 3min to -2.4V, 15min. None of these two methods showed any deprotection; therefore, it cannot be said that upon optimization these methods could become efficient. In contrast, given that the electrochemical setup has been inconsistent, these methods could not be written off completely. The idea of reducing piperidine hydrochloride to piperidine electrochemically is promising, as we have seen approximately 25% deprotection of Fmoc groups. Perhaps the efficiency of this reaction could be improved by playing with several titration conditions and the employment of different modes of counter electrodes.

APPENDIX C

STUDY OF PEPTIDE CONTAMINATION DURING MICROARRAY SYNTHESIS

During the studies involving peptide synthesis yield determination and optimization, we encountered contamination of peptides from a different region of the chip in the concerned region. Such a moderate to high level of contamination could lead to false positives. Consequently, we went ahead and studied the problem of contamination carefully. The probable reasons for contamination could be (a) due to non-specific application of voltage to silent electrodes during the gating step, (b) due to diffusion of protons, generated from electro-acids during the gating step, to the silent electrodes region, or/and (c) the deterioration of the functionalized polymer of the chip during the gating step or/and during synthesis.

The pyrrole electro-polymerization experiment was performed to determine whether or not any hardware issues existed. As a result of which the silent electrodes were getting addressed. Results of the experiment suggested no non-specific addressing of electrodes, as no electro-polymerization took place on silent electrodes (Figure C-1).

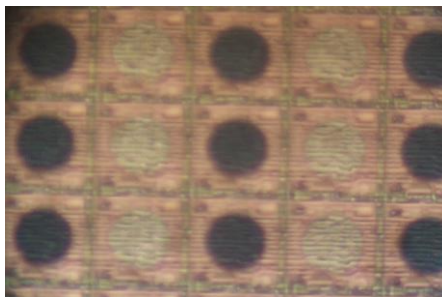


FIGURE C-1: The dark circular region in the Figure is due to pyrrole electro-polymerization. Electric potential of 1.0V for 10s was applied on selected electrodes. The electrodes that were not selected did not form pyrrole polymer on its surface, as can be seen from Figure C-1 (bright electrodes).

From the experiment results, we were able to strike out the option of non-specific application of voltage to the electrodes. To determine whether or not the diffusion of protons generated during the gating step was the reason behind contamination, two detailed experiments were conducted. In these experiments, five different peptides were synthesized in five different regions of the chip. There was a sixth region present in the chip, which was a control region. Here, no gating step was involved. A diagram of the chip with the locations of six different regions and the peptides synthesized in it is shown in Figure C-2.

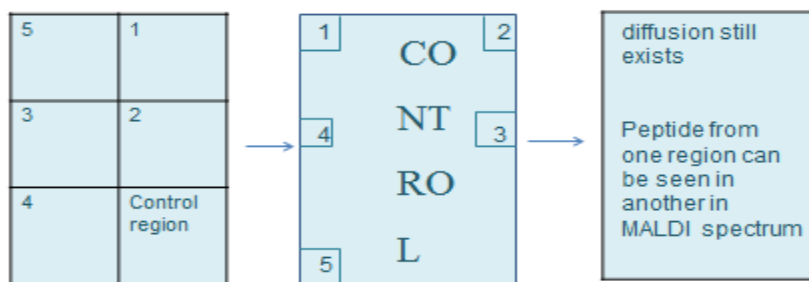
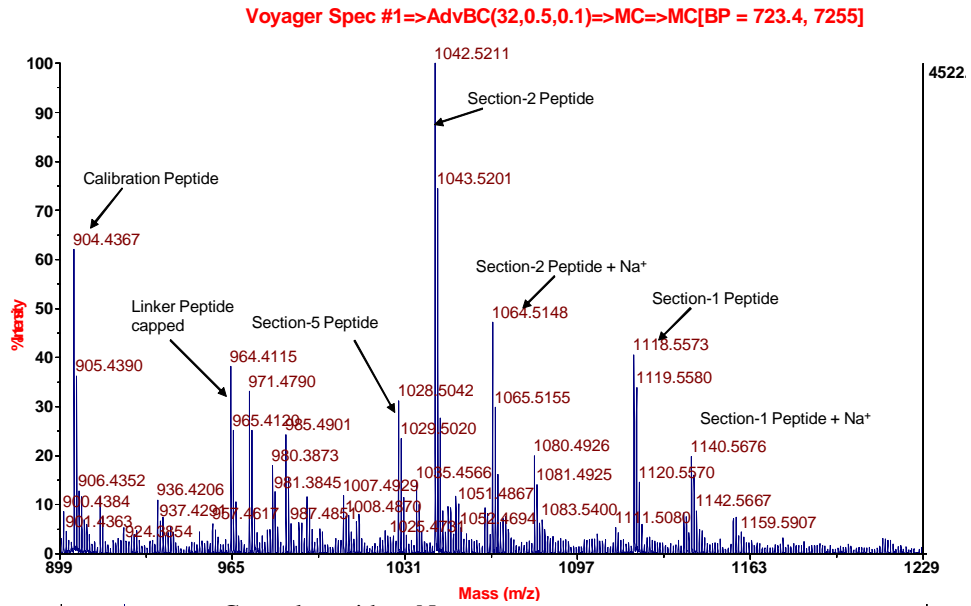


FIGURE C-2: Chip design of two experiments conducted for peptide contamination study. In the first experiment, the chip was divided into six large regions and different peptides were synthesized in the six regions. In second experiment, the chip was divided into six small regions, each region further apart from other regions compared to first experiment. In both the experiments contamination could still be seen.

In the second experiment, the dimensions of these regions were further shortened to determine if the contamination of peptides could still be seen. The idea behind the second experiment was that if the contamination of peptides could still be seen after shrinking the regions and thereby increasing the distance between any two regions, then the contamination is not due to the diffusion of protons during the gating step. A detailed description for this reasoning is given in the subsequent paragraphs. In these two experiments, it was observed that peptides from one region contaminated the other region. The contamination was seen even among the two regions that were farthest apart from each other. For example, in experiment 1, a peptide NH₂-KMAFGAFGAFG-CONH₂, which was synthesized in section-5, could be seen in the MALDI spectrum of section-2, in which peptide NH₂-KFAFGAFGAFG-CONH₂ was synthesized. Similarly, a peptide NH₂-KGAFGAFGAFG-CONH₂ synthesized in section-1, in the second experiment, was seen in the MALDI spectrum of section-2, in which peptide NH₂-KFAFGAFGAFG-CONH₂ was synthesized. These two regions were quite far from each other on the chip. The abovementioned MALDI spectrum of the two experiments can be seen in Figure C-3a and Figure C-3b respectively.

Section – 2 (Alanine coupled)

C-3a.



C-3b.

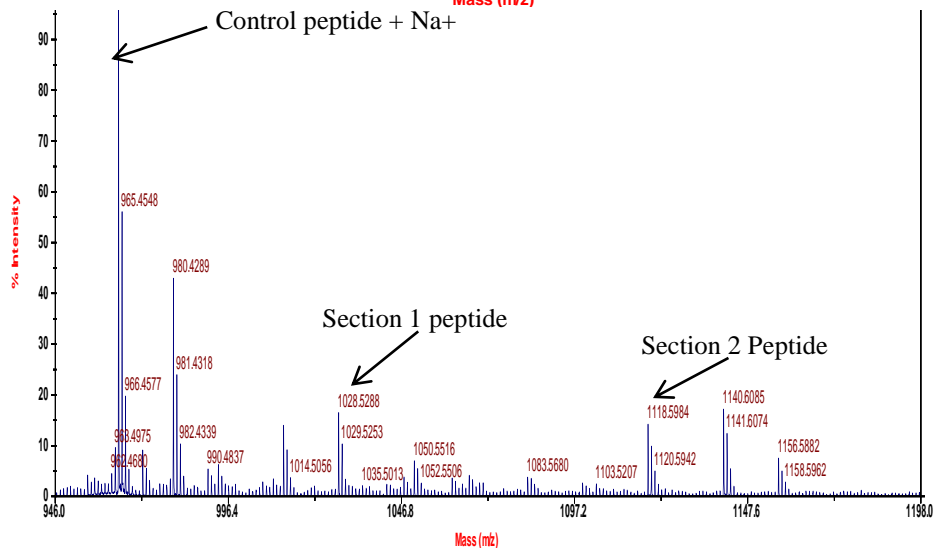


FIGURE C-3: MALDI-MS characterization of experiments conducted for peptide contamination study. MALDI spectrum in Figure C-3a corresponds to Section-2 of the Diffusion experiment 1. Along with the peptide that was synthesized in Section-2, peptides synthesized in other regions, such as the peptide from Section -1, Section-5, and

the control peptide were also seen in the Section-2 spectrum. Similarly, Figure C-3b corresponds to Section-2 of experiment 2. Along with the peptide that was synthesized in Section-2, peptides synthesized in other regions were also seen in the Section-2 spectrum.

From these two experiments, it was concluded that the contamination of peptides into one region from another is not taking place due to the diffusion of protons during the gating step. The reasoning behind our claim is as follows: the active area of CBMX chip has a dimension of 10mm X 2.5mm, which translates to 25mm² area. Each region designed during the first experiment had a set of 10 X 10 electrodes, which translates into 2 mm² area. For instance, if the electrodes in section-5 were addressed, the maximum area that the protons generated could diffuse in ten minutes (the electrical condition employed during gating step was 3.0V for 10 minutes) would be 9.31xE-5mm² (assuming proton is moving in water + electrolyte medium). The diffusion of protons is fastest in a water + electrolyte medium. The medium in our gating step is that of an organic solvent (aprotic solvent) + electrolyte, in which the diffusivity of protons will be less than in a water + electrolyte medium. If the diffusivity of protons in a water + electrolyte medium itself is not sufficient for protons to reach from one region to another, it is not possible that the protons would diffuse and reach far-off sections in an aprotic solvent medium. Also, the electric field which is present in the medium between two counter electrodes will always direct the motion of the diffusing protons towards the counter electrode, a bulk platinum electrode, at a distance of 5mm. In our setup, it is minimizing the time that a proton can spend on the silent electrode region. Professor N.J. Tao, director of Center for Bioelectronics and Biosensors at Arizona State University, and an expert in

Electrochemistry, suggested the maximum diffusion of protons that can take place in our set up , in ten minutes, under 3.0V equivalent electric field and N,N'-dimethylformamide + tetra-butyl ammoniumhexafluorophosphate as a medium, would be about $10^4 \mu\text{m}^2$. This area is less than one-hundredth of the chip surface area and, therefore, it would not be possible for the protons to diffuse into other regions and lead to contamination.

It should be noted that several precautions to prevent diffusion are employed in our setup. Firstly, (a) the EGA-P precursor, N,N'-diphenylhydrazine, itself can act as proton acceptor and thus plays the role of chemical scavenger for protons in the EGA-P solution, and (b) in the chip fabrication, every electrode is surrounded by a thin, circular, ring-like electrode called a getter electrode. Opposite polarity can be employed to these getter electrodes, which can prevent the diffusion of protons (we were unable to utilize this feature for most of our experiments, only at a later stage did the company realize that we did not possess this ability and the instrument was upgraded to utilize this capability).

From the above analysis, it can be concluded that the contamination of a specific region with peptides from another region is not taking place due to (a) non-specific addressal of electrodes or (b) diffusion of protons at the gating step. At this point, a plausible explanation is the deterioration of the polymer present on the chip surface due to strong electrical conditions employed during each gating step. Small, functionalized pieces of the partially degraded chip polymer move across the chip surface and get stuck onto different regions of the chip. These bits of polymer somehow remain stuck to the chip during the synthesis and, in fact, participate in the further steps of the synthesis. The

peptide thus fabricated on these bits of polymer show up in the MALDI spectrum as contamination.

APPENDIX D

SEARCH FOR A MILD ELECTRICAL CONDITION TO ELECTROCHEMICALLY DEPROTECT TRITYL GROUPS

As a result of the analysis concerning contamination discussed in Appendix C, we searched for mild, yet optimized electrical condition for proton generation at the gating step. In the first several rounds of experiments, the assay involved five components as follows: (1) coupling of a trityl protected amino acid to the polymer present on the chip, (2) deprotection of trityl group from different sets of electrodes at different electrical conditions, (3) coupling of the biotin molecule to the deprotected amine groups, (4) labeling of the biotin molecule with streptavidin-fluorophore molecule, and (5) fluorescence based detection to find the efficiency of titration conditions. The EGA-P used was hydroquinone rather than N,N' -diphenylhydrazine. Researchers at CBMX have used hydroquinone as EGA-P for oligonucleotide microarray fabrication and have reported a very mild condition, $0.26\mu\text{A}$ 30s, for acid generation. The results of all of the trials were inconsistent, due to suspected hardware malfunctioning. Upon evaluation at CBMX, it was discovered that the instrument failed to employ any other mode of counter electrode other than the bulk platinum electrode of the instrument's reaction chamber. The instrument, once upgraded at CBMX, was then capable of employing different modes of counter electrodes. In further experiments, the grid was employed as a counter electrode. Such an arrangement could be more efficient than bulk electrodes as a counter electrode in preventing diffusion of protons produced at gating step. After upgrading the instrument, experiments to search for mild electrical condition were resumed. The biotin-based assay was not successful, and even though different parameters were changed - for example, a change in composition of blocking from 3% BSA to 30% BSA - no consistent results were seen. As a result, an N-terminal endorphin sequence – antibody interaction

assay was employed. In these experiments, an N-terminal endorphin sequence (YGGFL) was synthesized. The N-terminal end, which was protected with Fmoc group, was replaced with a Trityl group. The trityl group was then electrochemically deprotected at twenty different electrical conditions, ranging from 0.25 μ A, 60s to 0.25 μ A, 210s and 1.2V, 60s to 3.0V, 60s. After deprotection, the chip was incubated with an anti-endorphin antibody conjugated with a fluorophore. Upon fluorescence detection, electrodes corresponding to 0.75 μ A, 45 seconds and all electrical conditions stronger than 0.75 μ A and 45 seconds showed fluorescence (Figure D-1). The mildest, yet consistent, electrical condition with the highest amount of fluorescence was 0.75 μ A for 45s.

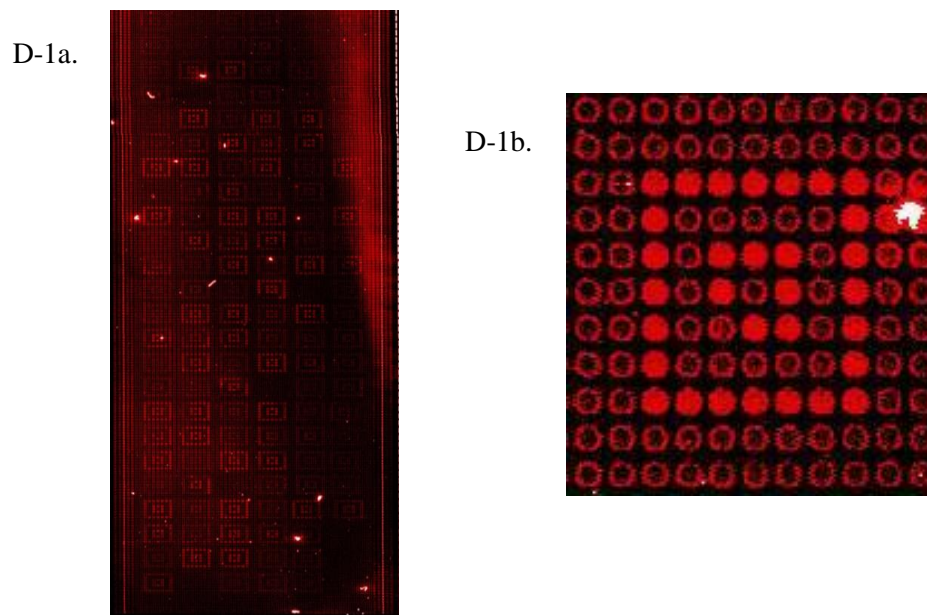


FIGURE D-1: D-1a is the fluorescence image of the chip on which twenty different electrical conditions were tested to search for the most efficient deprotection condition for trityl groups using Hydroquinone as EGA-P. Figure D-1b, shows the fluorescence

image of one of the replicates of 0.75 μ A, 45s condition. All of the replicates of 0.75 μ A, 45s condition and stronger electrical conditions showed high fluorescence intensities.

It should be noted that different assays such as biotin-fluorophore conjugated to streptavidin interaction, MALDI mass spectrometry, and N-terminal endorphin sequence – antibody interaction were performed for mild, yet efficient electrical condition determination. Out of the three different assays, only N-terminal endorphin – antibody interaction revealed best electrical conditions for trityl deprotection. A similar experiment with a different detection method did not reveal the best electrical condition, even after multiple trials. All the above-mentioned assays are extremely sensitive and should have shown similar results. A probable explanation could be that the MALDI detection method and biotin-based method involve chemical steps which may not be efficient. For example, in the MALDI detection method, peptides are chemically ionized using alpha-hydroxycinnamic acid as proton donor. The biotin-based detection method involves chemical coupling of biotin to the N-terminal of the peptide sequence, which is a very difficult reaction due to the high hydrophilicity of the biotin molecule. The solvents used for coupling reactions are not hydrophilic enough to dissolve the biotin molecule at a desired concentration. Unlike MALDI and biotin-based detection methods, N-terminal endorphin sequence interaction, with its antibody, does not involve any chemical steps. It may be for this reason - it is a more efficient method for the best electrical condition determination. It seems that the MALDI based detection method, which has proved very useful in direct characterization of synthesis, could in some cases be an inefficient method due to the chemical ionization step involved. Perhaps it can be replaced by an

electrospray ionization mass spectrometry (ESI) based method to characterize simple peptide synthesis, as it only involves physical methods for ionization and no chemical step is involved. At this point in our research, there were several issues with instrumentation involved in this project and further analysis of microarray synthesis, such as stepwise yield, chemical nature of side-products, and total yield of peptide synthesis involving three gating steps at $0.75\mu\text{A}$, 45seconds electrical condition could not be performed. Issues related to instrumentation are described in detail in Appendix E.

APPENDIX E

PEPTIDE SYNTHESIZER AND ELECTRO-SYNTHESIS INSTRUMENT

INTEGRATION AND OTHER INSTRUMENTATION ISSUES

The electrosynthesis instrument and the peptide synthesizer are two very different instruments, one designed to apply voltage across the CBMX chips and conduct electrochemical reactions and the other designed to execute peptide synthesis on beads. To make the microarray synthesis setup fully automated, it is necessary to integrate both these instruments. A very clever approach from Kevin Brown, a software professional at the Center of Innovations in Medicine (ASU), helped us achieve the integration of the two instruments. Rather than making the instruments communicate with each other, peptide synthesizer was programmed to wait at different time intervals during the synthesis, and during this time electrosynthesis instrument was activated automatically using LabVIEW software. Specifically, microarray synthesis was conducted in a reaction chamber of the electrosynthesis instrument. The chamber was connected to the peptide synthesizer and all of the synthesis steps were carried out in an automated mode through the peptide synthesizer. The peptide synthesizer was programmed so that it would load the reagents needed for electrochemical reaction into the chamber, and then temporarily halt the synthesis for a few minutes. During this time interval, through LabVIEW software, the cursor of the computer screen would automatically move and activate the electrosynthesis instrument software. Once this task was performed, the peptide synthesizer would take charge of the synthesis once again. Such an arrangement can potentially save labor time because it is not required for any professional to be physically present at the station in order to conduct the gating step manually every three hours. The reaction could now be conducted overnight. However, due to some issues with chamber design, this advantage of complete automation could not be leveraged yet.

The four reaction chambers present in the electrosynthesis instrument have a volume of 100 microliters each. Each chamber has electronic circuitry present. In addition to these four reaction chambers of the electrosynthesis instrument, there is a manifold with four reaction chambers, each having a volume of 200 microliters. These chambers do not have any electronic circuitry. It was observed that if complete microarray synthesis is conducted in the reaction chambers of the electrosynthesis instrument, the electronic circuitry of the chamber deteriorates quickly, due to the seeping of chemicals into the circuitry. It is not feasible to sacrifice the chambers for complete automation, as these chambers are quite expensive (\$1100 per chamber) and the deterioration starts taking place in as little as a month. Although the capability to perform synthesis in fully automated mode is possible, a professional is needed at the station to transfer the chip between the instrument's chambers during each gating step.

The manual chamber is not compatible with peptide synthesizer because the synthesizer's internal pressure is not enough to push the solution present in the chamber forward. As a result, solutions of different steps gets mixed and fail the reaction. The alternative is to use the reaction chambers of the electrosynthesis instrument, which can hold only 100 microliters of reagent. The peptide synthesizer is able to easily push the solution forward. The problem with this alternative is that the reagents could seep into the circuitry and destroy the electrical capabilities of the chamber. Doug Daniel, an associate research scientist at the Center for Innovations in Medicine, helped solve this problem. He designed a manual chamber that can hold only 100 microliters and is therefore compatible with the peptide synthesizer instrument. At present, we have one such

redesigned chamber as well as the details of the design, which can be used in the future to produce more such chambers. As stated previously, the CBMX chips are delicately designed and have a certain region that is very sensitive to chemicals. The thirteen connecting pads of the chip surface, which establish electrical connection between the electro-synthesis instrument and the microelectrodes of the chip, should be protected from exposure to chemicals for the proper functioning of the chip. A Teflon-based acid resistant chamber was built to save the chip from losing its electrical functionality.

The electro-synthesis instrument, in the past, has often either failed to apply potential to the addressed electrodes or has applied potential non-specifically. It is because of this that a diagnostic test is necessary to check the proper functioning of the electro-synthesis instrument. In this regard, a pyrrole electro-polymerization test is conducted every now and then to ensure proper functioning of the instrument. The test is simple to execute and can be completed within two hours. Pyrrole undergoes electro-polymerization upon application of potential across the chip. The mildest electrical condition to execute polymerization test is 0.5 V and 10 seconds. The stronger the electrical condition employed, the thicker the polymer becomes. The difference in thickness can be seen via a change in the color of the polymer under a microscope.

The electro-synthesis instrument can potentially employ different kinds of counter electrodes, such as a bulk platinum electrode of the reaction chamber, a grid present in the chip, and neighboring electrodes in the chip. The instrument could previously be used only with a bulk electrode as a counter electrode, but upon upgrading the instrument's software, the grid as a counter electrode option is now possible. To switch the instrument

to a grid as a counter electrode, two of the three pins of the instrument chamber are connected using a jumper. Neighboring electrodes cannot yet be employed as a counter electrode in the instrument that we possess due to some technical difficulties.

Two different peptide synthesizers were used in this project. One of them was 9050 plus peptide synthesizer manufactured by Millipore, and another was a Pioneer peptide synthesizer built by Applied Biosystems. We had mixed experiences with both of the synthesizers. Contamination was an issue with both of the synthesizers. The pneumatic valves of 9050 plus synthesizer were easily contaminated with solutions, whereas the Pioneer synthesizer's recommended internal pressure was not enough to push solution forward from the synthesis reaction chamber. This issue led to contamination of the solutions in the reaction chamber. Spare parts of 9050 plus synthesizer are very difficult to secure, but its robotic station is quite robust compared to that of the Pioneer Synthesizer. Because we had two Pioneer synthesizers, securing spare parts for proper functioning of one synthesizer was not an issue. Overall, our impression of the 9050 plus peptide synthesizer was better than Pioneer's, and if its spare parts can be secured, it should be given first priority for future experiments. It is probable that the use of microwave synthesizers will be an even better option. Microwave assisted peptide synthesis is far more accelerated than conventional synthesis, and results in high overall yields. It is considered favorable for long sequence synthesis and it is known to prevent aggregation because of heating and electrical frequency fields involved in the reaction. It also prevents lot of wastage of solvents and therefore lowers the cost of an experiment.

Some constraints with the microarray synthesis have been the incompatibility of the chip to strong acids and an inability to monitor the amino acid coupling and protecting group's deprotection efficiencies. Issues due to incompatibility to strong acids are averted since the t-butyl group can be used as side-chain protecting group - the chip can sustain the acidic strength required for its deprotection. However, monitoring the efficiency of coupling and deprotection steps have proved to be difficult. Two strategies, (1) using IR spectroscopy to analyze chemical modification of the surface qualitatively, and (2) using bromophenol blue test to monitor the steps, have not been successful. It is probable that these two strategies could not be successful on this platform due to the reflective platinum surface and generation of very small amount of peptides on the surface.

APPENDIX F

PEPTIDE MICROARRAY FABRICATION ON SILICON SUBSTRATE USING
PHOTOLITHOGRAPHY TECHNIQUE

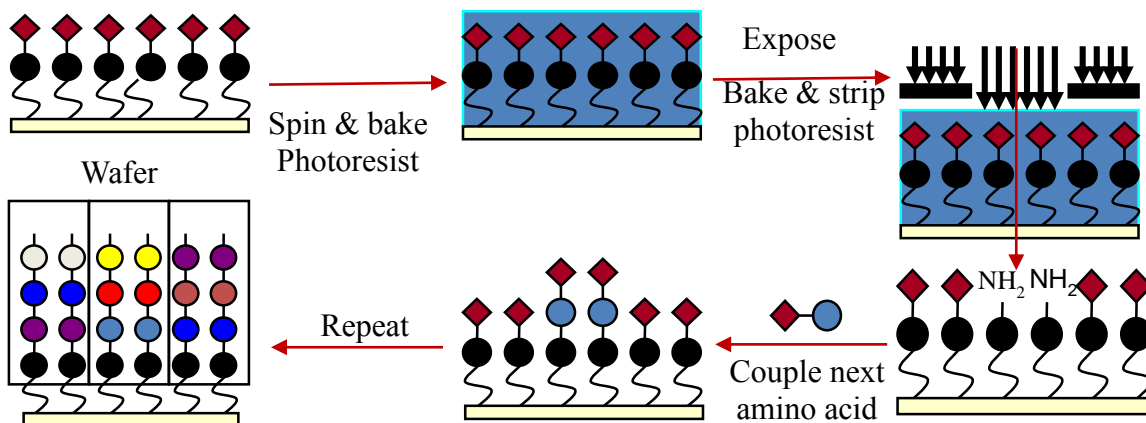
Peptide and peptidomimetics microarrays have the potential to become a powerful research and medical diagnostics tool. Using microarrays, a vast amount of chemical space can be searched for development of catalysts, drugs, synthetic antibodies etc. It can also serve as a medical diagnostics tool for various illnesses. In the process of microarray-related research and development, several algorithms can be developed and new concepts in science can be discovered.

The Center for Innovations in Medicine at The Biodesign Institute at Arizona State University intends to use peptide microarray technology to meet customer's unstated needs by providing treatment of illnesses at the presymptomatic stage. Using microarray technology, researchers at the center would be able to aid individuals in figuring out an individual's predisposition to diseases, before the onset of the disease or in very early stage. This is so that the disease can be treated before it becomes life threatening. Towards this end, the center has been working in close collaboration with its spin-off company, *HealthTell* Inc., to fabricate peptide microarrays on silicon substrates using a photolithography technique.

General Synthesis Scheme

The initial treatment of the silicon wafers, such as thermal deposition of oxide and chrome deposition needed for peptide microarray fabrication, was provided by the collaborators at Sandia National Laboratory and the Center for Integrated Nanotechnologies (CINT). Each silicon wafer used is approximately 1 mm in thickness and 4 inches in diameter. A silicon substrate modified with chromium doping is also being tested, in parallel, for peptide microarray fabrication. Chromium doping provides a

better signal to noise ratio during the fluorescence characterization of synthesis. The silicon wafer, once ready for fabrication, is first silanized with (3-Aminopropyl)triethoxysilane (APTES). The silanization is possible with various kinds of linkers, such as hydrophobic, hydrophilic etc. After silanization, a boc-protected amino acid is coupled to the free amines present on the surface. The wafer is then spin-coated with photoresist mixture (PRM). After spin-coating and washing with DMF, the wafer is spatially patterned by a localized generation of photoacid using photolithography instrumentation. The photoacid generated at specific areas by shining light removes the boc groups from amines and thus activates the irradiated features for the next coupling step. Multiple rounds of such spatially defined deprotection and coupling steps leads to the fabrication of a peptide microarray. A schematic diagram of general synthesis is shown in Scheme F-1.

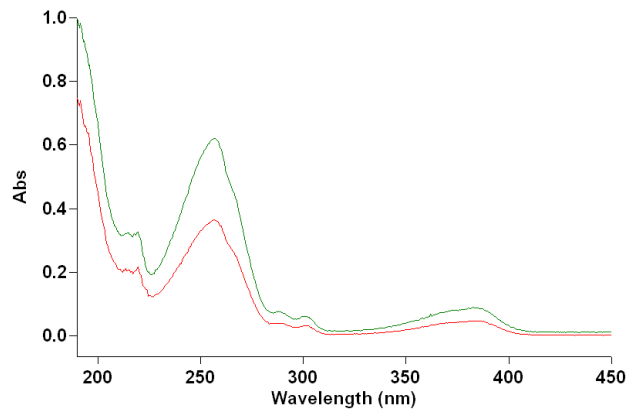


SCHEME F-1: General synthesis scheme of peptide microarray fabrication on silicon substrates.

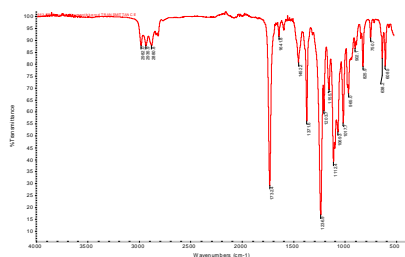
Photoresist Mixture Composition Determination

The PRM used in the fabrication process consists of PAGTf, Isopropyl thioxanthone (ITX), polymethylmethacrylate (PMMA), and propyleneglycolmonomethyletheracetate (PGMEA). The accurate concentration of each of these components in PRM, used by a previous team, was determined by IR and UV-visible spectroscopy and HPLC analysis. It was found that PRM is made up of 5% w/v PAGTf, 5% w/v ITX, and 2.5% w/v PMMA in PGMEA. A comparison of UV-Vis, IR, and HPLC data of (5,5,2.5) PRM, and a sample of old PRM can be seen in Figure F-1.

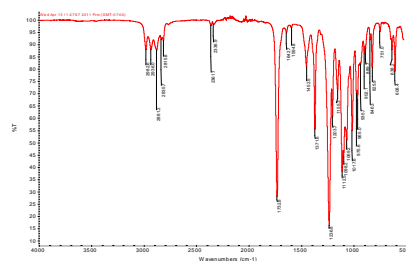
F-1a



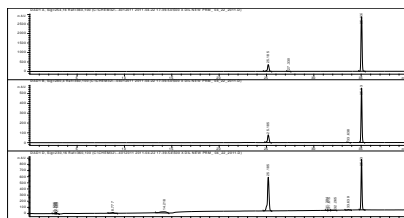
F-1b



F-1c



F-1d



F-1e

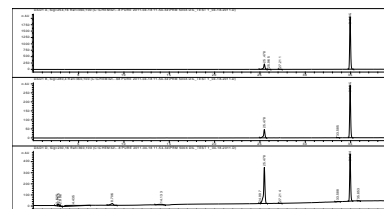


FIGURE F1: UV-Vis, IR, and HPLC analysis to determine composition of photoresist mixture. Image (F-1a) shows absorbance spectrum of (5,5,2.5) and old PRM. Image (F-1b) and (F-1c) correspond to IR spectrum of (5,5,2.5) and old PRM. Image (F-1d) and (F-1e) correspond to HPLC analysis of (5,5,2.5) and old PRM.

In situ Peptide Synthesis Optimization

Following tasks were tested towards the development of peptide microarray fabrication on silicon wafers.

Determination of Boc-protected amino acid coupling efficiency to available free amines on silanized silicon wafer. The amino acid coupling efficiency to a silanized silicon wafer was determined. Fluorescence signals from a silanized silicon wafer, taken as reference, was obtained by coupling Alexa-555 dye to APTES present on the surface. To a similar silanized silicon wafer, boc- β -alanine was coupled followed by capping with acetic anhydride. The wafer was then chemically deprotected using TFA and Alexa-555 dye was coupled to it. Results suggested that a substantial percentage of APTES did not couple to boc- β -alanine. Comparison of fluorescence signals can be seen in Figure F-2.

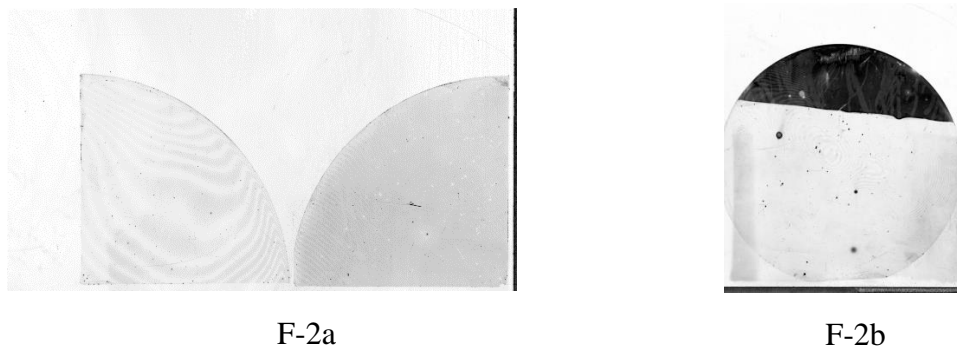


FIGURE F-2: Fluorescence images of the experiment to determine coupling efficiency of boc-protected amino acids to available free amines on silicon substrates. The right portion of the image (F-2a) is a control region and the left portion corresponds to a section of wafer to which boc- β -alanine and dye (Alexa-555) was coupled. Similarly, in

image (F-2b) the dark portion corresponds to section of wafer to which dye was coupled and the lighter region corresponds to control section (section in which no dye was coupled).

Fluorescence based comparison of efficiency of derivatization of silicon substrates with β -alanine and Peg 6 linker modified with a glycine. One of the silanized silicon wafers was coupled with Peg-6 linker on top of which a glycine amino acid was coupled. β -alanine was coupled to another silanized surface. Both the derivatized wafers were then labeled with Alexa-555 dye. The wafer derivatized with glycine and Peg linker showed better fluorescence and signal-to-noise ratio compared to a wafer derivatized with β -alanine. The comparison of fluorescence signals from the two wafers can be seen in Figure F-3.

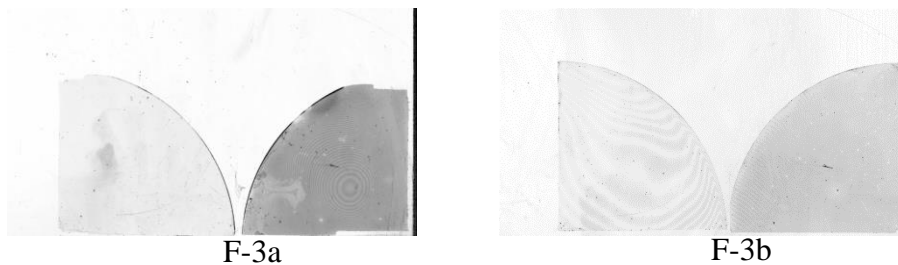


FIGURE F-3: Fluorescence images of the silicon substrates derivatized with β -alanine and Peg 6 linker modified with a glycine. The darker region of image F-3a & F-3b corresponds to the section of the wafers to which glycine + Peg-6 and β -alanine were coupled respectively. The lighter regions correspond to control sections of the two wafers. The wafers were imaged using Alexa-555 dye.

Comparison of photo-deprotection efficiency at 260nm and 365nm. Photo-deprotection efficiency at two different wavelengths, deep UV (260 nm) and near UV (365 nm) was determined by coupling Alexa-555 dye after irradiating two silanized wafers with the mentioned wavelengths. The silicon wafers were further sub-divided into regions where photo-exposure for different time intervals (0s, 1s, 2s, 3s, 14s) was carried out. Results of the experiment can be seen in Figure F-4. Photo-deprotection efficiency at 260 nm seemed to show higher fluorescence signals compared to 365 nm. Also, photo-deprotection efficiency seemed to improve from a 1s to a 3s time interval. Photo-deprotection efficiency at 3s and 14s seemed equally efficient.



FIGURE F-4: Fluorescence comparison of photo-deprotection efficiency at 260nm and 365nm. The darker region of image F-4a & F-4b corresponds to section of the wafers which was irradiated at 260 nm and 365 nm respectively for different time intervals (1s, 2s, 3s, 14s). The lighter regions correspond to control sections (no irradiation) of the two wafers. The wafers were imaged using Alexa-555 dye.

Comparison of photo-deprotection efficiency to chemical deprotection efficiency. One of the silanized silicon wafers, derivatized with Boc-Gly-Peg-6 and later baked with PRM, was irradiated at 260 nm. Another similar wafer was chemically

deprotected using TFA. Both the slides were then labeled with Alexa-555 dye. A comparison of fluorescence signals can be seen in Figure F-5. Chemical deprotection seemed to give marginally better fluorescence signals compared to photo-deprotection.

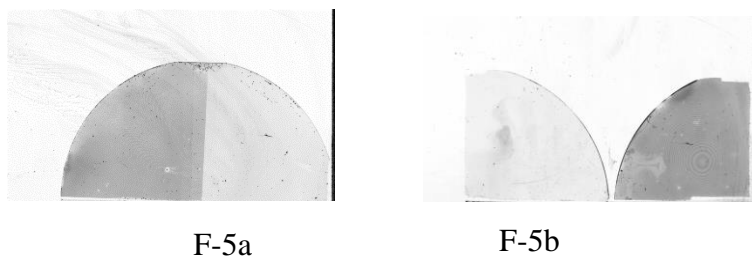


FIGURE F-5: Fluorescence comparison of photo-deprotection efficiency to chemical deprotection efficiency. The darker region of image F-5a & F-5b corresponds to section of the wafers which were photo and chemically deprotected respectively. The lighter regions correspond to control sections of the two wafers. The wafers were imaged using Alexa-555 dye.

Experimental Protocol

UV-Vis, IR spectroscopy and HPLC analysis. UV-Vis analysis was carried out in a 2.00 mL-quartz cuvette with a total reaction volume of 1.00 mL. For each PRM sample (5,5,2.5 PRM and old PRM), background spectrum of the solvent (acetone) was first recorded followed by 2.00 μ L addition of PRM sample. The cuvette was then scanned for absorbance from 200 – 450 nm range using a UV-Vis spectrophotometer at the Center for Innovations in Medicine (CIM), Arizona State University. The absorbance spectrum of the two PRM samples were compared. IR analysis was performed using an FT-IR instrument at the Single Molecule Biophysics Research Center, at ASU. A background spectrum of the instrument was first recorded, followed by a recording of the

spectrum for 100 μ L of each PRM sample. Peaks corresponding to each component of a PRM sample for the two samples were compared. For the HPLC analysis, a 500x diluted solution of each PRM in CH₃CN with 0.1% TFA was prepared. Each PRM was then analyzed with HPLC and areas corresponding to each component of PRM sample for the two samples were compared.

Silanization with APTES. The wafer was first washed with 20mL of Piranha solution (50% sulfuric acid + 50% hydrogen peroxide) for 30 min. It was then washed 2x with 20mL deionized water and 2x with 20mL 95% ethanol. The wafer was then incubated with 20mL of 3% APTES in 95% ethanol for 30min. After incubation, the wafer was washed 2x with 20mL 95% ethanol and dried in an oven at 100°C for 60 min.

Amino acid coupling reaction. The coupling reaction of Boc-Gly-OH and Boc- β -Ala-OH to free amines is similar, the difference being only in concentrations. To achieve amino acid coupling, the silicon wafer terminated with free amines is exposed to a mixture of amino acid (boc-glycine: 37mg, 137mM, boc- β -ala: 52mg, 137mM), HBTU (*O*-benzotriazol-1-yl-*N,N,N',N'*-tetramethyluronium hexafluorophosphate, 95mg, 137mM), HOBT (*N*-hydroxybenzotriazole, 33.5mg, 137mM), and diisopropylethylamine (130.5 μ L, 350mM) in DMF (2mL) for 30 minutes. The wafer is then rinsed with DMF 3x, dichloromethane 3x, and again with DMF 3x, then re-exposed to the coupling mixture for another 30 minutes. After repeating the washing procedure (with an additional ethanol rinse to remove any residual DMF or dichloromethane), the chip is allowed to dry.

Capping with acetic anhydride. The wafer is first washed 3x with 20mL DMF. It is then incubated with 50% acetic anhydride in DMF solution for 30 min. The wafer is then washed 3x with DMF, 3x with DCM, and dried with Argon gas.

Dye-labeling and fluorescence detection. The surface of the chip was labeled with Alexa-555 dye (1 mg of Alexa-555 succinimidyl ester, plus 1XPBST to 50 mL) for 1 hour at room temperature in the dark. The wafer was then removed and washed 3x with 1XTBST for five minutes each. The wafer was then washed 3x with ddH₂O, five minutes each. The wafer was then scanned at 650nm wavelength with 70%PMT and 100% laser. The Typhoon 9200 instrument at Center for Innovations in Medicine (CIM), ASU was used for fluorescence imaging.

Acid based chemical deprotection. Boc groups were chemically deprotected using a cocktail of 94% TFA (Sigma-Aldrich, St. Louis, MO) + 2.5% triisopropylsilane (TIS) (Sigma-Aldrich, Milwaukee, WI) + 3.5% water. The wafer was placed in an acid-resistant chamber and exposed to the deprotection cocktail for thirty minutes. At regular time intervals, the setup was shaken for better reaction. After thirty minutes, the solution was discarded in acid waste and the reaction setup was rinsed 5x with dichloromethane, 5x with 5%DIEA in dichloromethane, 3x with DMF, and 5x with water. The chip was then dried with argon gas.

APPENDIX G
TECHNIQUES

Continuous Flow Peptide Synthesizer^{1,2}

A peptide synthesizer instrument is used to achieve automation of solid phase peptide synthesis. Peptide synthesizers can be classified as continuous flow, batch, parallel, and micro-wave peptide synthesizers. In continuous flow peptide synthesizers, the process solution is re-circulated through the reaction vessel using pumps. The reaction progress is usually monitored photometrically. Batch synthesizers are useful to produce a small batch of peptides in large scale (depending upon the instrument design, peptides can be produced even at the kilogram scale). Parallel peptide synthesizers are useful to generate a large library of peptides. These synthesizers are based on split-mix-synthesis strategy. Microwave synthesizers allow microwave heating of process solutions, which can reduce synthesis time and can be useful in achieving the synthesis of difficult sequences. There are several vendors for the instrument, such as Invitrogen, Protein Technologies Inc., or PerSeptive Biosystems Inc. However, basic instrumentation of most of the continuous flow peptide synthesizer is quite similar. The important components of a peptide synthesizer are the pneumatic pump, nitrogen supply, the valve system, the amino acid delivery system, the solvent supply system, waste system, reaction vessel, fluid sensors, and the user interface software to manage the synthesizer (Figure G-1).

A pneumatic pump is used in the instrument to apply pressurized air to produce mechanical motions, such as opening and closing of valves. Regulators are installed in the instrument to remove excess air pressure that occasionally builds up in the pneumatic system. Generally, 80 – 90psi air pressure is maintained in the unit. A nitrogen or inert

gas, such as argon, is connected to the unit to transfer pressurized nitrogen for the transfer and mixing of solutions. Regulators are employed to maintain desired pressure (roughly 6psi) in the unit. The valve system is a unique combination of valves, which provide common solution supply ports to the reaction vessel. They are made up of chemical resistant materials such as Teflon. Additionally, there are electromechanical valves which actuate the regular valves.

An amino acid delivery system generally includes a stage where 20 vessels, corresponding to 20 amino acids, can be held. A robotic system, which as per the software, prepares and delivers the correct activated amino acid solution to the reaction vessel. A solvent reservoir system is also present in the unit to deliver solvents, such as DMF, DCM, acetonitrile, and capping solution to the reaction vessel. The reagents in the solvent delivery system are pressurized under nitrogen. The waste system is the only exit route for the solutions in an otherwise fully enclosed unit. Waste sensors present in the unit identify when the waste reagent bottle is filled and needs replacement. The reaction vessel in a unit could be multiple volumes designed for small scale, medium scale, and large scale synthesis. Fluid sensors present in the unit constantly monitor the supply status of reagents in the unit.

The user interface software of a peptide synthesizer controls the execution and monitoring of peptide synthesis. The software executes each chemical step and moves to the next on completion through a serial communication. Files for the execution of synthesis can be manipulated to customize synthesis protocols. The software program also generates a synthesis report and performs data calculations.



FIGURE G-1: A picture of continuous flow peptide synthesizer manufactured by PerSeptive Biosystems.

Matrix-assisted Laser Desorption Ionization (MALDI) Mass Spectrometry^{3,4,5}

MALDI mass spectrometry, developed by Hillenkamp and Karas, is a powerful analytical technique for identification and characterization of peptides, proteins, oligonucleotides, carbohydrates, and many other biomolecules. In this technique, a sample is first co-crystallized with a large excess of matrix compound. The matrix usually is a UV absorbing, weak acid. Some of the commonly used matrix compounds are α -cyano-4-hydroxycinnamic acid, 2,5-dihydroxybenzoic acid, and sinapinic acid. The matrix solutions are commonly prepared in a mixture of nanopure water and HPLC grade acetonitrile or methanol containing 0.1% Trifluoroacetic acid (TFA). The matrix absorbs laser light energy and transfers some of the energy to a sample, resulting in vaporization of the sample-matrix mixture. At the same time, the matrix also ionizes the sample molecules by accepting or donating protons with the sample molecules. It produces quasi-molecular ions for MALDI detection.

In a MALDI instrument there are three types of mass analyzers. They are (1) a linear time-of-flight (TOF) analyzer, (2) a TOF reflectron, and (3) a Fourier Transform analyzer. In linear TOF analysis, ions of different masses are provided with same amount of energy and allowed to pass through a field-free path of usually 1-2 m in length (Figure G-2). Here, they are separated in space and time-of-flight, according to their motion equation $t = c \times m \text{ per } U^{1/2}$ (where t denotes the flight time, m the ion mass and U the acceleration potential, respectively). At the end of the drift path, ions, within a time span of some tens to some hundreds of μs , arrive at the detector (an ion with lower mass will show up before an ion with higher mass). In a TOF reflectron, the time spent by ions in the TOF tube is increased and kinetic energy distribution is decreased, with the help of an electrostatic analyzer. The TOF reflectron analyzers provide peaks with high resolution when compared to linear TOF analyzers. This is at the expense of sensitivity. Better resolution in TOF analyzers can also be achieved by a method called delayed extraction (DE). In this method, ions are allowed to cool for approximately 150ns before accelerating to the analyzer. This helps by lowering the K.E distribution among ions, leading to a decrease in the temporal spread of ions. As a result, an increase in resolution and accuracy can be seen in a MALDI spectrum.

In a Fourier transform analyzer, ions orbit in the presence of a magnetic field. While orbiting, the ions are excited by a radio frequency radiation. Excitation of the ion generates a detectable image current. The time-dependent image current is Fourier transformed to obtain component frequencies, which, in turn, is dependent on mass to charge the ratio of ions. High accuracy and increased resolution can be achieved using

Fourier transform analyzer. The analyzer is also well suited for tandem mass spectrometry.

The MALDI peaks of amino acids and different groups widely used in peptide synthesis can be found in Appendix H.

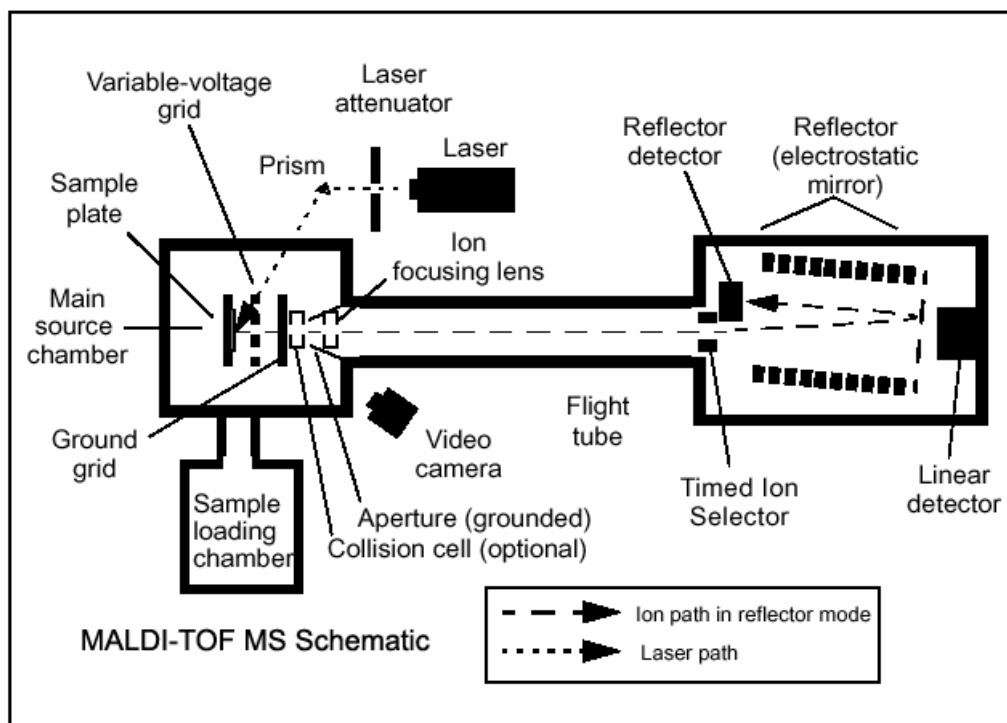


FIGURE G-2: Schematic of MALDI-TOF⁶

Ultraviolet-visible (UV-Vis) Spectroscopy⁷

Ultraviolet-visible (UV-Vis) radiation wavelengths range from 100Å – 7800Å. The energy associated with the UV-Vis radiation, when absorbed by molecules, can excite electrons from a lower energy level to higher energy level. Three types of electrons are present in a molecule: sigma-bond electrons, pi-bond electrons and non-bonding electrons. Sigma-bond electrons are most stable, and require higher energy for transition.

These electrons generally absorb deep-UV radiations for transition. Pi-bond electrons are less stable compared to sigma-bond electrons, and can be excited with UV and visible light radiations. Non-bonding electrons are generally the least stable electrons and can be excited from their ground state by UV and visible light radiations.

A sample, when exposed to a UV-visible radiation spectrum, absorbs radiation with a frequency that matches the energy difference between a possible electronic transition within the molecule. A spectrophotometer records and plots the degree of absorption (A) of different wavelengths of the UV-visible region. At λ_{max} , the sample absorbs the maximum amount of light. Conjugation can lead to reduction in the energy difference between HOMO and LUMO of the molecule, thereby making the molecule absorb radiations of near UV and visible region.

Beer-Lambert Law can be used to determine concentration of absorbing species in a sample.

$$A = \log_{10} (I_0/I) = \epsilon \cdot c \cdot L \quad (\text{G-1})$$

Where 'A' is absorbance, I_0 is the intensity of incident light, I is the intensity of transmitted light, ' ϵ ' is a constant known as the extinction coefficient, 'c' is the concentration of the sample, and 'L' is the path length through the sample.

The ratio I/I_0 is known as transmittance. A UV-Vis spectrophotometer measures absorbance based on transmittance.

$$A = -\log_{10}(\%T/100) \quad (\text{G-2})$$

A sample is generally placed in liquid phase in a UV spectrophotometer for measurement. The sample holder, known as cuvette, is a transparent cell usually made of

fused quartz, as it is transparent to UV and visible radiations. The internal width of these cuvettes is generally 1cm.

A spectrophotometer usually consists of a radiation source, a sample holder, a monochromator with a diffraction grating, and a detector (Figure G-3). Common radiation sources employed in spectrophotometers are a tungsten-halogen lamp, a deuterium arc lamp, a xenon arc lamp, and light emitting diodes. The two most common types of detectors employed are photocell and photomultiplier tube detectors. In a photocell detector, a photon hits the cathode of the cell to eject an electron, which moves towards the anode. The electric current signal thus generated is proportional to the energy of the photon. The electric signal is processed and converted into the absorption spectrum. A photomultiplier detector (PMT) is based on the photoelectric effect. Photons eject electrons from the surface of a photomultiplier tube, which then ejects secondary electrons from the collision to another surface. The secondary electron then produces multiple electrons through several collisions with photosensitive material placed in the PMT setup. Multiple secondary electrons, thus generated, are directed towards the anode generating an amplified electric signal. Due to the capability to amplify signals, a photomultiplier tube is sensitive to photons of low energy.

A spectrophotometer instrument can be based on a single-beam or a double-beam technique. In a single-beam technique, the radiation can reach the detector only through the sample cell. Therefore, I_0 can be measured only in a different step, without the presence of a sample in the instrument. In a double-beam technique, the radiation is split into two beams, one passing through the sample cell, which measures ' I ', and another

avoiding it, which measures 'I₀'. Some double-beam instruments have two detectors, measuring I and I₀, at the same time. Others have a single detector in which one beam is blocked to measure the intensity of the other beam at a certain time.

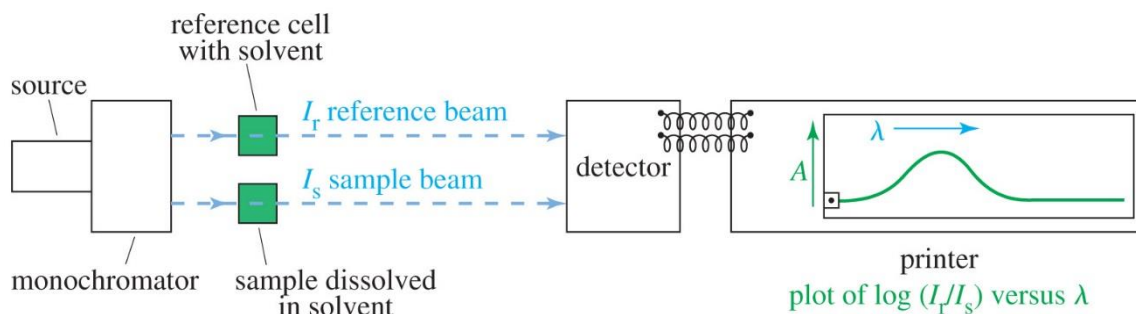


FIGURE G-3: Working principle of a UV-vis spectrophotometer⁸.

Infra-Red (IR) Spectroscopy⁸

Infrared spectroscopy, one of the two types of vibrational spectroscopy, involves irradiation of a sample with infrared radiations. The infrared radiations with similar frequency to that of different vibrational modes of bonds and groups of a molecule are absorbed by the sample and reflect in the IR spectrum. Only vibrations which involve a change in dipole moment are IR active. The vibration that does not involve a change in dipole moment is analyzed through Raman spectroscopy. The infrared region spans from 4000 – 400 cm⁻¹. The frequencies of the radiations of the infrared region can resonate with rotational frequencies and fundamental vibrational frequencies as well as overtones and harmonics of bonds and groups of molecules.

An IR instrument records and plots transmittance or absorbance of different frequencies of an IR region. An IR spectrum of each molecule is unique, since every molecule has a unique environment, due to the different atoms and bonds present. Thus,

the IR spectrum is also known as a molecular fingerprint of a compound. The intensity of the peaks in the IR spectrum also gives an idea about the concentration of the compound present in the sample.

Fourier Transform Infrared Spectrometry (FTIR) involves the measurement of all infrared frequencies simultaneously (Figure G-4). FTIR instruments consist of an optical device known as interferometer. The interferometer produces a signal encoded with all of the infrared frequencies that can be read quickly, allowing analysis of several samples in a small time frame.

Generally, interferometers possess a beam splitter, which divides the incoming infrared beam into two beams. One beam is reflected from a fixed mirror and another is reflected from a moving mirror. The two reflected beams are then recombined. The signal exiting from the interferometer is the result of the two beams interfering with each other. This signal is called an interferogram, and its every datapoint is a unique piece of information about all of the IR frequencies radiated through the sample. Thus, all of the IR frequencies are measured simultaneously using the interferometer. The interferogram encoding all of the IR frequencies is decoded computationally using the Fourier transformation. Once processed computationally, a frequency spectrum plotting intensity vs wavenumber is collected.

With the advent of FTIR spectrometers, sample preparation has become simplified to a great extent. A very small amount of solid or liquid sample that can cover the diamond tip of the stage of the instrument is sufficient for collecting spectrum. It is a

non-destructive technique, and the sample can be recovered after analysis. Furthermore, a sample can be placed directly in the instrument without any sort of preparation.

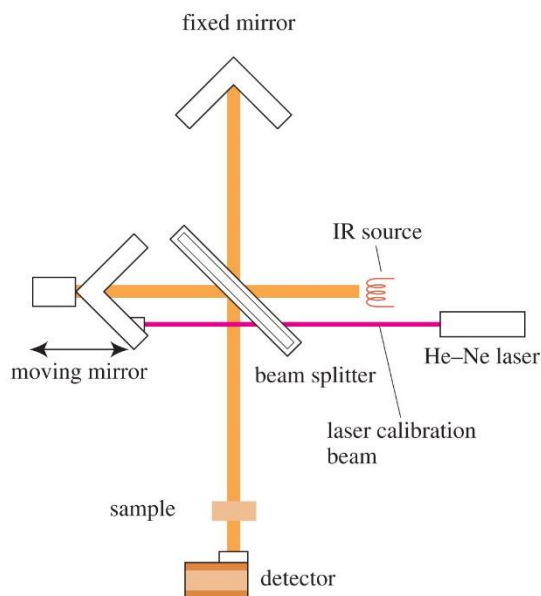


FIGURE G-4: Working principle of a FT-IR spectrometer⁸.

Nuclear Magnetic Resonance (NMR) Spectroscopy⁹

NMR spectroscopy is an extremely powerful analytical technique for structural determination of organic molecules. A wide variety of nuclei such as ^1H , ^{13}C , ^{15}N , and ^{31}P are studied in this technique. A nucleus with an odd number of protons and/or neutrons is associated with a nuclear spin. A nucleus (charged species), when spinning, generates a magnetic field. When an external magnetic field is applied to the spinning nucleus, the nucleus aligns itself in either alpha-state (lower energy state; the direction of magnetic field of nucleus is the same as the direction of external magnetic field) or beta-state (higher energy state; the direction of the magnetic field of the nucleus is opposite to

the direction of the external magnetic field). An alpha-state nucleus, when irradiated with a photon of radio frequency equal to the energy difference between alpha and beta states, absorbs the energy and flips to beta state. The frequency at which such flipping takes place is called a resonating frequency. For example, in proton-NMR, a radio frequency radiation of 300MHz is applied to flip a nucleus if the strength of the external magnetic field is 70459 gauss. However, all of the protons do not have the same environment in a molecule. The surrounding electrons of each proton have influence with their magnetic fields, altering the value of the net external magnetic field acting upon a specific proton. Thus a stronger magnetic field than 70459 gauss would be required to flip a proton with surrounding electrons at 300MHz radio frequency radiation. Protons that are more shielded with electrons resonate at higher field (upfield) and protons that are less shielded with electrons resonate at a lower field (downfield). The more the proton is downfield, the more its corresponding signal will be towards the left side of the spectrum.

The number of signals in a $^1\text{H-NMR}$ spectrum shows the number of different kinds of protons present in a molecule, and the location of the signals show the extent of the de-shielding effect on the proton. The schematics of a NMR spectrometer can be seen in Figure G-5.

In order to prevent interference in signals from solvent, generally deuterated compounds such as deuterated water, acetone, methanol, chloroform, dimethylsulfoxide or compounds containing no protons such as carbon tetrachloride and carbon disulfide are used as solvents. In a sample preparation, a small amount of tetramethyl silane (0.1% v/v) is added as an internal standard. Because silicon is less electronegative than carbon,

protons in tetramethyl silane are highly shielded, and the location of its signal is given an arbitrary value of zero in the spectrum. Signals from organic molecules are generally found downfield to the TMS signal.

The x-axis of the NMR spectrum is called delta-scale. The location of a signal on the delta-scale is called a chemical shift of the proton. It is defined as a ratio of shift downfield from TMS (Hz) to spectrometer frequency (MHz). The units of chemical shift is parts per million (ppm).

$$\text{Chemical shift} = \frac{\text{shift downfield from TMS (Hz)}}{\text{Spectrometer frequency (MHz)}} \quad (\text{G-3})$$

In ¹H-NMR, the splitting of signals can be seen. Equivalent protons do not split the signal, but neighboring non-equivalent protons split the signal according to the 'N+1 rule': N+1 peaks are observed within a signal if it is split by 'N' number of equivalent protons. When non-equivalent protons are four or more bonds apart, generally, splitting of signals is not observed. The distance between peaks in a signal is called the coupling constant. Two nonequivalent protons splitting each other will have the same coupling constant. Protons whose imaginary replacement can form stereoisomers are non-equivalent and split each other in the ¹H-NMR spectrum.

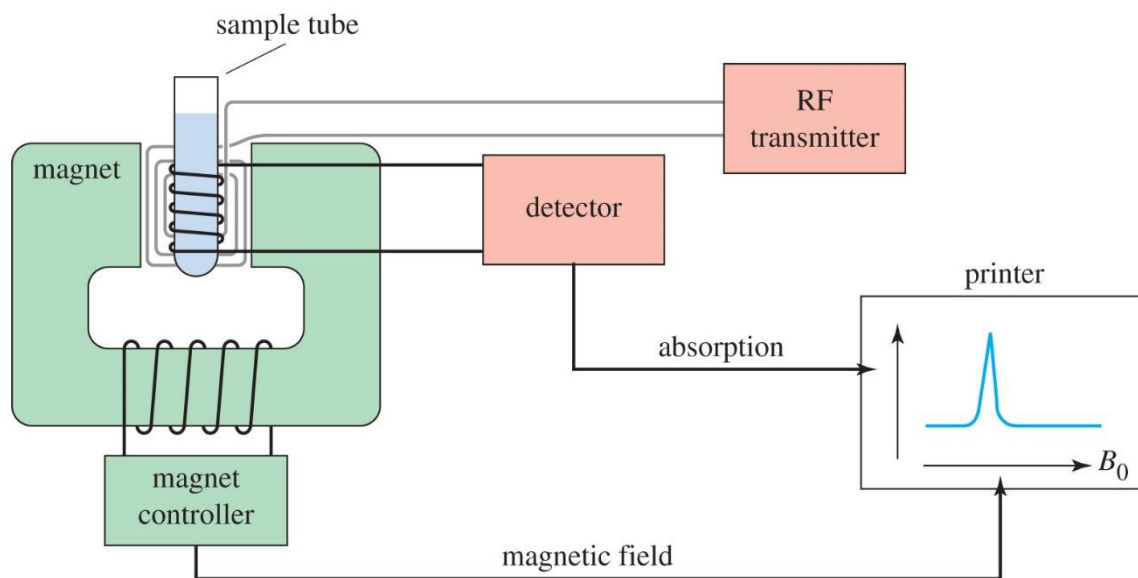


FIGURE G-5: Working principle of a NMR instrument⁹.

Fluorescent Microarray Image Scanner^{10,11}

Fluorescence based microarray imaging systems involve excitation of dye incubated on a microarray substrate, collection of fluorescence signals, and generation of a digital image of a fluorescence signal (Figure G-6). Laser excitation, along with a photomultiplier tube (PMT) detector, is the common method used in these systems to acquire images. A laser with a wavelength similar to λ_{max} of dye and a few microns in diameter scans the substrate exciting the dye. Laser excitation of a dye can be achieved in a few microseconds, as higher power density monochromatic light can be focused on a small spot of the surface while scanning. The emitted fluorescence signals are collected by the PMT. The signal is amplified by PMT, which is then processed into a digital image, showing the fluorescence signal intensity from each pixel position. Compared to

other kinds of detectors, the PMT detector is considered to have a high signal to noise ratio (SNR). SNR is calculated as:

$$\text{SNR} = (\text{signal} - \text{background}) / \text{standard deviation of background} \quad (\text{G-4})$$

The magnitude of the emitted signal can be changed by adjusting the electric potential applied to the PMT. An electric current produced by incident light can be amplified as much as 10^8 times using a PMT. PMTs have optimum electric potential range. An incident photon colliding with a PMT set at lower potential than its optimum range would not generate an electric signal. At the same time, if the PMT is set at a higher potential than its range, SNR efficiency is likely to go down. Although quantum efficiency (the amount of electronic signal emitted from a device relative to the number of incident photons) of PMTs is less than CCD detectors, PMTs are preferred in microarray imaging scanners due to their high resolution and other design parameters.

Laser design in scanners could be confocal or non-focal. A confocal design is generally used to image a thick sample, such as cells or tissues. A confocal design has a narrow depth of focus. Because of this, only thin slices of the sample are imaged at a time. By repeated scanning at different depths, all layers of a thick sample can be imaged. All of the images can then be stitched together to construct a 3D image of the sample. Because microarray surfaces are generally flat and background signals are emitted from the same plane as the real signals, confocal design may not provide an added advantage compared to non-focal design.

Two types of microarray scanners are available: one in which lenses move and the platform is fixed while scanning, and another in which lenses are fixed and the platform

moves while scanning. Performance of the scanners with fixed lenses are usually better, due to less scanning errors. Another feature of a scanner that affects its performance is the numerical aperture. It is defined as:

$$N = n \sin \Theta \quad (\text{G-5})$$

Where ‘N’ is numerical aperture, ‘n’ is the refractive index of environment in which lens is working, and ‘ Θ ’ is the half-angle of maximum cone of light that can enter or exit lens.

Scanners with high numerical aperture values are considered to be efficient microarray scanners. Some other parameters that decide efficiency of a scanner are reproducibility, sensitivity, scanning speed, and durability.

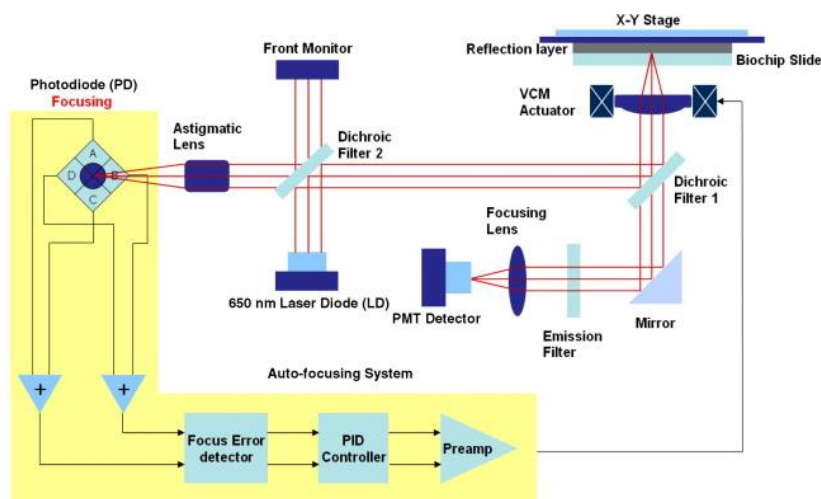


FIGURE G-6: Working principle of a fluorescent image scanner¹².

High-performance Liquid Chromatography¹³

It is a powerful analytical tool used to separate solution-phase mixtures into its chemical constituents. The basic principle of HPLC is the same principle as column

chromatography. Instead of letting the solution-phase drip through the column by gravity, in this technique, the solution-phase is run through the column under high-pressure (approximately 400 atm). This makes the separation process faster. Owing to smaller particle size and efficient packing of the stationary phase, the interaction between the molecules of the mobile phase and the stationary phase is greatly improved. This leads to an efficient separation of mixtures.

Depending on the polarity of the stationary and mobile phase, there are two types of HPLCs: (1) Normal phase HPLC and (2) Reverse phase HPLC.

Normal phase HPLC. In this type of HPLC, the stationary phase is a highly polar material, usually silica, and the mobile phase is relatively non-polar. The most non-polar component of the mixture to be separated is eluted first, and the least non-polar/most polar component of the mixture is eluted last.

Reverse phase HPLC. In this type, the polarities of the stationary and the mobile phase are reversed, compared to the polarity of the phases in Normal phase HPLC. Usually, silica is modified with an 8 or 18-carbon long hydrocarbon chain to make the stationary phase non-polar. Common solvents used for mobile phase are usually ethanol or a mixture of water and ethanol. The most polar component of the mixture is eluted first, and the most non-polar component of the mixture is eluted last.

Generally, the length and inside width of the column for both normal and reverse phase is 150-250 mm and roughly 4.6mm respectively.

Retention Time. Retention is the time taken by a specific component of the mixture to pass through the column. Retention time of a chemical compound depends

upon various factors. These may be the nature of the stationary and mobile phase, pressure, and temperature. There is a possibility that two different chemical compounds have the same retention time under similar conditions. Therefore, it is valuable to characterize the separated component through UV-Vis, IR, NMR, and mass spectrometry. Nevertheless, retention time can serve as quick indicator of the nature of the chemical component.

UV-Vis spectroscopy based detection. Quantitative determination of components of a mixture can be done using a UV-Vis spectrophotometer as a detector in the HPLC instrument. Many organic compounds absorb radiation of wavelengths falling in UV-Vis region. The amount of light absorbed by a compound is proportional to its concentration. The retention time and concentration of a pure sample of a component under similar HPLC conditions could be used to determine the concentration of the component.

HPLC coupled to mass spectrometer. The HPLC and mass spectrometer, coupled together, is widely used in analytical chemistry. The components, separated through the HPLC column, are fed into the mass spectrometer instrument. It then ionizes the compound, accelerates it through the time-of-flight tube and detects the m/z peaks of the molecule and its fragments. The mass spectrum can be compared to the database to find the chemical nature of the compound.

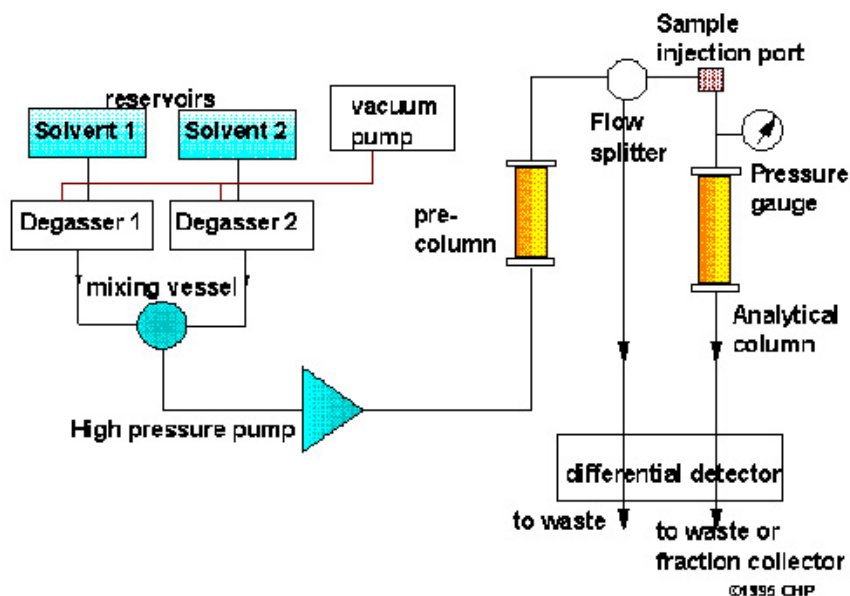


FIGURE G-7: Schematic of a HPLC instrument¹⁴.

References

1. R.P. Andrews, Automated continuous flow peptide synthesis. *Nature* **319**, 429-430.
2. <http://www.aapptec.com/equipment-solid-phase-peptide-synthesis-i-249.html>
3. R.J. Cotter, Time-of-flight mass spectrometry for the structural analysis of biological molecules. *Anal. Chem.* **64**, A1027–A1039 (1992).
4. B.T. Chait, S.B.H. Kent, Weighing naked proteins: Practical high accuracy mass measurement of peptides and proteins. *Science* **257**, 1885–1894 (1992).
5. M.B. Comisarow, A.G. Marshall, Frequency-sweep fourier transform ion cyclotron resonance spectroscopy. *Chem. Phys. Lett.* **26**, 489–490 (1974).
6. http://cbsu.tc.cornell.edu/vanwijk/images/massspec/massspec_schem_maldi.gif
7. T. Owen, Fundamentals of modern UV-visible spectroscopy, Agilent Technologies. www.chem.agilent.com/Library/primers/Public/59801397_020660.pdf

8. L.G. Wade Jr. *Organic Chemistry* (7th ed.), Prentice-Hall (2009).
9. P.A. Paula, J. De, *Elements of physical chemistry* (5th ed.), Oxford: Oxford U.P., p. 459 (2009).
10. S.C. Pickett, *IVD Technology* **9**, 4: 1-6 (2003).
11. Technical features to consider when purchasing a microarray scanner
www.corelifesciences.com
12. K.H. Kim, S.Y. Lee, S. Kim, S.G. Jeong, DNA microarray scanner with a DVD pick-up head. *Current Applied Physics* **8**, 687-691 (2008).
13. Y. Xiang, Y. Liu, M.L. Lee, Ultrahigh pressure liquid chromatography using elevated temperature. *Journal of Chromatography A* **1104** (1–2), 198–202 (2006).
14. Osmania University, Central Facilities For Research And Development
<http://14.139.82.43/cfrd/hplc.html>

APPENDIX H

ABBREVIATIONS, SIDE-CHAIN RESIDUES, AND ACID DISSOCIATION

CONSTANT VALUES OF AMINO ACIDS

TABLE H-1. Abbreviations, side-chain residues, and pKa values of amino acids

Amino Acid, 3-let. abbr., 1-let. abbr.	Side chain residue (R)	Acidic/basic /neutral	pKa (α-carboxylic acid, α-amino, side-chain)
Alanine, Ala, A	-CH ₃	Neutral	2.35, 9.87
Asparagine, Asn, N	-CH ₂ CONH ₂	Neutral	2.02, 8.80
Cysteine, Cys, C	-CH ₂ SH	Neutral	2.05, 10.25, 8.00
Glutamine, Gln, Q	-CH ₂ CH ₂ CONH ₂	Neutral	2.17, 9.13
Glycine, Gly, G	-H	Neutral	2.35, 9.78
Isoleucine, Ile, I	-CH(CH ₃)CH ₂ CH ₃	Neutral	2.32, 9.76
Leucine, Leu, L	-CH ₂ CH(CH ₃) ₂	Neutral	2.33, 9.74
Methionine, Met, M	-CH ₂ CH ₂ SCH ₃	Neutral	2.28, 9.21
Phenylalanine, Phe, F	-CH ₂ (C ₆ H ₅)	Neutral	2.58, 9.24
Proline, Pro, P	-CH ₂ CH ₂ CH ₂ -	Neutral	2.00, 10.60
Serine, Ser, S	-CH ₂ OH	Neutral	2.21, 9.15
Threonine, Thr, T	-CH(OH)CH ₃	Neutral	2.09, 9.10
Tryptophan, Trp, W	-CH ₂ (C ₈ H ₆ N)	Neutral	2.38, 9.39
Tyrosine, Tyr, Y	-CH ₂ (C ₆ H ₄ OH)	Neutral	2.20, 9.11, 10.07
Valine, Val, V	-CH(CH ₃) ₂	Neutral	2.29, 9.72
Aspartic Acid, Asp, D	-CH ₂ COOH	Acidic	2.10, 9.82, 3.86
Glutamic Acid, Glu, E	-CH ₂ CH ₂ COOH	Acidic	2.10, 9.47, 4.07
Arginine, Arg, R	CH ₂ (CH ₂) ₂ NHC(NH)NH ₂	Basic (strong)	2.01, 9.04, 12.48
Histidine, His, H	-CH ₂ (C ₃ H ₃ N ₂)	Basic (weak)	1.77, 9.18, 6.10
Lysine, Lys, K	-CH ₂ CH ₂ CH ₂ CH ₂ NH ₂	Basic	2.18, 8.95, 10.53

APPENDIX I

MASS TO CHARGE RATIO VALUES OF AMINO ACIDS AND FEW GROUPS

FREQUENTLY USED IN PEPTIDE SYNTHESIS

TABLE I-1. m/z values of amino acids and few groups frequently used in peptide synthesis

Amino acid	Monoisotopic residue mass	Monoisotopic mass	Hydrophobicity	Other groups	m/z value
Alanine	71	89	1.0	Fmoc	+223.25
Arginine	156.1	174.1	-7.5	Boc	+101.125
Asparagine	114	132	-2.7	Trt	+243.325
Aspartic acid	115	133	-3.0	t-bu	+57.116
Cysteine	103	121	0.17	Acetyl	+43.045
Glutamic acid	129	147	-2.6	Piperidide adduct	+67
Glutamine	128.1	146.1	-2.9	Tmpp	+575.69
Glycine	57	75	0.67	CONH ₂	+44.033
Histidine	137.1	155.1	-1.7	alloc	+85.082
Isoleucine	113.1	131.1	3.1	Bn	+91.133
Leucine	113.1	131.1	2.2	Bz	+105.116
Lysine	128.1	146.1	-4.6	Pbf	+253.336
Methionine	131	149	1.1	Cbz	+135.142
Phenylalanine	147.1	165.1	2.5	H ₂ O	+18.015
Proline	97	115	0.29	Na	+22.989
Serine	87	105	-1.1	K	+39.098
Threonine	101	119	-0.75	H	+1.008
Tryptophan	186.1	204.1	1.5	DMT	+303.381
Tyrosine	163.1	181.1	0.08	NH ₂	+16.023
Valine	99.1	117.1	2.3	COOH	+45.017